Final Report

Personal Air Transport System

AE3200: Design Synthesis Exercise

Group 22

Delft University of Technology

TU Delft

This page is intentionally left blank.

Final Report

Personal Air Transport System

by

Group 22

Student Name	Student Number
Job Ruijters (JR)	5073138
Diaa Abbasi (DA)	5490626
Ashcharyaa Rajesh (AR)	5807239
Fedor Selivanov (FS)	5756227
Amer Alshehab (AA)	5519438
Anthonie Moggré (AM)	5647452
Gonzalo Fernandez (GF)	5730651
Sohye Lee (SL)	5712831
Katie Sok (KS)	5683319
Martin Průcha (MP)	5552710

Principle Tutor:	Dimitrios Zarouchas
Coaches:	Guus Aerts, Shantanu Purohit
Project Duration:	April 2025 - June 2025
Faculty:	Faculty of Aerospace Engineering, Delft University of Technology

TU Delft

Executive Summary

Traffic congestion is an ever-growing problem in large cities, with significant implications for social and environmental well-being. For instance, the average New Yorker travelling during peak times sits in traffic for 60 hours longer than in 1987, culminating in increased stress and exposure to pollution. While New York and other large Western cities can combat this problem through a combination of improved public transport and pedestrianisation, these solutions are notably more difficult to implement in post-modern cities with harsh climates. A prime example of this is Dubai; its unorthodox urban planning and limited public transport infrastructure leave road expansion as the primary economically viable remedy to congestion. This underscores the urgent need for an innovative transportation solution.

Owl-22's vision is twofold. First, to provide a novel long-term solution, one that isn't constrained by land connections, to traffic congestion in postmodern cities. This approach enables the continuous expansion of travel corridors through the introduction of vertical layers. Secondly, Owl-22 aims to redefine the daily commute experience. In highly congested cities like Dubai, travelling to work typically requires leaving at unconventional times to avoid rush hour and a general feeling of dread is associated with the entire experience. Through this vehicle, which introduces intuitive, aerial travel, users can not only reduce their travel times, but also come to enjoy the experience of going back and forth from work.

This report aims to document the design process that has led to the final configuration of Owl-22. Throughout this process, the team was guided by the following mission statement, which encapsulates the project's core vision:

Provide a sustainable air travel option for personal daily use in urban areas, helping to decrease traffic congestion and the need for more high-density infrastructure.

Product Overview

Owl-22 is a compact, energy-efficient personal air vehicle designed with both functionality and aesthetic appeal in mind. Its user-friendly interface, featuring a car-inspired control setup with a yoke, pedals, and an integrated iPad-based control panel, enhances accessibility for the target audience in the United Arab Emirates. Furthermore, for the convenience of storing the vehicle, it is foldable, fitting in a volume of 4 [m^3] when stowed away. A visual representation of the deployed vehicle is shown in Figure 1.

Figure 1: Owl-22 external view.

The main design specifications are summarised in Table 1:

Table 1: Owl-22 specifications.

Specification	Value
Range	30 [km]
Cruise Velocity	60 [km/h]
Flight Time	30 [min]
Minimum Cruise Altitude	20 [m]
Selling Price	$99,575
Operational Empty Weight	197 [kg]
Payload Mass	105 [kg]
Noise level	71 [dB]

Business Case

Before conducting technical design, a market analysis was conducted to establish a customer base to guide the design processes. Based on comprehensive PESTEL, Porter and SWOT analyses, the UAE market was selected for its supportive regulatory framework, advanced infrastructure and strong cultural acceptance of emerging technologies, creating a favourable environment for market entry. Furthermore, alternative markets outside of the UAE were analysed to allow for future expansion. The countries explored include: the Kingdom of Saudi Arabia, Singapore, Qatar and the United States. These countries share common characteristics with the UAE in terms of high income, innovation investment and urban congestion problems.

Following the market evaluation, a detailed financial analysis was conducted using NASA's aerospace cost modelling methodology. Costs were divided into recurring (COTS components, manufacturing, and assembly) and non-recurring categories (R&D, certification, and production facilities). Incorporating learning curve effects for the recurring costs and a conservative risk-based contingency model, a target selling price was established. With a profit margin of 22.5%, the final price was set at **$99,575.09** as presented in Table 2, meeting the stakeholder requirement to stay below $100,000 while maintaining long-term financial viability.

Table 2: Total per-unit price breakdown at a production volume of 1,000 units per year.

Cost Component	Per-Unit Value [$]
Recurring Costs	64,936.89
Non-Recurring Costs (Amortised)	16,360.74
Total Cost (before profit)	81,297.63
Per-unit Profit (22.5%)	18,277.46
Final Selling Price	**99,575.09**

In order to determine the financial viability of Owl-22, two investment analyses were performed. The return on investment (ROI) calculation resulted in a value of 1.11 over a projected production run of 15,000 units across 15 years. Nevertheless, the obtain a more accurate indicator of the financial viability of the investment, the Net Present Value (NPV) was calculated. The NPV remained negative across conservative discount rates (4–12%), indicating that the investment will likely not be profitable. In order to improve the financial performance of the investment, clear pathways have been identified, including scaling production, securing development grants, and optimising the revenue model over time.

The resulting business case positions Owl-22 as a financially viable, strategically differentiated, and market-aligned solution in the emerging personal air mobility sector.

Vehicle Design Overview

Owl-22 is designed as a compact, efficient and safe personal aerial vehicle which optimises performance. At the heart of these performance characteristics lies the propulsion system selection. A hybrid configuration has been selected, consisting of two coaxial rotors at the rear and two cyclorotors at the front. This layout was chosen to control noise emissions while maximising manoeuvrability and lift. The cyclorotors provide 360° thrust vectoring. This enhances control at low speeds and hover stability. The cyclorotors operate at 60% of their maximum capacity to extend their lifespan. They are positioned lower than the coaxial rotors in order to avoid aerodynamic interference.

The coaxial rotors are powered by separate brushless motors, which increases the lifespan of the system. The rotors are made of carbon fibre. The coaxial rotors setup is designed to minimise the blade-vortex interaction noise. This is done through corotation and unequal rotor diameters. Furthermore, trailing-edge serrations has been added to optimise the turbulence of the propellers resulting in noise reduction. The final configuration consists of two-bladed propellers with NACA 4412 airfoils. This selection enables the vehicle to operate at 50-60% of its maximum thrust, ensuring reliability and efficiency. Aerodynamic simulations have shown minimal flow interference between the propulsion systems. Safety is enhanced through physical separation and structural offsets, preventing damage propagation in the event of blade detachment or motor failure.

Powering this propulsion system is a high-voltage solid-state battery (SSB) pack, selected for its thermal stability, high energy density, and long-term reliability. The battery contains energy of approximately 19.8 [kWh] with a mass of just 66 [kg], enabling a typical range of 30 [km] under standard flight conditions. A modular layout was adopted to support fault tolerance and ease of maintenance, allowing safe continued operation in case of localised failure. Although structural batteries were considered, their added complexity could not be justified without a substantial performance benefit. Battery safety is further supported by a modular Battery Management System (BMS), which monitors both cell- and module-level performance and interfaces with the flight controller via a Controller Area Network (CAN) bus. The BMS handles thermal regulation through a combination of passive heat sinks and active air-based cooling. Liquid cooling is excluded in this iteration but remains an option for future redesigns, should thermal constraints tighten.

As part of the avionics suite, Owl-22's Human-Machine Interface (HMI) features a yoke with an iPad in the middle of it, mimicking a Formula One-style steering wheel. To best utilise the iPad screen, an Electronic Flight Instrument System (EFIS) is used to digitally display the required instruments. Additionally, vertical and horizontal vehicle translation can be done through the iPad directly if preferred. Lastly, to ensure an easier learning curve for users, the pedals are used as acceleration inputs to better resemble a car.

To ensure safe operation, Owl-22's external avionics were divided into a communication suite and a sensing-and-navigation suite. Together, the two parts would constitute the necessary data flow on a hardware, as well as a software level. For the communications suite, the components are summarised in Table 3.

Table 3: Communication suite components.

Component	Use
Two-way very-high frequency (VHF) radio	All voice communications.
Aircraft Communications Addressing and Reporting System over IP (AoIP)	Data communication with both Air traffic control and Owl-22 HQ.
Automatic Dependent Surveillance-Broadcast (ADS-B) Out	Relaying position information.
Basic visual flight rules (VFR) instruments	Communicating vehicle state to user.

The VFR instruments consist of an airspeed indicator, altimeter, temperature gauge, magnetic compass, an Emergency Locator Transmitter (ELT), for relaying location after a crash and both navigation and anti-collision lights for visibility. By adhering to VFR only, the user would need to undergo minimal flight training and face an easier learning curve compared to learning the significantly more complex instrument flight rules (IFR).

The navigation and sensing suite consists of an inertial measurement unit (IMU), a GNSS transponder and LiDAR for primary state measurements, such as altitude, attitude, position and velocity. For this, they would need to be integrated in a tight architecture including filtering techniques to adjust for measurement errors. The LiDAR would also be responsible for obstacle detection, providing a 20-meter omnidirectional detection range. Moreover, a camera would be positioned nadir for extending the user's vision, for example, during landing. This architecture is complemented by the iPad, which provides redundant navigation and inertial sensors.

Outside of human control, Owl-22 features semi-autonomous capabilities, leveraging a deep Reinforcement Learning (DRL) algorithm for automated take-off and landing. Specifically, the Returns Uncertainty-Navigated Distributional Soft Actor-Critic (RUN-DSAC) algorithm is used due to its fine-tuning of model riskiness, as well as an improved ability to generalise. To provide the ideal user experience in terms of safety, timeliness and energy efficiency, Proximal Policy Optimisation (PPO), another DRL algorithm, is used to determine the optimal path for a given journey.

Given the high ambient temperatures expected in the UAE and the criticality of vehicle safety, a Prognostics and Health Monitoring (PHM) system was integrated into Owl-22 to ensure safe, reliable, and maintainable operation. The PHM system enables real-time fault detection, isolation, and health state prediction by combining onboard with ground-based systems. Using a top-down approach, the system is structured across functional, logical and physical domains. The system consists of five core modules: data acquisition, data processing, fault diagnostics, prognostics and health management. These modules operate in sequence to support predictive maintenance. The battery PHM system is further elaborated since it is identified as the most risk-sensitive subsystem of the vehicle. A physical architecture was developed that mitigates risks such as thermal runaway, cell imbalance and over-voltage. Future work should expand the PHM framework to other subsystems and select specific hardware and algorithms to further mature the design.

The structure of the vehicle would need to house the person as well as carry the propulsion loads on the vehicle. Furthermore, it would need to fold to ensure the vehicle would comply to the volume requirements set on it. For this reason, it was split into two parts, with the main airframe connected to the propulsion units and carrying the loads introduced onto it by the user-supporting structure. The main airframe would be made out of Al7068-T6511, manufactured using primarily extrusion. The skin of the airframe, which would also assist the aerodynamic properties of the vehicle, would use the same material.

The user-supporting structure would then consist of the floor, also made of aluminium alloy, the seating and the side-skin of the vehicle. As depicted in Figure 2, such a separation of the structure would facilitate folding the vehicle in the longitudinal direction. This would make use of telescoping beams and an accordion-like side-skin made of polyphenylsulfone (PPSU) plastic and Dyneema fabric. The canopy, which would be made out of impact-modified polymethyl methacrylate (PMMA), would fold over the folded structure, with the arms of the coaxial rotors folding inwards of the structure.

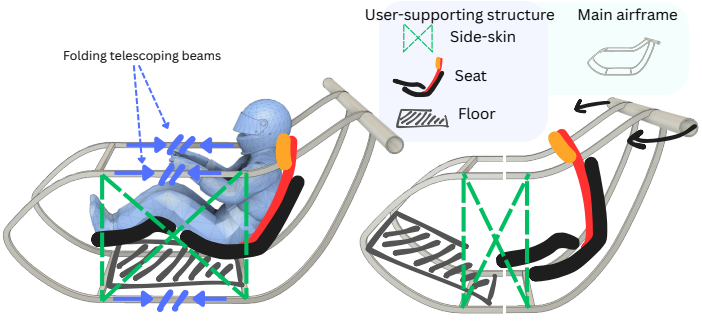

Figure 2: Owl-22 folding concept.

Finally, to ensure compliance with performance and safety objectives, the systems engineering process included a full verification and validation (V&V) plan, requirement compliance matrix, and technical risk

assessment. The verification and validation plan outlined the strategy employed to ensure the software and hardware products function correctly, and furthermore, the plan highlighted the procedures that must be taken in order to ensure that the final product will meet the requirements set at the beginning of this project. The requirement compliance analysis was conducted to guarantee that the design outputted thus far complies with the requirements, followed by a justification for the cases where a requirement has yet to be met. The technical risk assessment evaluated the critical risks that the system is expected to face, followed by a mitigation plan detailing the measures taken to prevent the risk, and a contingency plan in the case of the risk occurring. From the risk assessment, it was evident that the health of the battery was a major concern, which was mitigated through a thorough design of the battery management system.

Mission Execution and Lifecycle Strategy

To ensure the Owl-22 is not only technologically progressive but also operable in daily life, a comprehensive operations and logistics framework was established. The vehicle is designed for seamless integration into urban environments, leveraging its compactness and VTOL capabilities to enable use without the need for large infrastructure. Its six-phase mission profile, from pre-flight to charging, is built around safety and minimal user effort. Interaction is centred on an iPad interface, supplemented with intuitive physical controls to ensure safe operation by non-professional users. The logistics support concept prioritises low-maintenance requirements, enabled by onboard diagnostics and predictive monitoring. A UAE-based production strategy ensures efficient distribution. A robust end-of-life concept embraces circular economy principles through a digital material passport.

Sustainability has been a guiding principle throughout the design of the Owl-22. The project integrates environmental, economic, and social sustainability into a unified framework. Environmentally, material selection prioritised long-term viability, and key design decisions, such as the use of energy-efficient cyclorotors and solid-state batteries, were made to reduce operational emissions. A lifecycle assessment (LCA) revealed that most emissions are generated during flight operations, reinforcing the importance of energy efficiency as a design priority. Social sustainability was addressed by minimising noise impact, which is particularly critical given the Owl-22's low cruise altitude of just 20 metres. In parallel, local manufacturing supports national employment objectives and aligns with initiatives such as "Make it in the Emirates." From an economic perspective, the Owl-22's ability to reduce travel time, combined with compatibility with green finance models, strengthens its long-term value proposition in the urban mobility landscape.

The post-DSE development of Owl-22 follows a structured six-phase roadmap to ensure technical maturity, regulatory approval, and market readiness. The roadmap begins with the finalisation of the detailed design, underpinned by extensive software and hardware testing. In the second phase, individual subsystems are tested to validate performance and identify potential issues early. These systems are then integrated into a full-scale prototype during the third phase, where ground and flight tests are conducted to verify system-level behaviour. Upon successful testing, the fourth phase focuses on certification readiness, followed by a gradual production ramp-up in the fifth phase. The final phase culminates in market entry, supported by tailored pilot training and early operational feedback loops to ensure smooth adoption and continuous improvement.

In conclusion, Owl-22 tackles urban congestion in postmodern cities like Dubai by introducing a personal aerial mobility solution that bypasses ground traffic entirely. Its compact, foldable design, vertical take-off and landing capabilities, and intuitive iPad-based controls enable accessible travel for everyday users. With a coaxial-cyclorotor propulsion system and a solid-state battery, Owl-22 delivers efficient, low-noise operation aligned with the UAE's sustainability goals. By combining advanced tech, user-centric design, and sustainable principles, Owl-22 offers a practical solution for future urban mobility.

Contents

List of Figures

List of Tables

Nomenclature

Abbreviations

Abbreviation	Definition	Abbreviation	Definition
AAM	Advanced Air Mobility	ML	Machine Learning
ACARS	Addressing and Reporting System	MSR	Maintainability, Safety and Reliability
AFCS	Automatic Flight Control System	NFZ	No-Fly Zone
ADS-B	Automatic Dependent Surveillance-Broadcast	NPV	Net Present Value
AOC	Air Operator Certificate	OBC	Onboard Computer
ATC	Air Traffic Control	OEW	Operative Empty Weight
BMS	Battery Management System	PA	Prognostic Assessment
CAAS	Civil Aviation Authority of Singapore	PAV	Personal Air Vehicle
CAD	Computer Aided Design	PCB	Printed Circuit Board
CAN	Controller Area Network	PCM	Phase Change Materials
CAGR	Compound Annual Growth Rate	PDU	Power Distribution Unit
CFD	Computational Fluid Dynamics	PESTEL	Political, Economic, Social, Technological, Environmental and Legal
COTS	Commercial Off-The-Shelf	PHM	Prognostics and Health Management
CSR	Corporate Social Responsibility	PMMA	Polymethyl Methacrylate
DA	Data Acquisition	PPO	Proximal Policy Optimisation
DCAA	Dubai Civil Aviation Authority	PPSU	Polyphenylsulfone
DNNs	Deep Neural Networks	RANS	Reynolds-Averaged Navier-Stokes
DOD	Depth of Discharge	RE	Reinforcement Learning
DP	Data Processing	RFLP	Requirements, Functional, Logical, Physical
DRL	Deep Reinforcement Learning	RL	Reinforcement Learning
DV	Design Verifier	ROI	Return On Investment
EASA	European Union Aviation Safety Agency	RTA	Roads & Transport Authority
EFIS	Electronic Flight Instrument System	RUL	Remaining Useful Life
ELT	Emergency Locator Transmitter	RUN-DSAC	Returns Uncertainty-Navigated Distributional Soft Actor-Critic
EOD	End of Discharge	R&D	Research & Development
eVTOL	Electric Vertical Take-Off and Landing	SAC	Soft Actor-Critic
FAA	Federal Aviation Administration	SIL	Software-in-the-loop
FCU	Flight Control Unit	SIMPLE	Semi-Implicit Method for Pressure-Linked Equations
FDA	Fault Diagnostics Assessment	SIMP	Solid Isotropic Material with Penalization
FEA	Finite Element Analysis	SOC	State of Charge
FVM	Finite Volume Method	SOH	State of Health
GCAA	General Civil Aviation Authority	SOP	State of Power
GDP	Gross Domestic Product	SOT	State of Temperature
GNSS	Global Navigation Satellite System	SPL	Sound Pressure Level
GWP	Global Warming Potential	SSL	Solid State Lithium

Abbreviation	Definition	Abbreviation	Definition
HIL	Hardware-in-the-loop	SWOT	Strengths, Weaknesses, Opportunities and Threats
HM	Health Management	TIMs	Thermal Interference Materials
IFR	Instrument Flight Rules	TMS	Thermal Management System
IMU	Inertial Measurement Unit	UAE	United Arab Emirates
ISA	International Standard Atmosphere	UAM	Urban Air Mobility
KSA	Kingdom of Saudi Arabia	UAV	Unmanned Aerial Vehicle
LCA	Lifecycle Assessment	V&V	Verification and Validation
LiDAR	Light Detection and Ranging	VFR	Visual Flight Rules
		VHF	Very High Frequency
		VTOL	Vertical Take-Off and Landing

Symbols

Symbol	Definition	Unit	Symbol	Definition	Unit
A	Area of cross section	$[m^2]$	A_m	Area of member	$[m^2]$
A_s	Area of skin	$[m^2]$	A_{stif}	Area of stiffener	$[m^2]$
C_D	Drag coefficient	[-]	C_L	Lift coefficient	[-]
$C_{1\epsilon}$	Const. in $K-\epsilon$ model	[-]	$C_{2\epsilon}$	Const. in $K-\epsilon$ model	[-]
$C_{D_{coaxial}}$	Coaxial rotor drag coeff.	[-]	$C_{D_{cyclo}}$	Cyclorotor drag coeff.	[-]
$C_{D_{fuselage}}$	Fuselage drag coeff.	[-]	$C_{L_{cyclo}}$	Cyclorotor lift coeff. at without blade pitch	[-]
$C_{L_{fuselage}}$	Fuselage lift coeff.	[-]	C_μ	Const. in $K-\epsilon$ model	[-]
E	Young's modulus	[Pa]	E_{ij}	Strain rate tensor comp.	[-]
F_m	Member force	[N]	F_s	Skin panel force	[N]
F_x, F_y, F_z	Net forces in x, y, z	[N]	G	Gravitational constant	$[m/s^2]$
I	Area moment of inertia	$[m^4]$	I_{circ}	Circular moment of inertia	$[m^4]$
$I_{xx,yy,zz}$	Moments of inertia	$[m^4]$	KV	Motor velocity const.	[rpm/V]
L	Length	[m]	L/W	Lift-to-weight ratio	[-]
L_1	Lateral CG offset	[m]	L_2	Longitudinal CG offset	[m]
L_{front}	Front strut length	[cm]	L_{rear}	Rear strut length	[cm]
M_x, M_y, M_z	Moments in x, y, z	[Nm]	P_f	Forward force	[N]
P_{cr}	Critical load	[N]	P_{ideal}	Ideal power	[W]
P_{real}	Actual load	[N]	Re	Reynolds number	[-]
T	Thrust	[N]	V	Velocity	$[m/s]$
Q	First moment of area	$[m^3]$	a	Square side length	[m]
bit_{depth}	Bits per axis meas.	[bits/sample]	$bitrate_{IMU}$	IMU bitrate	$[bps]$
$bitrate_{cam}$	Camera bitrate	$[bps]$	c	Chord	[m]
$colour_{depth}$	Bits per pixel	$[bits/px]$	d	Diameter	[m]
f, g, h	Body forces per unit mass	$[N/kg]$	f_{ps}	Frames/sec	$[1/s]$
f_s	Sampling freq.	$[Hz]$	f_n	Natural freq.	$[Hz]$
g	Gravity accel.	$[m/s^2]$	h	Serration height	[mm]
$h_{1,x}, h_{2,x}$	Cyclorotor radial vel. (x)	$[\frac{rad^2}{s^2}]$	$h_{1,z}, h_{2,z}$	Cyclorotor radial vel. (z)	$[\frac{rad^2}{s^2}]$
h_3, h_4	Coaxial radial vel.	$[\frac{rad^2}{s^2}]$	h_{res}	Height resolution	[px]
k	Turbulent kin. energy	$[m^2/s^2]$	k_1	Cyclorotor lift eff.	$[\frac{N}{rad^2}]$
k_2	Coaxial lift eff.	$[\frac{N}{rad^2}]$	λ	Serration wavelength	[mm]
m	Vehicle mass	[kg]	n_{axes}	Num. of axes	[-]
p	Static pressure	[Pa]	r/R	Radial pos. ratio	[-]
$ratio_{compress}$	Compression ratio	[-]	t	Thickness	[m]
u, v, w	Flow velocity comps.	[m/s]	u_i'	Velocity fluctuation	[m/s]
$\bar{u}_i$	Mean velocity	[m/s]	v_{max}	Max deflection	[mm]
w_{res}	Width resolution	[px]	δ	Deflection	[m]

Symbol	Definition	Unit	Symbol	Definition	Unit
δ_{ij}	Kronecker delta	[-]	$\ddot{x}, \ddot{y}, \ddot{z}$	Linear acceleration	$[m/s^2]$
$\ddot{\phi}, \ddot{\theta}, \ddot{\psi}$	Angular accel.	$[rad/s^2]$	β	Mode shape const.	$[1/m]$
ω_n	Natural ang. freq.	$[rad/s]$	τ	Shear stress	[Pa]
μ	Dyn. viscosity	[Pa·s]	μ_t	Eddy viscosity	[Pa·s]
ν	Kin. viscosity	$[m^2/s]$	ν	Poisson's ratio	[-]
ρ	Density	$[kg/m^3]$	$\tilde{m}$	Mass per length	$[kg/m]$
σ_b	Buckling stress	[Pa]	σ_{cc}	Crippling stress	[Pa]
$\sigma_{cc_{panel}}$	Panel crippling stress	[Pa]	σ_{cr}	Critical buckling stress	[Pa]
σ_ϵ	Const. in K–ϵ model	[-]	σ_k	Const. in K–ϵ model	[-]
σ_y	Yield stress	[Pa]	θ, ϕ, ψ	Angular displacements	[rad]

1 Introduction

Cities worldwide are approaching a critical inflexion point in transportation infrastructure. Conventional forms of transport, such as cars, subways and buses, are starting to reach their limits under escalating congestion, worsening air quality, and an ever-growing demand for personalised mobility solutions. These challenges demand transformative solutions that either optimise existing networks or find efficient alternatives. Among the emerging solutions, urban air mobility stands out as a promising option, offering the potential to bypass ground-level constraints. While much of the current attention has focused on air taxis for shared use, there remains a largely unexplored niche: personal aerial transport that is swiftly deployable and can be stored within a small volume.

This report documents the development of such a system, which has been named 'Owl-22'. The primary objective of this report is to provide a detailed design for the project itself, the vehicle and its subsystems. Before advancing to the detailed design stage, the project underwent a preliminary design phase during which concepts of the Owl-22 were reviewed through a series of system and sub-system level trade-off analyses. A wide range of design options was evaluated, ensuring the selected designs comply with the mission requirements and design philosophy. The selected design concepts and components are examined in greater detail in this report. The different concepts are then systematically integrated to form the final complete vehicle architecture.

The report begins with establishing the selected concepts in Chapter 2. It then delves into the subsystem design by first discussing the propulsion subsystem in Chapter 3, where the rotor design alongside its aerodynamic and acoustic properties. The power subsystem is detailed in Chapter 4, which outlines the battery characteristics and also introduces the battery management system that aims to preserve the health of the battery. This is followed by the avionics suite design is presented in Chapter 5, which describes the main electronic components required for the basics functioning and safety of the vehicle. The prognostics and health management framework is then introduced in Chapter 6, elaborating on the diagnostic architecture employed by the vehicle to ensure effective fault detection and health management. Subsequently, the stability and control characteristics of the vehicle are discussed in Chapter 7. The subsystem design is concluded in Chapter 8, where the structural design is established along with the integration of all the subsystems to produce the final system design.

Consequently, the report then shifts focus to the overall system perspective. Chapter 9 discusses the operations and logistics concept, detailing how the vehicle would achieve mission objectives while remaining affordable and scalable. This is followed by the sustainability assessment performed in Chapter 10, which evaluates the Owl-22's impact on the environment, society and economy. The business case for this project is elaborated in Chapter 11, including a comprehensive market analysis and financial planning. Chapter 12 discusses the systems engineering aspects for the vehicle, covering topics such as verification and validation, requirement compliance, and risk analysis. The project design and development logic are then presented in Chapter 13, which outlines the strategic roadmap for future development beyond the current design phase. Finally, the report is concluded in Chapter 15, presenting a summary of key findings.

2 Concept Design

For the detailed design process, a concept design must be established. This is done to outline the functions and development process of the entire system. This chapter details the conceptual design of the Owl-22, a personal aerial vehicle for urban transport in the UAE. This is done by firstly establishing the design enabler, which would provide a guideline in the design selection. The design enabler would be explained and elaborated in Section 2.1. In Section 2.2 the stakeholder requirements would be addressed. This would include the requirements for performance, usability, safety and sustainability. In Section 2.3, a functional analysis would be conducted, determining the actions the Owl-22 would need to perform. Finally, in Section 2.4 the system architecture and the interface between the subsystems.

2.1. Design Enabler

When designing products with a vast design space, it is important to follow a consistent philosophy to motivate the selection of design options. For example, assuming that two design options perform very similarly in a trade-off, the decision would be quite challenging. To provide a uniform method that consistently assess both macro and micro-level trade-offs, it was decided that a 'performance' based philosophy will be followed. This is done for multiple reasons. Firstly, this approach hinges largely on the concept of energy-efficiency, since aircraft performance depends on a delicate balance between propulsive output and its Operative Empty Weight (OEW). This means that one of the central tenets of this project aligns directly with the project's approach to sustainability, thereby enabling their compatibility.

Moreover, a vital reason for this choice was the decision to target the UAE market. Here, locals and expats share a materialistic, trend-centric culture, which is best exploited by designing a visually attractive and unique product. While it is not the aim for Owl-22 to feed into such a culture, it is financially essential that this social behaviour is sufficiently considered by the final design. Another method to attract customers would be by designing a luxury vehicle. However, such an enabler would largely be antithetical to the goal of making a compact vehicle, as well as sustainability goals.

To better illustrate how this enabler is enforced, consider a simple example between two (hypothetically) closely ranked designs. Design A is more compact and foldable than Design B, which is a larger, more aerodynamic option. In this case, Design B would be chosen since it better adheres to the performance policy. Hence, adopting a performance design enabler recalibrates the vision of Owl-22, originally intended for the more cost-wary, sustainability-oriented European market, thereby aligning the design more with the Emirati market whilst still maintaining its core aims.

2.2. Stakeholder Requirements

To determine how the system performs, the requirements it should fulfil must be analysed. The stakeholder objectives provide a foundational set of specification, which are later expanded into a comprehensive requirements framework, which would be formulated in each relevant chapter. The stakeholder objectives, covering performance, usability, safety and sustainability criteria are included in Table 2.1.

Table 2.1: Initial stakeholder objectives.

Specification	Detail
Maximum transportable mass	200 [kg], transportable by one person
Maximum volume	4 [m^3]
Range and speed	30 [km] range, 60 [km/h] max speed
Deployment time	Less than 2 minutes
Flight capabilities	VTOL, min cruise altitude 20 [m]
Power supply	Rechargeable battery preferred (≤ 35% of total weight)
Control	Operable via electronic device
Payload capacity	One passenger (max 100 [kg]) + 5 [kg] utilities
Usage frequency	5 days/week, 500 flights/year
Maintenance	Maintenance-free for first 2 years
Security	No-fly zones enforced
Diagnostics	Real-time monitoring of system faults and structural damage
Noise level	Max 75 [dB] (urban ambient level)
End-of-life considerations	Service extension, recyclability, down-cycling, or waste treatment
Regulation	Compliance with relevant airspace and certification regulations
Safety	Safety of pilot and bystanders is ensured
Production volume	1000 units/year
Selling price	≤ $ 100,000 per unit

Table 2.1 includes the updated requirements. As the initial requirements have been updated based on feasibility. Where the maximum volume was initially 1 [m^3] volume and it has been updated to 4 [m^3]. The battery total weight was initially 30% of the total weight, however after evaluating and assessing this requirement it has been updated to 35% of the total weight. Also, the minimum range and maximum speed were 20 [km] and 40 [m/s] respectively, and have been updated to 30 [km] and 60 [m/s]. Finally, the initial flight altitude has been adjusted to a minimum cruising altitude of 20 [m], as it initially was a maximum altitude of 20 [m].

2.3. Functional Analysis

In order to determine what actions the personal air transportation vehicle needs to be able to perform and aid the creation of requirements for the design process, a functional analysis is performed. The functional analysis is performed in two stages. First, the functional flow diagram (FFD) is created, in order to identify the timeline of tasks and their dependencies. The outcomes of the (FFD) in Subsection 2.3.1. Afterwards, the functional breakdown structure (FBS) is created, where the identified functions are organised in an 'AND tree' based on the stages of the aircraft operation. Further description of this is included in Subsection 2.3.2.

2.3.1. Functional Flow Diagram

The first tool to determine the system functions is the functional flow diagram. This is crucial for the later compiling of the requirements, as the process identifies the necessary functions and actions related to the aircraft lifecycle. In this case, the flow diagram is constructed by chronologically going through the lifecycle of the aircraft. This process identifies key functions the aircraft must perform during operation, as well as essential functions required for its design, certification, delivery, maintenance and retirement. These functions are then broken down further into smaller, more specific functions, such that each higher-level function has its own functional flow presented. Overall, the flow diagram is divided into five functional levels, outlining their dependencies. It includes both AND and OR junctions, indicating

whether functions should be performed simultaneously (AND) or if only one need to be performed (OR).

2.3.2. Functional Breakdown

Another tool used to analyse the aircraft's functions is the functional breakdown. While the functional flow diagram displays the functions depending on the order in which they need to be logically performed, the functional breakdown provides insight into the functions' hierarchy. This helps with determining how to separate subsystems and organise the design process.

The functional breakdown is an 'AND tree' structured such that the first level shows the different life stages of the aircraft. On the second level, these functions are broken down further into different high-level actions of the aircraft, such as 'Deploy the System'. These are then divided into different aspects of each action, such as 'Turn on on system electronics' and 'Check airworthiness' on level 3. Lastly, levels 4 and 5 present small-scale functions such as 'Establish system state', which is broken down further into functions like 'Perform Diagnostics'.

Functional Flow Diagram

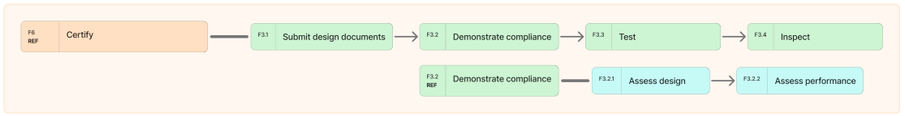

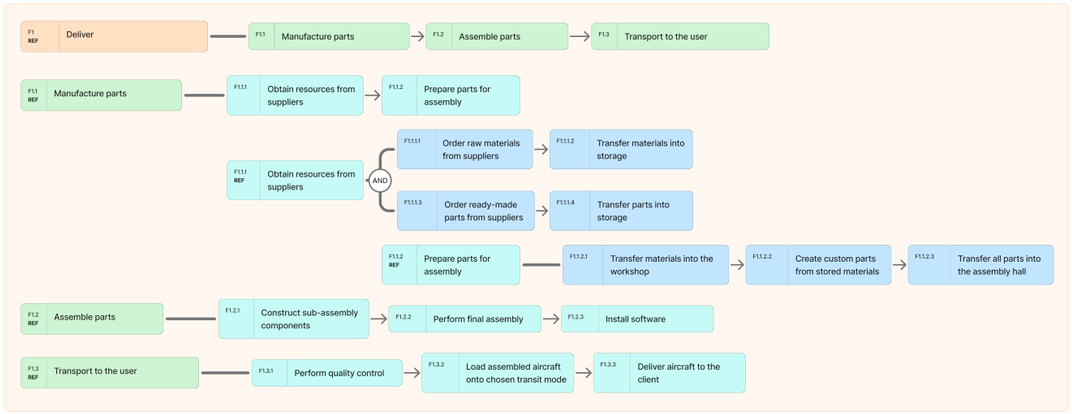

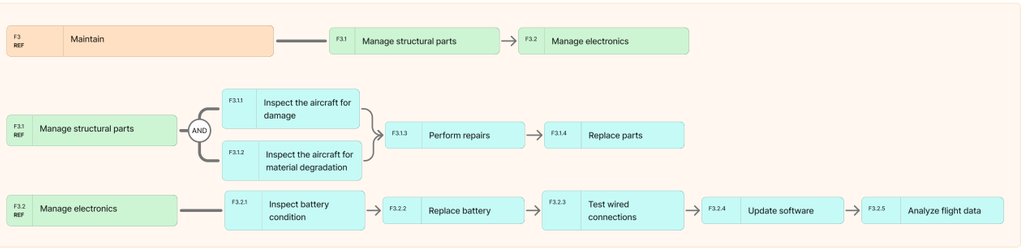

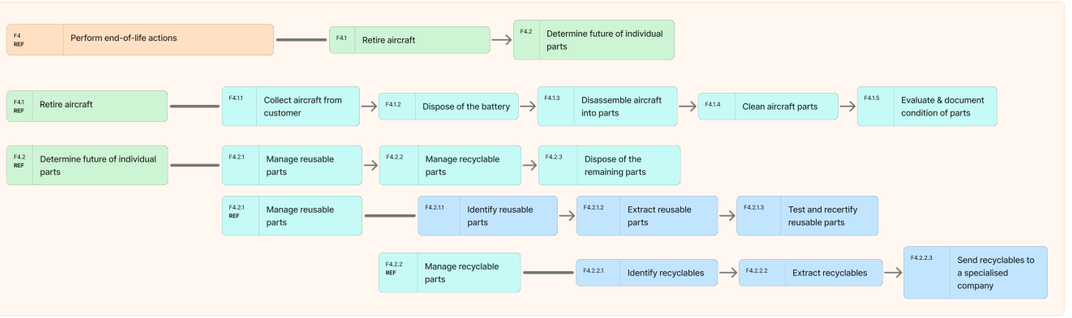

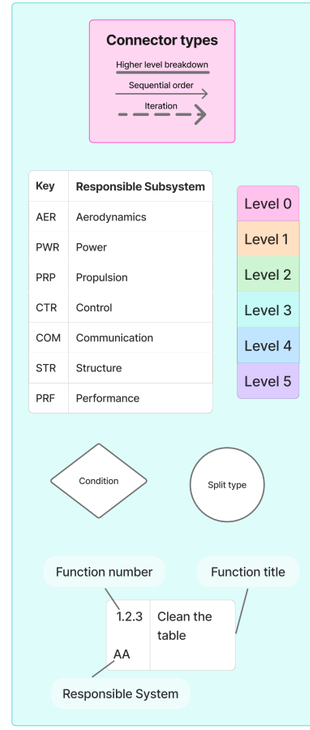

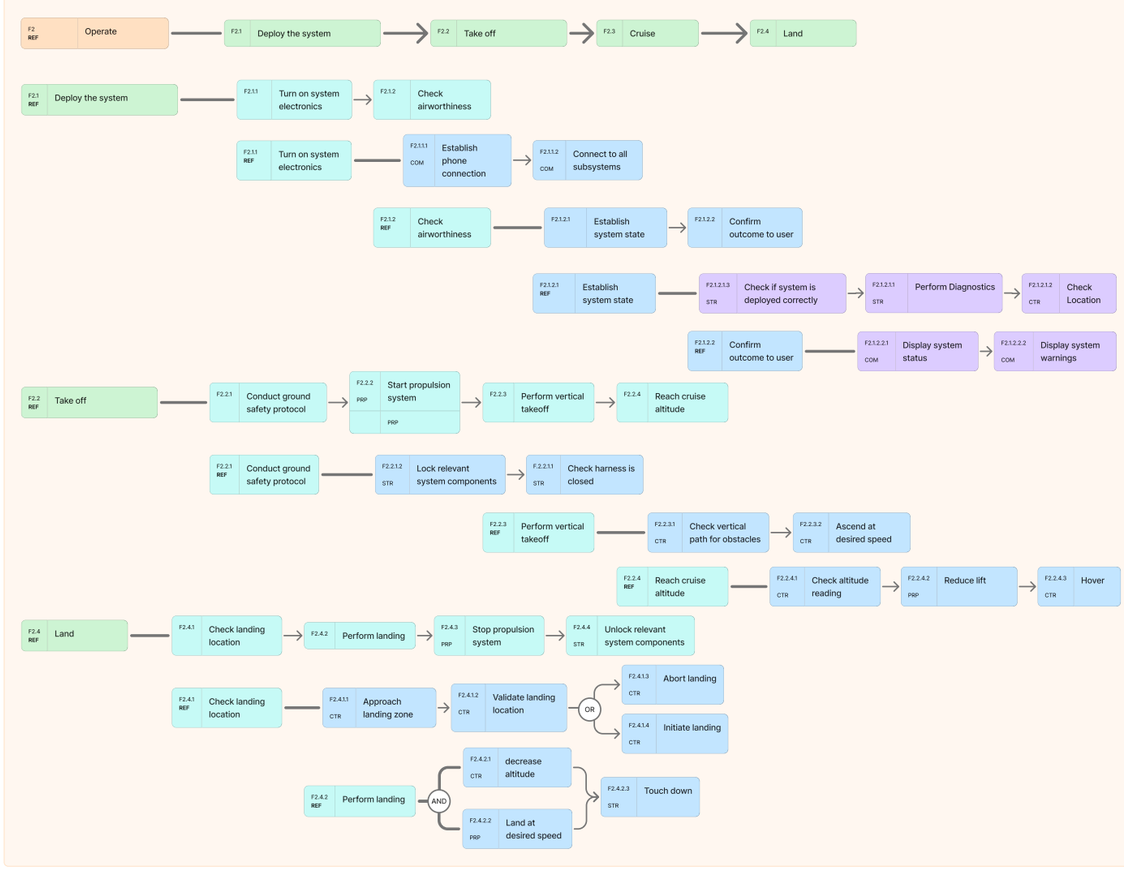

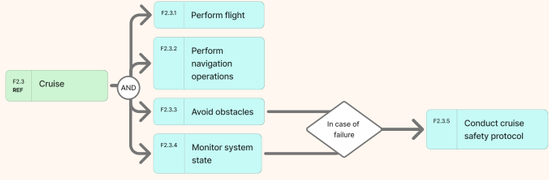

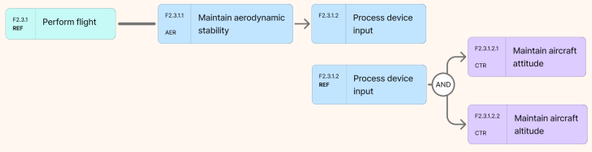

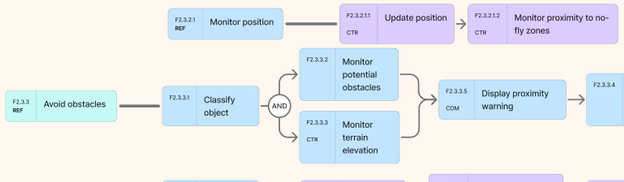

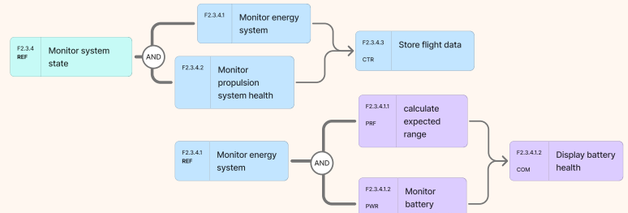

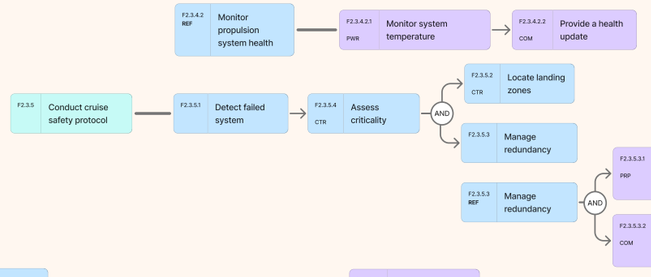

Functional Breakdown Structure

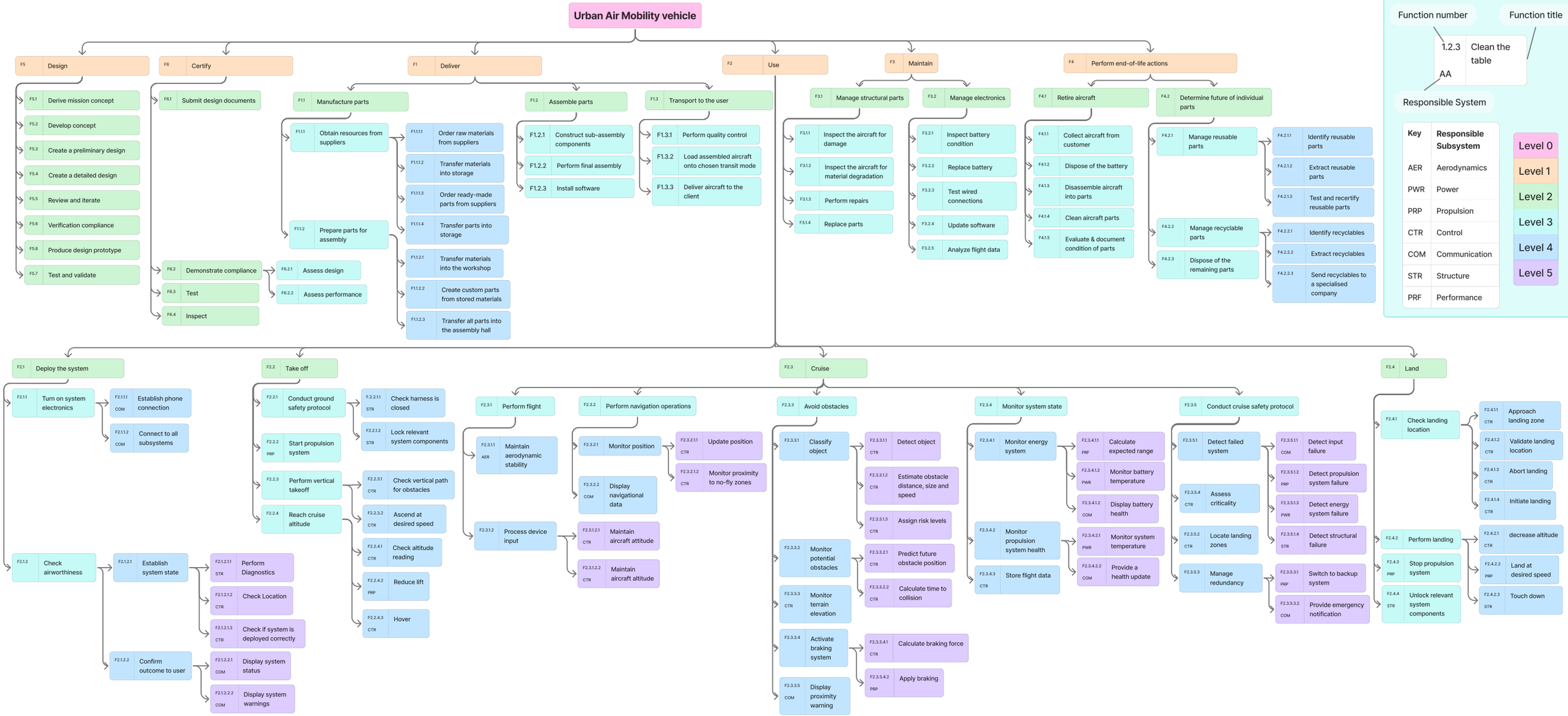

2.4. System Architecture and Interface Definition (N2)

The Owl-22 system will be an intricate web of connections between the subsystems. Figure 2.1 presents these interconnections between subsystems and the environment. Everything inside the grey boundaries demarcates the operations within Owl-22. The different arrows represent flow of data, commands and energy.

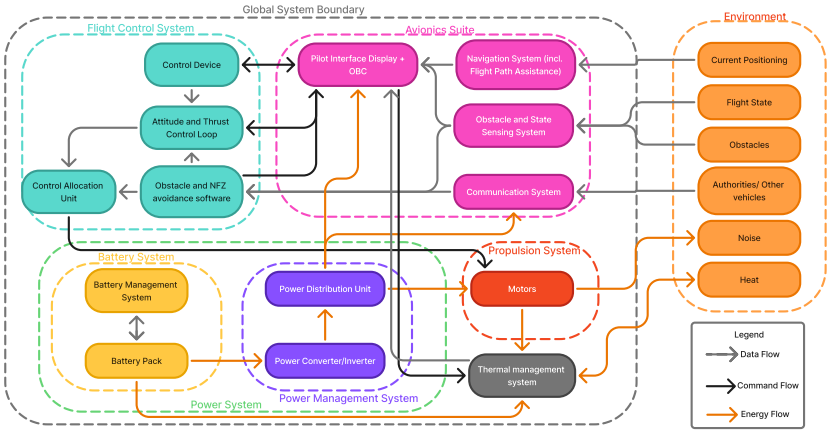

Figure 2.1: System architecture flowchart.

An alternative way of viewing the architecture is provided in Table 2.2 where the interaction with the structure is also presented.

Table 2.2: N2 system architecture chart.

Environment	NFZs, Weather changes	Obstacles, Current State, Signals from Space		Outside reference		Wind, Damage Risks	Heat	Damage risks, Aero Loads, Heat
To ground/in air signals	**Communications**	Map, NFZ updates	Weather, NFZ updates, Vertiport assistance, Remote control instructions*	Data from other UAMs and authorities				
Signals to space	Position Data	**Navigations and sensing**	Obstacle detection. Altitude, Attitude, Position information, Diagnostics feedback					
	Collision Warnings and Position information to other vehicles.	Sensing instructions, Fault scenario commands	**OBCs*** **	Visual/audio feedback, including path generation**	Power distribution commands	Automated/ user-induced (stab. and control) commands.	Nominal Temperature	
	Authorities and other UAM call-outs.		Wanted temperature, User control inputs	**User interface**				Manual deployment
	Allocated Power	Allocated Power	Allocated Power, Diagnostics feedback		**Power System**	Allocated Power	Heat	
Noise			Diagnostics feedback			**Propulsion (and Lift)**	Heat	Propulsion loads
Heat			Temperature information, Cooling		Cooling		**Thermal management**	Cooling/Heating
	Coms. integration	Sensor integration	Diagnostics feedback	Ergonomics	Power system housing	Motor housing, Lift and Drag	Thermal state	**Structures**

* This can be implemented in future development, though it would require significant bandwidth and would introduce extra risks.
** Initially, used as feedback helping the user. In future development stages, this can become automated feeding directly into prop. and lift.
*** OBCs stands for On Board Computers, including computations on the tablet.

3 Propulsion

The propulsion system is a critical system, which is responsible for generating the necessary thrust to achieve lift and controlled flight. In Section 3.1, the requirements that the propulsion has to fulfil are established. Section 3.2 includes the design, selection and sizing process of the propulsion system, which consists of coaxial and cyclorotors. Followed by Section 3.3, which indicates the noise mitigation process for both propulsion subsystems, the coaxial and cyclorotors. In Section 3.4, an aerodynamic analysis was conducted, estimating the forces, pressure, turbulence and its effect on the environment. Finally, the maintainability, safety and reliability of the propulsion system have been discussed, which could be found in Section 3.5.

3.1. Propulsion System Requirements

The propulsion system is a critical system for the vehicle's performance, which would have to fulfil some essential requirements. The requirements relevant to the propulsion system are presented in Table 3.1.

Table 3.1: Propulsion system requirements.

ID	Description
REQ-STR-TPT-01	The total mass of the fully assembled vehicles in its operational configuration shall not exceed 200 [kg], excluding the pilot and any external control device.
REQ-FP-PAY	The vehicle shall be capable of transporting a total payload of at least 105 [kg] over the full mission profile.
REQ-FP-VTOL	The vehicle shall be capable of vertical take-off and landing (VTOL) from a stationary position on flat terrain, without the need for external launch or recovery infrastructure, within a ground footprint of 8 [m] x 8 [m].
REQ-SUS-NOI	The system shall produce noise levels no greater than 75 [dB].
REQ-SAF-PIL	The vehicle shall protect the pilot from life-threatening injury during all phases of nominal operation.

REQ-FP-PAY and REQ-STR-TPT-01 indicate the weight of the vehicle and payload, which results in a 305 [kg] take-off weight, which the propulsion system must provide. However, the system also has to account for upward acceleration. This would require higher thrust levels than the maximum take-off weight. To ensure the system can meet this, the requirement is set to be 310 [kg].

3.2. Propulsion System Design/Selection

This section outlines the selection and design process of the propulsion components, focusing on cyclorotors and coaxial rotors; the chosen lift devices from the conducted trade-off. Where two cyclorotors would be positioned in front of the vehicle and two coaxial rotors would be positioned in the rear, slightly higher than the cyclorotors. This was done to avoid the interaction between the two propulsion systems. Both coaxial and cyclorotors would be required to provide a minimum thrust of 155 [kg] separately, as the centre of gravity is assumed to be in the centre of the vehicle.

3.2.1. Cyclorotors

Cyclorotors were chosen as a part of the propulsion system for their unique characteristics. As it could provide 360° thrust vectoring, making it highly manoeuvrable and smooth in the transitioning phase between hover and forward flight. The two cyclorotors that would be used for the propulsion system of the vehicle will be acquired from Cyclotech. To provide sufficient lift for the entire system, the CR-84 cyclorotor would be used, which could be seen in Figure 3.1. As the CR-42 does not provide enough

thrust and the CR-60 would have to operate at its maximum thrust throughout the entire mission, to provide sufficient thrust. This would make the CR-60 very inefficient and would not account for any safety margin. Also, comparing the CR-84 to the CR-42 and CR-60, the CR-84 has a higher efficiency and has a higher thrust-to-mass ratio [1].

Each CR-84 can provide a maximum thrust of 152.8 [kg]. However, the cyclorotors would be required to provide only 60% of their thrust, for higher efficiency, to maximise their lifespan and to increase the reliability and safety of the system [1].

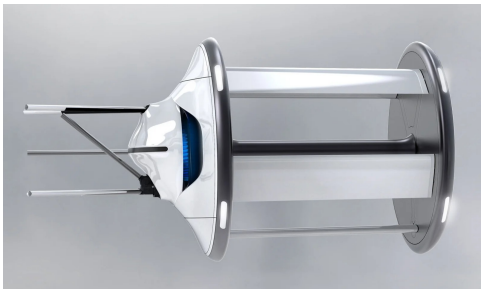

Figure 3.1: The CR-42 model [1].

3.2.2. Coaxial Rotors

The coaxial rotors consist of two main components, the propellers and the motors. To optimise the system's design and minimise mechanical complexity, each propeller within the coaxial setup is directly driven by its own dedicated motor. This independent motor-propeller configuration simplifies the overall mechanism by eliminating the need for intricate gearboxes or power-splitting devices that would otherwise be required to drive multiple propellers from a single motor.

Design Decisions

In the propeller designing process, the main consideration was the noise. That is due to REQ-SUS-NOI, which has to be fulfilled while providing sufficient thrust to lift the system. Especially due to the high noise level that the coaxial rotors generate, as they are considered to be the main source of noise.

To reduce the noise the coaxial rotors generate, the noise generated by the propellers is split into three main noise components. This is done considering the propellers are the main source of noise in the coaxial setup. The three noise sources are the thickness, loading and blade vortex interaction noise. The thickness noise accounts for the displacement of air due to the propeller motion. This is mainly relevant for the airfoil selection. The loading noise is dependent on the loads that the air applies to the propellers [2].

Looking at the three noise types, the blade vortex interaction is considered to be very high in a coaxial setting. To reduce the vortex interaction noise of the coaxial propellers, two decisions have been made. The first decision is to have a corotating propeller instead of contra-rotating propellers, as this has a considerable interference reduction, resulting in a lower noise [3]. However, this also reduces the thrust output of the coaxial rotors compared to counterrotating by 10% [4]. The second decision is to use a smaller spanned propeller for the lower propeller, compared to the upper one. This is done to ensure the vortex of the upper propellers does not interfere with the lower propellers.

To reduce the loading noise and the tip vortices, a serration would be applied on the trailing edge of the propellers. This design option is inspired by serration on the owl's wings, which results in their silent flight [5]. This would improve the aerodynamic property, reducing the turbulence at the trailing edge. As a result, the noise would be reduced.

Propeller Sizing

The main aspect of the coaxial rotors is the thrust generation. The coaxial rotors would be required to provide thrust, which is equal to 155 [kg]. To achieve this thrust the propellers would be sized accordingly. As mentioned earlier in the section, each propeller of the coaxial rotors would have a different span length, thus each propeller would be sized separately.

The first decision that was made regarding the propellers was to have a two-blade propeller. This is because the propellers with two blades generate less drag, improving their efficiency [6]. Also, the two-bladed propellers require less material, which saves on weight and manufacturing cost. Furthermore, two-bladed propellers are more compact and easier to store compared to multi-bladed propellers, which require more space due to their extended blade arrangement.

Based on the database of MadComponents and Hobbywing, a comparison was done to select a propeller. This was done based on the essential thrust requirement and the size requirement, as the propellers would require a large area. The coaxial rotors are expected to operate around 50% of their maximum thrust. This assumption is made to include the safety factor. This percentage was obtained by comparing the propeller's maximum thrust to its operational thrust, which is around 50% [7, 8].

From the database, the propellers that provided the required thrust and had the smallest area were chosen. Based on this selection, two propeller options remained. These two propeller designs that were chosen are the Hobbywing P50M 64x20" and 54x23", which could be seen in Figure 3.2 and 3.3 [8]. The propeller with the larger span is attached above the motor, whereas the 54" counterpart will be placed beneath it.

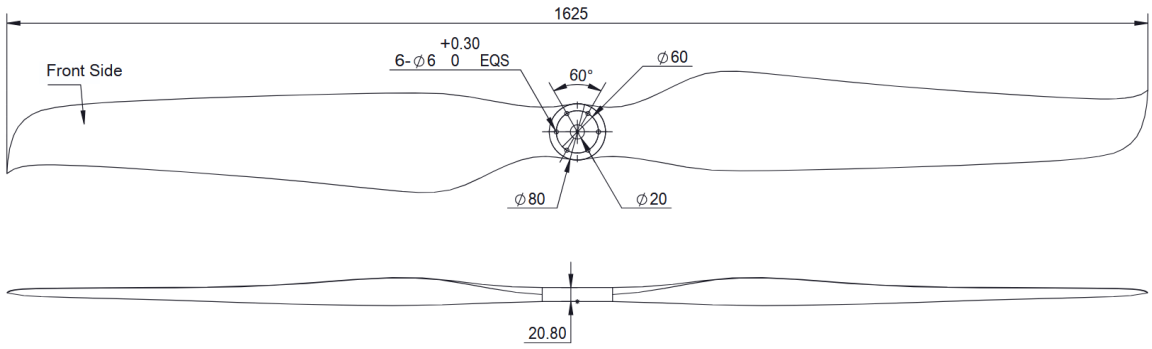

Figure 3.2: CAD drawing of the P50M 64"x20" propeller design, including the dimension in [mm] [8].

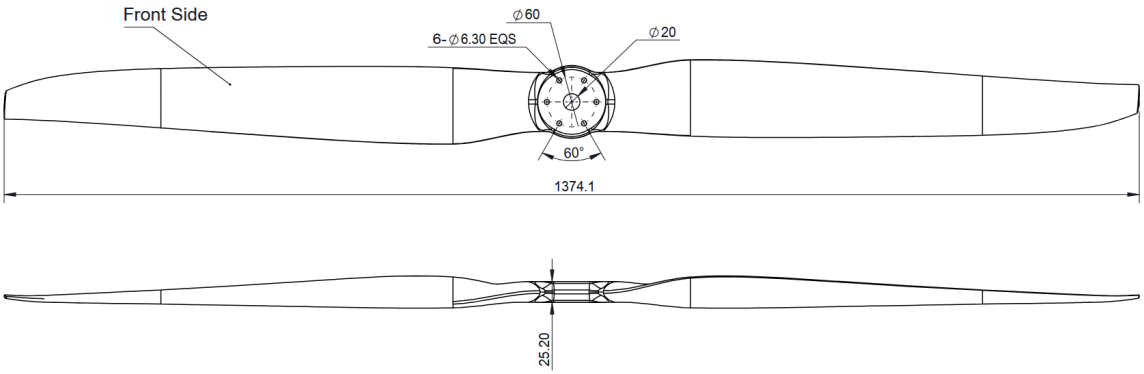

Figure 3.3: CAD drawing of the P50M 54"x23" propeller design, including the dimension in [mm] [8].

Based on the chosen propellers, the chord and twist distribution could be found. This could be found in Figure 3.4. The airfoil, however, is not known; therefore, an airfoil had to be selected to achieve similar results. For the airfoil selection, it is important to note that, as long as the airfoil selected has a reasonable drag polar, it does not have a huge effect on the performance of the propeller, as optimising the twist would have a larger effect [9]. Thus the airfoil selection is done based on the commonly used airfoil, which are NACA 4412 and Clark-Y airfoils [10]. To find the optimal airfoil, the drag polar, which is the lift coefficient divided by the drag coefficient of these two airfoils, was compared. This was done by first finding the Reynolds number and airspeed of the propeller. Along the span of the propeller, different airspeed is observed on each cross-section; thus, it was determined to look at 75% of the

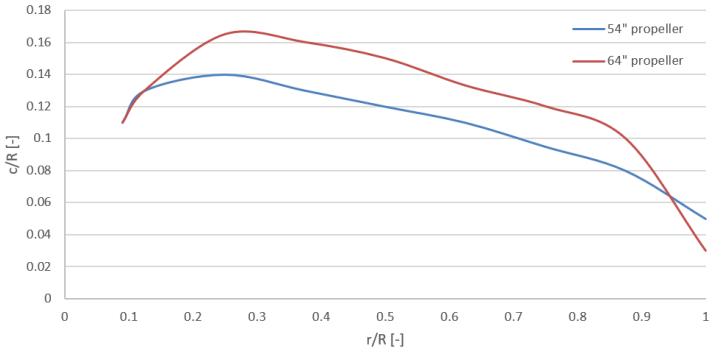

Figure 3.4: Chord distribution of the chosen propellers.

blade span, as this position is usually used as a representative reference point [11]. Looking at both the 54" and 64" propellers, which would be rotating at around 2600 and 2200 $[rpm]$ respectively. This would result in approximately a Reynolds number of 400000 and an airspeed of approximately 70 $[m/s]$ [12]. Based on this, the drag polar was computed, which could be seen in Figure 3.5.

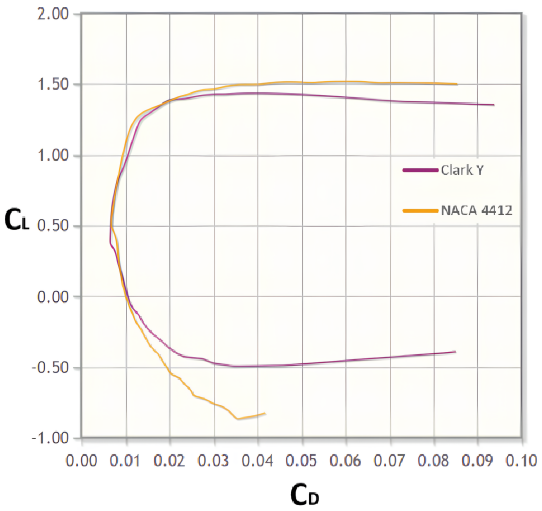

Figure 3.5: The drag polar of Clark Y and NACA 4412 airfoils [13].

Based on Figure 3.5, it could be seen that the NACA 4412 has a higher lift to drag ratio and also has a higher maximum lift coefficient. For that reason this airfoil was chosen for both propellers.

Since the airfoil used in both Hobbywings propellers is similar to the NACA 4412 airfoil, and because the performance of the propellers is mainly dependant on the twist and chord of the blade, which is also similar to the existing propellers, an assumption could be made that the performance is going to be similar [8].

Finally, after the propeller design, the serration at the end of the trailing edge was applied. A serration along the entirety of the propeller span has been avoided to reduce the manufacturing cost. Thus, a decision has been made to cover only 50% of the ends of both propellers with the serration. This decision has been made because the main thrust of the propellers is produced around 75% of its radius with respect to the root. Thus, at 75%, the main loading noise would be generated, and the serration would be applied for 25% of each side of that point. This could be seen in Figure 3.6, where the serrated part is indicated by red. This would ensure a noise reduction of the main noise source.

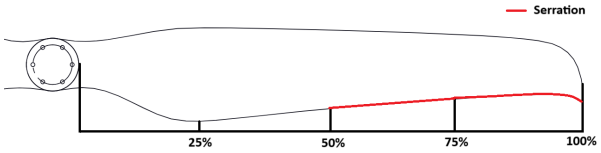

Figure 3.6: CAD drawing of the propellers with the serration location.

For the serration, a sawtooth configuration has been used. The associated dimensions are indicated in Figure 3.7, where λ indicates the serration wavelength and $2h$ indicates the serration height. Where the ratio $\lambda = 2h$, as this is the optimal ratio as it ensures approximately a noise reduction of 7 [dB], compared to a non-serrated surface [14]. The serration would be applied along the second half of the trailing edge of the propeller. The serration would be applied with $\lambda = 0.1d$, assuming d is the total serration distance, which is indicated in Figure 3.6 [15]. The serration distance is 343.75 [mm], which is calculated from the propeller's dimensions. This would result $\lambda = 34.4$ [mm].

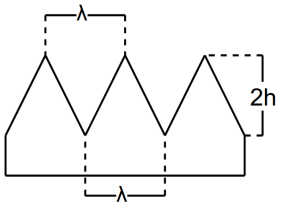

Figure 3.7: The sawtooth serration dimensions.

Finally, to ensure the two coaxial rotors' tip vortices do not interact, a clearance has been added. This results in a more efficient system and noise reduction. The minimum clearance that must be maintained is 20% of the propeller radius, ensuring no vortex interactions occur between both rotors [16].

Propeller Material selection

The material selected for the propellers is carbon fibre reinforced polymers. Even though the material cost is higher, it has a very light weight compared to aluminium and stainless steel, which complies with the strict weight requirement. It also performs quite well with respect to durability, as it does not significantly degrade under sunlight (UV) radiation. They also provide great corrosion resistance, increasing the reliability of the system [17].

Since the same material will be used for the propellers as the reference propellers, and because the geometry of the propellers used is also similar, the weight of the propellers could be found. The weight of the 64" and 54" propellers is 860 and 707 [g] respectively [8].

Motor Selection

Two motors would be powering each coaxial rotor. The motor would be required to produce at least 100 [kg] of maximum thrust, as the motor would be operating between 40-50% of its maximum output. This is done to ensure a reliable and safe system and also to prolong its lifespan. For the motor design, a brushless motor would be selected over a brushed motor. Although brushed motors are cheaper, brushless motors have higher efficiency, longer lifespan and require less maintenance. To compare the motors for the selection, the rotation per voltage of different motors would be compared, which is indicated as KV. A few motors that are capable of providing sufficient power were selected from the Hobbywing and Madcomponent databases, which could be found in Table 3.2 [8, 7].

Table 3.2: Motor selection for the coaxial rotors[7, 8].

Motor	KV	Motor Weight [kg]
M90C60 [7]	9.9	12.7
M60C60 [7]	8.5	9.20
M60C50 [7]	9.5	7.50
P50M [8]	11	4.25

Comparing the KV value of different motors, the P50M motor has the highest value, meaning it has a higher efficiency. Also, it has the lowest weight compared to other motors. With that, the P50M motor is selected, which would be used for the coaxial rotors. This would be done by installing two P50M motors, for each coaxial rotor, where each motor would be powering one of the propellers on each of the coaxial rotors.

3.3. Noise Mitigation

The vehicle will operate in urban environments, requiring strict noise compliance to minimise disturbance and ensure sustainability. The primary noise source is the propulsion system, which consists of four subsystems: two cyclorotors and two coaxial rotors.

The noise the cyclorotros generate is computed using the results of the noise test performed by Cyclotech. This test was done by operating the cyclorotors at their maximum performance and measuring the noise at 100 [m] distance. Converting the results to 20 [m], which is the cruising altitude, results in 66 [dB] [1, 18].

The noise levels of the cyclorotors were estimated using test data from Cyclotech. During testing, the cyclorotors were run at maximum performance, with noise measurements taken at 100 [m] distance. Converting these results to the vehicle's cruising altitude of 20 [m] results in a noise level of 66 [dB] [1, 18].

Estimating noise generated by coaxial rotors presents significant challenges. To address this, the analysis first computes the noise of a single propeller and then extends the results to the coaxial configuration. After that, design decisions are incorporated into the noise estimation.

To estimate the single rotor noise, Hanson's Model was implemented. This model calculates both tonal noise (from blade passing frequencies) and broadband noise (from turbulent flow) based on propeller geometry, operational parameters, and observer position. The model required inputs including propeller dimensions, flight conditions, aerodynamic coefficients, and measurement distance. This would provide a maximum sound pressure level of 70 [dB] for the single rotor configuration [19, 20].

While both the single-layered and coaxial rotors operate at the same fundamental blade passage frequency, the coaxial rotors produce a 10 [dB] higher sound pressure level (SPL) compared to single rotors. This increase results from aerodynamic interactions between the counter-rotating propeller pairs [21].

Implementing different-sized propellers reduces the blade vortex interaction, resulting in a SPL reduction of 6 [dB] [22]. Additionally, using corotational upper and lower rotors instead of contrarotational ones provides a 4.5 [dB] noise reduction [3]. Finally, applying serration to the blades results in an additional SPL reduction of 7 [dB], as mentioned in the previous section. An overview of the impact of these design decisions on the noise of the coaxial rotors could be found in Table 3.3.

Table 3.3: The impact of the design decision on the overall noise of the coaxial rotors.

Design decision	Effect on noise
Coaxial rotors	+ 10 [dB]
Different sized propellers	- 6.0 [dB]
Corotational	- 4.5 [dB]
Serration	- 7.0 [dB]

Based on the above effects, the maximum noise generated by a single coaxial rotor is approximately 63 [dB] at 20 meters distance. However, the vehicle contains four noise sources, two coaxial and two cyclorotors. Accounting for the noise interaction of these four sources results in 71 [dB] at 20 meters distance [23]. Based on this value, it can be concluded that the vehicle is able to comply with the noise requirement.

Yearly, 1,000 vehicles are produced, meaning approximately 10,000 will be produced in the first decade. This would result in a considerable number of vehicles flying in the same city at the same time, resulting in noise interaction, increasing the noise observed by people on the ground. To estimate the maximum noise observed on ground, it is assumed that all the 10000 vehicles are flying at the same time with a maximum distance of 30 meters between them and at a 20-meter altitude. It is also assumed that the noise of the vehicle would be omnidirectional. Based on this, the maximum noise observed would be 82 [dB]. However, having 10,000 vehicles flying simultaneously in one city is an overestimation. In reality, far fewer vehicles are expected to occupy such compact airspace simultaneously, meaning that the real noise levels would be lower and the estimation is conservative.

To reduce this noise, three main mitigation strategies could be considered. Firstly, reducing the number of vehicles that are flying simultaneously. However, this would be difficult to manage, as the pilots have no restrictions on flight within designated flying zones. Besides, reducing the number of vehicles that are operating at the same time from 10000 to 1000, would result in noise reduction of approximately 1 [dB], as could be seen in Figure 3.8a. This proves that the number of vehicles does not have a huge effect on the noise reduction.

Secondly, increasing the flight altitude. By increasing the altitude from 20 to 80 meters, a noise reduction of 2.5 [dB] could be achieved as could be seen in Figure 3.8c.

The third method is by increasing the minimum distance between the vehicles. By slightly increasing the separation distance, a noticeable noise reduction could be achieved. Decreasing the distance from 10 to 60 meters results in a 12 [dB] of noise reduction, as can be seen in Figure 3.8b. This also enhances safety by ensuring a greater clearance distance.

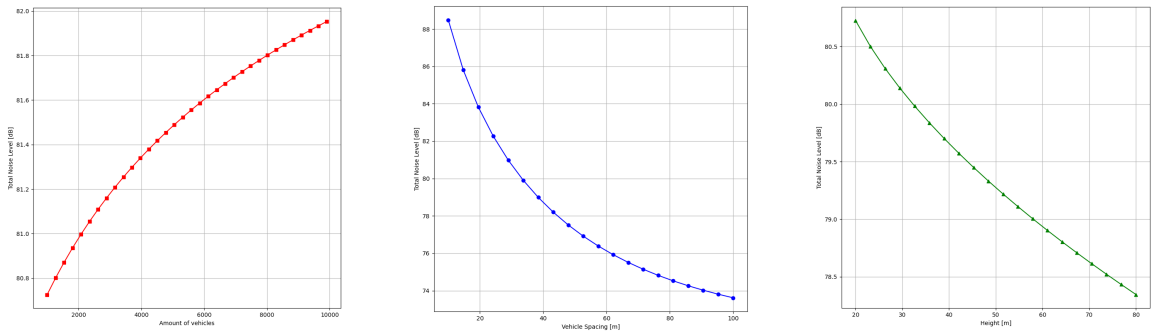

(a) The impact of the number of vehicles flying simultaneously on the total noise.

(b) The impact of the vehicle's distance on the total noise.

(c) The impact of the flight altitude on the noise.

Figure 3.8: The impact of different considerations on the total noise.

3.4. Aerodynamic Analysis

Aerodynamic analysis allows for the estimation of the forces, pressures, turbulence, and other characteristics crucial for understanding the propulsion system and its influence on the surrounding environment. CFD simulations were then run to simulate the two propulsion system types as well. Due to the element number limit imposed by the Ansys software, together with being computationally expensive, the propulsion system and the structure were simulated separately. The validity of this approach is evaluated later in this section once the characteristics of the flow around the propulsion system types are known.

In this section, the simulation set up is first discussed in Subsection 3.4.1. Then, the numerical model and the solver algorithm are presented in Subsection 3.4.2. After these steps, the analyses for the cyclorotors and the coaxial rotors are presented in Subsection 3.4.3 and Subsection 3.4.4 respectively.

Later in Chapter 8, similar analysis was performed for the structure, where characteristics like $C_{L_{fuselage}}$ and $C_{D_{fuselage}}$ were determined for both the preliminary and the updated structure.

3.4.1. Simulation Preparation

The simulation is carried out using the Ansys Workbench. This is a commercial software developed by Ansys, Inc.; however, it offers free student access. For the purposes of this project, the tools integrated into Ansys Workbench are considered to already be verified and validated [24]. The process starts with simply importing the 3D model of the studied part. After this, an enclosure with an inlet and outlet is created around the body, which represents the surrounding air. After this step, the body surface and the enclosure need to be discretised, in order to allow for the computational method to be used. This can be done in many ways; nevertheless, in this case, a fine mesh was used on the aircraft surface in order to capture its complex shape. Meanwhile, a coarser mesh was used to discretise the enclosure. Buffer layers were set up between these two entities to improve the smoothness of the transition from one to the other. An unstructured mesh consisting of tetrahedra was used for the discretisation, since it allows for the capture of complex shapes while retaining relatively high-quality elements. Overall, the mesh element size was refined to approach the 10^6 element limit of the Ansys student license.

The first propulsion system type to be analysed was the cyclorotor. In order to analyse moving parts like a propulsion system, relative movement needs to be imposed on parts of the mesh. Thus, multiple enclosures were created, one of which represented the stationary air domain, and the other(s) representing the immediate vicinity of the rotating object. There was a significant limitation in terms of the ability to realistically simulate the cyclorotor. This is because a model with 6 moving meshes would be necessary, as there is the general rotation of the cyclorotor, but within the rotating reference frame, each airfoil is rotating at a different angular velocity, which is also changing continuously. This would firstly be computationally expensive to simulate and secondly, it would presumably require an extremely high-quality, fine mesh to decrease the risk of divergence. In conclusion, it was decided to study the cyclorotor without the airfoils being deflected, which should still provide a reasonably accurate estimate of its parasitic drag.

3.4.2. Numerical Model

Fluid flow is described by the Navier-Stokes equations. These consist of the continuity equation describing conservation of mass and 3 momentum equations describing conservation of momentum in 3D. An incompressible case is considered due to flight at low Mach numbers. The equations are outlined below [25]:

$$\frac{\partial u}{\partial x}+\frac{\partial v}{\partial y}+\frac{\partial w}{\partial z}=0 \tag{3.1}$$

$$u\frac{\partial u}{\partial x}+v\frac{\partial u}{\partial y}+w\frac{\partial u}{\partial z}=-\frac{1}{\rho}\frac{\partial p}{\partial x}+\nu\left(\frac{\partial^2 u}{\partial x^2}+\frac{\partial^2 u}{\partial y^2}+\frac{\partial^2 u}{\partial z^2}\right)+f \tag{3.2}$$

$$u\frac{\partial v}{\partial x}+v\frac{\partial v}{\partial y}+w\frac{\partial v}{\partial z}=-\frac{1}{\rho}\frac{\partial p}{\partial y}+\nu\left(\frac{\partial^2 v}{\partial x^2}+\frac{\partial^2 v}{\partial y^2}+\frac{\partial^2 v}{\partial z^2}\right)+g \tag{3.3}$$

$$u\frac{\partial w}{\partial x}+v\frac{\partial w}{\partial y}+w\frac{\partial w}{\partial z}=-\frac{1}{\rho}\frac{\partial p}{\partial z}+\nu\left(\frac{\partial^2 w}{\partial x^2}+\frac{\partial^2 w}{\partial y^2}+\frac{\partial^2 w}{\partial z^2}\right)+h \tag{3.4}$$

Here, $\frac{\partial u}{\partial x}$ is the spatial derivative of the u-component of the local flow velocity with respect to displacement in x. A similar relation applies to the other partial derivatives. In addition, ρ is the fluid density and p is the static pressure. Lastly, f, g, and h are the body forces ρg_x, ρg_x, and ρg_x respectively.

In practice, direct numerical simulation is extremely computationally expensive. Thus, models utilising assumptions and simplifications are usually implemented. In this case, it was decided to use Reynolds-averaged Navier-Stokes equations. This model uses Reynolds decomposition to convert the velocity of the flow into a mean term and a fluctuating term.

$$u_i = \bar{u_i} + u_i' \tag{3.5}$$

The RANS equation itself will be written in Einstein notation for the sake of brevity. In this notation, multiplication between a variable and a spatial derivative with certain subscripts is used to express summation. An example is provided below.

$$\bar{u_j}\frac{\partial \bar{u}}{\partial x_j} = \bar{u}\frac{\partial \bar{u}}{\partial x} + \bar{v}\frac{\partial \bar{u}}{\partial y} + \bar{w}\frac{\partial \bar{u}}{\partial z}$$

The full RANS equation is as follows [26]:

$$\bar{u_j}\frac{\partial \bar{u_i}}{\partial x_j} = \rho\bar{f_i} + \frac{\partial}{\partial x_j}\left[-\bar{p}\delta_{ij} + \mu\left(\frac{\partial \bar{u_i}}{\partial x_j} + \frac{\partial \bar{u_j}}{\partial x_i}\right) - \rho\overline{u_i' u_j'}\right] \tag{3.6}$$

Familiar variables appear here, except for dynamic viscosity, which follows $\mu = \nu * \rho$. The last term ($-\rho\overline{u_i' u_j'}$) is the so-called Reynolds stress. Further equations need to be introduced in order to close the system of equations. For this purpose, the $K - \epsilon$ turbulence model, together with the Boussinesq eddy viscosity hypothesis, is applied. The Boussinesq hypothesis states the following [27]:

$$-\rho\overline{u_i' u_j'} = \mu_t\left(\frac{\partial \bar{u_i}}{\partial x_j} + \frac{\partial \bar{u_j}}{\partial x_i}\right) - \frac{2}{3}\delta_{ij}k \tag{3.7}$$

In this case, μ_t is the eddy viscosity and k is the turbulent kinetic energy. They can be obtained with the following expressions [28, 27]:

$$\mu_t = \rho C_\mu \frac{k^2}{\epsilon} \tag{3.8}$$

$$k = \frac{1}{2}\overline{u_i' u_j'} \tag{3.9}$$

In this case, C_μ is a constant with a typical, empirically obtained value of 0.09. The $k - \epsilon$ turbulence model by Launder and Spalding is then used to obtain expressions for the transfer of k and ϵ[28].

$$\frac{\partial(\rho k u_i)}{\partial x_i} = \frac{\partial}{\partial x_j}\left[\left(\mu + \frac{\mu_t}{\sigma_k}\right)\frac{\partial k}{\partial x_j}\right] + 2\mu_t E_{ij}E_{ij} - \rho\epsilon \tag{3.10}$$

$$\frac{\partial(\rho \epsilon u_i)}{\partial x_i} = \frac{\partial}{\partial x_j}\left[\left(\mu + \frac{\mu_t}{\sigma_\epsilon}\right)\frac{\partial \epsilon}{\partial x_j}\right] + C_{1\epsilon}\frac{\epsilon}{k}2\mu_t E_{ij}E_{ij} - C_{2\epsilon}\rho\frac{\epsilon^2}{k} \tag{3.11}$$

Similarly to the previous case of C_μ, σ_k, σ_ϵ, $C_{1\epsilon}$, and $C_{2\epsilon}$ are constants.

With the model equations set up, a 3D finite volume method (FVM) is used to numerically solve the PDEs at all the nodes created by the mesh that was generated during the setup of the simulation. The FVM essentially uses neighbouring cells or boundary conditions to calculate the derivatives and values at inner nodes of the mesh [29]. Unfortunately, the mathematical expression for the 3D case and its derivation are too long to include in a report like this, where the numerical method is not the main focus.

The SIMPLE algorithm is utilised for the calculation of the equation terms themselves. First, boundary conditions are set. This is a crucial step with a significant effect on simulation convergence. In this simulation, Dirichlet boundary conditions were used for all boundaries, meaning a variable had a fixed value on the boundary. Firstly, the inlet into the test enclosure had a fixed inlet velocity of 17 [m/s]. Secondly, a no-slip condition was imposed on the walls of the enclosure, meaning that the velocity was zero immediately on the surface. Lastly, a fixed pressure condition was set on the outlet of the

enclosure. Next, as previously mentioned, the solver computes the gradients of velocity and pressure on the individual nodes, using the FVM. Next, the momentum equations are solved and the intermediate velocity field is computed. Then, the uncorrected mass fluxes are computed at the faces. The pressure correction is then calculated and under-relaxation is applied for more conservative correction, in order to not make the simulation unstable. Then, the boundary pressure corrections are applied and the mass fluxes on the faces are corrected. The gradient of the pressure corrections is then used to correct cell velocities. This process is iterated multiple hundreds of times over the whole mesh and the convergence of desired characteristics like drag or lift, together with the ”residuals”, is monitored. The residuals are a useful tool to observe the amount of correction being applied between iterations and should decrease and stabilise as the simulation progresses. Once the simulation converges, efforts shift to post-processing.

3.4.3. Cyclorotor Aerodynamic Analysis

The drag coefficient obtained for the cyclorotor from the simulation was $C_{D_{cyclo}} = 0.022$. Meanwhile, lift is also created by spinning the cyclorotor at 1700 [rpm] without any angle of attack on the airfoils, purely by accelerating air over its top. This was found to be equal to $C_{L_{cyclo}} = 0.027$. The flow over the symmetry plane of the cyclorotor is visualised in Figure 3.9.

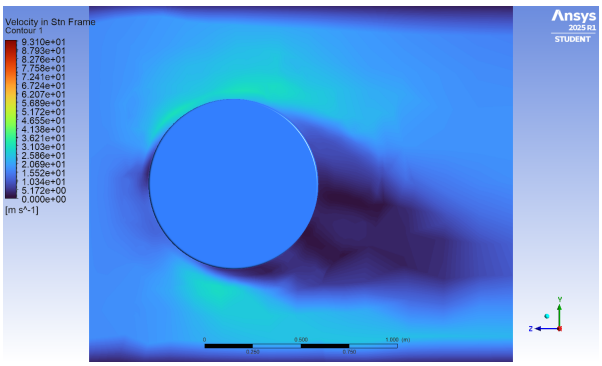

Figure 3.9: Airflow over the symmetry plane of the cyclorotor when in forward flight (positive z-direction) at 17 [m/s] airspeed.

In this figure, the cyclorotor is rotating clockwise. It can be observed that the flow accelerates on both the top and bottom sides of the cyclorotor. However, due to the rotation, the top part accelerates the flow more. This results in the top having lower static pressure and thus exerting a lift force.

Having examined the flow around the cyclorotor, its effects on the rest of the aircraft were evaluated. It had been assumed that the rotor could be analysed separately. This is still considered a reasonable assumption, as the cyclorotor draws the vast majority of the air from the clean flow in front, not from the side where the structure interferes with it. This is illustrated in Figure 3.10.

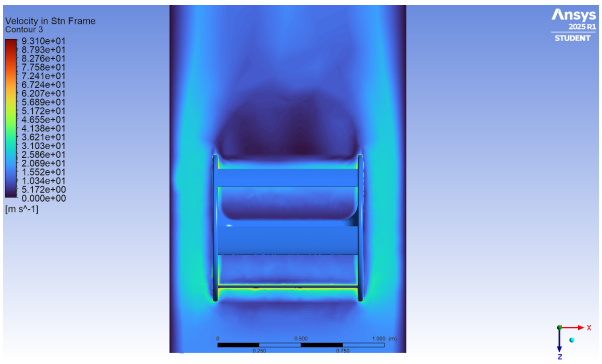

Figure 3.10: Top view of the velocity field around the cyclorotor when in forward flight (positive z-direction) at 17 [m/s] airspeed.

It can be seen that while the air passes around the cyclorotor on the structure side, its performance will not be affected, since it is far forward and draws air in front of it, not from the side. The air that is passing around it will now need to be divided and pass over the top and bottom, which could cause minor extra drag. Nevertheless, this effect is omitted from the analysis.

Another characteristic of the cyclorotor that should be examined is the wake. The wake was found to be straight in the longitudinal direction (z-axis), which is not expected to change significantly when mounted onto the structure. Furthermore, the wake is angled down by approximately 30 degrees. This is desirable behaviour, as it suggests that the wake of the cyclorotor will not interfere with the functioning of the rear coaxial rotors. It has also been confirmed by other research that this angle will further increase when the cyclorotor operates as it normally would [30].

3.4.4. Coaxial Rotors Aerodynamic Analysis

Lastly, the properties of the coaxial rotors will be examined. A higher-fidelity analysis can be performed than in the case of the cyclorotor, as there is inherently only one rotating frame, which can be accurately modelled. The propulsion system was isolated such that the two corotating rotors were simulated with the mount in between, since it likely has some effect on the efficiency and thrust of the overall coaxial rotor.

The simulation determined that the coaxial rotors will add approximately $C_{D_{coaxial}} = 0.007$ to the overall configuration. This value is rather low but reasonable, since the rotors are analogous to a thin, circular plate, which would have negligible pressure drag [31]. A visualisation of the flow around the coaxial rotors is presented in Figure 3.11.

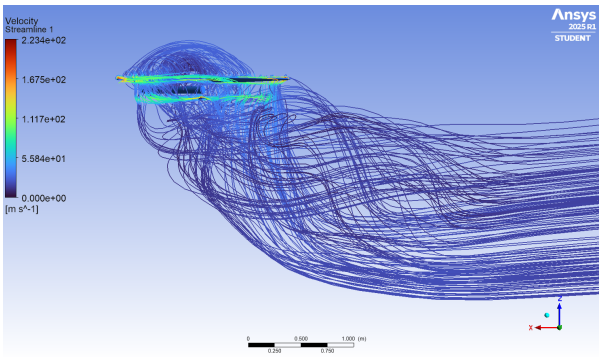

Figure 3.11: Visualisation of the airflow through the coaxial rotors when in forward flight (positive x-direction) at 17 $[m/s]$ airspeed.

The coaxial rotors are at the very rear of the aircraft. In previous analysis, it was not identified that the fuselage or the cyclorotors would significantly affect the flow in that location, meaning that the assumption that the components can be analysed separately is considered valid.

3.5. Maintainability, Safety, and Reliability

The propulsion system is a critical component of the vehicle, requiring continuous maintenance to prevent potential failures. Ensuring its safety and reliability is essential for long-term operation. This section evaluates the system's operational robustness, focusing on maintenance strategies, redundancy measures, and safety considerations.

3.5.1. Maintainability

The maintainability of the system is crucial, as it ensures the system is fulfilling the safety and reliability requirements. To simplify and decrease the cost and time of the maintainability and inspection process, the entirety of the propulsion system is positioned outside the structure of the vehicle. This is done to improve the accessibility for inspection and maintenance, as the full system does not require disassembly.

Furthermore, to reduce the maintainability cost, the subsystems of the propulsion system could be inspected and maintained separately. As for the coaxial rotors, propellers and motors could be inspected separately and could be replaced independently, as this also does not require disassembly of the entire system.

3.5.2. Safety

The propulsion system is a crucial part of the vehicle, which should comply with the safety requirements. To account for the safety requirement, the propulsion system would be able to provide sufficient thrust even when one of its components fails. This is done by having each subsystem operate at around 50-60% of its maximum output.

The propulsion system incorporates fail-safe measures to mitigate risks from component failures. For the cyclorotors, the rotational plane ensures that any ejected parts will be emitted outward away from the vehicle structure due to their rotational axis orientation. In the coaxial rotor assembly, the upper propeller's rotational plane is offset from the main airframe, ensuring no ejected parts would be emitted toward the main airframe. While the lower propeller rotates parallel to the airframe, a clearance gap is maintained between the propeller's blade and main airframe structure. This design redundancy prevents certain failure scenarios, enhancing system safety.

3.5.3. Reliability

To account for a reliable system, a few decisions have been made. The use of a brushless motor has been chosen, which has a higher reliability and durability than brushed motors. Also, the material used for the propellers is carbon fibre reinforced polymers, which ensures the propellers are more fatigue and erosion resistant [17].

Also, the propulsion system would be operating at approximately half of its maximum output limit. The cyclorotors operate at 60% of their maximum capacity. The motors and propellers are operating around 50-60% of their capacity. This would increase the reliability and lifespan of the system.

3.6. Future Recommendation

Implementing serrations on the cyclorotor blades could significantly enhance performance by reducing turbulence during rotation. This modification would improve efficiency and decrease noise levels. However, since adding serrations may increase production and testing costs, this remains a consideration for future development.

The performance of coaxial rotors largely depends on propeller design, particularly the chord and twist distribution. Optimising these parameters could lead to substantial improvements in aerodynamic efficiency. However, this process would require extensive computational analysis and testing, making it a longer-term goal.

Additionally, refining the serration design, such as using iron-shaped, ogee, or sinusoidal type serration, could further reduce noise. While these advanced serrations offer acoustic benefits, their complex shapes may pose manufacturing challenges. Future development in manufacturing techniques could make these designs more feasible.

4 Power

This chapter presents the design of the power system. It begins with the selection of the battery type, followed by the development of a battery management system, including thermal management and cell balancing strategies. The chapter then outlines the architecture of the power distribution network, detailing how the electrical energy is managed and routed to various subsystems. The maintainability, safety, and reliability of the entire design are highlighted, after which the chapter concludes with a summary of key design decisions.

4.1. Power System Requirements

During the initial stages of the project, requirements were formulated for the entirety of the design process of the Owl-22. Below, in Table 8.1, all the requirements relevant to the power system can be seen.

Table 4.1: Updated structures relevant requirements.

ID	Description
REQ-SAF	The vehicle shall ensure occupant and bystander safety during all phases of operation with active and passive safety measures that prevent hazardous system failures and minimize injury risk.
REQ-FP-RAN	The vehicle shall have a minimum operational range of 20 [km] under standard urban flight conditions, based on a full fuel cycle, including take-off, cruise, and landing phases.
REQ-FP-VEL	The vehicle shall be capable of sustaining a cruise speed of at least 60 [km/h] in level flight under standard atmospheric conditions at cruise altitude.
REQ-OP-USE-01	The vehicle shall have a maximum refuel time of 30 [min].
REQ-SUS-BAT	The vehicle shall include an onboard battery system as part of its energy storage architecture by default.
REQ-SUS-BAT-01	The battery shall retain at least 80% of its original capacity after 1000 full charge-discharge cycles under standard operating conditions (ambient temperature 297.15–318.15 [K]).
REQ-SUS-BAT-02	The battery shall be rechargeable.
REQ-SUS-BAT-03	The battery shall support repeated charge-discharge cycles without replacement during the first 2 years of operation.

4.2. Battery Characteristics

Owl-22's energy source will consist of a solid-state lithium (SSB) battery. This decision was reached after performing a detailed trade-off that considered several non-battery energy sources and also different types of batteries. The main characteristics of a SSL battery are its very high energy density, good durability and excellent safety (low fire risk). Furthermore, it is important to note that the battery and battery performance assumed in the design of the Owl-22 are not currently commercially available, but rather are expected to be in approximately five years time; around the time the Owl-22 is expected to begin production.

A big design decision to make regarding the battery of the vehicle is whether it will carry any loading or not. Batteries are inherently delicate components and as such, without careful considerations, any force acting on them could critically damage them. The concept of a structural battery is defined by Jin et al. as follows: "an energy storage device that is able to bear structural loads and act as a replacement for

structural components such that the weight of the overall system is reduced" [32]. There are two main types of structural batteries: cell-level and material-level. The former consists of surrounding the cells in external reinforcements, while the latter consists of developing components that act as load carriers and valid battery components [32]. The second type of structural batteries are both very expensive and still a very novel area of research; therefore, if a structural battery were to be used, the Owl-22 would use of the first type.

Initially, it was believed that in order to minimise Owl-22's weight, and following from the design enabler: performance, a structural battery would be designed. However, although conceptually this is reasonable, in reality the improvement in performance from a structural battery was found to be minimal for the Owl-22. As the loads of the vehicle are not particularly large, the airframe does not require the battery to sustain any loads, and if it were to do so, the reduction in mass would be very small. On the other hand, making the battery structural carries with it many complications. Firstly, structural batteries are clearly more expensive than their non-structural counterparts. These costs are not only manufacturing or production costs, but also include maintenance and fatigue analysis costs. Overall, it was determined that for the Owl-22 the advantages proposed by a structural battery were not enough to make up for the complications it brought. As such, Owl-22 has a non-structural battery.

4.2.1. Battery Capacity

Before defining any of the battery characteristics, it is important to mention that the following calculations were performed under the assumption that the mass of the vehicle is 305 [kg] during flight. This consists of 200 [kg] of the vehicle itself with an addition of 105 [kg] from the pilot and belongings. It is possible that the mass budget that has been allocated to each system overestimates the true mass of said system. Therefore, it is possible that the empty vehicle will have a mass lower than 200 [kg]. To facilitate this, the battery sizing and energy capacity will be iterated on at the end of the design phase. The results of this iteration concerning the battery can be seen in Section 8.6.

The very first step in determining the dimensions and characteristics of the battery was to determine the required battery capacity for the Owl-22. This required an estimate of the maximum energy required for a trip using the Owl-22. The energy required for the lift devices was calculated, and then it was assumed that the energy used by them would be 80% of the energy used by the whole vehicle. Therefore, using specifications from Cyclotech and Equation 4.1, ideal power for rotors equation, the total energy needed for the lift devices in a maximum trip by the Owl-22 could be found to be 15.91 [kWh] for a trip of maximum range (30 [km]), with up to 4 minutes of hovering [33, 1].

$$P_{\text{ideal}} = T \cdot \sqrt{\frac{T}{2\rho A}} \tag{4.1}$$

The variables in Equation 4.1 are the following: T is thrust, ρ is the air density and A is the area of the circle covered by the rotors.

However, although this is the energy demand of the maximum trip, lithium batteries cannot fully charge and discharge without their battery health being damaged. As such, the battery of the Owl-22 will only operate within 10% and 90% of its total capacity; although it is recommended for current lithium batteries to stay within 20% and 80%, these values are expected to improve in the future [34]. Therefore, when applying the fact that the lift devices use 80% of the total energy of the vehicle and that the energy needed must be 80% of the full battery capacity, the energy capacity of the battery of the Owl-22 would be 22.91 [kWh].

4.2.2. Weight and Dimensions

Having determined the total capacity of the battery, its sizing and weighting can be conducted. Firstly, for the weight, an energy density of 450 [Wh/kg] can be expected from SSBs in 5 years [35]. As such, the mass of the cells in the battery can be calculated to be 50.9 [kg]. However, this mass does not include the casing of the battery, the thermal management, or the battery management systems. Assuming that the cells compose 77% of the total mass of the battery, the actual mass of the entire battery pack for the Owl-22 is 66.1 [kg] [36].

To derive pack volume, we adopt a volumetric energy density of approximately 900 [Wh/L], yielding an estimated volume of 25.5 [L], or about 0.0255 [m^3] [37]. Packaging this volume in a prismatic layout suggests a rough envelope on the order of 50 [cm]× 50 [cm] × 10 [cm]. Therefore, in conclusion, the battery pack of the Owl-22 has the following characteristics: capacity of 22.91 [kWh], a mass of 66.1 [kg] and a volume of 25.5 [L] (with dimensions 50 [cm] × 50 [cm]× 10 [cm]).

4.3. Battery Management System Overview

The battery pack of an electric vehicle consists of many cells that must run efficiently, be protected against fire and failure, and communicate and function together as a unit. To facilitate this, a Battery Management System (BMS) is used. The BMS is an electronic control unit that communicates with other electronic systems and exchanges battery data, while simultaneously monitoring and regulating the battery during charging-and discharging cycles [38].

The design of the BMS entails first selecting a system architecture, which establishes a framework for how the BMS is constructed and how the system communicates. Then the functionality of the BMS is established by detailing its state determination, thermal management and cell balancing techniques. Finally this section will be closed off by presenting the final system architecture.

4.3.1. BMS Architecture Type Selection

The optimal design for a BMS entails making the system compact and cost-effective. Most BMS architectures/topologies fall within three categories: centralised, distributed, and modular. The centralised BMS is a type of battery monitoring where all the measurement processing and control functions are executed in a single control unit. A modular BMS is a system architecture that divides the system into multiple modules that consist of a group of cells, with each module having its own control unit, the slave BMS. These control units are then managed by a master controller, the master BMS. Finally, a distributed BMS architecture is where each battery cell is connected to its own dedicated BMS Printed Circuit Board (PCB) that performs all the tasks of a control unit, but for the individual cell. Then each of the BMS PCBs are connected to a a main control unit by one communication network [39]. A visual representation of these BMS topologies can be seen in Figure 4.1.

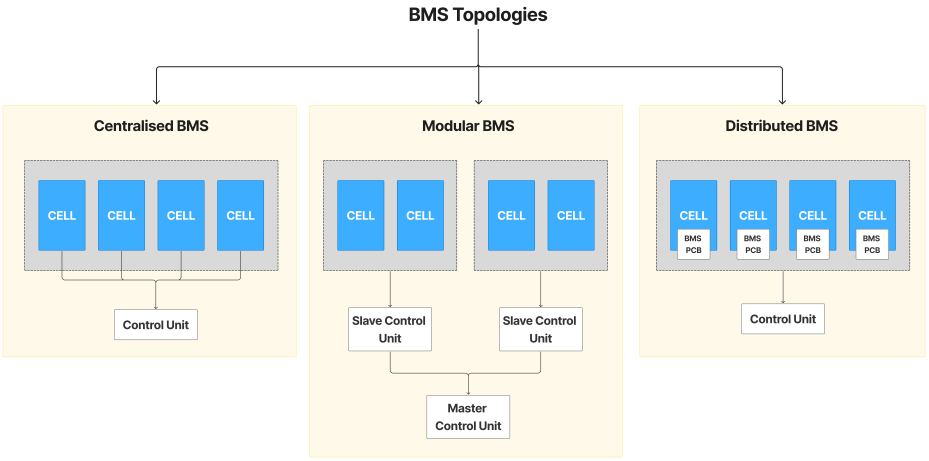

Figure 4.1: BMS topologies.

The ideal topology for an electric vehicle such as Owl-22 is the modular BMS, because it balances cost, scalability, and reliability better than the centralised and distributed BMS [40].

A modular BMS outperforms a centralised BMS in critical aspects such as redundancy, scalability, and ease of maintenance. Unlike centralised systems, where a single failure can disable the entire battery pack, modular designs can isolate failures while the remaining system can continue its operation [41]. After failure has occurred, maintenance procedures can be executed with ease since only affected modules must be replaced instead of an entire system renovation [40]. The architecture's modularity

also allows for scalability through the addition or removal of modules depending on its application [41].

Concurrently, the modular BMS also presents distinct advantages over fully distributed BMS designs. Modular BMS is more cost-effective since fewer components must be used as the modular topology groups cells and eliminates complex wiring. Thus, the modular architecture is the strategic middle ground between centralised and fully distributed systems, striking a balance between performance and cost [39].

4.3.2. Battery State Determination

Having selected a system architecture, the system functionality was allocated between master and slave units to optimise performance. This would distribute the key responsibilities of the BMS; state estimation, thermal management and cell balancing [42]. This section addresses the battery state determination techniques employed.

The state determination function of BMS includes determining the State of Health (SOH), State of Charge (SOC), State of Power (SOP), and State of Temperature (SOT). In order to establish these parameters and understand the performance of a battery, a battery model must be decided upon. Battery models translate complex models into interpretable mathematical expressions, which aids the designing, analysis and optimisation of battery algorithms [43]. In future design iterations, a suitable battery model must be selected for Owl-22's batteries, since the battery model selection process will not be conducted at this phase of the project.

Similarly, a thermal model must also be selected such that the model will allow for the system to understand and predict how heat is generated, distributed and dissipated during the different operational phases [44]. This modelling is especially vital since based on preliminary risk analyses, the thermal conditions of the battery pose a number of concerns on the safety and efficiency of Owl-22. As mentioned, the selection of the thermal model will not be conducted at this stage of the project; however, the general thermal management strategies will be discussed in the following section.

4.4. Thermal Management System

Delving deeper into the BMS, an integral part of maintaining the battery integrity is the incorporation of a Thermal Management System (TMS). SSBs, as mentioned in Section 4.2, have many advantages such as high power, high specific energy and higher durability; however, temperature can affect these attributes negatively [45]. Hence, the TMS must be designed to ensure the battery's safety, performance and longevity.

4.4.1. Heat Generation Within the Battery

Before analysing the thermal management techniques, it is necessary to analyse the sources of heat that affect the battery. Heat is generated within a SSB due to three main reasons: joule heating, charging and discharging cycles, and interfacial resistance.

Joule heating occurs due to the internal resistance of the battery, resulting in Ohmic losses [46]. In SSL batteries, the ionic conductivity of the solid electrolyte is usually lower than that of liquid electrolytes, which leads to greater ohmic heating [47]. Therefore, overheating is a risk that must be tackled through the design of the TMS. The charging and discharging cycles are another cause of heat generation within the battery. Due to the changes in Gibbs free energy during these cycles, not all the energy is transferred into useful electrical energy; some of it ends up being dissipated in the form of heat [47]. Finally, the last source of heat in the SSL battery would be the heat generated due to interfacial resistance. This occurs at the junctions between the solid electrolyte and electrodes, which is specific to SSL batteries since the solid electrolytes struggle to maintain close, continuous contact with the electrode materials [47].

Based on the sources of heat, an appropriate TMS design was curated. The TMS would consist of both passive and active forms to ensure a well-rounded management of heat within the battery system.

4.4.2. Passive Thermal Management

Passive thermal management techniques control temperature using natural heat transfer mechanisms without relying on external power sources [47]. A heat sink is a fundamental form of passive thermal management, where heat generated by electronic components is dissipated. Heat sinks are typically made from materials with high thermal conductivity and are constructed to maximise surface area through fins, or other design considerations that promote airflow through the battery system [47]. In order to amplify the system's performance, the use of a heat sink must be combined with another form of thermal management method, which is the use of Thermal Interference Materials (TIMs). TIMs are essential for improving the thermal contact between components and the heat sinks, as they fill microscopic air gaps and surface irregularities that can hinder efficient heat transfer. However, if the battery is subjected to thermal loading beyond the capacity of the sink or the TIMs, their effectiveness would diminish. Hence, other forms of thermal management were explored.

An alternate way to have passive thermal management would be through the use of Phase Change Materials (PCMs). PCMs are substances that absorb and release thermal energy during phase transitions such as melting and solidifying allowing for effective thermal regulation [48]. Although PCMs have a large effective functioning temperature range, its high weigh and volume characteristics caused the team to avoid its implementation in Owl-22 [48].

Therefore, to comply with battery weight constraints, alternative thermal management systems must be explored to optimise cooling performance relative to the system's weight and volume, namely active thermal management techniques.

4.4.3. Active Thermal Management

Active thermal management refers to use of external energy and mechanical systems to control the temperature of a battery system [47]. The most common TMS types are air based and liquid based TMS. In air-based TMS, fans and blowers are essential components for forced convection cooling. While passive airflow can cool the battery during light thermal loads, during times of higher ambient temperatures or heavier performance demand from the battery, passive airflow techniques could result in uneven temperature distribution or inadequate cooling [48]. Thus, fans are placed at the inlet or the outlet of the battery pack to actively drive air through the pack. This approach allows the TMS to remain lightweight and cost-effective. On the other hand, considering the ambient temperatures in the UAE, the air based cooling systems alone may not be sufficient for the batteries.

On the other hand, liquid based TMS use liquid coolants that circulate in the battery pack to regulate temperatures. For an electric vehicle such as Owl-22, the liquid based TMS in question would make use of an indirect heat exchange. In the indirect heat exchange system, the battery cells would not be in direct contact with coolant, instead they would use intermediate structures such as cooling plates, to transfer heat away from the battery. This configuration isolates the coolant from electrical components, it allows for better heat exchange and more uniformity, but it comes at the risk of higher cost and weight.

Given the lack of certainty surrounding the exact battery structure, namely the number of cells and modules present in the battery pack, the exact type of active thermal management employed cannot be finalised.

4.5. Cell Balancing

Another critical aspect of the BMS is battery cell balancing. This is essential because variations in manufacturing or cell usage can cause differences in cell voltage and SOC of the cell. Without effective balancing, some cells may overcharge while others remain undercharged, leading to reduced efficiency and possible damage to the battery pack [49].

There are two forms of cell balancing: passive and active cell balancing methods. Passive balancing involves releasing excess energy from higher-voltage cells as heat using resistors [42], whereas active balancing systems use additional circuitry to transfer energy between cells, redistributing charge from higher-voltage cells to lower-voltage cells. Active cell balancing techniques are often more energy efficient as it uses precise monitoring and modification of each cell. For an electrical vehicle such as Owl-22, it is imperative to prioritise safety while simultaneously ensuring energy efficiency [49]. Hence, both passive and active cell balancing methodologies will be utilised.

4.6. Final BMS Architecture

Having examined the core components of the BMS, namely the type of BMS in Section 4.3, the TMS in Section 4.4, and the cell balancing technique in Section 4.5; the final BMS architecture for Owl-22 was designed. This section will detail the implemented architecture, outlining the placement of the key components and their impact on the system's overall design. Figure 4.2 presents the final BMS architecture design.

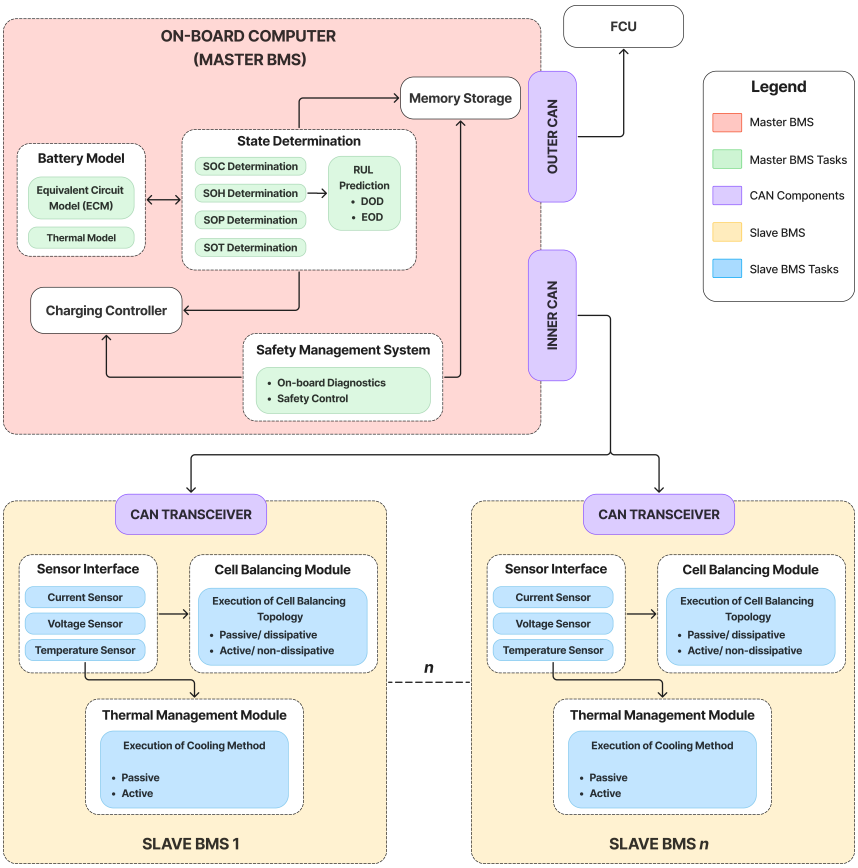

Figure 4.2: BMS architecture.

The modular BMS architecture presented in Figure 4.2, shows a Master-Slave configuration that features a centralised BMS, which in this case will be the On-Board Computer (OBC), and multiple Slave BMS modules to monitor and manage battery operations. The system utilises an inner Controller Area Network (CAN) connecting the Master BMS to the slave units, and an outer CAN that links the Master BMS to the Flight Control Unit (FCU).

The Master BMS executes the state determination, including Remaining Useful Life (RUL) prediction and manages Depth of Discharge (DOD)/ End of Discharge (EOD) thresholds. Additionally, the Master BMS handles charging protocols through the charging controller, implements safety measures via the On-Board Diagnostics (elaborated in Chapter 6), and stores necessary information regarding the battery health. The OBC was selected to perform the tasks of the master BMS, since the OBC will have the computational power to perform the necessary tasks of the Master BMS. This decision also allows for scalability since adding more battery modules will not overload the OBC, since the OBC's resources can be scaled with vehicle needs. Additionally, it is more cost and weight-effective because using the OBC as the Master BMS leverages the OBC's existing hardware rather than requiring a separate Master BMS unit.

The Slave BMS units perform real-time monitoring and balancing operations at the cell module level.

Each Slave BMS unit manages one cell module consisting of typically 6-12 cells [50]. Each Slave BMS will be designed to include necessary TMS and cell balancing technologies to ensure the safety and health of each battery module.

The system operates through a coordinated workflow where Slave BMS units transmit cell-level data to the Master BMS via the inner CAN. The Master BMS processes this information and relays the critical data to the FCU via an outer CAN interface. Such an architecture offers significant advantages, including scalability for larger battery packs, redundancy through distributed control, and precise monitoring at a cell level.

4.7. Electrical Block Diagram

A key aspect of the power system architecture is its design for efficient power distribution and integrated data communication across all major subsystems. A visual representation of the architecture is presented in Figure 4.3.

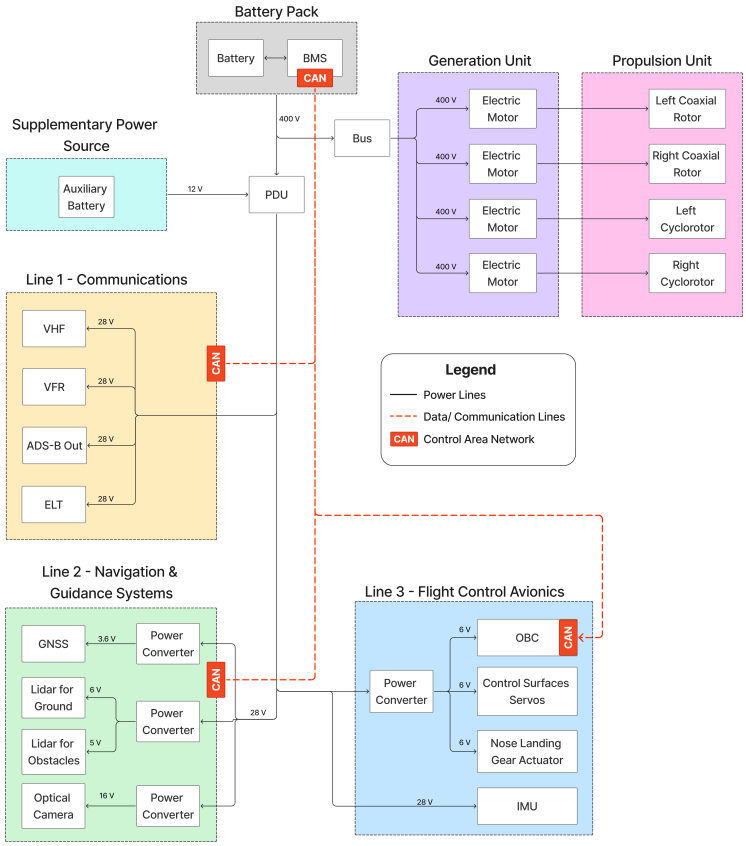

Figure 4.3: Electrical block diagram.

The architecture is centred around a high-voltage battery pack rated approximately 400 [V] [51]. The battery outputs 400 [V] to the Power Distribution Unit (PDU) and the propulsion generation unit. A supplementary 12 [V] auxiliary battery also provide voltage to the PDU to ensure backup power during startup or emergency conditions. The PDU then steps down the input voltage to 28 [V]. A power converter is used at locations where the power needs to be stepped up or stepped down, depending on the subsystem component needs. All the voltages for subsystem components in Figure 4.3 come from the component selections made in Chapter 3 and Chapter 5.

Furthermore, the electrical block diagram also illustrates the CAN bus for digital communication across key subsystems. CAN bus is responsible for connecting the OBC with the BMS, communications systems, navigation sensors and the flight control avionics. This allows for real-time data exchange

and health monitoring.

4.8. Maintainability, Safety, and Reliability

The Maintainability, Safety and Reliability (MSR) of the power system can be divided into three aspects; the MSR of the type of battery, the BMS, and the power system as a whole.

The use of SSB brings a number of advantages, in terms of MSR, to the vehicle. Due to the higher thermodynamic stability of a solid-state electrolyte than that of a liquid-state electrolyte, no violent chemical reaction can occur at high operational temperatures, guaranteeing a high level of safety [52]. The higher electrochemical stability of SSBs also ensures a more consistent performance of the battery over a longer lifespan, which reduces the need for constant maintenance.

The use of a modular BMS, as mentioned in Subsection 4.3.1, allows for damage isolation, increasing the safety of the battery pack. The modularity and the presence of an auxiliary battery also allow for redundancy in the case of modules failing, making the design more reliable.

The entire power system architecture provides additional safety since the high-voltage components are separated from the rest of the components, which prevents the low-voltage components from being exposed to dangerous voltages. The CAN bus allows for robust communication with error checking, increasing data reliability.

5 Avionics Suite

Avionics refer to all electronic systems used onboard an aircraft. This involves a complex, intertwined system of software and hardware. As such, this chapter will outline the main electronic components related to vehicle Navigation, Communication, Control and Data Handling. Within each of these functions, the relevant components will be chosen and then placed in a hardware diagram to highlight the connections between different parts of the suite. Moreover, a detailed explanation of the semi-autonomous system will be provided, followed by a high-level software diagram. Notably, the embedded systems architecture will be missing from this diagram, since this will be designed at a later stage. Lastly, a Data Handling diagram will also be presented to complete the overview of Owl-22's avionics.

5.1. Communications Suite

All aircraft communications are heavily regulated by aviation authorities, and the components required for a certified commu cations suite are well defined. For user-friendly, urban eVTOLs, the essential instruments typically include: a two-way very high frequency (VHF) radio for voice communications; an altitude-reporting transponder; an automatic dependent surveillance–broadcast (ADS-B) Out system for transmitting position data; an emergency locator transmitter (ELT) for broadcasting location in the event of an accident; and a set of basic visual flight rules (VFR) instruments for displaying key flight information.

Given the relative infancy of the current design, specific component selection for the suite is not particularly relevant. However, to help complete the electrical diagram presented in Figure 11.1, a VHF radio was selected to better estimate the required voltage and determine whether a step-down converter is necessary. Thus, the Garmin GTR-205 was selected due to its aerospace heritage, relatively low cost and dual channels for communication and navigation, respectively. Although not legally mandated, the Aircraft Communications Addressing and Reporting System (ACARS) will also be included to help ease the learning curve of aircraft communications for unfamiliar users. More specifically, the ACARS over Internet Protocol (AoIP) system will be used, which allows for communication via cellular connectivity. This drastically increases the amount of data that can be sent and received both to air traffic control (ATC) and the Owl-22 HQ.

Moreover, while most of the listed components are self-explanatory, the VFR instruments require further explanation. VFR refers to a mode of operation where the pilot can rely on visual references for navigation. Conversely, instrument flight rules (IFR) rely entirely on reading navigation instruments and communication with ATC to fly. In essence, IFR is only used for low-visibility conditions since it is significantly harder to follow. Since Owl-22 focuses on delivering a vehicle that requires little or no formal training to operate, it is essential that the vehicle is operable under VFR at all times. However, a pilot is still unable to perform all flight operations using vision alone. Thus, VFR instruments are required to be on board to allow the pilot to perform all nominal operations. In the case of an eVTOL, these are the following mandatory instruments and equipment: airspeed indicator, altimeter, (battery) temperature gauge, anti-collision lights (always) and navigation light (for night flights only), magnetic compass, and ELT.

Luckily, VFR compliance is quite easy to guarantee during the day. Since the operating altitude is 20 meters, the typical visibility threat posed by clouds is nullified. Regarding the instruments themselves, they can mostly be displayed digitally on the iPad by leveraging an electronic flight instrument system (EFIS). This also significantly simplifies the cockpit electronics. However, since the iPad itself is attached to the yoke, reading the display during a turn could be challenging. Of the aforementioned instruments, only the magnetic compass is required to be easily readable during turns, since it is actively used by the pilot to determine the correct heading if necessary. Of course, it should be mentioned that due to the ultra-low altitude of the vehicle, the pilot would mostly be navigating using a map software. However, the magnetic heading remains the navigation standard for all authorities, and so users must

be able to view this value at all times in cases of emergency. One point of consideration is stress-testing the iPad, since the scorching summer sun in the UAE could cause critical overheating issues. The results of such a test would then determine the need to include stand-alone, backup flight instruments. However, since it is not legally mandatory to include these redundancies, they will be assumed unnecessary for the time being.

Adhering to VFR at night is a more complex issue. To ensure visibility, Owl-22 would need to provide additional navigation lighting. Ideally, the relevant requirements would be quantified via the GCAA. However, since these are not yet fully outlined for Urban Air Mobility vehicles (UAMs), the FAA's clearer regulations are instead used as a reference. Lastly, the list below typically refers to a helicopter. This is because the FAA allows VTOLs that 'have demonstrated a capability to autorotate or conduct an approved equivalent manoeuvre' to follow the same VFR regulations as a helicopter [53]. Thus, the following regulations apply [53]:

- Flight visibility means the average forward horizontal distance, from the cockpit of an aircraft in flight, at which prominent lighted objects may be seen and identified by night.
- **14 CFR 91.155 - Basic VFR weather minimums** No person may operate a helicopter under VFR when the flight visibility is less than one statute mile
- **14 CFR 91.205** The aircraft must have position (navigation) lights and an anti-collision light system.

Clearly, some additional measures, such as the aforementioned light systems, have to be taken into account, whilst also considering the unique flight case of Owl-22. In particular, the 20-meter flight altitude is rather advantageous; it means that the light pollution, particularly from street lights, would make the city significantly more visible for the pilot. Despite Dubai being an exceptionally well-lit city, there are still substantially darker suburbs. To mitigate this, the Owl-22 team proposes a separate, night no-fly zone, which would be significantly more strict and be designed roughly along highways due to their higher levels of visibility. Another reason for this is Owl-22's proactive approach to the social implications of this vehicle. Currently, there are no procedures in place to detect inebriation, which would be a particular concern for night drivers. By having a stricter airspace at night, it becomes easier to regulate and design procedures to check for drunk driving and other reckless behaviour, thereby making it easier for law enforcement to regulate the use of this vehicle.

Regarding the lights themselves, the navigation and anti-collision lights are heavily regulated and must be placed in specific positions to help with visibility and indicate the direction of other aircraft relative to the pilot. These are indicated in Figure 5.1.

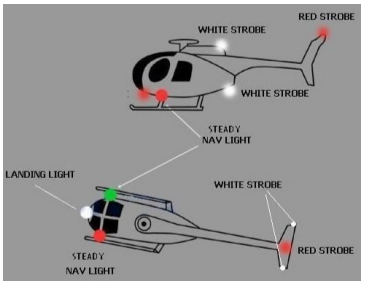

Figure 5.1: Regulated colour and position of VTOL lights.

5.2. Sensing and Navigation

To enable safe operations in urban environments, Owl-22 requires an integrated sensor architecture designed to tolerate potential failures. The risk analysis done in an early stage of the project identified that the failure of GNSS, IMU or LiDAR poses serious risks to operations. While MEMS sensors offer advantages in terms of cost, size, and weight, these must be integrated carefully to achieve the level of accuracy required for UAM applications [54]. This outline of the sensing architecture can be observed in Figure 5.2.

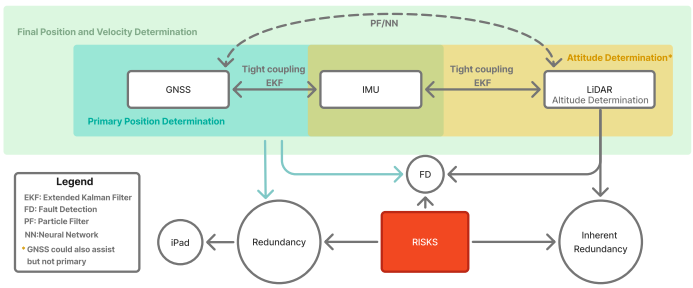

Figure 5.2: Owl-22 sensors architecture.

With the GNSS providing global positioning and IMU providing inertial measurements, the combination of these systems can provide a more accurate and robust system, which can operate in GNSS outages [55, 56]. It is an extensively studied subject, and for a further integration with LiDAR, the proper coupling of these two systems should be ensured first [57]. There are three coupling strategies: loosely, tightly and ultra or highly tight. For autonomous urban operations, a tightly coupled system using an extended Kalman filter offers the best trade-off between accuracy and complexity [54, 55, 58].

To ensure system integrity, especially in safety-critical applications, fault detection is essential. In line with diagnostic requirement **REQ-CON-DET**, Fault Detection and Exclusion (FDE) methods are recommended for the tightly coupled GNSS/IMU system and should be implemented in future development stages [54]. For Owl-22, the GNSS/IMU redundancy was chosen to be implemented through the tablet. Since the iPad would be connected to the yoke, its attitude measurements would need to be corrected for the yoke movements. It should be noted that LiDAR would need to come with an independent redundancy and fault detection, as it would be positioned alone.

5.2.1. LiDAR and Camera Positioning

LiDAR will serve multiple functions in the design of Owl-22, including real-time obstacle detection and precise altitude measurement. For this, it would need to be able to provide sufficient coverage to map out the surface around and below the vehicle. As an externally mounted sensor, it will have independent redundancy and fault detection. Flying at 20 $[m]$ with a 45$[^\circ]$ cone would necessitate a 360-degree LiDAR of a range of at least 30 $[m]$. This sensor would be connected to the rear bottom part of the vehicle, outside of the folding mechanism. Another 360 degree LiDAR sensor could then be connected to the top of the vehicle next to the connection with the canopy. An extra four LiDAR sensors would then be positioned around the four corners of the vehicle. These sensors would be long range, slanted slightly downwards to also act as redundancies for the altitude measurements, while providing long range obstacle detection in the oriented direction.

Finally, a camera will be pointed nadir for obstacle detection as well as landing assistance. However, due to its high computational cost relative to LiDAR, it will not serve as an active sensor. Instead, it will provide visual information to the pilot, such as runway markings, landing pad detection, and visual obstacle recognition.

5.2.2. Obstacle and NFZ Detection

To comply with **REQ-SAF** and **REQ-SAF-OBJ**, Owl-22 must avoid both obstacles and No-Fly Zones (NFZs). Obstacles may be static or dynamic, ranging from birds or pedestrians during emergency landings to other aerial vehicles as urban airspace becomes more congested. While NFZs are typically static, they can become dynamic in situations such as terrorist threats [59]. Additionally, the environment evolves over time, with infrastructure like roads and buildings degrading [60].

The baseline implementation would consist of using map data, which has improved precision with the help of particle filter coupling between LiDAR and GNSS [60]. As previously discussed, this would also improve LiDAR accuracy, but would mainly enable avoiding static objects. The planning for static NFZs and 2D objects could be done offline, before flight, with management of these obstacles performed online, during flight, using the 3D RTAB-Map mapping technique [59]. This mapping technique is a proper

combination of ease of integration, necessary for a modular approach, accuracy, cost and necessary computational complexity [61].

To avoid the obstacle during flight, the system would also have to differentiate between static and dynamic objects. For this, a protocol of ”detect, categorise, respond” could be employed, inspired by Figure 9 in [59]. Depending on whether the obstacle is static or dynamic, the system would have to respond accordingly. The response will be discussed below; however, detection and categorisation would need to be verified and validated depending on the chosen algorithm. This would have to be developed in further development stages and would likely use AI to adequately respond to dynamic objects. The necessity to respond to dynamic NFZs would have to be communicated through the communication system. The overall flowchart for obstacle and NFZ can be observed in Figure 5.3.

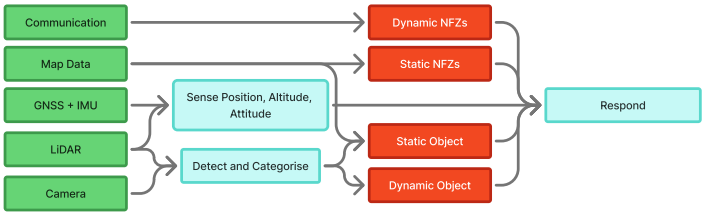

Figure 5.3: Approach for tackling static and dynamic obstacles and No Fly Zones (NFZs) flowchart.

After categorising the object as static or dynamic, the system would have to respond accordingly. For this, passive or active strategies could be used and the best would have to be chosen during verification. The response necessary could furthermore be learnt through RL or be a predefined protocol. For static objects and NFZs, given accurate position determination, passive vector potential methods could be used, repelling the vehicle from the locations identified before the flight [59]. This could be applied to detecting other UAVs in the future; however, it would necessitate their position being monitored, as well. As previously discussed, obstacle avoidance could also be assisted with the communication system. For more unpredictable obstacles, RL would need to be applied.

5.2.3. Flight Path Assistance Strategy

Owl-22 will employ a modular approach, building upon a simple take-off, cruise, and landing flight plan. This is inspired by unmanned aerial vehicles (UAVs) that follow predefined, mission-adaptable flight steps [62]. The flight path follows a ”goalpost” trajectory with perfectly vertical take-off and landing. To reduce complexity and accelerate development, the first iteration will use a semi-autonomous system operated by a pilot, allowing for real-world validation of key technologies before introducing full autonomy. This approach aligns with EASA’s phased integration of automation [63], but is primarily driven by engineering prudence and risk reduction. Thus, Owl-22 initiates vertical take-off and landing using an autopilot system that can be overridden by the pilot if needed. The cruise phase will be partially automated, supporting obstacle detection and flight stability. These specific choices will be justified in Section 5.3 and Subsection 5.2.4 respectively. With the modular approach in place, future developments will be able to develop the system to full mission autonomy, including path generation, though such endeavours would be significantly more complex and expensive.

5.2.4. Path Optimisation

Path optimisation for urban eVTOLS is particularly important. This is because a careful balance of safety, comfort, energy efficiency and noise pollution must be achieved. As such, Owl-22 aims to implement a solution that improves as more simulation and flight data is obtained. Additionally, it is very likely that this algorithm will only be introduced after the initial launch of Owl-22, since its success will most certainly require significant amounts of in-flight data.

Traditional deterministic path-planning algorithms such as A* or Dijkstra’s algorithm, which often prioritise single objectives, are insufficient for this multi-objective problem due to the stochastic nature of urban environments. Metaheuristic methods, particularly genetic algorithms, are great at multi-problem optimisation, but require vast amounts of data and time [64]. Furthermore, supervised deep learning

architectures are especially susceptible to overfitting. Thus, deep Reinforcement Learning (RL) was selected due to its ability to learn optimal policies through trial-and-error interactions with complex environments, mimicking biological systems' strategies for energy-efficient navigation. For example, birds optimise flight paths by dynamically balancing energy expenditure and risk avoidance—a process analogous to deep RL's reward-maximisation framework. A more in-depth explanation of the RL framework is provided in Section 5.3. While deep RL does also suffer from the high-data, overfitting constraints of other deep learning models, recent studies have demonstrated deep RL's superiority in air vehicle path optimisation, particularly in urban settings [65, 66]. Specifically, the method outlined in [66], using an adapted form of Proximal Policy Optimisation (PPO) will be followed. This algorithm considers dynamic obstacle avoidance, adherence to noise regulations, and energy efficiency when optimising any given path. The associated pipeline is outlined in Figure 5.4.

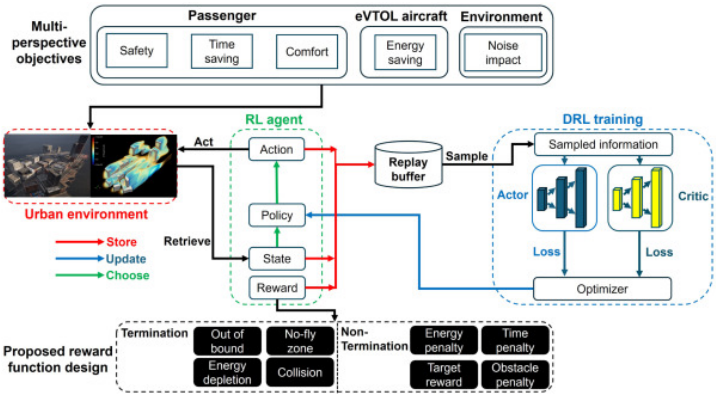

Figure 5.4: Modified PPO pipeline [66].

5.3. Automated VTOL System

In line with the modular approach outlined in Subsection 5.2.3, Owl-22 will initially only implement fully automated takeoff and landing. This is because the VTOL phase is significantly more constrained than the cruise phase, making it easier to model and solve. This greatly reduces both the time and data required to achieve automated flight control. Traditionally, Automatic Flight Control Systems (AFCS), comprising of a complex set of control algorithms, are used due to their extensive reliability and validity. However, they pose several issues; Modelling the extremely complex system dynamics, followed by extensive verification and validation, is computationally, financially and temporally expensive. Furthermore, they are unable to operate reliably in non-modelled conditions, placing a direct dependence on model fidelity and validity [67]. These issues are amplified significantly when considering the novel nature of both this vehicle and the UAM industry in general. As such, an alternative, model-free approach is considered. Of course, there are a vast number of these methods, some of which involve deep neural networks (DNNs), and others, more traditional Machine Learning (ML) algorithms. For the sake of conciseness, this section will only elaborate on deep RL methods, which were shortlisted due to their ability to learn complex tasks related to robotics and autonomous navigation [68, 69]. Deep RL is a framework that combines the benefits of DNNs with the agent-reward RL approach. Figure 5.5 gives a brief description of a model-free deep RL model. Note that the DNN is used to output a policy, π, based on a current system state, s.

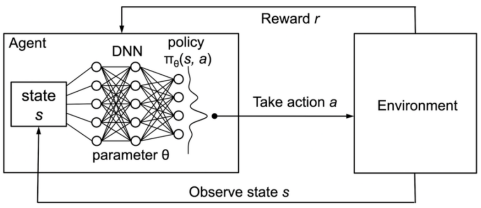

Figure 5.5: Deep Reinforcement Learning architecture [70].

More specifically, Figure 5.5 outlines an *on-policy* method. Here, the action-value function, Q, is trained on the same policy that generates the agent's actions, a. This is mathematically represented by Equation 5.1

$$Q^{\pi}(s_t, a_t) = \mathbb{E}\left[\sum_{t=0}^{\infty} \gamma^t R(s_t, a_t)\right] \tag{5.1}$$

where Q is defined as the expectation of the sum of the reward, R, and discount factor γ at every time-step. However, deep RL methods can also employ *off-policy* learning strategies. The distinction between these approaches lies in how the agent utilises experience to update its policy parameters, θ:

- **On-policy methods** require the agent to learn exclusively from trajectories generated by its current policy $\pi(a|s;\theta)$. This ensures that the training data reflects the policy's latest behaviour but limits sample efficiency, as old data becomes obsolete after each policy update.
- **Off-policy methods** decouple the policy used for exploration (*behaviour policy*) from the policy being optimized (*target policy*). By storing past experiences in a replay buffer, these methods can reuse historical data, improving sample efficiency and enabling better exploration. However, the mismatch between behaviour and target policies can introduce instability during training.

In robotics and autonomous systems, off-policy methods are often favoured for their sample efficiency and improved ability to generalise [71], while on-policy approaches remain prevalent in scenarios requiring precise policy alignment [72]. Hybrid techniques, such as proximal policy optimisation (PPO) [72], blend aspects of both to mitigate their respective limitations. Another hybrid technique is the Soft Actor-Critic (SAC) algorithm [73], an off-policy actor-critic method that introduces entropy regularisation to enhance exploration. Here, entropy refers to the stochasticity of an action; *How many possible states are left after this action is taken?, and how random is the probability of exploring each state?* This way, SAC optimises a modified objective function that maximises both expected reward and policy entropy, $\mathcal{H}(\pi(\cdot|s)$:

$$J(\pi) = \mathbb{E}\left[\sum_{t=0}^{\infty} \gamma^t \left(R(s_t, a_t) + \alpha \mathcal{H}(\pi(\cdot|s_t))\right)\right] \tag{5.2}$$

Where $\alpha > 0$ controls the trade-off between reward maximisation and entropy deterministic strategies. SAC's entropy-aware formulation improves sample efficiency (inherited from off-policy learning) while maintaining robust exploration, making it particularly effective in continuous control tasks. Conversely, its inclination towards entropy maximisation raises serious questions regarding generalisation, an extremely common problem with 0 methods [74]. This is an even bigger concern for aircraft controllers, since safety is paramount. Thus, this project proposes the use of Returns Uncertainty-Navigated Distributional Soft Actor-Critic (*RUN-DSAC*), a state-of-the-art algorithm developed and tested by the Control & Simulations department at TU Delft [71]. This method deploys several additional terms to aid with quantifying risk and creating a model that generalises well without being too risk-seeking. This is a particularly important problem when training the model on a simulation, since there is a risk that it will generalise poorly compared to real life. While there are still many points to discuss, they will be omitted for the sake of conciseness. Instead, the reader is referred to [71], which provides an excellent breakdown of RUN-DSAC, as well as other state-of-the-art alternatives. Figure 5.6 also shows the more complex actor-critic architecture of RUN-DSAC.

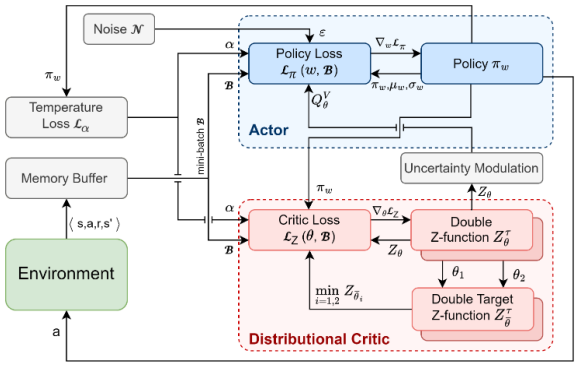

Figure 5.6: RUN-DSAC architecture [71].

5.4. System Overview

Owl-22's complex system contains a vast array of different hardware and software interactions. Documenting these inter-connections is essential to ensure a logically sound architecture with the appropriate protocols in place. Furthermore, it is important to provide estimates of different data flows in the system to ensure the data budget is reasonable and can be handled adequately using the selected components. Lastly, outlining the chosen components is also important to verify the related budgets. As such, two diagrams are displayed below, showcasing the data-handling and software diagrams sequentially.

Note that the data-handling diagram also contains bandwidth estimates for the different flows. In some cases, such as the GNSS, the bitrate could be found directly from the data sheet [75]. For the camera, the required bitrate can straightforwardly be calculated using Equation 5.3:

$$bitrate_{cam} = w_{res} \times h_{res} \times fps \times colour_{depth} \times ratio_{compress} \tag{5.3}$$

where w_{res}, h_{res} denote the resolution width and height respectively, fps is the camera's frame-rate, $colour_{depth}$ is the colour bit depth and $ratio_{compress}$ refers to the compression codec used. In the case of the Walksnail Avatar Pro camera, assuming the vehicle would display Full HD, 16-bit, 60 fps video, the resulting bitrate, including the H.264 compression codec, would equal $1920 \times 1080 \times 60 \times 16 \times 1/5 = 398[Mbps]$.

Calculating the bitrate IMU sensor follows a similar logic. For the IMU case, Equation 5.4 is used, with f_s denoting the sampling frequency. The chosen IMU sensor does not state its sampling frequency. For that reason, a value of 400 [Hz] was chosen since it is commonly used for objects moving at similar speeds.

$$bitrate_{IMU} = f_s * 2(n_{axes} * bit_{depth}) \tag{5.4}$$

$$= 400 * 2(3 * 16) = 38.4[Kbps] \tag{5.5}$$

For the LiDAR, the calculation is significantly more difficult to obtain since certain required information, such as the Pulse rate and number of returns, is very difficult to acquire. In this case, a value of 60 [Mbps] was obtained from literature analysing LiDAR sensors on semi-autonomous vehicles [76]. However, since Owl-22 uses a combination of different LiDAR sensors with varying field of view values, an arbitrary 20% overhead is added to mitigate any potential oversights. Even with a larger overhead, the bitrate of these sensors remains way below the capacity of the Apple M4 chip, and so any underestimation poses little threat to the system's feasibility.

Lastly, note the omission of any values related to the diagnostics and temperature sensors. For the former case, it is too difficult to estimate a concrete value due to the relative infancy of the system, whereas the latter was ignored due to its extremely low bitrate.

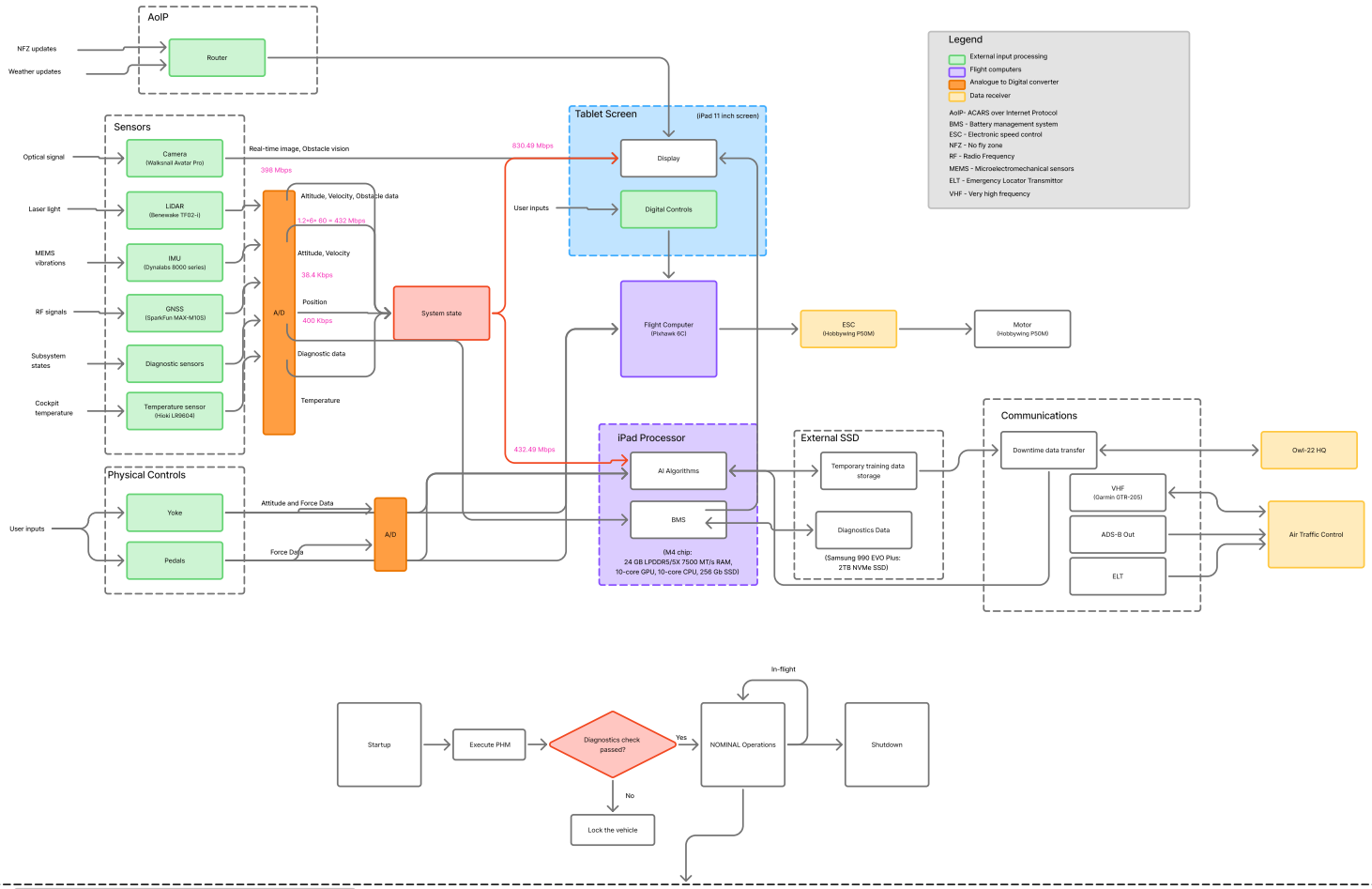
AoIP
NFZ updates
Weather updates
Router
Legend
External input processing
Flight computers
Analogue to Digital converter
Data receiver
AoIP- ACARS over Internet Protocol
BMS - Battery management system
ESC - Electronic speed control
NFZ - No fly zone
RF - Radio Frequency
MEMS - Microelectromechanical sensors
ELT - Emergency Locator Transmitter
VHF - Very high frequency
Sensors
Optical signal
Camera (Walksnail Avatar Pro)
Real-time image, Obstacle vision
398 Mbps
Laser light
LiDAR (Benewake TF02-i)
MEMS vibrations
IMU (Dynalabs 8000 series)
RF signals
GNSS (SparkFun MAX-M10S)
Subsystem states
Diagnostic sensors
Cockpit temperature
Temperature sensor (Hioki LR9604)
A/D
Attitude, Velocity, Obstacle data
1.2×6× 60 = 432 Mbps
Attitude, Velocity
38.4 Kbps
Position
400 Kbps
Diagnostic data
Temperature
System state
Tablet Screen
(iPad 11 inch screen)
830.49 Mbps
Display
User inputs
Digital Controls
Flight Computer (Pixhawk 6C)
ESC (Hobbywing P50M)
Motor (Hobbywing P50M)
iPad Processor
AI Algorithms
BMS
M4 chip:
24 GB LPDDR5/5X 7500 MT/s RAM,
10-core GPU, 10-core CPU, 256 Gb SSD)
432.49 Mbps
External SSD
Temporary training data storage
Diagnostics Data
(Samsung 990 EVO Plus:
2TB NVMe SSD)
Communications
Downtime data transfer
Owl-22 HQ
VHF (Garmin GTR-205)
ADS-B Out
ELT
Air Traffic Control
Physical Controls
User inputs
Yoke
Pedals
Attitude and Force Data
Force Data
A/D

In-flight
Startup
Execute PHM
Diagnostics check passed?
Yes
No
NOMINAL Operations
Shutdown
Lock the vehicle

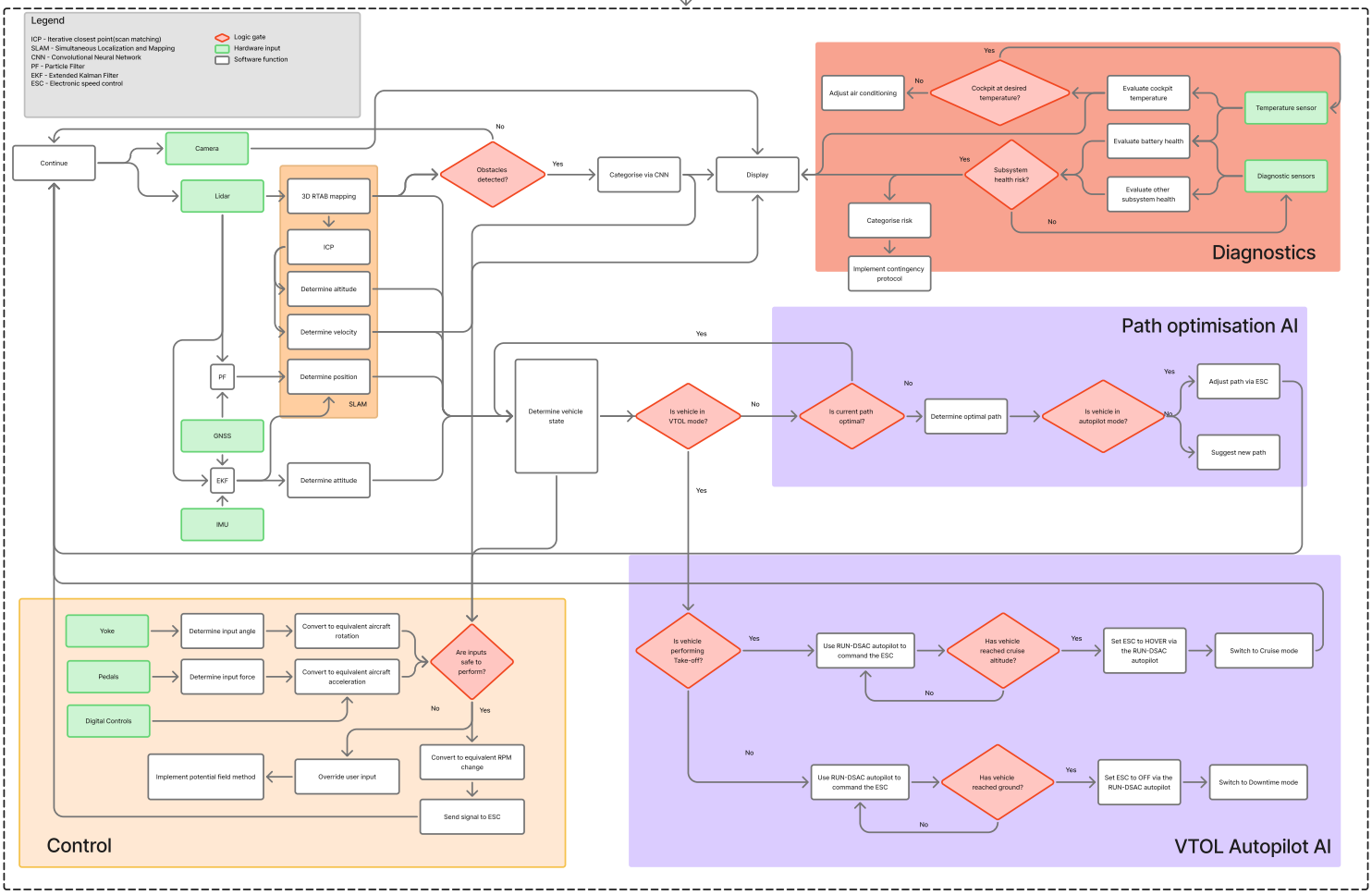
Legend
ICP - Iterative closest point(scan matching)
SLAM - Simultaneous Localization and Mapping
CNN - Convolutional Neural Network
PF - Particle Filter
EKF - Extended Kalman Filter
ESC - Electronic speed control
Logic gate
Hardware input
Software function
Continue
Camera
Lidar
3D RTAB mapping
ICP
Determine altitude
Determine velocity
Determine position
SLAM
PF
GNSS
EKF
IMU
Determine attitude
Obstacles detected?
Yes
No
Categorise via CNN
Display
Determine vehicle state
Is vehicle in VTOL mode?
Yes
No
Diagnostics
Cockpit at desired temperature?
Adjust air conditioning
Evaluate cockpit temperature
Temperature sensor
Evaluate battery health
Subsystem health risk?
Diagnostic sensors
Evaluate other subsystem health
Categorise risk
Implement contingency protocol
Path optimisation AI
Is current path optimal?
Determine optimal path
Is vehicle in autopilot mode?
Adjust path via ESC
Suggest new path
Control
Yoke
Pedals
Digital Controls
Determine input angle
Determine input force
Convert to equivalent aircraft rotation
Convert to equivalent aircraft acceleration
Are inputs safe to perform?
Override user input
Implement potential field method
Convert to equivalent RPM change
Send signal to ESC
VTOL Autopilot AI
Is vehicle performing Take-off?
Use RUN-DSAC autopilot to command the ESC
Has vehicle reached cruise altitude?
Set ESC to HOVER via the RUN-DSAC autopilot
Switch to Cruise mode
Use RUN-DSAC autopilot to command the ESC
Has vehicle reached ground?
Set ESC to OFF via the RUN-DSAC autopilot
Switch to Downtime mode

6 Prognostics and Health Management System

The implementation of a diagnostic and prognostic system is essential for ensuring the safety, reliability, and maintainability of the Owl-22. Personal use introduces unique challenges as tight turnaround times and integration with user-centric planning. To address these, a Prognostics and Health Management (PHM) system is embedded in the vehicle architecture. This enables the vehicle to detect, isolate, and predict faults across subsystems. Being able to predict failures, efficient maintenance scheduling is made possible.

This chapter presents the design of the diagnostic architecture based on the systematic, top-down approach by Rui Li et al.[77]. This framework encompasses functional, logical, and physical layers. The PHM system consists of onboard, communication, and ground layers. Fault detection, prognostics, and health management are distributed over a modular, sensor-redundant architecture. The following sections cover first the general architecture of the PHM system. This includes the design approach, functional breakdown and functional flow. Afterwards, a physical architecture will be presented for the battery system, specifically as this subsystem was identified to be the most risk-sensitive.

6.1. General Architecture

The process of designing the PHM system consists of three sequential design steps: the functional, logical and physical design following the RFLP methodology. This methodology ensures the traceability of the requirements towards the physical implementation of the design.

6.1.1. Design Approach

The PHM system architecture for the personal aerial vehicle is developed following a structured top-down methodology. The architecture definition process begins with defining a design approach and decomposing the design process into manageable parts. This decomposition aligns with the “RFLP-methodology” [77] (Requirements, Functional, Logical, Physical), as illustrated in Figure 6.1. This ensures that each functional requirement can be traced to a physical implementation and vice versa. Notably, the methodology supports iterative refinement and allows for the integration of feedback from lower architectural levels back into the system framework.

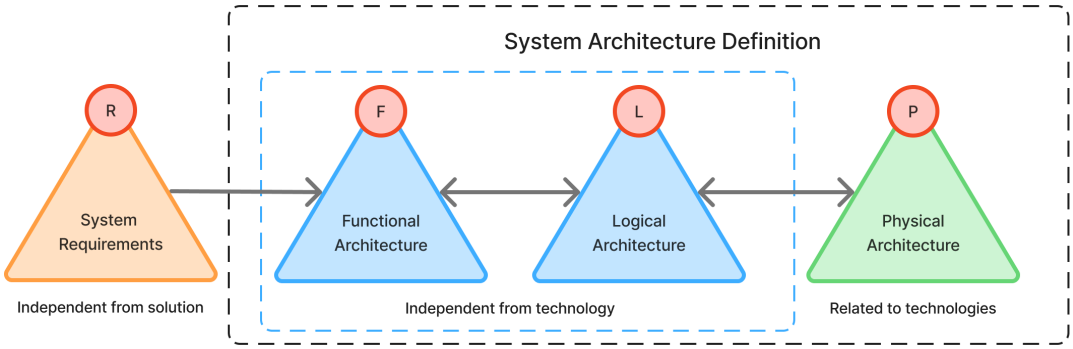

Figure 6.1: Top-down architecture development based on the RFLP methodology.

The top-down approach proceeds through the development of three complementary architectural views:

- **Functional view**: Defines *what* the system must do to fulfil PHM-related requirements, independent of technology or implementation. It establishes the functions and their hierarchy.
- **Logical view**: Captures *how* these functions are related in terms of sequencing and data flow, without yet specifying physical implementation.
- **Physical view**: Realises the functions and logical flows using specific hardware and software components, including sensors and communication interfaces.

The PHM-system is not conceived as a single entity, but as a set of components interacting across onboard, communication, and on-ground layers as displayed in Figure 6.2. This layered approach is essential for the integration of onboard health monitoring with maintenance planning.

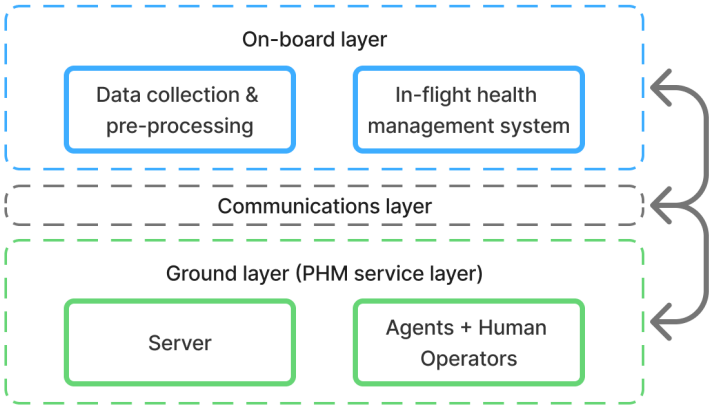

Figure 6.2: The 3-layered structure of the PHM-system.

6.1.2. System Architecture Definition

The PHM-system architecture of the Owl-22 is defined by integrating functional, logical, and physical views following the RFLP model. This integration ensures a coherent system architecture capable of real-time monitoring, fault isolation, and health forecasting across the vehicle's critical subsystems.

At the core of this architecture is the three-layer PHM-system framework displayed in Figure 6.2. The onboard layer includes distributed sensor networks and processing units responsible for real-time data collection and (pre-)processing. The communication layer provides data transfer capabilities via the 5G network, ensuring that collected health data is transferred to the ground-based prognostic and maintenance environment. The 5G network is chosen for data transfer since the Owl-22 will fly at altitudes where the connection is still strong. The ground layer hosts the centralised prognostics-computing and maintenance infrastructure. Here, the more computationally intensive tasks, such as prognostics, model updates, and health management advisory generation, are performed.

Functional architecture: The PHM system is functionally decomposed into five primary modules:

- **F1 – Data Acquisition (DA)**: Gathers in-flight data from various sensors and avionics subsystems and stores it temporarily.
- **F2 – Data Processing (DP)**: Applies data manipulation and transmission to make the data suitable for fault analysis.
- **F3 – Fault Diagnostic Assessment (FDA)**: Implements algorithms for fault detection, isolation, and identification.
- **F4 – Prognostic Assessment (PA)**: Estimate health state and remaining useful life (RUL).
- **F5 – Health Management (HM)**: Integrates diagnostic and prognostic results to generate maintenance advisories considering operational constraints.

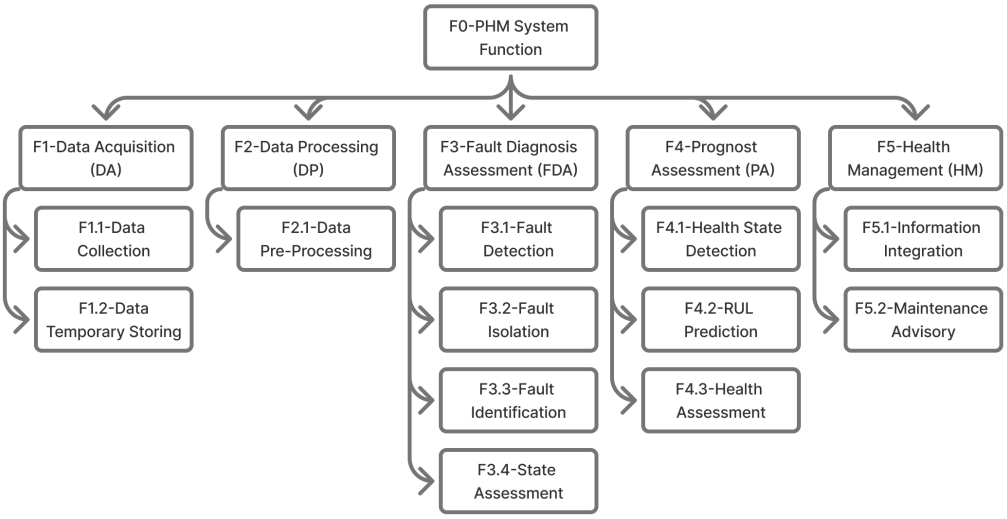

Figure 6.3: PHM function hierarchy diagram.

These functions, represented in Figure 6.3 form the foundational elements of a diagnostic pipeline. However, they do not yet constitute an operationally connected sequence. While each function is modular and adaptable to evolving requirements or operational scenarios, the current breakdown lacks the interdependencies and data flows needed to form a cohesive pipeline. Therefore, a logical architecture must be established.

Logical architecture: The functional flow of the PHM-system, as illustrated in Figure 6.4, commences with *F1: Data Acquisition (DA)*, where real-time sensor data is collected onboard and temporarily stored for initial processing. This raw data is subsequently routed to *F2: Data Processing (DP)*. The DP module is responsible for manipulating the data into a desired form that characterises features of interest in the condition monitoring and diagnostic process. This function can be configured with algorithms to perform signal transformation (e.g., Fast-Fourier Transforms [FFT]) [77].

Depending on whether a critical fault is detected, the preprocessed output is transmitted to *F3: Fault Diagnostic Assessment (FDA)*. If no critical fault is detected, the data will be transmitted to *F4: Prognostic Assessment (PA)* for further analysis.

When a critical fault is detected, the data proceeds to the *F3: Fault Diagnostic Assessment (FDA)*. This module sequentially performs fault detection, isolation, and identification through dedicated software algorithms. The resulting fault information is then used to perform a comprehensive state assessment. Ultimately, the resulting health states are transmitted to the Health Management (HM) module to support decision-making for appropriate maintenance actions.

When non-critical data is involved, the processed information is forwarded to *F4: Prognostic Assessment (PA)*. Here, the system performs health state estimation and prediction of Remaining Useful Life (RUL), leveraging either model-based or data-driven prognostic algorithms (depending on the specific subsystem).

The outputs from both the diagnostic and prognostic processes converge in module *F5: Health Management*, which combines the information and generates maintenance advisories. These advisories are communicated via *C1: Data Sharing Network* with the *G2: Maintenance Management System*, which factors in available inventory, technician capacity, and scheduled maintenance windows to determine and execute optimal maintenance actions. All outputs are archived in the *G1: Database*, and communicated across subsystems again via the *C1: Data Sharing Network*.

An essential component supporting the PHM system is the *In-Flight Health Management System*. This system is responsible for acquiring comprehensive operational data during flight, which is subsequently transmitted to the ground-based infrastructure. The system integrates several onboard modules such as the indicating/recording system, onboard maintenance system, battery management system, and a data management unit [77]. This routine collection and evaluation of flight data enhances safety and

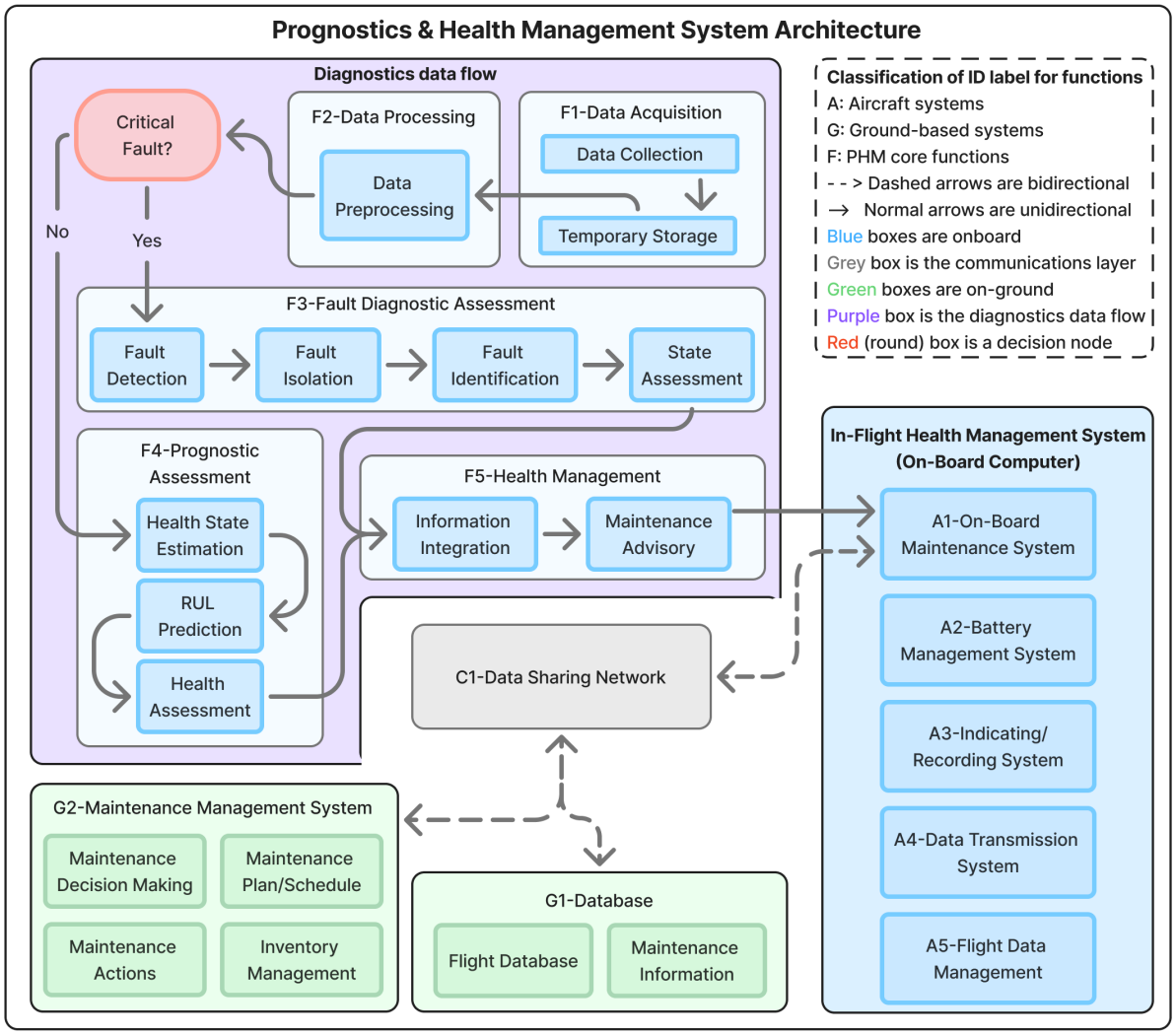

Figure 6.4: Prognostics and Health Management system architecture.

maintenance efficiency by identifying anomalies which indicate maintenance necessity before parts break.

Physical architecture: Physically, the diagnostics system is realised using three key hardware components as proposed by Rui Li et al. [77]:

- An **integrated computing module** executing PHM software functions (FDA, PA, HM).
- A **data acquisition cabinet** interfacing with sensor networks, performing initial signal filtering and buffering.
- An **auxiliary power module** ensuring uninterrupted diagnostics in case of main power failure.

Each hardware element must be designed with modularity in mind to make future changes to the architecture possible. In reality, the physical architecture will differ significantly per subsystem. Due to time constraints and advice from Dr. Dimitrios Zarouchas, this paper will treat the physical architecture of the PHM system for the battery.

6.2. Physical Architecture of the Battery PHM-system

The battery is the most safety-critical component in the Owl-22, as acknowledged by Section 12.3. Therefore, it is essential that a robust PHM system is integrated into the battery module in order to ensure long-term operational safety, maintenance efficiency, and prevent severe battery degradation.

The integration of the PHM system into the battery of the vehicle enables early fault detection, RUL

prediction, and predictive maintenance planning.

This section proceeds by defining what variables should be measured by the battery PHM and how the data will be used. The architecture is based on findings from NASA's battery PHM framework proposed by Chetan Kulkarni and Mohit Mehta [78]. This framework outlines a dedicated PHM architecture for the battery of eVTOLs used in Urban Air Mobility (UAM). The structural health of the battery PHM system is not discussed in this section as it is considered to be part of the structural PHM subsystem.

6.2.1. System Requirements and Risk-Based Motivation

The robust physical implementation of a PHM system in the battery of an eVTOL is pivotal in ensuring regulatory compliance and ensuring safe operation. Batteries in eVTOLs are high-risk components [78] due to the following reasons:

The first is their potential for thermal runaway, which is defined as a self-sustaining chain reaction in which a battery's temperature rises uncontrollably, leading to dangerous consequences like fire or explosion [79]. The second risk for the battery is the effect of charging and discharging the battery at different current rates, also known as C-rate [80]. Charging the battery under high C-rates can lead to battery degradation in the long term. As a third, cell imbalance can lead to overheating, voltage fluctuations, and even failure of the entire battery subsystem [81]. Another possible point of failure, identified by Manuel Ank et al. [82], is the risk of physical contact loss between the battery and electrodes as a consequence of mechanical vibrations. The study finds that exposing battery cells to vibrations leads to increased resistance and capacity fade of the battery, harming the long-term performance. Finally, repeated discharging of the battery under varying environmental conditions imposes a high risk of thermal runaway. Consequences could be, in this case, gas leakage and jet flames [83].

In summary, the 4 main risks for the battery are: thermal runaway, capacity degradation, cell imbalance, over-voltage, and connector detachment. A more elaborate listing can be found in Section 12.3.

To mitigate the risks described above, the PHM system for the battery must satisfy a set of requirements. The requirements are derived in accordance with the method described by Rui Li et al [77]:

- **PHM-DR-B1:** The system shall detect early signs of runaway with a confidence level $> 95\%$ under nominal flight conditions.
- **PHM-DR-B2:** The PHM-system shall support accurate estimation $(\pm 10\%)$ of Remaining Useful Life (RUL) based on degradation models or data-driven approaches.
- **PHM-DR-B3:** The PHM-system shall operate independently of the main BMS to ensure fault tolerance and enable post-landing health reporting.
- **PHM-DR-B4:** The PHM-system must ensure sensor redundancy to tolerate single sensor failures.
- **PHM-DR-B5:** Data logging and transfer to ground infrastructure must be completed within 5 minutes post-landing.

6.2.2. Battery PHM Architecture

The functional architecture for the PHM system of the battery inherits from the five core functions (F1-F5) proposed in Figure 6.3. It follows the logical flow proposed in Figure 6.4. This general architecture will be tailored for the battery system. Details of the battery PHM architecture are discussed below.

F1 - Data Acquisition (DA): Based on multiple research papers, the parameters which need to be monitored are listed below. These variables are collected from the sensors and relayed to the data preprocessing unit:

- Voltage and current at the cell and module level
- Temperature at the busbars, middle of the battery pack and along the coolant flow path. This layout was proposed by Ozge Yetik et al. [84]
- Impedance [85]
- Ambient air temperature [86]

F2 - Data preprocessing (DP): The raw data coming from the sensors is then preprocessed. This includes noise filtering and feature extraction. Furthermore, a time stamp is added to the raw sensor

data in order to enable traceability.

F3 - Fault Diagnostic Assessment (FDA): This module identifies and isolates faults such as over-voltage and battery heating. Diagnostic algorithms for the battery system leverage rule-based thresholds for the voltage and temperature assessment that come with a low computational cost. The Fault Diagnostic Assessment runs both during vehicle operation and charging. Charging will be monitored at all times to prevent battery damage and extend its lifespan as much as possible.

F4 - Prognostic Assessment (PA): The prognostic assessment estimates future health states of the battery. It particularly monitors capacity fade and resistance growth in the electrical circuits. Based on this, a Remaining Useful Life prediction for the battery is established.

F5 - Health Management (HM): The health management module of the battery PHM-system combines the output of the Fault Diagnostic Assessment and Prognostic Assessment. Based on the information received, the HM module then generates maintenance advice if necessary. Maintenance can then be planned directly onboard via the iPad. Furthermore, the health management system will communicate via the Data Sharing Network (C1) with the maintenance management system (G2). When non-critical faults are detected, the user will be alerted via the control display on the iPad.

Below, in Figure 6.5, the Data Acquisition module and the Data processing module are visualised for the battery PHM system specifically.

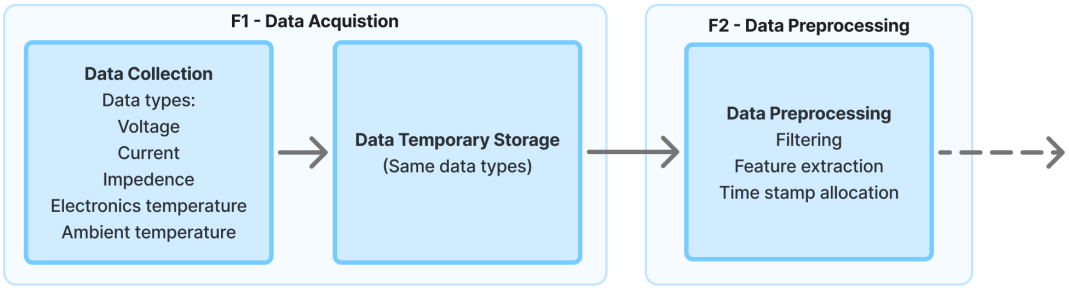

Figure 6.5: PHM architecture for the battery.

6.2.3. Redundancy, Fail-Safe Architecture, and Risks

In order to ensure a robust battery PHM system, the architecture is designed to maintain safe operation under degraded conditions. This is essential as the battery was identified in Section 12.3 as the subsystem carrying the highest risk of all subsystems.

The architecture is designed with redundancy in mind. This means that sensors of the DA module are installed at multiple critical locations. Sensors are installed both at the cell and module levels to enable the vehicle to localise faults precisely. In this way, if the cell-level sensor does not work, the module sensor can take over its task and vice versa. In the DA module, the gathered data is temporarily stored with redundancy in mind. In this way, no data gets lost in case of a communication loss. This enables the vehicle to analyse all gathered data when communication is re-established.

In the electrical circuits of the vehicle, fail-safes are implemented to ensure anomalies do not result in unsafe situations or vehicle damage. As an example, charging will halt in case of a short-circuit or over-voltage is detected. As a result, the risk of fire and long-term battery damage is significantly reduced.

As detailed in Section 12.3, the battery subsystem of the Owl-22 is subjected to key risks. The battery PHM-system monitors these risks in the following ways:

- **Thermal runaway**: Redundant temperature sensing and trend analysis.
- **Capacity fade**: Impedance monitoring and resistance growth tracking.
- **Cell imbalance**: Redundant voltage monitoring and generation of state of charge estimations.
- **Connector detachment**: Monitoring of voltage drops.

- **Over-voltage during charging**: Continuous voltage monitoring during charging and cut-off if voltage exceeds a certain threshold.

6.2.4. Conclusion and Recommendations

This chapter first discussed the design of the general architecture of the PHM system. Afterwards, a physical implementation for the battery PHM system is presented. The system is designed to detect and predict key failures before they can pose a significant safety risk. The architecture includes both real-time fault detection and post-flight trend analysis. Its functionality includes temperature and voltage monitoring, the tracking of capacity degradation and predicting the remaining useful life of the battery. The proposed system mitigates known risks as over-voltage, thermal runaway and connector detachment. The system aims to catch anomalies promptly and inform the user when necessary.

The main recommendation for further development of the PHM-system of the Owl-22 is the implementation of a PHM-system for subsystems as propulsion and the structure. Furthermore, for the battery PHM system, the proposed architecture could be further elaborated by selecting the specific sensors and algorithms. These were not included in this paper due to time and resource constraints.

7 Stability and Control Design

Unlike most fixed-wing aircraft, the Owl-22 is not stable and needs active control, as will be explained in the first section of this chapter. Therefore, the design of a robust (7.4) control system is necessary in order to have a safe flight. In that case, the vehicle will be able to move due to pilot inputs and correct for disturbances by the control system. This chapter presents the design of this system. There are a number of examples of quadcopter software publicly available. However, for the cyclorotor's thrust vectoring capabilities, original work was required to be done. The model was made with the intention of being as robust as possible. The big assumptions emphasise why this is preferable in accordance with pilot comfort.

7.1. Stability

The Owl-22 is very similar to a quadcopter in terms of stability. During hover, as well as during horizontal movement, there are no significant restoring aerodynamic forces that bring the vehicle back to an equilibrium state when opposed to a disturbance. However, the quadcopter does not tilt over further. Therefore, the Owl-22 has statically neutral stability and dynamical instability and needs active control adjustments [87].

7.2. Coupling

An interesting fact about the Owl-22 is that it has thrust-vectoring capabilities. Due to this, it can perform translational movement in the forward and backwards direction without having to tilt. This means less coupling and allows for easier pitch control. The coupling means that a certain manoeuvre is always connected to another manoeuvre. In the case of tilting to translate, the vehicle would be very prone to overshooting. This could be especially dangerous during landing. Furthermore, not having to tilt to translate forwards is more comfortable for the pilot since tilting is not something most people experience regularly.

Instead, there is coupling between the pitch-up moment of the cyclorotors due to the lift created and the pitch-down moment due to the cyclorotors because of the torque. Because this coupling is about the same motion, the control system can correct this by robust tuning instead of aggressive tuning.

7.3. Dynamical model

In order to design a software system that would be able to correct the Owl-22, the dynamics of the hardware are required. This chapter shows how the equations of motion go into the state space model and which assumptions need to be made. The state space model is used for the design of the control system.

Equations Of Motion (EOM)

In order to simulate a control system for the Owl-22, the dynamics first need to be known. These are described by the equations of motion, which are shown below 7.1.

$$
\begin{aligned}
\sum F_x &= k_1 \cdot h_{1,x} + k_1 \cdot h_{2,x} - mg\theta = m\ddot{x} \\
\sum F_y &= mg\phi = m\ddot{y} \\
\sum F_z &= -k_1 \cdot h_{1,z} - k_1 \cdot h_{2,y} - k_2 \cdot h3 - k_2 \cdot h4 + m \cdot g = m\ddot{z} \\
\sum M_x &= L_1 \cdot k_1 \cdot h_{1,z} - L_1 \cdot k_1 \cdot h_{2,z} + L_1 \cdot k_2 \cdot h_3 - L_1 \cdot k_2 \cdot h_4 = I_{xx}\ddot{\phi} \\
\sum M_y &= L_2 \cdot k_1 \cdot h_{1,z} + L_2 \cdot k_1 \cdot h_{2,z} - L_2 \cdot k_2 \cdot h_3 - L_2 \cdot k_2 \cdot h_4 = I_{yy}\ddot{\theta} \\
\sum M_z &= L_1 \cdot k_1 \cdot h_{1,x} - L_1 \cdot k_1 \cdot h_{2,x} = I_{zz}\ddot{\psi}
\end{aligned}
\tag{7.1}
$$

These equations of motion make use of the body-fixed reference frame. This means that the x-axis points in the direction of forward flight, the y-axis to the right and the z-axis points downwards in order to finish the right-handed frame. Angles roll, pitch and yaw are the rotations around the x, y and z consecutively. The EOM makes use of a constant 'k' for $F_{propellor} = k \cdot \omega^2 = k \cdot h$. This is the lift efficiency and is specific for the coaxial rotor and the cyclorotor [88]. This number contains the relation between force created by the propulsion device and the angular velocity squared. This relation was statistically confirmed to be present and is known to be proportional to the size and lift coefficient of the propulsion devices. It tells how much force is created due to the rotation of the lift devices.
The symbol 'h' is defined as the square of the lift devices. The control system modifies this quantity directly.

The left cyclorotor has a lift efficiency k_1, $h_{1,x}$ tells the forward thrust and $h_{1,y}$ upward thrust. The right cyclorotor similarly produces thrust with the same lift efficiency k_1, but now has $h_{2,x}$ and $h_{2,y}$. The coaxial rotors have lift efficiency k_2 and produce an upwards force by modifying $h3$ and $h4$ for the left and right rotors consecutively. In reality, the cyclorotors can do thrust vectoring by modifying the angular velocity and the lift efficiency in the x- and z-directions. However, this translates one-to-one to the assumption of constant lift efficiency and then modification of the apparent angular velocity that contributes to a force forward and upward. This was done in order to save one input parameter and make the model simpler. An overview of what every symbol in the EOM means is provided in Table 7.1.

Table 7.1: Quantities in the EOM.

Quantity	Description	Value
	Hardware parameters	
k_1	Lift efficiency of the cyclorotors	0.04610 [$\frac{N}{rad^2}$]
k_2	Lift efficiency of the coaxial rotors	0.01326 [$\frac{N}{rad^2}$]
m	Vehicle Mass	305[kg]
L_1	Difference in y-position from the CG to a lift device	0.5[m]
L_2	Difference in x-position from the CG to a lift device	0.8[m]
I_xx	Mass moment of inertia around the x-axis	130[$kg \cdot m^2$]
I_yy	Mass moment of inertia around the y-axis	100[$kg \cdot m^2$]
I_zz	Mass moment of inertia around the x-axis	90[$kg \cdot m^2$]
	Control actuators	
$h_{1,x}$	Radial velocity squared for the x-component of the left cyclorotor	[$\frac{rad^2}{s^2}$]
$h_{1,z}$	Radial velocity squared for the z-component of the left cyclorotor	[$\frac{rad^2}{s^2}$]
$h_{2,x}$	Radial velocity squared for the x-component of the right cyclorotor	[$\frac{rad^2}{s^2}$]
$h_{2,z}$	Radial velocity squared for the z-component of the left cyclorotor	[$\frac{rad^2}{s^2}$]
h_3	Radial velocity squared for the left cyclorotor(z-component)	[$\frac{rad^2}{s^2}$]
h_4	Radial velocity squared for the right cyclorotor(z-component)	[$\frac{rad^2}{s^2}$]

State Space

Inspired by to the work of a paper on 'State Space System Modelling of a Quad Copter UAV' [89], a state space model was formulated for the Owl-22. The general form of the continuous time-invariant

state space model is stated below in equation 7.2.

$$\begin{aligned} \dot{x} &= Ax + Bu \\ y &= Cx + Du \end{aligned} \tag{7.2}$$

Using the EOM from the previous section, the following state space model is set below in equation set 7.3.

$$\begin{bmatrix} \dot{x} \\ \dot{y} \\ \dot{z} \\ \ddot{x} \\ \ddot{y} \\ \ddot{z} \\ \dot{\phi} \\ \dot{\theta} \\ \dot{\psi} \\ \ddot{\phi} \\ \ddot{\theta} \\ \ddot{\psi} \end{bmatrix} = \begin{bmatrix} 0 & 0 & 0 & 1 & 0 & 0 & 0 & 0 & 0 & 0 & 0 & 0 \\ 0 & 0 & 0 & 0 & 1 & 0 & 0 & 0 & 0 & 0 & 0 & 0 \\ 0 & 0 & 0 & 0 & 0 & 1 & 0 & 0 & 0 & 0 & 0 & 0 \\ 0 & 0 & 0 & 0 & 0 & 0 & 0 & -g & 0 & 0 & 0 & 0 \\ 0 & 0 & 0 & 0 & 0 & 0 & g & 0 & 0 & 0 & 0 & 0 \\ 0 & 0 & 0 & 0 & 0 & 0 & 0 & 0 & 0 & 0 & 0 & 0 \\ 0 & 0 & 0 & 0 & 0 & 0 & 0 & 0 & 0 & 1 & 0 & 0 \\ 0 & 0 & 0 & 0 & 0 & 0 & 0 & 0 & 0 & 0 & 1 & 0 \\ 0 & 0 & 0 & 0 & 0 & 0 & 0 & 0 & 0 & 0 & 0 & 1 \\ 0 & 0 & 0 & 0 & 0 & 0 & 0 & 0 & 0 & 0 & 0 & 0 \\ 0 & 0 & 0 & 0 & 0 & 0 & 0 & 0 & 0 & 0 & 0 & 0 \\ 0 & 0 & 0 & 0 & 0 & 0 & 0 & 0 & 0 & 0 & 0 & 0 \end{bmatrix} \begin{bmatrix} x \\ y \\ z \\ \dot{x} \\ \dot{y} \\ \dot{z} \\ \phi \\ \theta \\ \psi \\ \dot{\phi} \\ \dot{\theta} \\ \dot{\psi} \end{bmatrix} + \begin{bmatrix} 0 & 0 & 0 & 0 & 0 & 0 & 0 \\ 0 & 0 & 0 & 0 & 0 & 0 & 0 \\ 0 & 0 & 0 & 0 & 0 & 0 & 0 \\ \frac{k_1}{m} & 0 & \frac{k_1}{m} & 0 & 0 & 0 & 0 \\ 0 & 0 & 0 & 0 & 0 & 0 & 0 \\ 0 & \frac{-k_1}{m} & 0 & \frac{-k_1}{m} & \frac{-k_2}{m} & \frac{-k_2}{m} & g \\ 0 & 0 & 0 & 0 & 0 & 0 & 0 \\ 0 & 0 & 0 & 0 & 0 & 0 & 0 \\ 0 & 0 & 0 & 0 & 0 & 0 & 0 \\ 0 & \frac{L_1 k_1}{ixx} & 0 & \frac{-L_1 k_1}{ixx} & \frac{L_1 k_2}{ixx} & \frac{-L_1 k_2}{ixx} & 0 \\ 0 & \frac{L_2 k_1}{iyy} & 0 & \frac{L_2 k_1}{iyy} & \frac{-L_2 k_2}{iyy} & \frac{-L_2 k_2}{iyy} & 0 \\ \frac{L_1 k_1}{izz} & 0 & \frac{-L_1 k_1}{izz} & 0 & 0 & 0 & 0 \end{bmatrix} \begin{bmatrix} h_{1,x} \\ h_{1,z} \\ h_{2,x} \\ h_{2,z} \\ h_3 \\ h_4 \\ step \end{bmatrix}$$

$$\begin{bmatrix} x \\ y \\ z \\ \phi \\ \theta \\ \psi \end{bmatrix} = \begin{bmatrix} 1 & 0 & 0 & 0 & 0 & 0 & 0 & 0 & 0 & 0 & 0 & 0 \\ 0 & 1 & 0 & 0 & 0 & 0 & 0 & 0 & 0 & 0 & 0 & 0 \\ 0 & 0 & 1 & 0 & 0 & 0 & 0 & 0 & 0 & 0 & 0 & 0 \\ 0 & 0 & 0 & 0 & 0 & 0 & 1 & 0 & 0 & 0 & 0 & 0 \\ 0 & 0 & 0 & 0 & 0 & 0 & 0 & 1 & 0 & 0 & 0 & 0 \\ 0 & 0 & 0 & 0 & 0 & 0 & 0 & 0 & 1 & 0 & 0 & 0 \end{bmatrix} \begin{bmatrix} x \\ y \\ z \\ \dot{x} \\ \dot{y} \\ \dot{z} \\ \phi \\ \theta \\ \psi \\ \dot{\phi} \\ \dot{\theta} \\ \dot{\psi} \end{bmatrix} + \begin{bmatrix} 0 & 0 & 0 & 0 & 0 & 0 & 0 \\ 0 & 0 & 0 & 0 & 0 & 0 & 0 \\ 0 & 0 & 0 & 0 & 0 & 0 & 0 \\ 0 & 0 & 0 & 0 & 0 & 0 & 0 \\ 0 & 0 & 0 & 0 & 0 & 0 & 0 \\ 0 & 0 & 0 & 0 & 0 & 0 & 0 \end{bmatrix} \begin{bmatrix} h_{1,x} \\ h_{1,z} \\ h_{2,x} \\ h_{2,z} \\ h_3 \\ h_4 \\ step \end{bmatrix} \tag{7.3}$$

The change in state is described by the non-zero or one entries of the system matrix. These are forward and sideward accelerations due to roll and pitch. The absence of restoring forces showcases the inherent lack of stability and the demand for constant active control for state-maintenance. Similarly, the establishment of the input matrix is almost a copy of the EOM. In order to include gravity in the model, a new entry in the input vector was made. While in literature, the upwards force input is modelled as the resultant after subtracting one-fourth of the gravity. This becomes very complex in the case of 2 types of propulsion devices. The disadvantage of our solution, however, is that in the control model, a constant step input is needed. The benefit of this method is that the inputs of the input vector exactly correspond to the propulsion system action.

The output vector is a subset of the state vector. Therefore, the output matrix only consists of ones for the state variables that will be controlled and zeros otherwise. As usual, the inputs do not directly feed through outputs. This results in a feed-through matrix that consists of zeros.

Assumptions

AS-CTRL-1: The angles for pitch and roll remain within $\pm$15 degrees.

This small-angle assumption is important for the EOM. The relation between pitch, roll and acceleration towards x and y is assumed to be linear. As long as it can be shown that the roll and pitch angles are small, this approximation is accurate. Angles bigger would give estimation errors bigger than 1.14%, which would make the model inaccurate.

AS-CTRL-2: Aerodynamic forces on the body can be neglected.
Since the speed limit is 16.67 [m/s], the aerodynamic forces are too small to take into account for this model. Neglecting it gives no unreasonable errors, although it would be a good suggestion to include for future models.

AS-CTRL-3: Preliminary dimensions are representative of the final design.
The model was made for the estimation of the dimensions and design options from the midterm review. Therefore, this model does not exactly apply to the final design. This means that the dynamics differ, leading to different optimal control gains. Fortunately, the control system can also correct itself by having gains that are not exactly optimal. This explains that the model is still useful.

AS-CTRL-4: No net torques on the body are created due to the coaxial rotors and cyclorotors.
Since the left coaxial rotor rotates in the opposite direction to the right coaxial rotor, the net moment is zero. The torque on the cyclorotors creates a pitch down moment on the vehicle, however the lift creates a pitch up force. Since the unexpected moment can be counteracted by the coaxial rotors and the robust design of the control system, it is reasonable to neglect this moment in the EOM.

AS-CTRL-5: Desired inputs can be reached instantaneously.
Using saturation, the forces that the system can give are limited, which is realistic. However, how fast the propellers accelerate is also limited in reality. Due to a lack of knowledge on hardware, no saturation can be added to how quickly a force can be reached. All that can be done is to make sure the control system does not make aggressive adjustments.

AS-CTRL-6: Propeller forces do not influence each other, resulting in constant lift efficiency .
The assumption that propeller forces have no effect on each other is a hard one to quantify. This would have to be done using dynamic CFD, which is outside of the scope of this project. However, if the propeller efficiencies turn out to be lower, the control system can correct it.

7.4. Control System

Now that the state space model was developed, simple code was made to represent it in MATLAB. It has to be noted that this consisted of the state space model as presented earlier, in addition to an initial condition of all zeros. This code could then be used in the Simulink package in order to make the control system from scratch. Below, in figure 7.1, the design of this system is shown.

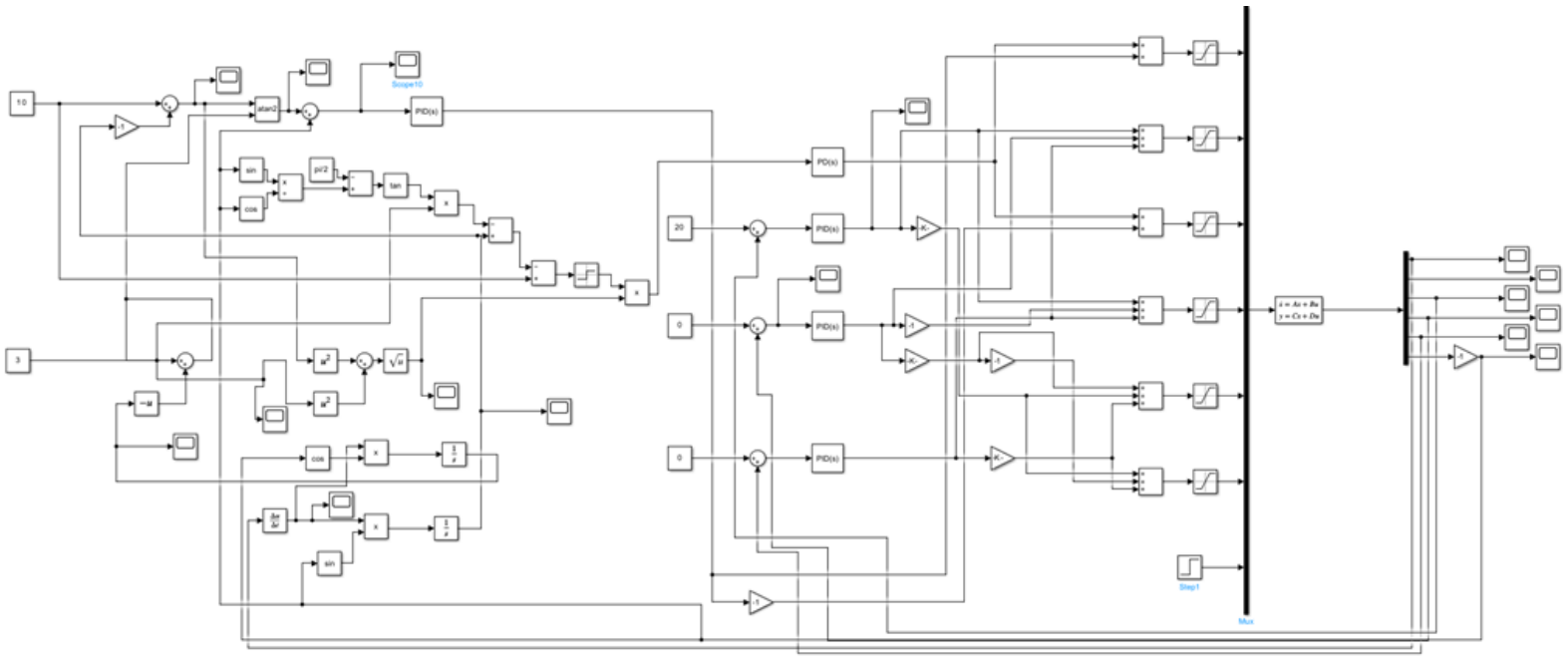

Figure 7.1: Screenshot of the developed control system (Simulink).

The state space model is the box that is in between the mux (left) and demux (right), which are the thick vertical lines on the right. As expected, the state space model takes in 6 control inputs and a step function for gravity. Via the mux, these inputs are matched to the dynamical model. From the columns of the matrix 'B' from the state space model, it can be shown why the 2 inputs are controlled by 2 PID's and 4 by 3 PID's. After these contributions are summed, they go through a saturation. This is explained in section 7.4.

From the old state and the inputs, the change in state and output are calculated. This goes through a continuous loop, and the outputs can then be plotted using the scopes to the right of the demux.

The 5 inputs to the system are the desired altitude (negative of z-position), the roll, pitch, x-position and y-position. These can be modified by the blocks that stick out on the left. The desired z-position was set to 20 metres because of the operational altitude and the roll and pitch to 0 for lateral and longitudinal equilibrium. Furthermore, the vehicle wants to fly to $(x, y) = (10, 3)$ in order to simulate how it moves.

The rest of the chapter will explain what the rest of the system does and how it was developed.

PID controls

The control system was developed that has several PID controllers in order to stabilise and go to a desired position. Figure 7.3 and 7.2 show what a PID controller does and give a schematic overview of the architecture for the altitude control.

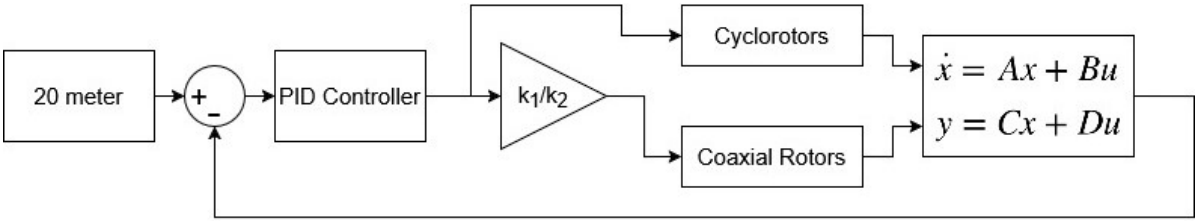

Figure 7.2: PID architecture for altitude control.

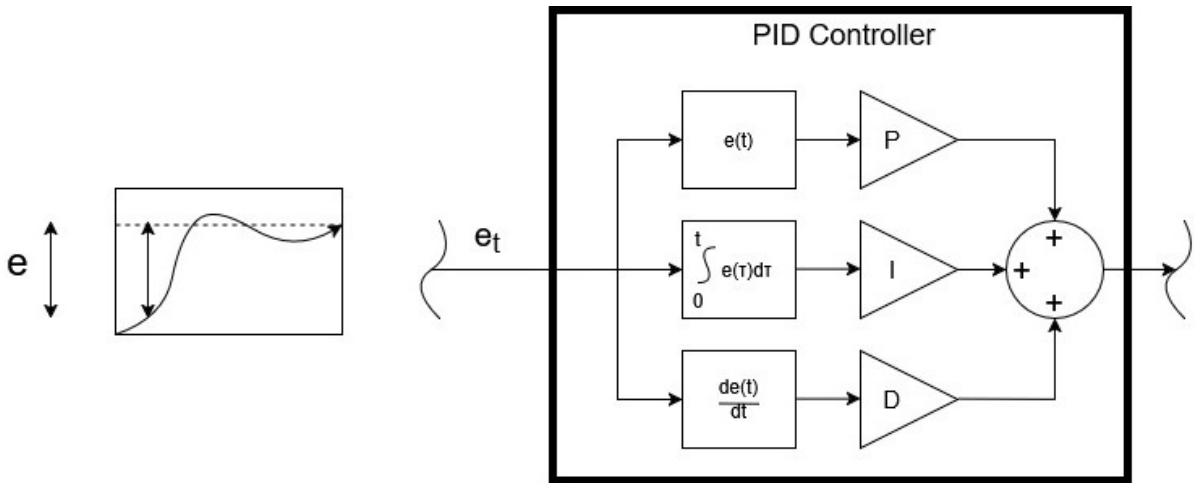

Figure 7.3: PID controller.

A PID controller takes in a signal, which is the comparison between an actual state component and the desired value. As an example, for the altitude, the Owl wants to climb to 20 metres. The differences give an error signal. Proportional to this error, a signal is fed through a gain. Therefore, the bigger the difference in state, the harder the cyclorotors and coaxial rotors will rotate in order to fly up. They are made sure to give the same lift by a correction of the lift efficiency ($k1/k2$). The problem is that the quadcopter will never reach the 20-meter altitude without the 'I' in PID. The propellers would shut off at 20 metres because the error signal is equal to 0. Therefore, the integral term is needed. This portion

counts the past error times in order to keep track of the error history. Using a gain of 'I', this makes sure that the vehicle will reach the desired altitude. The last gain D is used with a prediction of future errors. When the derivative of the error to time is either very big or very small, this component gives an opposing signal. This makes sure the vehicle does not overshoot too much, and goes to the desired position quicker.

The Owl-22 is designed to fly to a variable position and to an altitude of 20 metres. Therefore, the control system consists of 5 PID controllers to control the components of the output vector, with the x and y combined. This was done because the vehicle is designed to face the direction it wants to go and then move forward without tilting. This forward movement is in the xy-plane and by defining a distance, the model saves a controller. This method requires yaw control to work, however, this would already be done. As shown in the next section, the choice to control for yaw and distance instead of x and y comes with a challenge.

Distance Definition

The Owl-22 is designed to fly at zero pitch and roll, also when it is flying forward. Therefore, it makes sense to make controllers for yaw angle and distance to the desired position instead of the difference in x-position and y-position.

PID controllers assume an error term that can be both positive and negative. When the actual state is below the desired state, a positive signal will be given and vice versa. Now, for the distance definition, this is done with the Pythagorean theorem. Since $\sqrt{(x_{actual} - x_{desired})^2 + (y_{actual} - y_{desired})^2} > 0$ for every location, a PID controller will not understand if the vehicle is in front of or behind the desired position. This leads to the vehicle flying away from the desired position when overshooting, since it thinks it is still in front. Therefore, a section was made that modifies a combination of the signals for position and orientation relative to the desired position. This was included as part of the control architecture in order to give unambiguous information to the distance controller. Unfortunately, this part did not work out.

Saturation

If not for saturation, the model would be able to give any input that is preferred the most. For example, if the preferred height was 200 metres, then the propeller force would be 10 times higher. This, however, is not physically possible. Therefore, saturation was implemented in order to make the model realistic. This means that there is a limit to the radial velocity of the cyclorotors and coaxial rotors. For the cyclorotor, there is a maximum rpm of 1722 [1] and for the coaxial rotors it is 3266 [8]. Therefore, the mechanical limits of the 'h' inputs are calculated as follows.

$$\begin{aligned} h^*_{1,limit} = h^*_{2,limit} = \omega^2_{cyclolimit} = (1722 * \pi/30)^2 = 32517 \frac{rad^2}{s^2} \\ h^*_{3_{limit}} = h^*_{4_{limit}} = \omega^2_{coaxlimit} = (2654 * \pi/30)^2 = 77243 \frac{rad^2}{s^2} \end{aligned} \tag{7.4}$$

This puts an upper bound on how fast the propellers are allowed to rotate. However, by requirement REQ-SAF-ASC, it is not allowed for the vehicle to ascend quicker than 3 metres per second. Therefore, the control system was designed to have a limit lower than this. Trying out various limits gave the following results.

$$
\begin{aligned}
h_{3_{limit}} = h_{4_{limit}} &= 65000 \frac{rad^2}{s^2} \\
h_{1,z_{limit}} = h_{2,z_{limit}} &= 65000 \cdot (k_2/k_1) = 18700 \frac{rad^2}{s^2} \\
h^*_{1,x_{limit}} = h^*_{2,x_{limit}} &\leq \sqrt{(h^*_{1,limit})^2 - (h_{1,z_{limit}})^2} = \sqrt{32517^2 - 18700^2} = 26602 \frac{rad^2}{s^2} \\
h_{1,x_{limit}} = h_{2,x_{limit}} &= 18700 \frac{rad^2}{s^2}
\end{aligned}
\tag{7.5}
$$

The limits on h_3,h_4,$h_{1,z}$ and $h_{2,z}$ resulted from plotting the z-position and lowering the limits until the vehicle did not move upwards faster than 3 metres per second. Here, again, a factor of k_2/k_1 was used because of the different lift force that is created per angular velocity when comparing the coaxial rotors to the cyclorotors. Since the limits set by the control system in equations 7.5 are lower than the limits of the hardware given in equation 7.4, the control system will not require the propellers to rotate harder than they actually can. The limits on the horizontal component of the cyclorotors have to be below 26602 [$\frac{rad^2}{s^2}$], because the sum of the square of the horizontal and vertical components cannot be higher than the square of the mechanical limit. However, it was set to the same level as the vertical component since the horizontal component will never be higher.

Tuning And Plotting

In order to have a robust control system, the PID controllers went through a long tuning procedure. This was needed in order to make sure that the responses would be as efficient and comfortable as possible. By robustness, it is meant that the vehicle smoothly goes to its desired state. The opposite would be aggressive and would make the Owl respond uncomfortably to small disturbances. The plots that will be shown come from a single simulation, where the desired state is $(x, y, z) = (3, 10, -20)$ in metres. This also means that the vehicle should face in the direction of $\arctan(10/3) = 1.279$ radians, meaning yaw. To begin, the plot for the altitude is shown below in Figure 7.4.

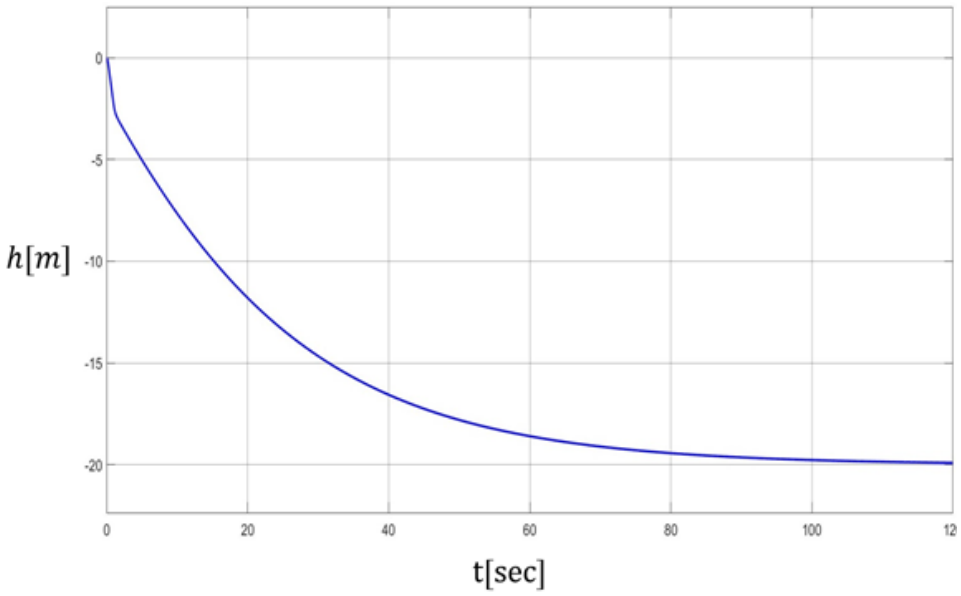

Figure 7.4: Z-position plot.

This plot shows the gradual climb to an altitude of 20 metres. Since the z-axis is directed downwards, the vehicle travels towards the negative z-direction. The absence of overshoot shows how pilot comfort was taken into account for the control system.

Next are the plots for roll and pitch. These are both controlled to stay at zero, meaning that a horizontal orientation would be preserved. The results are shown below in figures 7.5 and 7.6.

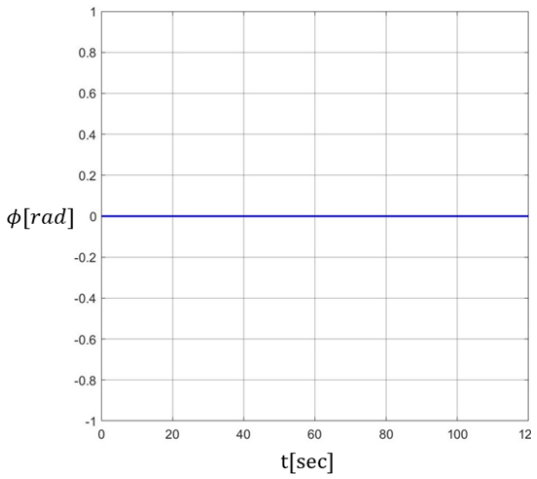

Figure 7.5: Roll plot

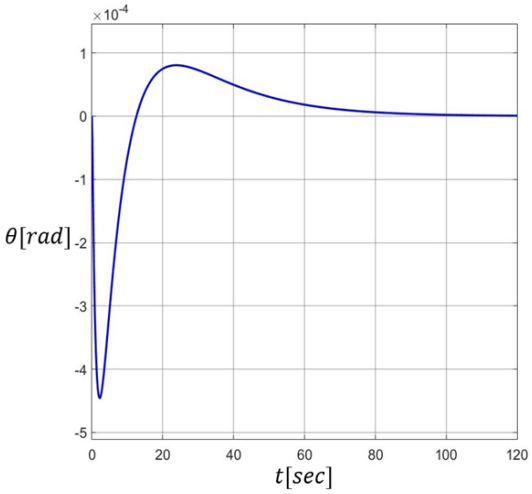

Figure 7.6: Pitch plot.

The plot for roll shows that in the simulation, no net roll moments are created. It was not possible to zoom in further. In order to be sure that roll control works well, it would ideally be tested with the presence of a disturbance. For the pitch control, there is a response during the take-off. However, the axis shows that this remains within $5 \cdot 10^{-4}$ radians from the horizontal position. This plot shows that the pitch correction control works well, that it gives a comfortable response and that the vehicle can move to a desired position in the horizontal plane without having to tilt. This would not be possible for a regular quadcopter.

For the yaw, the vehicle needs to go to an angle of -1.279 radians. The result is shown below in Figure 7.7.

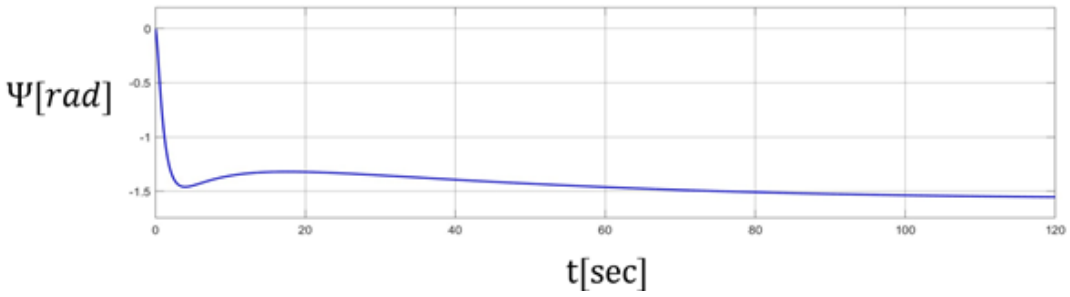

Figure 7.7: Yaw plot.

It can be seen that in about 4 seconds the vehicle is oriented in the right direction and then it stabilises. This is what is desired from the control system. However, after this, it approaches an angle of pi over 2. This means that the vehicle faces the y direction.

Lastly, there are the plots for the x and y positions in figure 7.8 and 7.9.

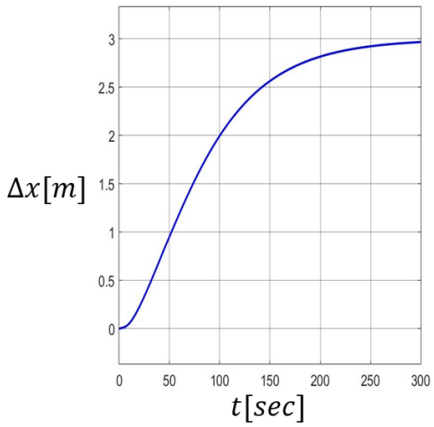

Figure 7.8: X-position plot.

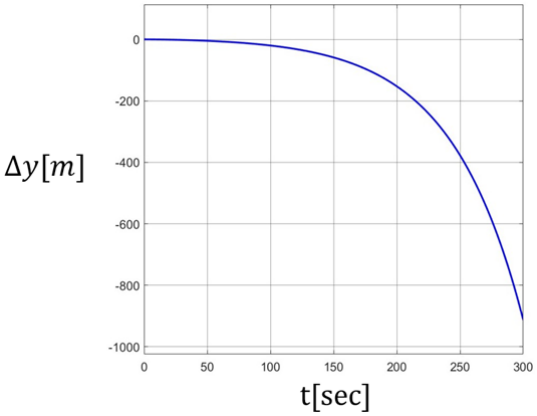

Figure 7.9: Y-position plot

Obviously, the control for the x-position succeeded and for the y-position it did not. From what can be read off, the vehicle goes to the desired x position of 3 metres. However, it accelerates in the y-direction. This means that the code that should account for the distance definition unfortunately did not work completely. Although the vehicle unintentionally flies off, the simulation shows that the vehicle does not need to tilt in order to go forward.

7.5. Verification and Validation

In this section, the verification and validation process of the control system model is presented. Here, the question of whether or not the model works as intended and whether or not the right model was built is answered.

Verification

For the verification and validation process of the control system, there has been looked at the responses of the different outputs have been examined. These consist of the following 4 measures: overshoot, delay time, rise time and settling time. These can be visually explained below in Figure 7.10.

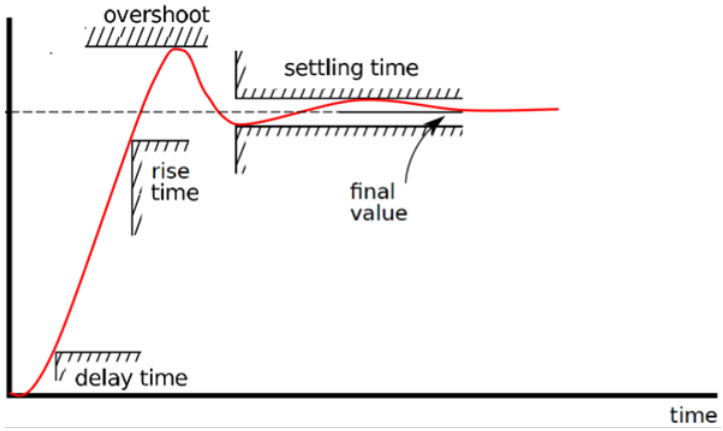

Figure 7.10: Response measures [90].

In the case of the study that was done, the delay time is defined as the time it takes for the response to rise to 10% of the final value. The rise time is defined as the time it takes to rise to 90% of the final value. The overshoot is defined as the maximum difference between the highest point and the final value. The settling time is defined as the time it takes for the response to enter a 5% difference from the final value for the last time without leaving this range afterwards. Below, the results of these measures are presented in Table 7.2.

Table 7.2: Verification table.

Overshoot[-]	Delay time[s]	Rise Time[s]	Settling Time[s]
Altitude			
N.A.	0.8963	51.1982	67.4306
Pitch			
-0.0255[rad]	N.A.	N.A.	56.1060
X-position			
N.A.	23.6574	211.2487	147.9224
Yaw			
N.A.	0.2321	1.3075	1.7065

These numbers display a comfortable experience for the pilot of the Owl-22 when travelling to an arbitrary position. However, the translation to the desired x-position takes a very long time. Therefore, the answer to the question of whether the model functions as it should would be answered by this. The model can translate differences in current states and desired states by giving beneficial output signals. For altitude, roll and pitch, it works perfectly. The simulation shows that the model slowly sends the vehicle to the desired x-position, but the control for the y-position doesn't work properly. For roll, the verification measures were also not applicable because of the final value.

Validation

Due to the realisation of the output vector, a model was built that intends to control the position and orientation. The user of the vehicle would, however, control the velocity. This means that a model was built that is more useful for an autopilot rather than a human pilot. Because of the autonomy ambitions of the Owl-22, the right model was built.

8 Structural Design and Integration

Much of the previous design phase focused on constraining the structural design through the configuration, lift device placement and seating position. As such, this chapter inherits these constraints and aims to iteratively converge to an optimal solution. First, the necessary requirements and budgets the structure would need to adhere by are discussed. Then, the design strategy is detailed, following that with preliminary and detailed sizing of the structural members. Informed by the aerodynamic considerations and Finite Element Analysis (FEA) simulations, the way the optimal design was converged on is detailed. Finally, the integration of subsystems and future recommendations are discussed.

8.1. Structures Requirements and Budgets

The requirements relevant to the structures design are presented in Table 8.1. Certain requirements still remain to be decided (<TBD>) at this stage of the design phase. The safety factor on the limit loads in **REQ-STR-LOAD** was set to 1.5 as recommended by the Federal Aviation Administration (FAA) and the European Union Aviation Safety Agency (EASA) [91, 92]. Furthermore, for **REQ-STR-PIL-01** the body height requirement was set to values corresponding to a range from the 5th percentile of female height data to the 95th percentile of male height data as is often used in designs with anthropometric (the study of body size ranges in a population) considerations [93, 94]. Also, the shoulder "width" requirement was reworded to a be a shoulder "breadth" requirement, a more precise definition when accounting for the shoulders width as well, setting the value to the 95th of male data with a small margin [95, 96]. Male data was used for the maximum values as they are on average higher than female numbers.

Table 8.1: Updated structures relevant requirements.

ID	Description
REQ-STR	The vehicle's structure shall support all mission phases - including ground handling, deployment, flight, and stowage - without permanent deformation or failure while minimizing weight and enabling single-person transport and operation.
REQ-STR-STAB	The vehicle structure shall remain stable and upright on flat urban surfaces under wind conditions up to <TBD> [m/s], without the need for external support or anchoring.
REQ-STR-LOAD	The structural components of the vehicle shall withstand all flight loads with a minimum safety factor of 1.5, without permanent deformation or structural failure.
REQ-STR-PIL	The vehicle shall be capable of transporting one pilot weighing up to 100 [kg] + 5 [kg] of utilities over a full mission cycle.
REQ-STR-PIL-01	The deployed structure shall provide a seating area that accommodates a pilot with a body height between 1.50 [m] and 1.94 [m] and a shoulder breadth up to 0.55 [m], without restricting control input or field of view during any phase of operation.
REQ-STR-TPT	The folded version of the vehicle shall be transportable by 1 person.
REQ-STR-TPT-01	The total mass of the fully assembled vehicle in its operational configuration shall not exceed 200 [kg], excluding the pilot and any external control device.
REQ-PHY-VOL	When fully folded for storage or transport, the vehicle shall fit entirely within a bounding volume of 4 [m^3].
REQ-STR-PROP	The structures shall house the propulsion elements, transferring the loads without discomfort to the user, or other systems.
REQ-STR-PROP-01	The displacement of structural members supporting the propulsion units shall not exceed 1/100th of the length of the supporting structural member.
REQ-OP-DEP	The vehicle shall be deployable from its fully retracted transport configuration to a flight-ready state by a single person in no more than 2 minutes.

What also should be noted is that **REQ-STR-PROP** and **REQ-STR-PROP-01** were added due to the consideration of integrating the propulsion and structures together. **REQ-STR-PROP** translated into a need for vibrational considerations, as well as volume considerations, and **REQ-STR-PROP-01** originated from the necessity of the propulsion system to be capable of fulfilling its lifting and control functions under the present structural deformations. The preliminary constraint on the displacement of coaxial rotor arms was set to be approximately 1/100th of the length of the arm, with a reference from existing quad-copter designs [97]. It should be acknowledged that this reference provides just a possible design, which has not been fully validated, and that the necessary deflection would not necessary scale with a large model. Nevertheless, the deflection angle of less than 1 [°] is assumed to be reasonable as a preliminary estimate to guarantee the functions of the propulsion system are fulfilled. With better knowledge of the control in future design iterations, a better estimate could be identified. **REQ-STR-PROP-01** would also have implications of the deformation constraint on the airframe as the propulsion integration arms would be connected to the structure itself, and with the airframe deforming, the connections would deform with it. For this reason, the maximum deflection of the body was decided to not exceed that of the coaxial arms by more than 50%. As a result, the sizing of the airframe would be both stress and displacement dependant, with the driving factor identified during the design.

Finally, the structure would need to stay within the budgets allocated to it in previous design reports. In particular, the mass allocated to the structure would have to not exceed 76 [kg], including canopy and interior, and the overall volume of the integrated structure with the propulsion would not exceed a volume of 4 [m^3], with **REQ-PHY-VOL** updated after renegotiating the requirement. This volume is defined as the bounding box around the vehicle without the consideration of wheels. In previous reports, this was budgeted for between the propulsion and the structures subsystems. However, since the structure would house the propulsion system, the budgeting here was done on the integrated system of the structures with the propulsions. Finally, although in previous design stages a certain percentage of the power budget was allocated to the structures for the folding mechanism, it was decided that it would not be electronically assisted, as detailed previously in the design stage reports. For this reason, no power considerations were made for the structures here.

8.2. Structures Design Strategy

While Al7068-T6511 was selected as the primary structural material due to its aerospace heritage, low cost and easy manufacturing, it is also overqualified for the Owl-22's flight profile, which experiences significantly lower loads compared to most aircraft. This left a lot of room to minimise the weight of the main load-bearing structure, which was done mainly through topology optimisation. A benefit of this method is the ability to form an initial idea about the stress distribution across a design [98]. By identifying the most loaded parts of the structure, a preliminary airframe was constructed and verified through a combination of simplified beam analysis and FEA. This pipeline is illustrated in Figure 8.1.

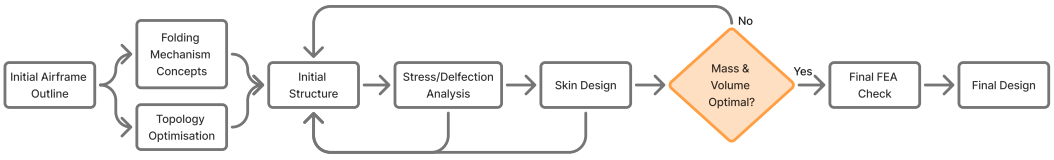

Figure 8.1: Structure design pipeline.

To perform the initial airframe outline design and topology optimisation, a host of Computer Aided Design (CAD) tools were considered, namely Rhino and CATIA. However, Autodesk's Fusion was chosen due to its versatile T-spline modelling technique known as *form*, as well as its shape optimisation tool which uses the well established Solid Isotropic Material with Penalization method (SIMP) [98]. By using Fusion, initial concepts could quickly be designed, iterated on and tested at a much faster rate than other CAD solutions. With this established, the initial outline for the outer airframe is presented in Figure 8.2a. The front of the vehicle resembles a typical aircraft cockpit, with the notable addition of two extruding elements on either side to account for the cyclorotor connection. At the back, the tip is raised in a generic spoiler-style configuration to account for the coaxial rotors. It should be noted

that this was not intended to be the final airframe outline and was to be iterated, with, for example, aerodynamic considerations. The outline's main purpose was to perform the topology optimisation, depicted in Figure 8.2b, where the colour key can be observed in Figure 8.2c. Red represents the region which needs most material.

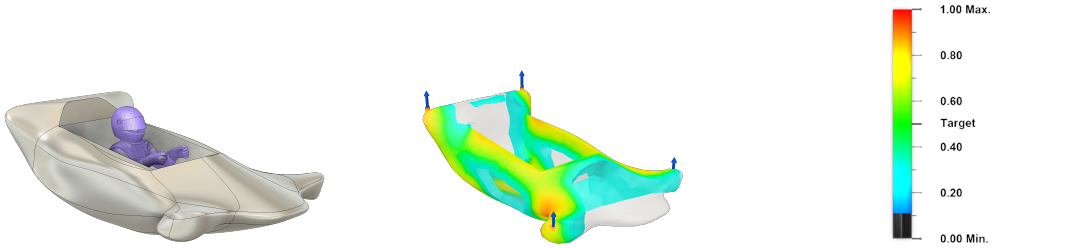

(a) Initial airframe outline. **(b)** Topology optimisation for initial outline. **(c)** Topology optimisation legend.

Figure 8.2: Initial airframe outline and topology optimisation.

Since topology optimisation operates using FEA, the load case and boundary conditions needed to be specified. For the loading case a combination of different situations were considered. The simplest case is the symmetrical, vertical loading case experienced during VTOL. There, the maximum thrust of the cyclorotor and coaxial propellers were used, since this represents the largest loads experienced by the structure during flight. This was tested alongside on-ground scenarios and the resulting optimisation netted a structure with similar key structural elements as in Figure 8.2b. For simulating the in-air load case, the structure was constrained at the bottom of the structure in the skin region where the person would sit. This generated a point-load-like reaction at the location of the constraint, simulating a static scenario in the local reference frame of the vehicle while in an inertial reference frame the vehicle is accelerating with maximum thrust output. This is returned to in more detail in Subsection 8.4.2, where the same boundary conditions are set for the FEA design iteration.

A limitation of this analysis was that the loads were introduced without consideration of how the propulsion system was to be integrated. This will be addressed in Subsection 8.3.2. Furthermore, topology optimisation generates structures which would be hard to manufacture without additive methods. Nevertheless, the main output from the topology optimisation was used as an inspiration for a simplified structure, which would have more easily manufacturable parts. Hence, returning back to Figure 8.1, with the topology optimisation performed, a very simple initial structure design was generated. This allowed to start sizing simple members by hand with simplifying assumptions, to then dimension a more streamline structure. Next, the design decisions were verified with a FEA to ensure confidence in complicated structure. Furthermore, the design was iterated to ensure compliance with other subsystems and volume and mass constraints.

8.3. Preliminary Sizing

The goal of the preliminary sizing was to determine the starting external and cross-sectional dimensions of the structural members. However, first the structural members needed to be identified. This was done with the consideration of a more streamline design, inspired by the initial airframe outline in Figure 8.2a and the topology optimisation in Figure 8.2b, for optimal structural members. Based on these, first a significantly oversimplified structure was proposed. However, under the assumption that the members are beam elements, even a simplified structure like the one outlined in grey in Figure 8.3 would be highly statically indeterminate due to normal, shear, and bending internal loads at each connection point carrying part of the introduced load. For this reason, the main structure was further simplified into two "L" shaped structure interconnected by one beam in the middle, and coaxial rotor arms to the side of the "L" members. For the "L" shape, the vertical part of the member would transfer the load of the coaxial rotor arms to the horizontal beam. The horizontal part of the "L" and the intermediate beam would carry the bending loads of both the propulsion devices, with the user weight also introduced through the intermediate beam. With the necessary dimension found for such an arrangement, the "lumps" of area could be redistributed into the real members, such that it would represent the structure in grey. Such a structure would be more applicable for housing a person, as it would have two horizontal

members on the sides. In other words, the preliminary sizing was performed on a “discretisation” of the structure and the results of the sizing informed the final design.

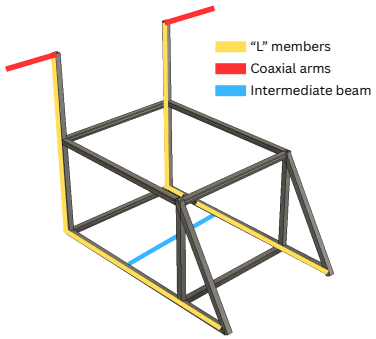

Figure 8.3: Simplified structure for preliminary sizing.

Since this would be a symmetric problem, for the preliminary analysis, the sizing was performed on one half of the structure. In asymmetric thrust conditions, some extra bending would likely need to be carried by the intermediate beam; however, as previously mentioned such a scenario would not be sizing as the asymmetric loads would not exceed the maximum thrust.

To size the external dimensions of the vehicle, **REQ-STR-PIL-01** was referenced, which limited the minimal possible vehicle dimensions. The initial guesses for the dimensions were set to 1 [m] width, 1.2 [m] height, and 2 [m] length resulting in a conservative 2.4 [m^3] for the volume with a margin accounting for the the integration of the propulsion and landing gears. These values were furthermore adjusted in the detailed design phase to accommodate for the volume constraint, as will be discussed in Section 8.4. However, before the sizing was performed, first, the loads were considered (thermal loads were assumed relatively negligible for the current sizing, given the operating conditions).

8.3.1. Weight Loads on Structure

While operating the vehicle, the user would introduce their loads onto the vehicle. For the maximal design conditions, the vehicle would need comply with **REQ-STR-PIL**, introducing a maximal total mass of 105 [kg]. It was assumed that this weight was distributed along the length of the structure supporting the user, for example, a beam, with 1/3 of the weight acting on the front part and 2/3 on the back part, where the main body of the person would be seated. This load was assumed to stay completely constant throughout the design iterations.

However, the user would also introduce more dynamic loads, while moving around in the vehicle or getting inside the vehicle. The dynamic loads are harder to account for. However, their consideration will be returned to during the detailed design. The battery loads on the structure will also be discussed in more detail in the detailed design alongside the positioning of the battery within the structure.

8.3.2. Propulsion Loads, Vibration, and Integration

When it comes to the loading from the propulsion devices, these were obtained from the propulsion subsystem with the maximum possible thrust provided by a single coaxial rotor and cyclorotor being 1669 [N] and 1499 [N] respectively.

The propulsion devices would also induce vibrational loads onto the structure. An approximation of the induced vibration on structure could be made using blade pass frequency calculated by multiplying the rotor speed by the number of blades [99]. This is used for calculating the frequency in helicopters and is assumed to be the major contributor of vibration from propulsion. The cyclorotors rotate at 1722 [RPM] [1], which is 28.7 [Hz] and with 5 blades, would result in an excitation of 143.5 [Hz] and its harmonics. In case of the coaxial rotor, both the bottom and top blades would rotate at 60% throttle at 2057 [RPM], or 34.3 [Hz], with two blades corresponding to a frequency of 68.6 [Hz] [8]. The angular position of the two blades would be offset, meaning that although the overall, vibrational frequency would remain the same, it would be less critical due to occasional destructive interference. It should be

noted that other sources of vibration would come from gusts and/or other aerodynamic effects, which were not evaluated at this design stage.

Besides the loads, the propulsion subsystem also created implications for the 4 [m^3] volume constraints set on the system. Namely, the spacing between coaxial rotors needed to be respected to avoid interference between the blades. Furthermore, to minimise volume, the top coaxial rotor would be positioned on the same vertical level as the highest point of the structure; the connecting arm would have to extend enough such that the lower blade would not collide with the structure. These considerations are depicted in Figure 8.4. The spacing between the top blades would need to be 20% of the rotor radius, meaning 0.1625 [m], and the spacing between the structure and the lower blade would need to be 10% of the lower propeller radius, meaning 0.07 [m] spacing from the structure [16]. This meant coaxial arms of at least 0.24 [m] to ensure sufficient inter-propeller spacing and arms of at least 0.76 [m] to ensure sufficient body-blade clearance. With the body-blade clearance sizing, a value of 0.8 [m] was chosen.

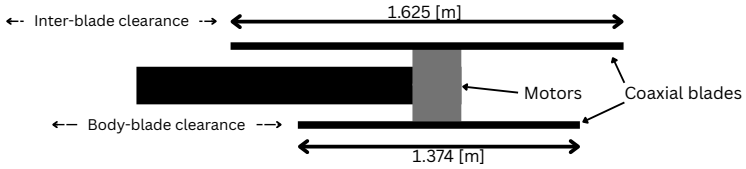

Figure 8.4: Coaxial rotor integration.

The dimensions of the newly selected cyclorotors would need to be considered as well. For the preliminary design it was assumed that with the connecting struts of the cyclorotors in the structure, they would span a maximum of 0.84 [m] outside of the body on either side [1]. They would be connected directly to the structure on the sides.

Finally, with the integration of the propulsion devices decided their torsional loads would need to be considered. In particular, since the coaxial rotors would be connected via an extending arm, as can be seen in Figure 8.4, they would not create a direct torsional load in the arm. Instead, they would introduce a torsion at the connection point, translating a bending moment into the arm. This value can be found to be 140 [Nm] [8]. When it comes to the cyclorotor, they would be connected to the structure by the two horizontal members extending from the triangular structure in Figure 8.3. This means that they would introduce a torque of 300 [Nm], which was calculated using Equation 8.1 [100],

$$T = \frac{P \cdot 9550}{RPM} = \frac{9550}{1722} = 292\ [Nm] \tag{8.1}$$

where P is the power in [kW] and RPM is the maximum rotational speed in [rpm], provided by Cyclotech [1]. To ensure a conservative estimate, the final value is rounded up to 300 [Nm]. In the final structure, the torque introduction would like in Figure 8.5.

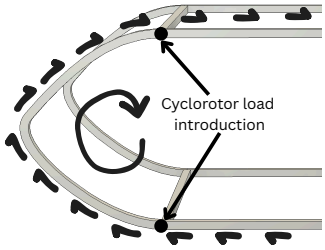

Figure 8.5: Cyclorotor integration and torque load introduction.

8.3.3. Loading Scenarios

In the previous reports, the design of different components was proposed for the different flight stages, designing the landing gear for on-ground operations, the coaxial rotor connections for take-off and landing, and the cyclorotors integration for cruise, where it would need to provide both thrust and lift. Designing for the critical flight conditions would ensure it would not fail in other nominal conditions. However, for the current design, the critical in-air design scenario was assumed to be the situation where the propulsion devices provide maximum thrust output vertically. In nominal operations, such thrust would never be provided and would never occur during cruise. As such, the sizing would also account for differential thrust conditions in cruise and engine failure scenarios. The wheels and certain parts of the skin; however, would still need to be evaluated during on-ground operations.

8.3.4. Preliminary Member Sizing

With the driving loading scenarios identified and the maximum propulsion loads found the preliminary sizing could be performed. However, to comply with **REQ-STR-LOAD** a slightly different approach was used than in the aviation industry, applying the safety factor on the allowed stress rather than on the loads, since the propulsion units could not produce higher than their maximum thrust. This mathematically yields the same result. In fact, this would most likely lead to an overdesigned structure, mainly due to the fact the propulsion devices would never operate at the maximum settings, and they would not be able to operate above them. Future designs would have clearer estimations of the operational limits, and more optimal sizing could be performed. This is especially relevant because at the maximum take-off weight, the maximum thrust setting of all propellers would result in a load factor above 2:

$$\frac{1669(2) + 1499(2)}{305(9.81)} \approx 2.1 = \frac{L}{W} \tag{8.2}$$

where L is the lift produced by the lift devices and W is weight of the vehicle. The obtained load factor could perhaps be a setting too high for the everyday user.

The material proprieties used for the the sizing can be seen in Table 8.2.

Table 8.2: Main airframe material properties.

Material	**Density([kg/m^3])**	**Young's Modulus([GPa])**	**Yield Strength([MPa])**
Al 7068-T6511	2850	71	650

Sizing the ``L'' Member and Intermediate Beam

For the sizing, it was early identified that the vertical member, loaded mainly in tension, would not be sizing if the “L” shaped beam was one continuous part, which would be beneficial for manufacturing and load introduction. To carry the tensile load introduced by the coaxial rotors, for example, this member would need an area of $2.42 \cdot 10^{-6}[m^2]$:

$$650 \cdot 10^6 = \frac{1669}{A}, \quad A = \frac{1669}{650 \cdot 10^6} = 2.42 \cdot 10^{-6}[m^2]$$

or around $4 \cdot 10^{-6}$ [m^2] rounding up with the 1.5 safety factor. This would correspond to, for example, a solid square cross-section with 2 [mm] sides, with a cross-section like this most definitely performing worse in bending and under compressive loads. The tension or compression induced by the 300 [Nm] torque of the rotating cyclorotor, as presented in Figure 8.5 would not generate a significant loads, as it would be introduced into the bending of those beams and the compression and tension of the side-members. Similarly, as could be expected for slender long beams, it was also not limited by failure under shear loads. However, for shear and bending sizing the cross-section first needed to be decided upon. For preliminary sizing, the “L” members were assumed to have a hollow square cross-section. A closed cross-section was chosen to avoid warping torsional effects in a 3D structure more effectively, and a square was chosen over a circular cross-section for easier assembly between the members and the skin. It should be noted that in future designs the square cross-section could be further optimised for the exact aerodynamic profile, and that it allowed for the optimal folding mechanism introduced later.

To simplify the initial sizing, thin-walled approximation was used. Without the simplification it would be more difficult to solve for the dimensions of the cross-section. The simplified second moment of area would be:

$$I_{xx} \approx 2(\frac{1}{12}ta^3 + \left(\frac{a}{2}\right)^2 ta) = \frac{2}{3}ta^3 \tag{8.3}$$

where a is the side of the square-cross section and t is the thickness.

Assuming that the bending moment of the coaxial propeller arms would act through half of the distance of the horizontal beam, that would result in a bending moment of 1669 [Nm]. Hence:

$$\frac{1669(a/2)}{\frac{2}{3}ta^3} = \frac{650 \cdot 10^6}{1.5}, \;\; ta^2 \approx 2.89 \cdot 10^{-6}[m^3] \tag{8.4}$$

The mass per length ($\bar{m}$), can be represented as:

$$\bar{m} = \rho A \approx 4\rho at = 4\rho \frac{2.89 \cdot 10^{-6}}{a} \tag{8.5}$$

where ρ is the material density. Hence to optimise for the mass of a thin-walled hollow cross-section, it would be best to decrease the thickness, while increasing the lengths of sides of the square cross-section. This is not surprising as parallel axis theorem contribution scales with the square of the distance.

For this reason, the thickness of the square cross-section was constrained to a minimal value first, yielding the necessary length of the sides for the cross-section. This was done with manufacturing, buckling, and assembly considerations in mind. In particular, extrusion was chosen as it is cost and material efficient for long hollow section production, and with reference to extrusion manufacturing capabilities of similar alloys, 5 [mm] was chosen as a realistic minimum thickness [101]. This minimum value was also informed by the fact the element would have to be connected to skin, which itself would not be much thinner than 1 [mm], as will be discussed later. This resulted in the necessary square dimension of:

$$a = \sqrt{\frac{2.89 \cdot 10^{-6}}{5 \cdot 10^{-3}}} = 0.024[m] \tag{8.6}$$

However, now the thin-walled assumption needed to be verified as the actual second moment of area is given by:

$$I_{xx} = \frac{1}{12}a^4 - \frac{1}{12}(a - 2t)^4 \tag{8.7}$$

and would give the value of $2.44 \cdot 10^{-6}[m^4]$, while the thin-walled approximation gives $4.608 \cdot 10^{-6}[m^4]$. As this is a order of 2 magnitude overestimation of moment of inertia, the following equation could be solved numerically:

$$\frac{650 \cdot 10^6}{1.5} = \frac{1669a/2}{\frac{1}{12}a^4 - \frac{1}{12}\left[a - 2(\frac{5}{1000})\right]^4} \tag{8.8}$$

leading to a value of $a = 3.1[cm]$. As a sanity check, the shear stress could be approximated using

$$\tau = \frac{VQ}{I_{xx}t} = \frac{1669}{2.44 \cdot 10^{-6}} \left[\left(\frac{3}{200} - \frac{5}{1000}\right)\left(\frac{3}{200}\right)\left(\frac{5}{1000}\right) + \left(\frac{3}{400}\right)\left(\frac{3}{200}\right)\left(\frac{5}{1000}\right)\right] \tag{8.9}$$

where V is the internal shear, and Q is the first moment of inertia. This results in a maximum shear stress of 0.2 [MPa]. It should be noted that even though this equation should be used for thin-walled cross-section and as previously shown, that assumption is not fully true. However, it is a reasonable order of magnitude check. The displacement considerations of the “L” structure will be returned to during the detailed design.

When it comes to sizing the intermediate beam in Figure 8.3, it would have to carry approximately twice the force. However, over half the distance, relative to the "L" member, the moment in Equation 8.8 would not change for it. With this also beneficial for assembly, the intermediate beam would have the same cross-section dimensions as the "L" member.

Sizing the Coaxial Arms

Before sizing the skin, the arms depicted in Figure 8.4 would have to be sized, as their weight would be important for designing the skin. To size for them, it would be necessary to ensure that they would not yield nor would they displace more than a 1/100th of their length as per **REQ-STR-PROP-01**. For the cross-section of the arms, a hollow circular section was selected, as this is optimal for bending. The second moment of area of this hollow cross-section can be found using:

$$I_{circ} = \frac{\pi d^4 - \pi(d - (2(5))/1000)^4}{64} \tag{8.10}$$

where d is the diameter of the cross-section and the thickness of the member has again been fixed to 5 [mm] due to the same reasons as in the square cross-section. Using the beam bending equation, Equation 8.11 could be set up with the maximum allowable deflection set to 0.8 [cm] as per **REQ-STR-PROP-01**.

$$\delta = \frac{0.8}{100} = \frac{1669(0.8)^3}{3(71 \cdot 10^9) I_{circ}} \tag{8.11}$$

Solving it numerically gives a necessary diameter of 6.83 [cm]. The necessary diameter to prevent yielding, with a safety factor of 1.5, can be found using Equation 8.12:

$$\frac{650 \cdot 10^6}{1.5} = \frac{[1669(0.8) + 140]d/2}{I_{circ}} \tag{8.12}$$

where the generic flexure formula is simplified for a symmetrical structure and the total moment contribution of the coaxial lift and torque, which induces moment, as discussed previously. Solving it numerically gives a necessary diameter of 3.60 [cm]. This means that the deflection condition is sizing. As a result, the dimensions of the hollow circular section would be set to a diameter of 7 [cm] and a thickness of 5 [mm].

Skin Design

With reference to Figure 8.2a, for aerodynamic, visual, and electronic protection purposes, the front and back parts of the vehicle would also be covered with aluminium skin. For reasons mentioned in Section 8.4, the side skin and floor would be designed separately. However, to analyse the stresses induced in the skin due to the connection with the structural members, the skin thickness would need to be decided. For this, aircraft were referenced, where the thickness tends to be in the 0.5-2 [mm] range [102]. Choosing the lower bound of this range would guarantee a safe yet weight optimal solution; there would likely not be the need for higher thickness, as such thickness is sufficient for aircraft. However, making it thinner would be associated with manufacturing and performance risks. Hence, the thickness of 0.5 [mm] was decided upon.

The critical case in tension of the skin would come from the back panel, which would induce the load from the two coaxial rotor arms. However, the skin would not carry a negligible part of the force, hence:

$$F_s + 2F_m = 3338[N] \tag{8.13}$$

where F_s is the force in the skin panel, and F_m is force in the member. Furthermore, assuming perfect joints and that the length of skin and E are equal for both, compatibility states that:

$$\delta_{skin} = \delta_m, \quad \frac{F_s L}{E A_s} = \frac{F_m L}{E A_m}, \quad F_m = \frac{A_m}{A_s} F_s \tag{8.14}$$

where δ_{skin} and δ_m are deflection of skin and the member respectively. Solving Equation 8.13 and Equation 8.14, using the skin width of 1 [m], from external dimensions, leads to an induced force of

1112.7 [N] in the skin, leading to an induced stress of 2.23 [MPa]. This the skin can withstand. However, the buckling is more critical.

In particular, the critical stress for buckling of the panel, assuming simply supported boundary conditions at the connection points of the panel, could be calculated using Equation 8.15 [103]:

$$\sigma_{cr} = 4\frac{\pi^2 E}{12(1-\nu^2)}\left(\frac{t}{b}\right)^2 \tag{8.15}$$

where ν is the Poisson ratio (about 0.33 for metals). The resulting critical buckling stress is 0.066 [MPa]. The actual compression load would come from the weight of the coaxial rotors, the coaxial rotor arms, the horizontal part of the "L" member and the skin above itself. The total mass would equal about 25.4 [kg]. Under the assumption that this load would be split between the skin and the vertical members as in Equation 8.13 and Equation 8.14, this would result in a load of 83.1 [N] and a stress of 0.166 [MPa]. As a result, the back panel would need to be reinforced with stiffeners to prevent buckling. An empirical equation for aluminium alloys, Equation 8.16, showed that L stringers with side lengths of 2 [cm] and a thickness of 2 [mm] would cripple:

$$\frac{\sigma_{cc}}{\sigma_y} = 0.8\left[\frac{0.425}{650\cdot 10^6}\frac{\pi^2(71\cdot 10^9)}{12(1-0.33^2)}\left(\frac{2/1000}{2/100}\right)^2\right]^{1-0.6} = 0.57 \tag{8.16}$$

Since an L stringer is composed of two equivalent area rectangles, this would correspond to a crippling stress of 370 [MPa] and using this stiffener for the skin would give the new buckling stress of 25.6 [MPa] via Equation 8.17.

$$\sigma_{cc_{pannel}} = \frac{\sum \sigma_{cc} A_{stif}}{A_{stif} + A_{skin}} \tag{8.17}$$

8.3.5. Preliminary Sizing Takeaways

The major takeaway from the preliminary structural analysis was that, as was expected, the loads acting on the vehicle are relatively small, and a relatively light structure can be employed. However, with the integration of the propulsion units, the volume bounding the vehicle would become:

$$Vol = 4.225 \cdot 2 \cdot 1.2 = 10.14[m^3] \tag{8.18}$$

Although it is possible to define the volume in different ways, the coaxial rotors would be an inconvenience to the user. For this reason, to abide by **REQ-PHY-VOL**, some sort of folding mechanism would need to be employed, and since the structure is relatively light, it would be possible to trade mass for volume. Additionally, what the preliminary sizing showed was that the vertical part of the "L" is not that demanding in tension, the member could be made more streamline, transition from the vertical member into the horizontal member, and it could follow the contour of the final external skin. This way it would be easier to make it look something like Figure 8.2a.

8.4. Detailed Design

The preliminary design gave the dimensions for the simplified structure. In this section, these dimensions will be translated into a more streamlined structure, such as the one depicted in Figure 8.6.

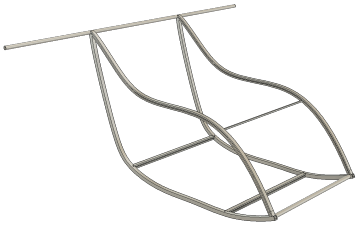

Figure 8.6: First airframe concept.

Furthermore, with the insight from the preliminary sizing, the approach to the design was informed by the necessity of folding the vehicle to fit the 4 [m^3] requirement. For this reason, the folding mechanism will be discussed first, with the decisions for the design of the main airframe and the structure supporting the user in the vehicle informed by the folding mechanism. Furthermore, since FEA was performed on the airframe without the folding mechanism, appropriate safety factors will be set and the reliability of the results will be discussed. To assist in meeting the volume constraint, the airframe dimensions were also adjusted, decreasing the width from 1 to 0.9 [m] and the height from 1 to 1.2 [m].

8.4.1. Folding Mechanism

With the coaxial rotor arms extending outside the vehicle, alongside the dimensions of the actual blades, see Figure 8.4, folding the arms would be an obvious first step in reducing the volume of the bounding box around the vehicle. Such technologies have already been tested and implemented in, for example, Jetson One [104]. However, it should be noted that the Jetson One weighs less, and the implementation of such a mechanism would need to be extensively tested. The detailed design of the folding arms will not be discussed here. However, when discussing future mass optimisations, the dimensions of the arms supporting the coaxial rotor will be reconsidered. Even with the coaxial arms folded, though, the cyclorotors would bound the width of the vehicle at 2.590 [m^3], resulting in a bounding box of:

$$Vol = 2.590 \cdot 2 \cdot 1 = 5.18[m^3] \tag{8.19}$$

With the new airframe dimensions mentioned in the introductory paragraph. As a result, the volume constraint would still not be met.

For this reason, it was decided to fold the structure down the middle with telescoping hollow square cross-section beams. However, now the vehicle would need to fold right where the person would be sitting. Hence, the structure was formalised more clearly by splitting the analysis into two parts. The first part would be the main airframe (consisting of the members sized in the previous section), which would be responsible for carrying the propulsion loads, as well as the user-induced loads transferred to it through the user-supporting structure. The user-supporting structure would then consist of the floor, seating, side-skin, and interior of the vehicle, so the parts with which the user would directly interact with. Both of the sub-parts of the structure would facilitate the folding, as depicted in Figure 8.7. The canopy would be raised in the folding process, coming back over the folded airframe, with the coaxial rotor arms folding by its side. Finally, since cables would likely be running throughout the vehicle, some sort of slack guiding would be necessary along the structure.

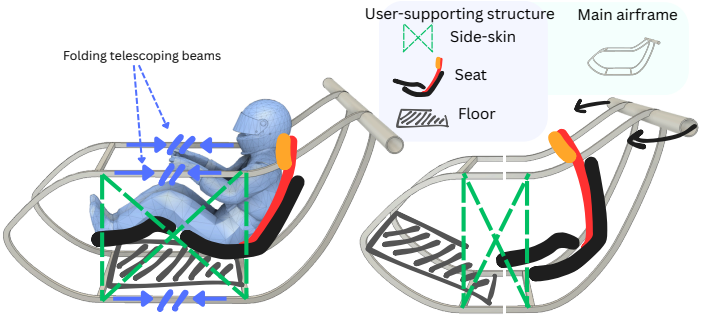

Figure 8.7: Folding concept visual.

However, the telescoping beams would now be positioned in a critical structural location and to guarantee safety in flight, a safety factor for the design would be necessary. Furthermore, the two halves of the telescoping beam would now necessitate different cross-sectional areas to allow the members to slide into each other. Also, with the structure folding down the middle, **REQ-STR-STAB** would still need to be ensured, preventing tip-over.

Now, to meet the volume requirement, if it was to be defined as specifically fitting the vehicle in a bounding box of 4 [m^2], the length of the vehicle would need to be reduced to 1.6 [m]. To reduce the

length of a telescoping beam by 0.4 [m], the length of the folding section would need to be at least 0.8 [m], with a region of intersection, for the pin preventing folding of the structure mid-air. This would mean that at least 0.8 [m] of the side members would have to be flat, allowing for the folding. In the initial CAD model, the flat section of the telescoping beams was indeed set to be 0.8 [m]. However, the beams would also need to intersect at some point. For this reason, the total flat section of the telescoping beam would have to be larger than 0.8 [m]. Alternatively, the telescoping beam could be split into several parts. This would be more volume efficient, but it would introduce the need for higher safety factors. The two concepts are presented in Figure 8.8 with "o" depicting the overlap length between the beams.

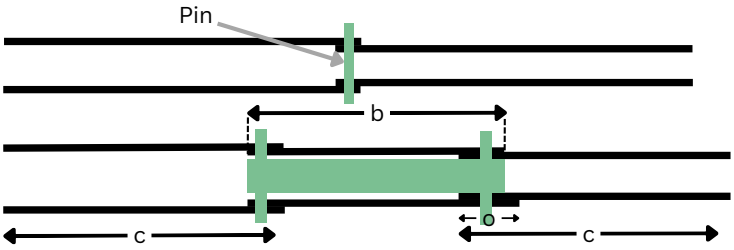

Figure 8.8: Telescoping beam concepts.

Prior to deciding between the two mechanisms, the pin joints fixing the telescoping beams in place needed to be sized first to get an insight into the necessary dimensions of the overlap between the telescoping beams. The pins would ideally be positioned along the neutral axis of the telescoping beams to avoid unnecessary bending stress. They would fail under shear, and although the cyclorotor torque would be a contributing factor in flight, trying to pull one part of the telescoping beam away, while the other is pushed in, as depicted in Figure 8.5, the preliminary sizing was done with a force of 1000 [N]. This magnitude of load could be a superposition of a dynamic load of a person "falling" onto the seat and transferring some of their weight in the horizontal direction, tensile propulsion loads in flight. However, even with such a load, the necessary area of the pin (A_{pin}) would be:

$$A_{pin} = \frac{1000}{325 \cdot 10^6} \approx 3.1 \cdot 10^{-6}[m^2] \tag{8.20}$$

which would correspond to a square cross-section pin of 2 [mm] sides. As a result it would be very easy to over-design the pins with a high safety factor. This meant that the intersection region between the telescoping beams could be relatively small, and it was reasoned that it would be beneficial to use a three-stage telescoping beam to save more length while folding the mechanism. To facilitate maximum folding, the dimensions "b" and "c" would have to be equal in Figure 8.8. With the constrained length of 0.8 [m] and a fixed overlap length of 5 [cm], which would be sufficient for the pin and would not result in critical stresses under transfer of bending moment, this would result in:

$$0.8 = 2c + (b - 2o), \quad 0.8 = 2c + (c - 2o), \quad c = \frac{0.8 + 2(5/100)}{3} = 0.3[m] \tag{8.21}$$

Hence, the flat section of the beams could be folded from 0.8 to 0.3 [m], saving 0.5 [m] of length and reducing the bounding box volume to:

$$Vol = 2.590 \cdot 1.5 \cdot 1 = 3.885[m^3] \tag{8.22}$$

As a result, if the flat section of the beam were made longer, increasing the part of the structure that could fold, even more volume could be saved. However, there would also be the need to prevent the telescoping beam from "pulling-out" during deployment. Furthermore, for easier deployment, it would be ideal to make the sliding of the beams relative to each other as smooth as possible. For this, the proposed folding mechanism is presented in Figure 8.9.

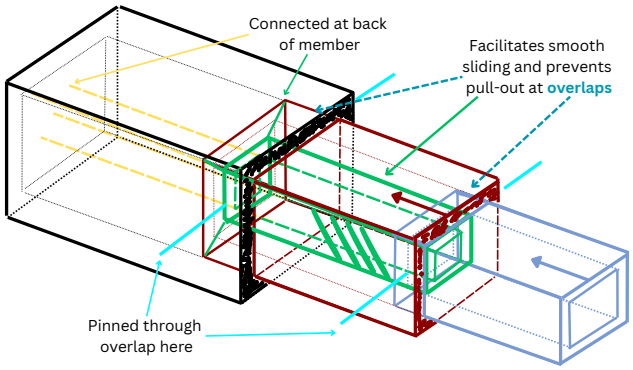

Figure 8.9: Proposed folding mechanism.

In Figure 8.9, the black and blue members are flat parts of the structural members depicted in Figure 8.7, extending further out into the structure. The rear element is the black one. The green beam is connected to the end of the middle beam, allowing the blue member to slide in. The green member simultaneously acts as a way of ensuring smoother deployment and preventing pull-outs during deployment via sliders. In the case of the rear beam, the slider is connected using the yellow bracket introduced during the assembly. The yellow bracket slides into the green member, while the blue member slides over the green beam.

8.4.2. Main Airframe

With the preliminary design of the airframe completed, it needed to be finalised and verified using FEA. In particular, firstly, the results of initial sizing needed to be translated to a more streamlined design, like the one in Figure 8.6. This would involve manufacturing considerations and cross-section dimensioning based on preliminary sizing and the new safety factors, due to the folding mechanism. When it comes to manufacturing considerations, the folding mechanism would be advantageous, allowing for splitting of the side member of the airframe, similarly to how it is depicted in the right image of Figure 8.7. This would allow to the manufacture the hollow parts with extrusion, as previously suggested, without more complicated techniques, which would be necessary for a closed member.

FEA Analysis Strategy

To verify the design, an FEA was performed on the design iterations. Since this was performed in Autodesk's Fusion, there were certain limitations to the simulations that could be performed. For one, simulating the condition of the aircraft in the air would necessitate different boundary conditions than the ones available in Fusion. To circumvent this, the structure was constrained at the bottom of the airframe with a beam which was not part of the airframe, as shown in Figure 8.10.

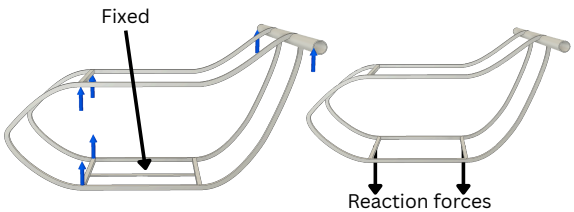

Figure 8.10: FEA boundary conditions simulation setup.

The reaction forces would simulate the weight from the human and the structure, which would be reasonable as the structure was indeed split into the user-supporting and airframe. Even though the reaction forces would likely be an overestimate, not all of the weight would be introduced through the

floor structure, with both the battery and the human introducing their weight in that part of the airframe, this was deemed a reasonable way of setting up the analysis.

When it comes to FEA, its results were split into displacement results and stress considerations. The displacement considerations were first used to check the convergence of simulation runs with different mesh sizes. The results of the convergence study can be observed in Figure 8.11. It was decided that a mesh with more than $2.5 \cdot 10^6$ nodes was sufficient for the current model. The results were deemed reasonably convergent when the displacement values were within a millimetre of each other.

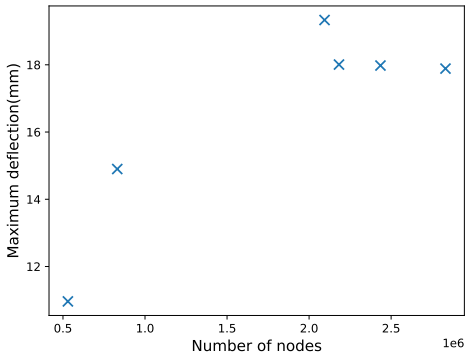

Figure 8.11: Convergence of FEA simulation results.

Secondly, the displacement results gave an insight into the deflection of the vehicle, and particularly, the amount by which the coaxial rotor arms would deflect under the loads. This needed to be verified to be within the **REQ-STR-PROP-01** requirement. It should be noted that as the airframe would also deform, and for this reason, the threshold of 20 [mm] was set as the initial constraint. It should further be reiterated that this constraint would need to be fulfilled for the FEA. However, with the introduction of the folding mechanism, the final deflection would differ and hence in future design iterations, FEA on the structure with the folding mechanism would have to performed.

8.4.3. FEA Member Resizing

With the simulation set up, two simulations were ran. Both had the same external dimensions, which were previously determined for the necessary fitting of the human in the vehicle. However, the cross-sections of the hollow square elements were varied, which was done in the context of the necessity of having different cross-sectional properties for a telescoping beam. The thickness remained the same, while the sides were increased from 3 [cm] to 4 [cm]. Furthermore, the diameter dimension of the coaxial rotor arm was increased from 7 [cm] to 8 [cm]. This allowed to comply with **REQ-STR-PROP-01**, decreasing the deflection of the structure from 34 [mm] to below 20 [mm]. The final result for the displacement can be seen in Figure 8.12.

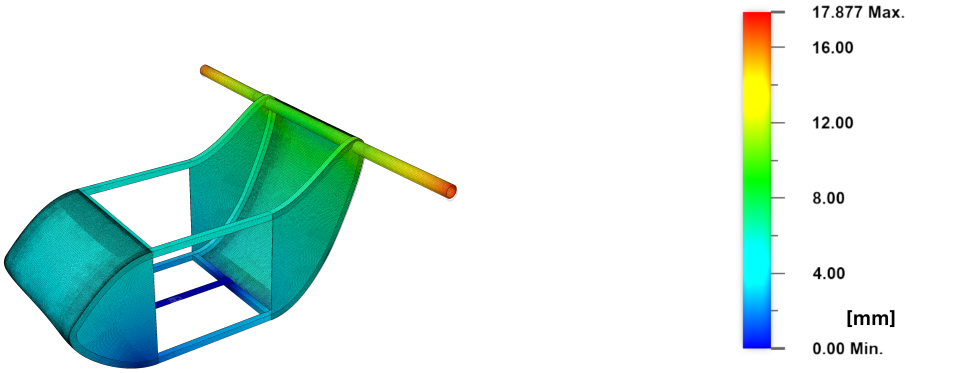

(a) Final FEA displacement diagram. **(b)** Final FEA displacement legend.

Figure 8.12: Final design FEA displacement results.

Note that the bottom panel does not deflect as it is modelled as a fixed constraint, as detailed in Figure 8.10. Since the beam would not be part of the actual structure, that is to be expected. This result was interpreted to be sufficient.

However, there still would be a disconnect between the real structure and the FEA results as the analysis was performed without the telescoping beams. For this reason, the stress analysis results were also referenced. In particular, the stresses in the parts where the folding mechanism would occur were studied in both the 3 [cm] and 4 [cm] FEA results. In both cases, the resulting stress in the members had a safety factor larger than 9. However, to facilitate the folding, the cross-sections would also need to be accessible and assembly would have to be possible. The cross-section dimensions were hence chosen to be 3 [cm] in the front, 4 [cm] for the intermediate telescoping beam, and 5 [cm] for the rear half of the structure. For other members not limited by such constraints, such as the intermediate beams, they will be optimised using the approach discussed in Subsection 8.6.2.

The final contribution of the stress analysis was instilling confidence in the design of the regions where connections would be made, as well as the skin rivet locations, which would lead to stress concentrations. It should be noted that this was done only for skin in tension, as more complex methods than the FEA in fusion would be necessary to study the skin under buckling. The preliminary hand calculations were deemed sufficient to guarantee the necessary performance in this failure mode. The main use case of FEA here was to identify regions of low stress in the interconnection between the skin and the stringers, as depicted in Figure 8.13a. This would verify that the skin could be joined with rivets there, even with a concentration factor of 4. The spacing of the rivets could then be identified in future development stages. What also could be observed from Figure 8.13b is the highest stress region, which happened at the interconnection between the boundary condition used for modelling the reaction forces. Such local effects were neglected as they were localised errors.

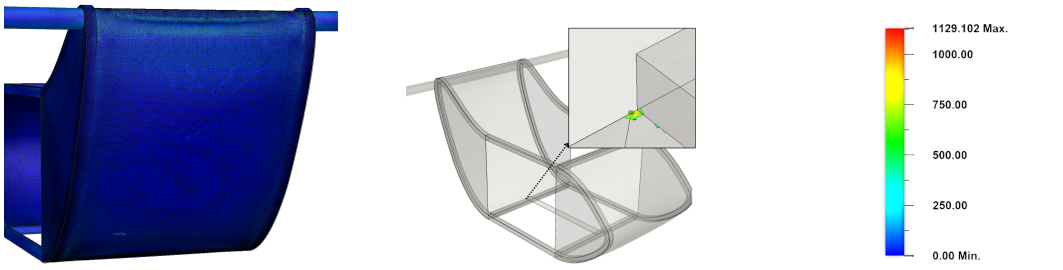

(a) Back panel stress. **(b)** Topology optimisation for initial outline. **(c)** Final FEA stress legend.

Figure 8.13: Final Design FEA stress results.

On a final note, the following design would fit constraints set on it, with a safety margin of around 3 on

the most critically loaded members, which happened to be the coaxial rotor arms, and a safety factor of 6 on the region where the folding mechanism would be. This is a significant overdesign also due to the deflection constraint, and future design iterations could aim to decrease the mass further through a more detailed analysis of the folding mechanism and a better estimate of the allowed deflections of coaxial rotors.

8.4.4. Vibrational Analysis

Due to the scope of the current design and the time-consuming convergence studies, the vibrational analysis was not performed using FEA. Instead, preliminary estimations were made for lateral vibration (since the beams would be long and slender) using the assumption that in the final structure, the beams would act as if fixed joints between the connection points, as pin joints would significantly underestimate the stiffness. It was deemed more reasonable to look at the critical members than the whole structure, to not ignore localised effects. For this Equation 8.23 was used [105].

$$\omega_n = \frac{(\beta L)^2}{L^2}\sqrt{\frac{EI}{\rho A}}, \quad f_n = \frac{(\beta L)^2}{2\pi L^2}\sqrt{\frac{EI}{\rho A}} \tag{8.23}$$

With ω_n corresponding to the radial natural frequency and f_n corresponding to the natural frequency. For the coaxial rotor arms, the boundary conditions would be assumed to be fixed and free, leading to $\beta L = 1.875$. With the chosen dimensions, this would lead to a natural frequency of around 115 [Hz] for the coaxial rotor arms, which would be around 22 [Hz] away from the second harmonic of the coaxial rotors. As such, future designs should be careful not to create excitation in the coaxial rotor arms through the implementation of dampers or isolation of vibration in the member [106].

8.4.5. User-supporting Structure and Battery Integration

With the user-supporting structure introducing the loads of the human onto the main airframe, the design of the floor would be critical for introducing all the weights. Since the floor would have to fold or get out of the folding telescoping beams, two concepts were considered for its design. The first one was using some sort of fabric, reinforced with ribs, that would fold together with the telescoping beams. However, in the end, the second option of just using aluminium was chosen and moving it upwards, out of the way of the folding. This was mainly chosen as an extra redundancy for locking the folding mechanism under the weight of the person; fabric would be in tension and would not assist in preventing the folding of the mechanism mid-air. Furthermore, such a design would be more aerodynamically favourable with aluminium skin flush on the outside. Finally, the user would be more likely to perceive this as safe.

It was decided that the battery would be introduced under the seat. Hence, to size the skin, the distributed weight of the person, seat and battery were considered. This would size the beams running through the two layers of skin. The top layer of skin would be for the user, and the bottom layer would interact with the airflow. Using the dimensions of the model in fusion, the mass of the two skin sections came down to 2.28 [kg]. To estimate the weight of the floor, the beams carrying the human load would also need to be estimated.

Using the assumption that 2/3 of the weight of the human would be towards the back of the floor, the preliminary sizing of the battery and the referencing existing seats, which tend to be in a range of 6-8 [kg] for F1 seats [107], the loading on floor as depicted in Figure 8.14 could be obtained. For the seat, an extra 2 [kg] were added to account for integration.

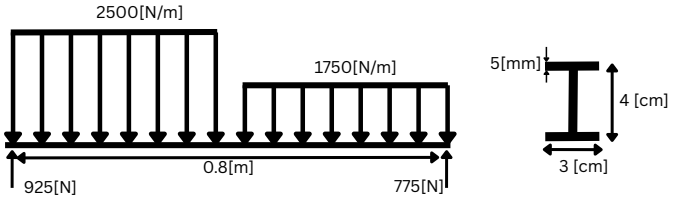

Figure 8.14: Approximate distributed load on floor structure, and floor I-beam cross-section.

This resulted in a maximum internal moment of 260 [Nm] with the load factor of 1.5. Three I-beams were sized for this, with the height dimensions bonded by the separation of the top and bottom skin of the floor. Together, they would provide the necessary rigidity for the floor. Their dimensions can also be observed in Figure 8.14. With such dimensions, three members would weigh around 3 [kg]. However, in reality, this would already be quite over-designed. As a result, a realistic budget for the total weight of the floor structure could be set to 5 [kg].

In future design iterations, it is recommended to verify that the folding mechanism would be easy for a user with a dynamic model. At the current stage, however, it was merely guaranteed that the structure was as light as possible. For this reason, the battery, which would be under the seat, would have to slide out of the way horizontally, due to its weight.

For the surrounding structure, the side skin of the vehicle in Figure 8.7, Dyneema was chosen due to its mechanical, water-resistant and abrasion-resistant properties. It is also FAR 25.853b certified for flammability [108]. To estimate its mass, the dimensions of the CAD model led to:

$$2(0.7)(0.8)(\frac{3}{1000})(970) = 3.3[kg] \tag{8.24}$$

However, Dyneema itself would not be able to house the person completely. For this, the proposed structure of the side skin would be reinforced with polyphenylsulfone (PPSU) thermoplastic, which is commonly used in aircraft interiors, in an accordion-like structure as can be observed in Figure 8.15 [109].

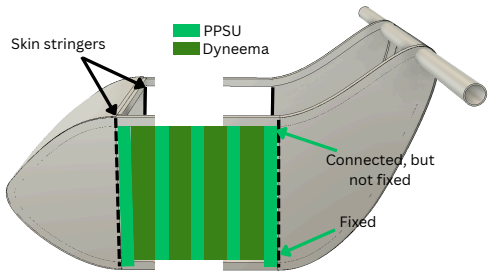

Figure 8.15: Side skin “accordion” structure for folding.

As the telescoping beams fold, the Dyneema and the PPSU members will follow. However, in air, the Dyneema might be loaded in shear and even though it is quite strong, unnecessary loading could be avoided through slack fabric in folds. However, the proposed solution here would be to first introduce stringers to the skin to also prevent having free skin. Then, alongside the stringer, a PPSU member would be fixed to the bottom part of the structure and connected but not fixed at the top, via a joint that allows some movement. This would also assist in introducing the user’s dynamic loads. With the skin connected to this member, it would carry less torsion and be mostly responsible for housing the person. The mass budget for the PPSU and Dyneema was set to 5 [kg]. Finally, the canopy around the user was designed after the aerodynamic iteration, as detailed in Section 8.6.

8.4.6. Landing Gears

Several decisions are made before the structural analysis of the landing gears is performed. Four landing gears are implemented in order to have better ground stability, especially when the vehicle vertically lands, and to prevent tip-overs. Each of them is assumed to carry the same amount of load. The landing gears are in the form of wheels so that they could also be used for transporting on the ground. The landing gear struts will be placed directly onto the bottom main airframe, the front two connection points of the beams and the back curved beam as shown in red points in Figure 8.16. The

tyres are selected from Electron Retracts with a diameter of 200 [mm], which are for up to 150 [kg] per pair [110]. Moreover, the struts are fixed, not retractable, in order to have a lighter and simpler structure. Finally, the material used for the landing gear struts is Aluminium 7068-T6511, which is the same as the main airframe material, resulting in consistency in material properties of the overall structure.

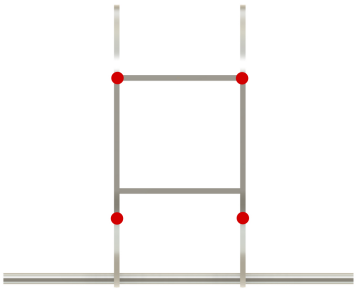

Figure 8.16: Position of landing gears on the main airframe (bottom view).

As demonstrated in Figure 8.17, the struts of the landing gears are hollow cylindrical beams. The thickness 't' is 5 [mm], which is the same as the thickness of the main airframe beams for efficient manufacturability. The outer diameter 'd' is 4 [cm], which is the side length of the square hollow beam cross section. With these values, the length L is determined based on the comparison between the buckling stress and the yield stress. Afterwards, it is assessed whether the strut design can withstand buckling for vertical landings and bending for forward movements on the ground.

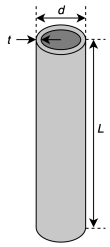

Figure 8.17: Dimensions of a landing gear strut including t, d, and L.

Buckling

First, for vertical landing motion, the strut must withstand buckling and compressive yield. Since yield before buckling is more desirable, the buckling stress 'σ_b' should be larger than the yield stress 'σ_y, resulting in Equation 8.25.

$$\sigma_b = \frac{\pi^2 EI}{L^2 A} > \sigma_y \cdot 1.5 \tag{8.25}$$

where E is the Young's modulus of the material, I is the area moment of inertia of the cross section, and A is the area of the cross section. To satisfy the condition above, L should be less than or equal to 32.69 [cm].

Based on the dimensions, it is essential to make sure that the actual load applied to each strut is below the critical buckling and yield loads. The analysis is conducted on a nominal landing scenario, where the maximum load on landing gears is the total weight of the aircraft. Extreme cases such as abrupt falling are not considered, but these could be investigated in future research. The total weight of the aircraft, including the pilot and payloads, 305 [kg], and the safety factor of 1.5, results in the actual load P_{real} of 1122.0 [N] per landing gear. The relationship between the critical load and the real load on the strut is shown in Equation 8.26.

$$P_{cr} = \frac{\pi^2 EI}{L^2} > P_{real} \cdot 1.5 \tag{8.26}$$

where the critical load P_{cr} is 579162 [N], the actual load P_{real} is 748 [N], based on the maximum L of 32.69 [cm] and with a safety factor of 1.5. Therefore, it means that the actual load is lower than the critical load.

Bending

Next, for the vehicle to move forward on the ground, the strut should withstand bending. To take into account the extreme case, it is assumed that the wheels are on the brakes so that the bottom end of the strut is fixed onto the ground. With the dimensions obtained from previous analysis on buckling, it is checked whether they comply with bending as well. The maximum forward force on the vehicle is when the two cyclorotors produce their maximum thrust in the forward direction, which is 2998 [N]. Therefore, each landing gear will experience one-fourth of the force P_f, 749.5 [N]. The deflection caused by the bending is calculated in Equation 8.27.

$$v_{max} = \frac{P_f L^3}{3EI} = 1.392[mm] \tag{8.27}$$

where v_{max} is the maximum horizontal deflection due to bending of vertical landing gear strut, which is slightly over than the total load deflection limit of aluminium, $L/240$ [111]. In order to have v_{max} within the deflection limit, L should be less than 31.68 [mm].

In conclusion, the dimensions and mass of the landing gears are specified in Table 8.3 and the length of the struts are demonstrated in Figure 8.18. Specifically, the front two landing gear struts have a length of 15 [cm], which is below 32 [cm], the maximum allowable length and above 10 [cm], the radius of the wheel. 5 [cm] margin from the top of the wheel to the bottom of the airframe provides clearance from the ground and the wheel, which complies propeller ground clearance requirement of EASA [112]. The rear two struts have a length of 31 [cm] and are placed as far back as possible while not letting the aircraft tilt backwards. This ensures the centre of gravity of the vehicle to be in between the front and back landing gear positions, preventing tip-over.

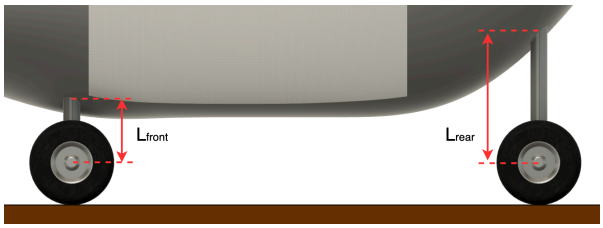

Figure 8.18: Length of front and rear landing gear struts.

Table 8.3: Landing gear dimensions and mass.

Thickness (t) ([mm])	Diameter (d) ([cm])	Front Strut Length (L_{front}) ([cm])	Rear Strut Length (L_{rear}) ([cm])	Mass per Strut ([kg])
5	4	31	15	0.51

The landing gears are exposed to cyclical loading over time, which could lead to fatigue. The fatigue strength at 10^7 cycles of Aluminium 7068-T6511 is 228.5 [MPa] [113], which is significantly higher than the actual stress on the strut, 1.36 [MPa]. This means that the actual stress is lower than the stress that would cause fatigue after 10^7 cycles. Due to the over-designed strut structure from buckling and bending analysis, the landing gears are safe under cyclical loading.

8.4.7. Tip-Over Prevention

Based on the positions of the landing gears determined in Subsection 8.4.6, it can be obtained that the front two landing gears are placed 0.4 [m] away and the rear two are located 1.5 [m] away from the nose. When the vehicle is deployed, the total centre of gravity is placed at the range of 0.96 [m] to 1.22 [m] from the nose and when folded, 0.53 [m] to 0.95 [m], using Equation 8.28. This is when the distance of the battery from the nose has a range of 0.4 [m] to 1.5 [m]. This indicates that wherever the battery is placed in between the front and back landing gears, the centre of gravity of the whole vehicle stays between the front and back landing gears in both deployed and folded state, preventing forward or backwards tipover. Moreover, all landing gears placed at the side edges of the vehicle also prevent tipping over sideways.

$$x_{cg} = \frac{\sum_i m_i \cdot x_i}{\sum_i m_i} \tag{8.28}$$

where x_{cg} is the distance from the nose to the centre of gravity of the whole vehicle, m_i are the mass of different components, including the airframe, coaxial rotors, cyclorotors, battery, and pilot, and x_i are the distance from the nose to the centre of gravity of the components. Nevertheless, to guarantee tip-over and ease of folding, the battery was placed as close to the centre of the vehicle after folding.

8.4.8. Maintainability, Safety, and Reliability

In order to facilitate successful operations, it would be important to ensure that vehicle structures are safe, reliable, and maintainable. For the safety and reliability aspect, the folding mechanism would be of particular importance and extensive testing would be crucial to guarantee a design that could be trusted. Furthermore, for example, the telescoping beams could have ways of access to ensure smooth folding procedures, via anti-friction coating, for example. When it comes to the structure overall, the safety will be reinforced with diagnostics, which monitor the structural health and ensure that the structural elements need to be serviced.

8.5. Aerodynamic Analysis

In order to ensure the aircraft can achieve the set performance requirements, the aerodynamic characteristics need to be assessed. In addition to modelling the general flow characteristics and creating points for improvement, a significant task of the aerodynamic analysis is drag estimation, which provides data required for range estimation. The analysis was performed separately for the structure and the two propulsion system types. This is a significant assumption, which was made in order to optimise the timeline of the analysis, as simulation of the full model would require a very fine mesh and long computational time. Its validity was further discussed in Chapter 3.

In this section, the preparation steps required to run the simulation are first briefly discussed in Subsection 8.5.1. Then, the analysis of the preliminary structure is carried out in Subsection 8.5.2.

8.5.1. Simulation Preparation

The process is similar to when the propulsion system was analysed. It starts with simply importing the 3D model of the part, after which an enclosure with an inlet and outlet is created around the body, which represents the surrounding air. After this step, the body surface and the enclosure need to be discretised, in order to allow for the computational method to be used. This can be done in many ways, but in this case, a fine mesh was used on the aircraft surface in order to capture its complex shape. Meanwhile, a coarser mesh was used to discretise the enclosure. Buffer layers were set up between these two entities to improve the smoothness of the transition from one to the other. A structured mesh consisting of hexahedrons was used for the discretisation, since it has been suggested that it leads to higher accuracy for the same number of edges when compared to its unstructured, tetrahedral counterpart [114]. However, some unstructured elements were still necessary in order to facilitate the transition from fine to coarser mesh, or to capture certain curves on the aircraft's surface without creating elements with high aspect ratio or otherwise bad quality. In the end, such elements were identified in limited cases, which could affect solution convergence. The overall meshing approach would need to be reconsidered in case of a diverging simulation; however, this was not necessary.

Overall, the mesh element size was refined to approach the 10^6 element limit of the Ansys student license.

8.5.2. Preliminary Structure Aerodynamic Analysis

With the computational method outlined, it is time to look at the results of the simulation. These consist of numerical values that can be extracted from the simulation, but it is also possible to plot certain variables and examine the development of their values depending on the chosen coordinates. Further visualisations, such as streamlines, can also be plotted. A key characteristic of the aircraft is the drag coefficient. The parasitic drag coefficient of the structure was found to be 0.037, which is a reasonable value when compared to general aviation aircraft, although higher than usual. For example, the Cessna 172 has a profile drag coefficient of 0.029 [115]. To evaluate points for improvement in the structure's shape, the velocity contour plot is shown on the symmetry plane of the aircraft in Figure 8.19, and on a plane offset by 0.530 [m] in the y-direction in Figure 8.20.

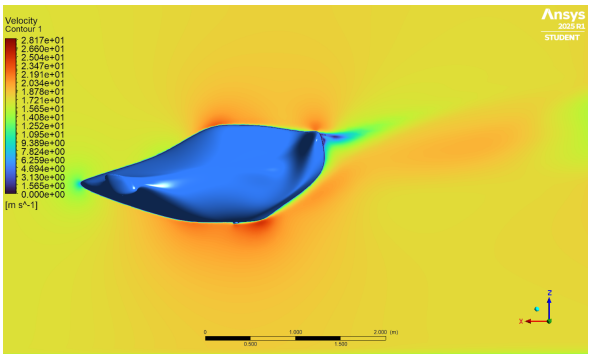

Figure 8.19: Contour plot on the preliminary structure centre line plane showing the velocity distribution.

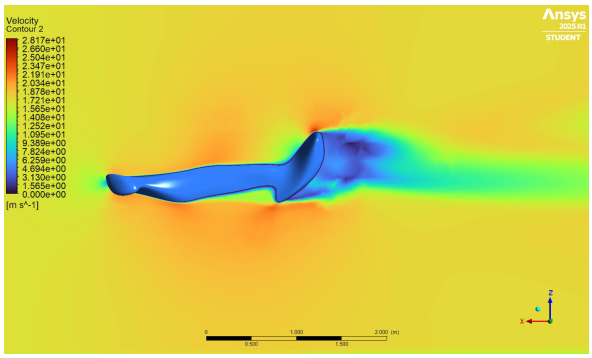

Figure 8.20: Contour plot on an offset plane (y=0.530 [m]) with the velocity distribution around the preliminary structure.

These contour plots already suggest that the preliminary structure might not be aerodynamically efficient. Firstly, there is an area of very low velocity at the rear of the aircraft, which could indicate flow separation. If that were the case, this would be causing additional drag to the aircraft when in forward flight. The phenomenon is accentuated on the plane shown in Figure 8.20, since the rear panel has a sharper edge in that region, and the skin surface at the rear is ascending more aggressively. This potential issue was further investigated using a contour plot of the velocity x-component (Figure 8.21), as well as the local velocity vectors in the region (Figure 8.22), and it was confirmed that the flow is separating at the rear of the aircraft, since the mean flow velocity in that region is in the opposite direction compared to the rest of the flow field.

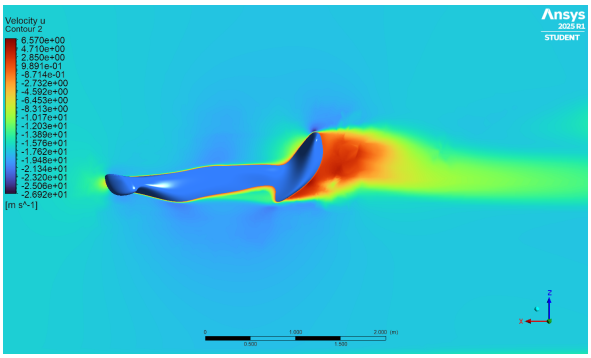

Figure 8.21: Contour plot on an offset plane (y=0.530 [m]) with the horizontal velocity distribution around the preliminary structure.

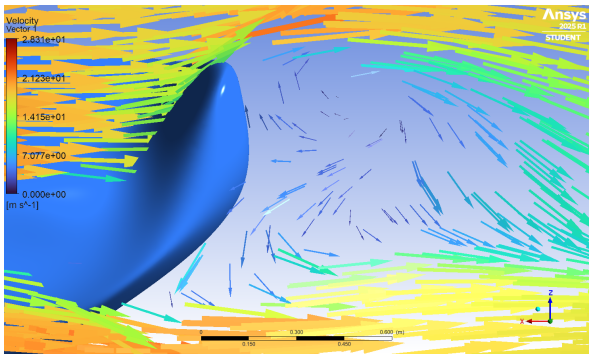

Figure 8.22: Local velocity vectors of the air flow around the rear extremity of the preliminary structure, plotted on an offset plane (y=0.530 [m]).

A number of potential solutions were proposed. The first option was to create slots through the structure from the high-pressure regions on the front side of the rear plate to the separation region. Alternatively,

the whole rear assembly carrying the coaxial rotors could be turned into a truss structure with large gaps between members. Either of these solutions would help transfer higher-pressure air to the separation region and prevent the formation of the separation bubble.

Alternatively, vortex generators could be placed at the bottom side of the aircraft. This approach aims to draw outer flow into the boundary layer and energise it, which leads to delayed separation and reduction of pressure drag [116]. However, this solution comes with its own disadvantages, such as increased friction drag [117].

One other potential solution to the separation problem would be to make a rather significant change to the structure's shape. In particular, a more gradual slope on the trailing side of the aircraft would delay or prevent separation. This would, however, require certain changes to the positioning and type of the coaxial rotor connection, and/or changes to the internal arrangement of other components, together with pilot repositioning. In case such changes were to be implemented, discussions and compromises would be necessary to accommodate other subsystems.

Another separate issue is that the airflow on the lower side of the aircraft is faster than on the upper side. It is reasonable to assume the Bernoulli equation is valid in this case, since the cruise Mach number is significantly lower (≈ 0.05) than the 0.3 where the equation usually stops being used.

$$P_1 + \frac{1}{2}\rho V_1^2 = P_2 + \frac{1}{2}\rho V_2^2 \tag{8.29}$$

Considering this formula and the accelerated flow over the aircraft's bottom, it can be concluded that the pressure on the lower side of the aircraft will be decreased. Thus, it can be expected that the aircraft to create negative lift when in forward motion. The resultant lift coefficient calculated from the simulation is $C_{L_{fuselage}} = -0.036.$. This could be mitigated by altering the shape of the aircraft, but would likely require the seating position and the overall internal arrangement to be changed. For this reason, and considering the relatively low magnitude of the negative lift, which can be compensated by the relatively high-thrust propulsion system (more information in Chapter 3), only limited effort was made to mitigate this effect. Namely, an attempt to flatten the floor and thus slow down the flow in the given region will be made in order to increase the local static pressure.

8.5.3. Aerodynamic Iteration

The aerodynamic analysis informed certain design decisions regarding the structure. Namely, the rear edge of the aircraft, on which the coaxial rotors are mounted, was made into a more streamlined, blunter shape with the intention to eliminate or at least reduce flow separation. An effort was also made to decrease the steepness of the back side of the Owl-22. Nevertheless, due to other constraints, mostly the volume limit and the functioning of the folding mechanism, the structure was not fully optimised for aerodynamic performance; in fact, the aerodynamic characteristics of the final design are worse than those of the preliminary concept. This is a result of changing the dimensions and shapes of the structure, since it is now taller, blunter, and more box-shaped in the front. The parasitic drag coefficient of the new design was found to be $C_{D_{fuselage}} = 0.037$, with the lift coefficient being $C_{L_{fuselage}} = -0.047$. Both of these worsened values make sense upon examination of the pressure distribution shown in Figure 8.23.

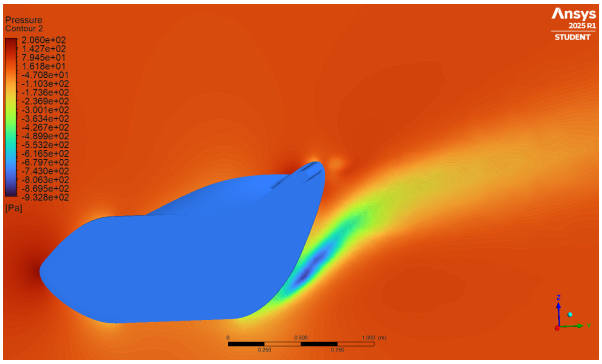

Figure 8.23: Pressure distribution around the final structure design on an offset plane at x=0.394 $[m]$.

Overall, the region of increased velocity and decreased pressure has shifted further backwards compared to the preliminary design, causing increased drag.

In terms of the other issue identified with the preliminary design, the flow separation region adjacent to the main body has been reduced in size. On the other hand, more separation was introduced with the implementation of the mounts for the coaxial rotors. These effects are presented in Figure 8.24 and Figure 8.25.

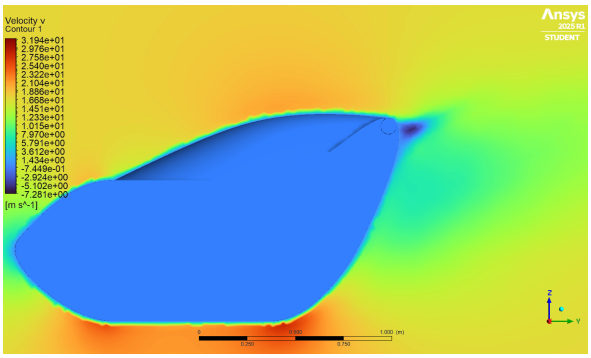

Figure 8.24: Contour plot on the symmetry line with the horizontal velocity distribution around the final structure.

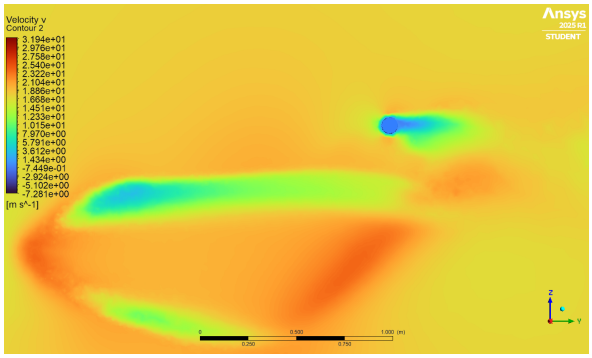

Figure 8.25: Contour plot one an offset plane at x=0.533 [m] with the horizontal velocity distribution around the final. structure.

8.6. Final Iteration and Final Design

The following section presents the iteration strategy and the final structural design of Owl-22.

8.6.1. Final Iteration and Sensitivity

As detailed in Figure 8.26, the final iteration step would include reconsidering the design with a new total mass estimated, which could differ from the initial value assumed when sizing the propulsion and battery systems. The initial value used was the maximum allowable mass from the requirements, and a lighter structure would necessitate a lower battery size and potentially a reconsideration of the propulsion system dimensioning.

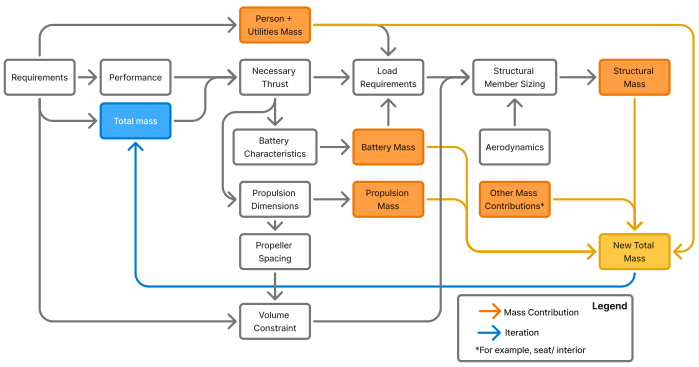

Figure 8.26: Detailed iteration flowchart.

However, before the iteration could be implemented, some other masses needed to be approximated. When it comes to the canopy, impact-modified PMMA was chosen as the material, with a density of 1150 [kg/m^3]. From the preliminary structure dimensioning a conservative estimated of the area it would need to cover would be 1.6 [m] x 1.8 [m], with products like Plexiglass manufacturing aviation certified canopy at a variety of different thickness, ranging mainly around 3 [mm] thickness for aviation purposes [118, 119]. This results in a mass of around 10 [kg], without a margin for considering the way it would

be integrated with the structure. It should, however, be noted that future design stages should create a more detailed design considering its integration with the airframe, with the recommendations for compliance from the FAA [120]. Using the external dimensions and the cross-sectional properties, the mass of the airframe could be calculated, resulting in the total mass breakdown in Table 8.4. Specifically, the members were sized to have a thickness of 5 [mm], for reasons discussed previously, with the side beams of dimensions of 3 [cm], 4 [cm], 5 [cm] for the telescoping beams, 8 [cm] diameter for circular beam, and 4 [cm] for the connecting beams.

Table 8.4: Mass budgeting with final dimensions.

Component	**Mass [kg]**
Airframe side beams	19.7
Airframe circular beam	8.4
Airframe connecting beams	5.2
Airframe skin(with stringers)	6
Seating	10
Floor	5
Canopy	10
Battery	66.13
Coaxial rotors	12.6
Cyclorotors	37.3
Landing gear	2
Dyneema + PPSU interior	5
Electronics + Controls	9.5
Total*	196.8

*Without battery mass iteration.

The mass budget for electronics was estimated from the budgeting completed in the previous design stages. However, the majority of components were selected in Chapter 5, as presented in Table 8.5.

Table 8.5: Electronics masses.

Component	**Mass [kg]**
Camera	0.0095 [121]
LiDAR sensors	0.45 [122] [123]
IMU	0.0275 [124]
GNSS	0.011 [75]
iPad	0.5 [125]
External SSD	0.009 [126]
OBC	0.06[127]
Radio	1.4[128]
Router	0.26[129]
Total*	2.73

*Without all the cabling

This would leave about 6.7 [kg] for the yoke, pedals, which have been dimensioned but not yet fully developed and cabling, which was not already accounted for in the table above. However, as detailed in previous design stages, the budgeting would also come with a 10% contingency, which would then lead to 7.72 [kg].

With the total mass equalling around 196.8 [kg], very close to the 200 [kg] used for propulsion decision and battery sizing, the full iteration step was not necessary. In particular, it was not necessary to select new propulsion devices. This is because the propulsion selection was made with existing devices in mind, which would otherwise need to be redesigned. Specifically, future design iterations should

consider collaborating with CycloTech to further optimise the propulsion and structure sizing. In this case, the strategy in Figure 8.26 could be fully employed. However, such decisions would come with increased costs.

Instead, the iteration consisted of resizing the battery and reconsidering the optimal cruising thrust, while still using the same propulsion devices. This was done using Equation 8.30

$$m_{i+1} = m_i - (66.13 - m_{b_i}) \tag{8.30}$$

where m_i constitutes the current mass estimate, 66.13 [kg] is the mass of the battery for 200 [kg] system weight and m_{b_i} is the battery mass for m_i system weight, which were calculated using the same method as in Section 4.2.

As will be discussed in Subsection 8.6.2, a sensitivity analysis on changing the structural mass and how that would affect the battery mass is described. What this meant for the structure was that it would be designed for the same ultimate loads, as the propulsion devices would still be able to output the same maximum thrust. The resizing of the battery would not have a significant effect on the structure; it would have a negligible weight change when compared to the driving factors sizing the structure; it would only slightly affect the distributed load onto the floor of the structure. With the iteration of the battery mass for the new total mass, the final total mass came down to **196.37** [kg].

8.6.2. Mass Sensitivity and Future Recommendations

It should be noted that the current mass estimate still does not account for certain masses, like riveting, although these are considered a reasonable allowance because in the places where there would be rivets/bolts, material would also be removed. Furthermore, as previously mentioned, the current structure was still over-designed, and although these values were completely verified using FEA due to time constraints, a sensitivity analysis was performed to see by how much future iterations could expect to decrease the mass. To do this, the mass contributions were split into constant and changing. This was done under the assumption that no major changes would happen to the design. For example, the propulsion device's mass was kept constant.

The seating, floor, canopy, and landing gear were also assumed to be fixed. Finally, the electronics can be considered with the contingency of 10% still allocated to it, as mentioned previously. This resulted in a range of mass of 9.5 - 10.45 [kg]. A margin of 20% would be applied to the Dyneema and PPSU interior to account for the fact that it would be a newly designed part [130], leading to a 5-6 [kg] range.

The current airframe mass estimate is 39.3 [kg], with the mass mainly depending on the cross-section of the beams. The external dimensions of the members were imported into Python, and cross-section elements that were initially oversized in the preliminary design and in the FEA analysis model were, leading to a mass range of 30 - 40 [kg] for the airframe. Specifically, the intermediate beams cross-sections were resized to be thinner, from 4 [cm] to 3[cm] and the circular cross-section of the member connecting the two coaxial rotor arms was resized to 5[cm] from 8 [cm], as the coaxial arms would be folded and it would not be a continuous member, as depicted in the airframes previously presented. Furthermore, the length and width of the vehicle were varied. This resulted in a mass range of around 180 - 200 [kg], limiting the maximum mass by the maximal requirement value. With the iteration using Equation 8.30, this would result in a mass range of 175.42 - 200 [kg]. To conclude, the mass would mainly depend on the redesign of the structure, changing the weight of the battery and hence of the whole vehicle again, and further optimisation could make the vehicle even lighter.

Future design iterations would need to identify more accurate operational limits to design a more optimal structure within those loads, as the current structure still assumes a load factor above 2. Furthermore, FEA simulations would need to be run with the proposed more light-weight structure, with optimised cross-sections. Finally, FEA simulations would need to be run to assess the feasibility of integrating the folding mechanism in the structure.

8.6.3. Final Design

The final external dimension of the deployed vehicle can be seen in Figure 8.27.

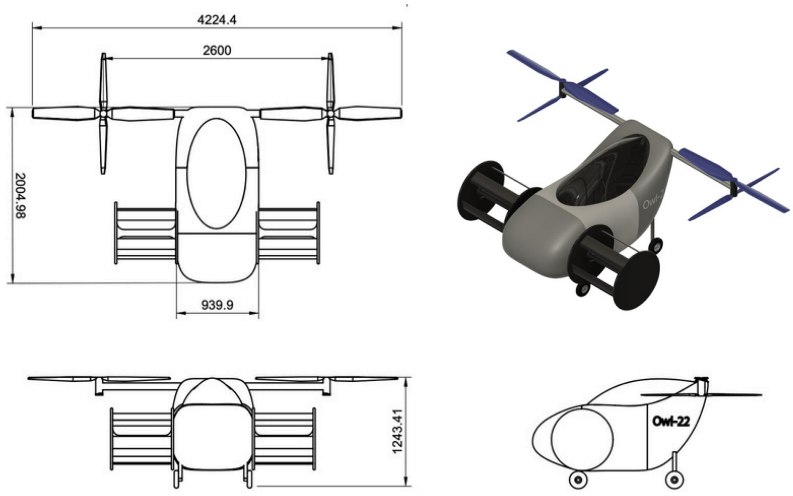

Figure 8.27: Deployed Owl-22 external dimensions.

The final external dimension of the folded vehicle can be seen in Figure 8.27. Note that the volume would be defined without the consideration of wheels.

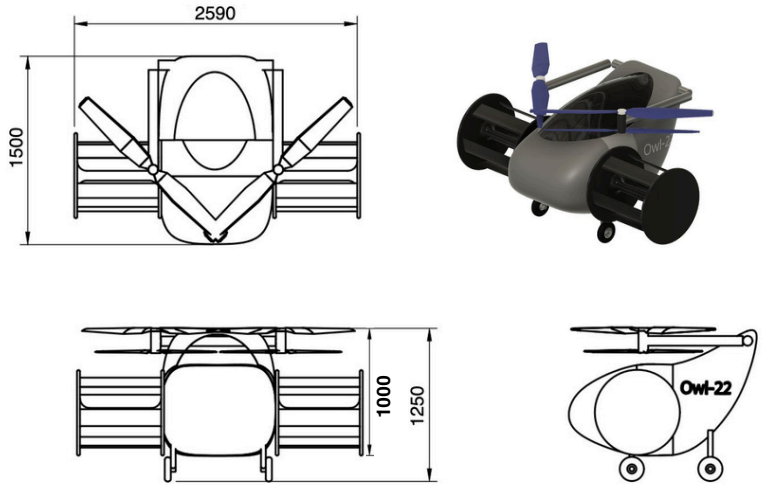

Figure 8.28: Folded Owl-22 external dimensions.

Lastly, simplified interior layouts with seat dimensions are displayed in Figure 8.29 and Figure 8.30.

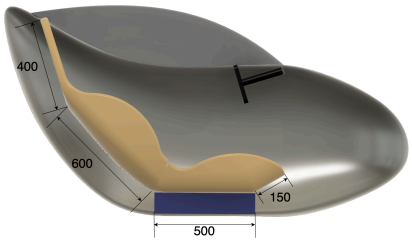

Figure 8.29: Simplified interior when deployed with seat dimensions in mm.

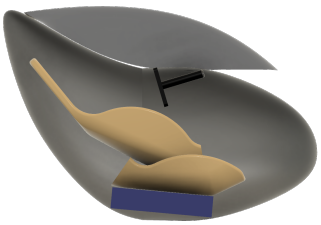

Figure 8.30: Simplified interior when folded.

9 Operations and Logistics Concept Design

The Owl-22 is a conceptual personal aerial vehicle designed for short-range urban transportation in the UAE. It aims to provide individuals with a compact, self-deployable air mobility system that minimises reliance on large infrastructure such as airports. The vehicle is capable of vertical take-off and landing, making it ideal for urban commutes and rapid point-to-point travel in densely built environments. The operational and logistical aspects of the system are central to its viability. These factors directly influence critical system-level requirements, including mass limits, foldability, charging infrastructure, maintenance strategies and safety protocols. This section outlines the operational concept and its logistics framework, ensuring that the vehicle meets its mission profile while remaining affordable, sustainable and scalable.

9.1. Operational Use Concept

The operational use of the Owl-22 is centred on simplicity, low maintenance, and minimal ground-dependency. The vehicle is designed to be stored and deployed from a private location, allowing the user to initiate a mission without relying on large infrastructure or ground crew support. Routine maintenance is embedded into the operational cycle, aided by real-time diagnostics and predictive fault detection. A typical mission is envisioned to consist of the following 6 mission phases:

1. Pre-flight and deployment
2. Take-off and climb
3. Cruise
4. Descent and landing
5. Post-flight and stowage
6. Charging

Mission Phases - The mission profile of the Owl-22 is designed around short-range, point-to-point transport for individual users in urban settings. The vehicle's operations are divided into six sequential phases, each governed by specific functional and environmental requirements to ensure safe, efficient, and low-maintenance travel, as represented in Figure 9.1.

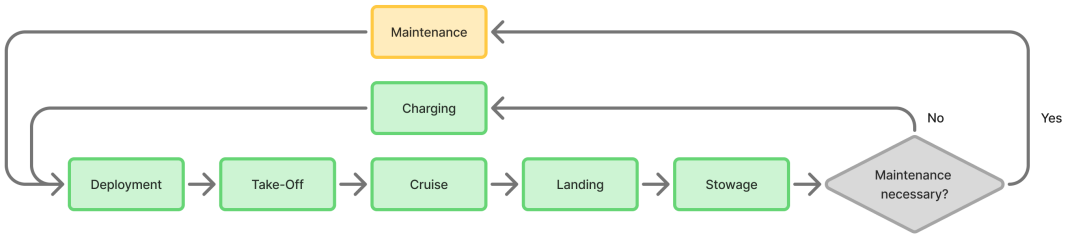

Figure 9.1: Operational phases of the Owl-22.

Pre-Flight and Deployment - The mission starts with user activation via a dedicated mobile application. Upon confirmation of weather conditions and airspace clearance through onboard systems and external data links, the Owl-22 initiates a self-diagnostic sequence. This includes structural integrity checks, battery state-of-charge assessment, sensor calibration, and control surface functionality verification. Predictive maintenance algorithms evaluate component health, ensuring issues are detected before flight. The vehicle then unfolds from its stowed configuration.

Take-Off and Climb - Once deployment is complete and all systems are verified as nominal, the vehicle engages its electric propulsion system to achieve vertical take-off. The climb is conducted under full autonomous control, using real-time sensor data (e.g. LiDAR, optical flow, inertial measurement) to stabilise the vehicle and avoid immediate obstacles. System performance is logged continuously to update maintenance models.

Cruise - During the cruise phase, the Owl-22 transitions to forward flight at a nominal speed of 40 [km/h] and an altitude of 20 [m]. This phase is piloted by the user, assisted by the onboard computer.

A navigation system will be implemented to make the pilot aware of any (temporary) no-fly zones. Real-time diagnostics monitor propulsion efficiency and sensor stability, and deviations are flagged for post-flight maintenance actions.

Descent and Landing - Upon reaching the destination, the vehicle transitions to vertical descent. Obstacle mapping ensures a safe approach path, and ground proximity sensors verify landing zone suitability. The final touchdown is executed with soft-landing protocols that dynamically adjust rotor speeds to minimise impact loads and reduce wear on structural components. Any anomalies detected during landing are recorded for deferred maintenance evaluation.

Post-Flight and Stowage - After landing, the Owl-22 automatically retracts its wings and rotors into the folded configuration. The vehicle logs mission and system data to the user interface and central monitoring system. Post-flight diagnostics assess system degradation, detect sensor drift, and evaluate component wear. If critical thresholds are reached, the system schedules a maintenance notification to the user. The vehicle becomes inactive and safe to handle once all systems confirm a secure and powered-down state.

Charging - The Owl-22 connects to either a fast or conventional plug-in charging system. Battery management software initiates controlled charging to prolong battery life and monitor for anomalies such as temperature spikes, voltage irregularities, or cell imbalances. Users are notified of charge progress and flight readiness through the mobile interface. Any faults detected during charging are recorded and scheduled for maintenance inspection. Charging is designed to complete within operational turnaround time, ensuring multiple daily flights are feasible.

9.2. User Interaction

The interaction between user and system for Owl-22 has been designed with a strong emphasis on simplicity, safety, and intuitiveness. This design philosophy is chosen since the vehicle will mainly be piloted by non-professional users. The majority of the control functions are executed via a tablet interface, integrated into the cockpit in a mount on the steering yoke. Supplementary physical controls are implemented for redundancy and as a possible alternative for the digital controls.

The team selected the Apple iPad (11-inch models) as the control device due to its market dominance in the UAE (with a 56.98% tablet market share [131]). The interface will be developed to be fully compatible with the iPad, iPad Air, and iPad Pro models. While many customers may already own a suitable device, Owl-22 will offer the iPad as an optional bundled product to ensure a seamless user experience. Mounted directly onto the steering yoke, the iPad serves as the primary interface for flight control. The control mapping is presented in Table 9.1.

Table 9.1: Overview of iPad-based controls for Owl-22.

Control Type	Functionality
Digital Sliders	• Acceleration / Deceleration • Vertical movement (Up / Down)
Digital Buttons	• Cruise Control Activation • Automatic Take-Off & Landing
3-Finger Swipe Gesture	• Hand Brake (Swipe from top to bottom of screen)

These controls are presented in a clear, high-contrast layout optimised for outdoor visibility. Real-time telemetry, such as altitude, velocity, attitude, and proximity warnings, is displayed alongside the controls, allowing users to maintain situational awareness at all times.

Despite the comprehensive use of the tablet interface, braking is controlled by a dedicated physical paddle. This decision was driven by the critical nature of braking in emergency and landing scenarios. The paddle is placed ergonomically on the ground to be controlled by the user's feet. Owl-22 is operated in semi-autonomous mode. The user provides high-level inputs via the iPad or physical controls, while core flight stability and control allocation are handled autonomously. Pre-flight system checks are initiated from the iPad, including system diagnostics, no-fly zone mapping, weather updates and route preview.

9.2.1. Safety and Human Factors

The safety of the user is central to the design of Owl-22 and its control interfaces. Since the vehicle is operated by non-professional users, controls are designed to be intuitive, while key safety functions are either automated or reinforced through redundancy.

Before each flight, the Owl-22 runs checks automatically. It verifies battery health, propulsion, structural deployment, and ensures the aircraft is not in a no-fly zone. If any check fails, take-off will be blocked, and a clear error message is shown on the iPad.

During flight, the system monitors critical parameters real-time. Warnings for low battery, obstacle proximity, or sensor faults are shown on-screen and signalled both visually and audibly. In the event of system degradation, an automatic landing protocol will be triggered. The main controls are digital sliders and buttons on an iPad mounted to the steering yoke. However, braking is handled by a physical breaking paddle at the pilot's feet to ensure quick access. A handbrake can also be triggered by a three-finger swipe gesture on the iPad—designed to be fast but hard to activate by accident. To reduce workload and error, all controls are placed logically, using familiar layouts and large, high-contrast elements.

9.3. Manufacturing and Assembly

Production of the aircraft, including shaping of parts and joining them together, could have major influence over the aircraft performance and safety overall. The suitability of shaping and joining processes depends heavily on the materials used and the desired shapes.

First, it is important to determine what manufacturing processes and machines are required for the production of the individual aircraft components. This is done in Subsection 9.3.1. Next, the off-the-shelf components required for the aircraft production are outlined in Subsection 9.3.2. Lastly, Subsection 9.3.3 shows the assembly plan for the Owl-22 aircraft.

9.3.1. Part Manufacturing

The aircraft consists of numerous parts that need to be manufactured in-house. These can be divided based on the material used.

Aluminium

Multiple processes will be used to shape the aluminium parts. The aluminium beams (airframe and landing gear) will be manufactured using extrusion. This complements the necessity to produce long beams with hollow cross-sections. Hot extrusion will be used to shape the aluminium parts, since the material is too stiff and strong to be used with cold extrusion, and could start cracking under this type of stress. The curved beams will use stretch forming in addition to extrusion, in order to achieve their desired shape. Again, stretch forming will be used to shape the surface skin of the aircraft, since it is expected to be delivered in sheet form.

CFRP

The Owl-22 uses two parts made of carbon fibre. These are expected to be the propellers of the coaxial rotors and the pilot seat. Production volume of 4000 units per year is required for the propellers, meaning that 11 units per day need to be produced. A potential failure of the propellers would endanger the life of the pilot. They must also last for a number of years, which overall means that they must be of the highest quality. For this reason, automated tape laying of CFRP pre-preg will be used to manufacture the propellers, after which they will be cured in an autoclave. The seat is another carbon fibre part of the aircraft, and will be made using vacuum infusion of resin into a dry carbon fibre part. This process was chosen because it is better suited for production of large parts and is usually cheaper

than working with pre-preg [132, 133].

Thermoplastics
Another material type which will need to be shaped into parts is thermoplastic. two processes will be used again, namely thermoforming and injection moulding. Thermoforming will be used for the canopy, since it needs to be a thin, curved, flowing shape. For the other thermoplastic parts (serrated end-pieces, PPSU side walls, yoke), injection moulding presents itself as a fast, low-cost solution with sufficient precision, and will be used for this reason.

Miscellaneous
There are two individual parts which require a separate manufacturing process. The pedals inside the aircraft will be machined from larger plates of aluminium. Machining might also be required to perform finishing touches on certain components like the airframe beams. Secondly, the interior will require cushioning surrounding the pilot, for the sake of comfort and safety. Sewing will be required to manufacture these parts.

9.3.2. Off-the-shelf Components
Certain items either cannot be manufactured or it is disadvantageous to manufacture them in-house. These parts appear in the propulsion subsystem, namely the cyclorotors, the electric motors for the coaxial rotors, and their ESCs. The battery, sensors, and components of the cooling system will also be purchased off-the-shelf. Lastly, the wires, Dyneema side sheets, and the landing gear wheels will also be bought, since it is more efficient to outsource their production rather than attempt to establish a new supply chain.

9.3.3. Aircraft Assembly
Once all the Owl-22 parts are manufactured and purchased, it will be necessary to assemble them together. In some cases, like the landing gear, it would be desirable to use welding as a joining method, however, this is generally not possible, due to the chosen material [113]. Thus, extensive use of mechanical fasteners will be made. In particular, bolting will be used in order to join the main airframe parts like the airframe beams, the coaxial rotor mounts, and the landing gear. Meanwhile, the skin will be riveted onto the structure, since it disrupts the flow on the aircraft surface less than bolts, and the removal and reuse of the skin is not planned, meaning a permanent fastener can be used. For the non-structural parts such as the serrated end-pieces on the propeller trailing edges and various interior pieces, adhesives will be used to save costs and keep surfaces smooth.

The Owl-22 production will be created in steps, some of which can be performed in parallel. The outcome of each step is a sub-assembly, all of which are eventually made into the full assembly. The overall assembly plan is presented in Figure 9.2.

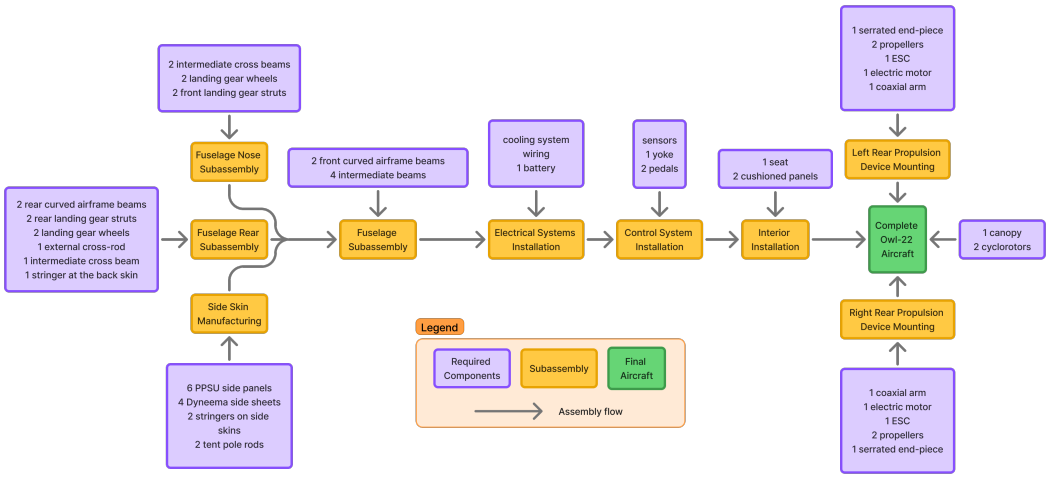

Figure 9.2: Assembly plan showing the flow from individual components to a completed Owl-22 aircraft.

9.4. Logistics Support Concept

To ensure operational reliability and user satisfaction throughout the service life of the Owl-22, a comprehensive logistics support concept is developed. This concept defines how the system will be sustained once deployed, including maintenance, supply chain, and support infrastructure tailored to the needs of a personal air transport vehicle. Given the goal of providing a low-maintenance mobility solution, the logistics framework focuses on minimising user burden while ensuring safety. The concept accounts for the urban context in which the system will operate. Subsequent sections detail the organisational structure and maintenance strategies.

9.4.1. Infrastructure and Deployment Requirements

To enable seamless integration into the daily routines of private users, the infrastructure requirements for the Owl-22 are intentionally minimal and tailored to urban environments. The vehicle is operable from residential and light commercial locations without the need for dedicated take-off or landing infrastructure. Its VTOL capability allows operation from compact, flat surfaces such as rooftops, courtyards, or driveways. A recommended area of 6 [m]x 6 [m] ensures safe rotor deployment and sufficient airflow during vertical manoeuvrers. The required surface load capacity is still under evaluation. Deployment of the vehicle is manual but spring-assisted to reduce user effort while minimising system weight.

Energy infrastructure is designed for flexibility. The Owl-22 supports both slow and faster charging modes, allowing users to preserve battery longevity when time permits or opt for rapid charging when needed. Compatibility with existing electric vehicle charging stations ensures ease of integration without the need for proprietary infrastructure. An optional wallbox may be installed to further reduce charging times. All pre-flight diagnostics are handled autonomously by the vehicle.

9.4.2. Production and Distribution

Production of the Owl-22 is planned to be UAE-based. This decision is driven by a combination of logistical, economic, and geopolitical factors. Local manufacturing significantly reduces the complexity and cost of supply chain operations, particularly for final assembly and customer delivery. The UAE's favourable trade relationships with key aluminum-exporting nations ensure stable access to primary structural materials. Additionally, relatively low labour costs in the region contribute to a competitive production model without compromising quality.

Final assembly will occur in a facility near DXB airport, allowing streamlined integration of imported components. The resulting proximity to early adopter markets further enhances deployment efficiency.

This centralised production and distribution model ensures control over quality, simplifies after-sales logistics, and aligns with the project's scalability objectives.

9.4.3. Maintenance

The maintenance strategy is designed to maximise reliability and to minimise downtime. In line with stakeholder requirements, the vehicle is intended to operate maintenance-free for the first two years under normal use conditions. This is achieved through robust component selection, conservative system design margins, and embedded health monitoring.

Core systems perform automated diagnostics before each flight, assessing battery status, rotor performance, and sensor functionality. Any deviations are communicated via the user interface. Critical faults result in disabling the vehicle, while non-critical issues are communicated and logged for later resolution. The maintenance framework distinguishes between user-level and service-level actions. Users are not expected to perform hardware interventions. All physical maintenance (beyond basic visual checks or online software updates) is reserved for certified technicians at authorised facilities. To ensure long-term airworthiness and support proactive servicing beyond the initial two-year period, the vehicle collects and transmits diagnostic data throughout its lifecycle. This enables predictive maintenance planning and allows the service centre to coordinate interventions efficiently, thereby enhancing availability and user convenience.

9.4.4. End-of-Life Logistics

To align with sustainability goals, the Owl-22 incorporates an end-of-life strategy grounded in circular economy principles. In the context of Owl-22, end-of-life is defined as the stage at which the vehicle is no longer viable for safe or cost-effective operation and is therefore withdrawn from service. At this point, the vehicle enters a managed retirement process focused on minimising environmental impact through responsible material handling and reuse.

A substantial portion of the vehicle's mass is intended to be reused, recycled, or safely disposed of using sustainable methods. Although precise targets are still being defined, material choices have been made to prioritise low-impact disposal and leverage established recycling pathways. Aluminium alloys are used extensively due to their proven recyclability and global processing infrastructure.

The vehicle is also designed for efficient disassembly. Fasteners, interface joints, and subsystem layouts are configured to enable straightforward separation of structural components, battery modules, and electronics. This facilitates both targeted recycling and the potential reuse of high-value components such as sensors and batteries. To support this strategy, a digital material passport is being developed to track component provenance, lifecycle data, and recycling compatibility. An overview of the retirement and disposal flow is shown in Figure 9.3, illustrating the decision pathways from initial evaluation to reuse, refurbishment, or material recovery.

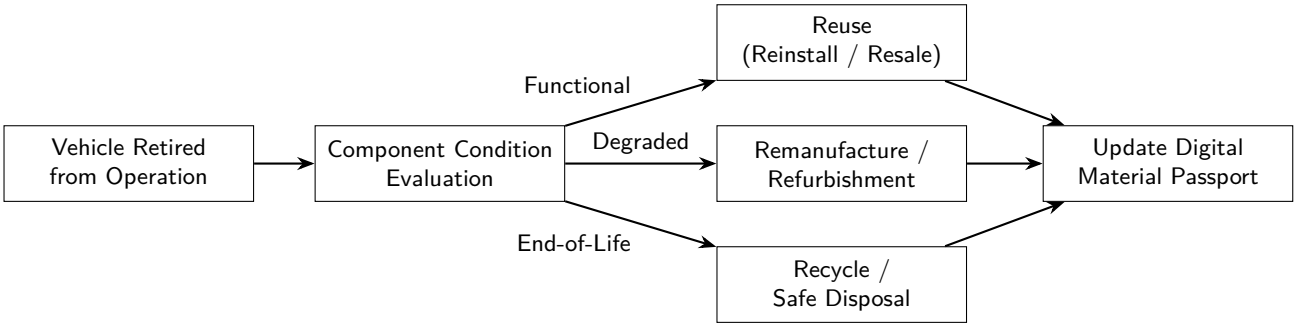

Figure 9.3: Retirement and disposal path of the Owl-22.

10 Sustainability Assessment

Product sustainability has been a notoriously difficult concept to quantify and report transparently, due to the complexity of the topic, as well as the deceptive nature of reporting undertaken by profit-generating businesses [134]. Current literature agrees upon the existence of three main pillars of sustainability: environmental, social and economic. However, despite this description having been generally accepted, sustainability remains an open concept with countless interpretations, resulting in a culture where corporate social responsibility (CSR) is almost always deceptive [135]. To avoid falling into these same pitfalls, a clear approach has been implemented throughout the design of the Owl-22. This method adheres to the concept of 'sustainable development' that was popularised by the Brundtland Commission [136], a sub-organisation of the United Nations: 'development that meets the needs of the present without compromising the ability of future generations to meet their own needs'. As such, this chapter has been divided into three sections, one for each of the main pillars, where the current and future impact of the Owl-22 will be analysed.

10.1. Environmental Sustainability

Before performing any environmental analysis, Aerospace material expert Dr. Irene Fernandez Villegas was consulted. Regarding carbon footprints, she explained that aircraft have one overwhelmingly dominant source of carbon, their energy source [137]. While the UAE's sourcing of electricity is beyond the control of Owl-22, its contribution can be minimised through the design of an extremely light-weight, energy-efficient and durable vehicle. To achieve this goal, several important design decisions were made. For one, the choice to incorporate the energy-efficient cyclorotors was made, in spite of their higher cost and more difficult integration. Another important consideration was related to the battery sizing; as explained in Chapter 4, a conscious decision was made to size the battery such that its charge-discharge cycle would occur in the 10-90% range of its overall capacity. The reason for this was twofold: to allow for an extra 10% of backup energy in case of serious emergencies, as well as to prolong the lifespan of the battery and mitigate its vastly decreased efficiency over time [138]. Another sizeable advantage to using solid-state batteries (SSBs) in particular is their potential to achieve full sustainability. At the current rate of improvement in energy density, durability and recycling technologies, the sustainability-focused non-profit organisation (NGO) RMI estimates that net-zero mineral demand for cobalt, lithium and nickel can be achieved by 2050 [139]. These are important ecological considerations which may not necessarily be reflected in the short-term assessment of this vehicle.

Of course, it is especially important to assess the environmental impact of Owl-22 using one of the many different frameworks and models. In this report, the widely adopted Life Cycle Assessment (LCA) method will be used to provide a comprehensive overview of Owl-22's environmental sustainability [140]. Furthermore, as there are several types of LCA's, the specific one that will be used in this report is one that focuses solely on the Global Warming Potential (GWP). This LCA indicator measures the impact on climate change by expressing the emissions of all greenhouse gases in terms of the equivalent mass carbon dioxide [$kgCO_2e$] required for the same warming effect. In order to perform a preliminary LCA, the following functional unit will be defined: kilometre travelled per vehicle. This allows for the easy comparison with more conventional modes of transport. The three main sources of environmental harm within the aircraft will be considered: the battery, UAE's electricity generation and the materials used in the vehicle's structure. It is important to note that, as the Owl-22 is a one-person vehicle, no adjustments need to be made in order to comply with the functional unit.

For the LCA of the battery, the fact that modern and cutting-edge SSBs have a 0.05 - 0.09 [$kgCO_2e/kWh$] is used [141]. Furthermore, 80% of the energy capacity of the battery is 18.98 [kWh] and this corresponds to a 30 [km] journey. Therefore, assuming the battery will last for 8000 cycles, the final [$kgCO_2e/km$] can be determined [142].

For the estimation of the carbon footprint of the electricity, two values were relevant: the 0.4041

[$kgCO_2e/kWh$] from the UAE and the energy consumption of a max-range 30[km] flight being 18.98 [kWh]. Therefore, assuming the same linear relationship between energy consumption and range mentioned previously, the [$kgCO_2e/km$] of the electricity used by the Owl-22 can be determined.

Finally, for the estimate of the material's LCA, the following information was used: an estimate for the LCA per km of a 122 [kg] piece of aluminium used in the aviation industry, assuming a lifespan of 30 years (1.05e4 [$kgCO_2e$]). Then this was scaled down to the mass of aluminium used in the Owl-22. Although other materials in the vehicle will have a carbon footprint besides the aluminium, the LCA for these is much harder to determine with the resources available. As such, it has been assumed that the GWP of the materials of the Owl-22 is double that of the aluminium in the vehicle.

With this information, the estimated LCA can be seen in Table 10.2:

Table 10.1: GWP of Owl-22's different sources

Source	$kgCO_2e$ **per km**
Battery	0.01971
Electricity	0.30685
Materials	0.0338
Owl-22	**0.36036**

Thus, as was previously suggested by our sustainability expert, it is immediately apparent that the operational emissions dominate the carbon footprint of the vehicle. This emphasises the need to continue prioritising energy efficiency in all design stages to effectively decrease Owl-22's environmental impact.

Furthermore, as this LCA represents the final design of the Owl-22, a comparison can be performed with respect to other modes of transport in urban areas. Before performing this comparison, it is important to realise that road vehicles will have to travel greater distances than the Owl-22 in order to reach their destination; this is due to the fact that the Owl-22 can just take the shortest straight path to the destination, while ground vehicles have to adhere to roads. Therefore, the direct route index - how much longer car journeys are compared to straight-line distances - for Dubai has been used to compare the LCA of the Owl-22 with alternative transport. This index is 1.6 for Dubai; therefore, this value will be used for the comparison [143]. The results of this comparison can be seen in Table 10.2 below:

Table 10.2: Life cycle GWP of different vehicle types adjusted for distance travelled.

Vehicle Type	**kgCO_2e per VTOL km**
Gasoline-powered internal combustion car	0.32 – 0.48
Hybrid electric car	0.27 – 0.40
Plug-in hybrid electric car	0.37 – 0.43
Battery electric car (2021 electricity grid)	0.32 – 0.40
Owl-22 vertical take-off and landing aircraft	**0.36036**

As can be seen in the table, the Owl-22 performs relatively well in comparison to cars. For all types of cars except plug-in hybrid electric, it is inside the range provided. However, the Owl-22 can only carry 1 passenger, while most cars can carry a minimum of 4. Therefore, if a car is carrying more than 1 person, it would already be less polluting than the Owl-22. While this is true, it is worth mentioning that this eVTOL will mainly serve as an alternative to cars for daily commutes. And daily car commutes in the UAE mostly have one person per car; to be exact, the average passengers per vehicle in Dubai is 1.3 [144]. In conclusion, although cars have the potential to be less polluting forms of commuting when compared to the Owl-22, this depends on the number of passengers in the car. And since for daily commute this number tends to be 1, the option of the Owl-22 is equally environmentally sustainable.

10.2. Social Sustainability

The social pillar of sustainability is harder to assess quantitatively than its environmental counterpart; however, this does not make it less relevant or important. Simply put, social sustainability focuses

on the well-being of people and their communities, promoting and protecting equity, human rights, and quality of life [136]. This subsection discusses how the Owl-22 has been developed with these concepts as core parts of the design.

Firstly, electric propulsion and cyclorotors in particular help reduce noise pollution when compared to traditional rotorcraft. Furthermore, reducing noise emissions has been, aside from providing sufficient lift, the most important factor considered during the design of the coaxial rotors at the back of the vehicle. In order to be as quiet as possible, serrations have been added to sections of the rotors, the top rotor is larger than the bottom rotor in order to avoid interactions between their tip vortices, and the rotors have been designed to be co-rotating. This aspect of the Owl-22 is critical in determining whether it will be accepted by the communities living in the major cities of the UAE, which is why so much effort has been invested in addressing it.

Furthermore, the design and operational performance of the Owl-22 are designed to preserve the pilot's health and well-being. The Formula-1 seat provides comfort under all the loads the vehicle will experience throughout its use. In addition, the cockpit will be air-conditioned in order to ensure the temperature remains within a safe range. This aspect is of particular importance in the UAE, as the ambient temperatures can exceed what a pilot would be able to withstand, without immediate health concerns, for a half-hour flight.

Another important aspect of the integration of the Owl-22 into the UAE society is its alignment with the country's visions for advanced mobility and sustainability under initiatives such as Dubai's Smart Dubai Vision [145] and Abu Dhabi's SAVI cluster—designed to cultivate autonomous and air mobility solutions [146]. These factors will make the adoption of the Owl-22 into the communities of Abu Dhabi and Dubai smooth, as the vehicle and what it represents will be supported by said communities.

Since the Owl-22 will be manufactured in the UAE, its development and production will contribute to local job creation in the aerospace sector from R&D and design to assembly, testing, and support services. This aligns with the government's 'Make it in the Emirates' initiative, which aims to bolster domestic manufacturing and reinforce national pride through home-grown innovation [147]. By connecting the Owl-22 to UAE facilities, the project will strengthen technical expertise and the workforce and also build a sense of ownership among the local community. Furthermore, the presence of high-skilled job opportunities will likely enhance public acceptance and enthusiasm for the vehicle. As national sentiment increasingly values Emirati-built advanced technologies, the Owl-22 will serve as a commute solution and as a symbol of UAE innovation.

During peak hours, a 30 [km] urban commute by car in the UAE often exceeds 60 minutes, sometimes reaching 75–90 minutes in congested corridors like Business Bay or Sheikh Zayed Road [148]. In contrast, the Owl-22's 30 [km] flight takes just 30 minutes, saving commuters 30–60 minutes per trip during rush hours. That's between 1 to 2 hours saved daily, equating to 5 to 10 extra hours of personal time each week. Research in psychology and public health shows that how free time is used—particularly time spent on meaningful leisure or social activities—strongly correlates with improved life satisfaction, reduced stress, and better mental health. Studies highlight that even modest boosts in discretionary time, when well-managed, significantly elevate well-being and strengthen mental resilience [149]. Therefore, by reducing commutes, Owl-22 does not just provide convenience, but it also delivers tangible improvements to life quality. Freed from traffic-induced stress and granted extra time for leisure, family, or creative pursuits, commuters gain autonomy and psychological relief. In urban environments where "time poverty" is increasingly common, these improvements are even more valuable.

10.3. Economic Sustainability

The economic sustainability of the Owl-22 focuses on three main areas: the time-saving value it provides by avoiding traffic, job creation across the aerospace sector, and accessible financing options that make the vehicle more attainable for potential buyers. Owl-22 offers significant value for professionals dealing with the UAE's heavy traffic congestion. During peak hours, saving commuters 45–60 minutes per trip, which translates to 1.5–2 hours saved daily, or 7.5–10 hours per week. These time savings represent real economic value. For professionals whose time has monetary worth, or anyone who values work-life balance, the Owl-22's ability to cut commute times in half makes the investment

worthwhile. This aligns with growing market trends where consumers are willing to pay premium prices for mobility solutions that deliver substantial time efficiency.

Furthermore, the Owl-22's production and adoption will create employment opportunities across the entire aerospace value chain. Manufacturing, assembly, testing, maintenance, and air traffic management will all require skilled workers. The vehicle fits directly into Abu Dhabi's SAVI cluster initiative [146], which aims to create 30,000–50,000 new jobs while contributing AED 90–120 billion to the economy. Beyond local impact, the advanced air mobility sector is projected to become a USD 1.4 trillion market by 2040, according to Morgan Stanley forecasts [150]. This growth potential reinforces the economic viability of vehicles like the Owl-22 and supports long-term investment in the sector.

Several UAE banks now offer attractive financing for electric and sustainable vehicles, making the Owl-22 more accessible to potential buyers. Emirates NBD [151] provides Green Auto Loans with up to 80% financing and interest discounts of 0.25–0.5%. ADCB [152] offers green car loans starting at just 1.94% flat rate. Dubai Islamic Bank [153], HSBC [154], and Rakbank [155] have similar green financing programmes with competitive rates and reduced fees. These green loan programmes reduce the financial barrier to entry and align with national sustainability goals.

Another, more indirect socio-economic consequence of Owl-22 relates to the real estate sector. Currently, expats are significantly constrained to living in certain locations, which reduces the likelihood of traffic. Often, this involves choosing areas which avoid the use of Sheikh Zayed Road, the most congested highway in Dubai [148]. Since expat-employing companies are usually found in one of Dubai's three main business sectors, the neighbourhoods surrounding these areas are typically very desirable, and consequently, very expensive. Owl-22 can redefine this socio-economic phenomenon by increasing the number of locations considered by expats. Not only does this ease the financial costs of housing without impacting one's daily commute, it also more evenly distributes the population across the city, bolstering Dubai's real estate market.

The combination of competitive financing rates, government policy support, and institutional backing creates favourable economic conditions for the Owl-22's market entry while supporting the UAE's broader economic diversification and sustainability objectives.

11 Business Case and Market Evaluation

In addition to the technical aspects of the Owl-22, it is equally important to evaluate the business aspect of the product. This chapter will focus on these aspects of the product. One of the first steps taken when designing Owl-22 was determining a target market for the vehicle; this market has been analysed thoroughly in the market analysis presented in Section 11.1. The market analysis is followed by a financial analysis presented in Section 11.2 which analysis both non-recurring and recurring costs related to the production as well as development of Owl-22. This section also includes the determination of the selling price of the vehicle. Lastly, an investment analysis is presented in Section 11.3 which evaluates the financial viability of Owl-22.

11.1. Market Analysis

To ensure the success of the Owl-22 project, a comprehensive market analysis is essential. This analysis provides the team with a clear understanding of the current market landscape and its key dynamics. Particular emphasis will be placed on the competitive environment, including Porter's Five Forces analysis, as well as a comparative assessment of Owl-22's direct competitors. Moreover, a future market expansion has been added to the market strategy to identify possible markets Owl-22 could also enter due to their similarities to the current market.

11.1.1. Market Overview and Target Audience

The United Arab Emirates (UAE) has been selected as the initial launch market for Owl-22 due to its highly supportive legislative and infrastructural environment for air mobility innovation. The country provides designated test zones, progressive airspace management plans, and a national push for advanced aviation technologies. Its rapid urban development and strategic vision to become a global innovation hub make it an ideal environment to introduce a personal air transport solution.

In addition, the UAE offers a highly attractive customer base. The population includes a high proportion of wealthy Emirati nationals and expats who are receptive to innovation and have a strong affinity for exclusive, technology-driven experiences. This audience is not only able to afford novel mobility solutions but also motivated to get them by the ability to bypass frequent traffic congestion in cities such as Dubai and Abu Dhabi. Moreover, the country's luxury-oriented lifestyle culture aligns closely with the premium positioning of Owl-22.

Owl-22 is specifically designed to meet this demand. Its compact folding architecture allows storage and operation from private properties or rooftops, while its semi-autonomous capabilities simplify piloting. With a targeted price below $100,000, it provides a cost-accessible yet aspirational option for high-income early adopters.

Globally, the urban air mobility market is expected to grow from $4.59 billion in 2024 to $23.47 billion by 2030, with a compound annual growth rate (CAGR) of 31.2% [156]. Regionally, the Middle East and Africa generated $138.3 million in UAM revenues in 2023 and is forecast to grow at a CAGR of 41.9% between 2024 and 2030 [157]. Although country-specific estimates are scarce, the UAE's early investment in regulatory frameworks and vertiport infrastructure suggests it will be a central driver of regional market growth. These factors confirm the UAE as a strategic location for the launch of Owl-22.

11.1.2. Stakeholder Identification

Following the assessment of the target market and the definition of the target audience, it is essential to identify the broader group of stakeholders that will influence or be affected by the introduction of Owl-22 in the UAE. To structure this identification, stakeholders have been mapped using a Power/Interest grid as depicted in Figure 11.1, categorising relevant parties based on their influence and interest in the project.

- **Manage Closely:** These stakeholders have both high influence and high interest, and will be

actively engaged throughout the project. This group includes regulatory bodies such as the General Civil Aviation Authority (GCAA), Dubai Civil Aviation Authority (DCAA), and the Road and Transport Authority (RTA), all of whom are critical in certifying and enabling airspace access. Customers are also key players in this category, as their expectations around convenience, safety, and luxury will shape the product experience. Additionally, strategic technology partners such as CycloTech, which supplies Owl-22's cyclorotor propulsion, are crucial for successful system integration and performance.

- **Keep Satisfied:** These stakeholders have high influence but lower interest in the day-to-day operations. Infrastructure providers and manufacturers fall into this group, particularly those involved in battery systems, software integration, or local production facilities. Municipal governments also belong here, as their noise and zoning regulations may influence take-off/landing permissions.
- **Keep Informed:** These are stakeholders with high interest but lower influence. They include future employees, media outlets, telecom and data providers (for flight communication), and the general public. Early and transparent communication with these groups will support public trust, employee recruitment, and social acceptance of semi-autonomous vehicles.
- **Monitor:** At this stage of the project, no stakeholders have been classified with both low influence and low interest. Given the innovation-driven and high-visibility nature of the UAE's AAM ecosystem, most stakeholders are currently engaged at some level. As the market matures, this may shift.

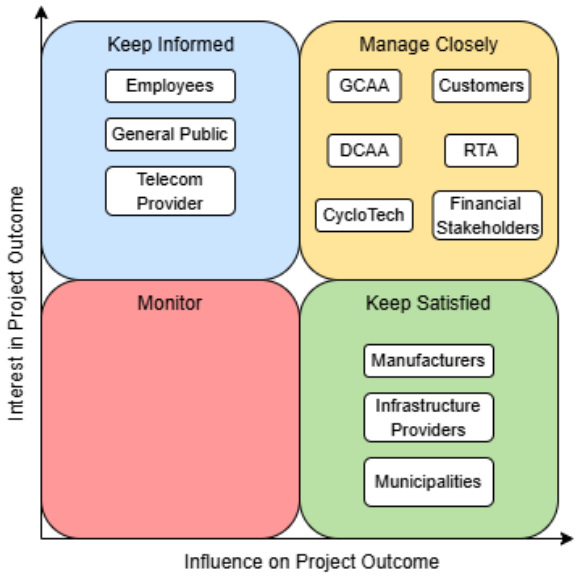

Figure 11.1: Power/Interest grid stakeholders.

Proactive engagement with regulatory bodies, technology partners, and future customers will be critical to ensure Owl-22's successful certification, deployment, and adoption in the UAE market.

11.1.3. PESTEL Analysis

The personal air transport industry in the UAE can be influenced by external factors such as the legislation of the UAE or economic factors. In a PESTEL analysis, these external factors are analysed to identify potential threats and opportunities in the UAE market.

Political and Legal Factors

The UAE has a stable government that actively promotes innovation, especially in the aviation and transport sectors. Key regulatory bodies such as the GCAA and DCAA have created a progressive framework to support experimental aircraft, including regulations on vertiports and air corridors [158, 159,

160]. The legal requirement for vehicle-specific pilot licensing aligns with Owl-22's semi-autonomous functionality, which is designed to assist less experienced users while remaining compliant.

Economic Factors
With one of the highest GDP per capita globally and low unemployment, the UAE supports a robust luxury market [161]. Dubai's aviation sector alone is projected to contribute $53 billion to the national GDP by 2030, reflecting its strategic importance. Policies such as zero income tax, free trade zones, and open skies agreements create a favourable climate for startups like Owl-22 to scale manufacturing and operations cost-efficiently [162, 163].

Social Factors
UAE residents are generally open to new technology, particularly high-income Emiratis and expats with a lifestyle aligned to exclusive experiences. This sociocultural readiness, combined with rising traffic congestion in Dubai and Abu Dhabi, creates demand for personal alternatives to ground-based transport [164, 165]. Owl-22 responds to this with its compact, individually owned design.

Technological Factors
The UAE actively supports VTOL innovation and has begun mapping air corridors to enable both piloted and autonomous operations [160]. Owl-22's semi-autonomous features align with these national goals, potentially accelerating certification and integration. Partnerships with local tech institutions and international suppliers like CycloTech further enhance its positioning within this tech-friendly ecosystem.

Environmental Factors
The UAE is committed to environmental sustainability by having signed the Paris agreement, with initiatives aimed at reducing carbon emissions and promoting green technologies in aviation [166]. The UAE has become aware that its wealth has been highly dependent on finite natural resources such as oil. Using its Net Zero 2025 strategy, the UAE's economy is shifting towards a more diversified and sustainable economy [167]. Owl-22's zero-emission electric drivetrain supports this goal while also appealing to environmentally conscious consumers. However, high temperatures and desert conditions may require specialised material and thermal solutions to ensure reliability.

Overall, the UAE presents a highly favourable environment for the launch of a personal eVTOL system. Political and economic conditions strongly support air mobility innovation, and the social and technological landscape aligns with Owl-22's premium, compact, and semi-autonomous offering. However, the project must still navigate regulatory complexity, climatic challenges, and consumer trust in automation to fully capitalise on these advantages.

11.1.4. Competitive Landscape

To assess the competitive pressures surrounding Owl-22, a Porter's Five Forces analysis is used. This framework evaluates the threat of new entrants, bargaining power of suppliers and buyers, threat of substitutes, and industry rivalry, providing insight into the intensity of competition and the potential profitability of entering the UAE's advanced air mobility (AAM) market.

- **Threat of New Entrants – Moderate:** While capital and certification requirements create barriers, the UAE's supportive regulation and recent developments attract new players.
- **Supplier Power – High:** The emerging eVTOL industry relies on a small number of certified component and propulsion system providers. Owl-22's reliance on CycloTech for its cyclorotors increases this risk. Moreover, dependencies on future vertiport infrastructure and airspace systems may increase supplier leverage if not mitigated through local partnerships.
- **Buyer Power – Moderate:** The novelty of personal eVTOLs limits buyer options, but high expectations for luxury and safety elevate customer influence.
- **Threat of Substitutes – Moderate:** Ground-based luxury transport, a well-developed public transport system and future autonomous vehicles offer alternatives. However, Owl-22 aims to differentiate by offering congestion-free travel and personal scheduling for more convenience.
- **Industry Rivalry – High:** UAE positions itself as a global pioneer in AAM, and at least four companies are entering the UAE AAM market, most focused on shared taxi services. Owl-22 aims to avoid direct rivalry by targeting the underdeveloped personal ownership niche.

As shown in the Porter analysis, the UAE positions itself as a hub for advanced air mobility. Several companies have already announced or initiated plans to deploy eVTOL solutions in the region. The following competitor analysis outlines four key players and highlights how Owl-22 differentiates itself within this evolving market.

1. Joby Aviation
Joby is a frontrunner in the air taxi sector with a piloted, five-seat eVTOL capable of vertical takeoff and a range of approximately 240 $[km]$. The company has partnered with Dubai's RTA and plans to launch air taxi services by 2026. They are the first company to apply for an Air Operator Certificate (AOC) from the GCAA and have started the construction of the first vertiport at Dubai International Airport [168]. Joby relies on a vertiport infrastructure and operates a shared-mobility service instead of a personal one.

2. Archer Aviation (Midnight)
Archer's Midnight targets high-frequency urban air taxi operations, designed for short flights with a maximum range. 30 $[km]$. It's a piloted, four-passenger vehicle aiming to begin service in Dubai in the near future, but it has not specified when yet. This vehicle will provide a similar service as Joby, making it highly dependent on infrastructure too. Moreover, Archer collaborated with Falcon Aviation to operate eVTOL flights connecting Abu Dhabi and Dubai, creating an air transport method that has a bigger range than Owl-22 [169].

3. Eve Air Mobility
Just like Joby and Midnight, Eve, backed by Embraer, will also pursue air taxi services with a strong focus on air traffic integration and vertiport infrastructure. This air taxi will mainly focus on tourism and fly the tourist routes from Atlantic The Palm, such as going to Downtown. Moreover, they collaborated with Kookiejar to develop urban air traffic management systems for operations in Dubai [170].

4. Autoflight and Xpeng AeroHT
Autoflight and Xpeng AeroHT are China-based companies developing eVTOLs aimed at private ownership. Autoflight's Prosperity I has already completed test flights in Dubai, showing interest in the UAE market, though its models are relatively large and depend on vertiport infrastructure [171]. Xpeng AeroHT is developing the X3, a flying car targeting the UAE for personal use, which also drives on roads [172]. While innovative, this dual-mode concept poses certification and operational challenges.

Table 11.1 allows a comparison between the main competitor of Owl-22 on the market presented above. In contrast to these competitors, Owl-22 is a compact, personal eVTOL designed for individual ownership rather than shared use. In the future, once legislation has been adapted to the growing demand, it would not require vertiport infrastructure and could operate from private properties, guaranteeing user convenience.

Table 11.1: Comparison of key eVTOL competitors in the UAE market.

Company	Product Type	Ownership Model	Infrastructure Dependency	UAE Entry	Key Differentiator (vs. Owl-22)
Joby Aviation	eVTOL air taxi	Shared service	High	Planned 2026	Larger, for shared use only
Archer Aviation	eVTOL air taxi	Shared service	High	Announced	Short-range, vertiport-reliant
Eve Air Mobility	eVTOL air taxi	Shared service	High	Under development	System integration focus
Xpeng AeroHT	Roadable eVTOL	Private	Medium	Uncertain	Dual-use (car/air) configuration
Owl-22	Personal eVTOL	Private	Low	Designed for UAE	Compact, personal use; lower infrastructure dependence

11.1.5. SWOT Analysis

Based on the PESTEL analysis and Porter's analysis, the opportunities and threats in the UAE market for personal air transport can be identified. Based on this information, a SWOT analysis can be made in which the strengths and weaknesses of the Owl-22 project are identified as well as the opportunities and threats in the market. The SWOT analysis is depicted in Table 11.2.

Table 11.2: Final SWOT analysis for Owl-22.

Strengths	**Weaknesses**
• Compact folding design with cyclorotors allows easy storage and private use. • Semi-autonomous features improve accessibility and ease of operation. • Target price <$100k makes it accessible for tech-forward luxury consumers. • Low dependency on vertiports and ground infrastructure. • Sustainable design supports UAE's Net Zero 2050 goals. • Strong product identity with innovative "transformer-style" appeal.	• Limited range (30 km) and low speed (60 km/h) restrict use cases. • Certification challenges due to novel cyclorotor and folding mechanisms. • Requirement for type-specific pilot license may deter casual users. • No flight test history or customer feedback yet available. • Lack of a defined maintenance and service infrastructure.
Opportunities	**Threats**
• First-mover advantage in UAE's personal eVTOL niche. • Partnership with CycloTech offers technological edge. • Strong regulatory support for air mobility innovation in UAE. • Tech-savvy, high-income customer base receptive to new luxury mobility. • Rising demand for decentralised, individualised transport post-COVID.	• Risk of larger players entering the personal eVTOL market. • Regulatory delays due to autonomous and cyclorotor features. • Dependence on CycloTech creates supplier vulnerability. • UAE infrastructure may prioritise air taxis over private vehicles. • Economic shifts could affect consumer spending on luxury tech. • Public concerns about safety or automation could slow adoption.

The SWOT shows that Owl-22's unique position in the personal eVTOL niche, combined with the UAE's strong regulatory support and tech-forward user base, creates a compelling opportunity for market entry. These insights directly inform the positioning and differentiation strategy outlined in the next section.

11.1.6. Market Strategy

Based on the SWOT analysis conducted in the previous section and the competitive landscape analysed in Subsection 11.1.4, a strategy can be constructed to successfully launch Owl-22 into the market. This market strategy will leverage the UAE's high-income demographic and technological openness. The strategy is built around three pillars: positioning, differentiation, and the future plan.

Positioning & Differentiation

Owl-22 will be positioned as a premium personal air mobility solution, designed for wealthy early adopters in urban UAE settings. Unlike competitors offering shared air taxi services such as Joby and Archer, Owl-22 is built for private ownership. This appeals to individuals seeking autonomy, exclusivity, and time savings in their daily or recreational mobility. The aircraft will be framed as both a practical tool for congestion avoidance and a status-enhancing, tech-forward lifestyle product.

Besides this exclusive positioning strategy, a successful differentiation strategy needs to be imple-

mented in order for Owl-22 to stand out in the increasingly personal air vehicle market. To create a competitive advantage in the market, Owl-22 will focus on:

- **Personal Use**: Unlike competitors such as Joby Aviation, Archer Aviation, and Eve Air Mobility, Owl-22 is designed for private ownership, allowing users to travel on their own schedule without relying on shared service providers. This caters directly to the privacy and flexibility expected by high-end users. While current legislation requires the use of designated take-off zones, Owl-22's compact design anticipates future regulatory shifts that will allow operations directly from private properties, further reducing infrastructure dependence over time.
- **Compact, Foldable Design**: Having analysed the direct competition for personal air vehicles like Joby S-4 and Archer Aviation's Midnight, Owl-22 distinguishes itself with a significantly more compact design due to having an undeployed volume of less than 4 $[m^3]$. The foldable and compact design of Owl-22 allows a more flexible use as it allows easier parking and storage, but also reduces infrastructure dependency, such as the need for large vertiports. The compactness of Owl-22 will align more with the luxury consumers' demand for convenience, exclusivity, and independence.
- **User Experience**: Owl-22 combines a sleek, aerodynamic design with a compact form to deliver a refined, premium look aligned with UAE luxury standards. The intuitive user interface, operable via iPad, simplifies flight control and reinforces the seamless, tech-forward experience expected by high-end users.
- **Semi-Autonomy**: Integrated flight path assistance and automated take-off/landing reduce pilot workload. This lowers the barrier for users who may be licensed but did not have an extensive professional training, while still meeting UAE regulations for vehicle-specific licensing.
- **Sustainability**: As a fully electric VTOL not emitting carbon dioxide during its operations, Owl-22 supports the UAE's Net Zero 2050 targets. This not only strengthens alignment with government policy but also appeals to environmentally conscious luxury consumers.
- **Affordability Within Premium Segment**: With a target price below $100,000, Owl-22 offers a more accessible alternative to personal aircraft like the Jetson-1 ($128,000), making it a competitive option for high-income individuals seeking private air mobility between luxury cars and helicopters.

Future Market Expansion

Following successful market entry in the UAE, Owl-22 plans to expand into regions with similar demand characteristics and emerging regulatory support. Target markets include:

- **Kingdom of Saudi Arabia (KSA)**: Vision 2030 includes major investment in advanced transport systems, particularly in smart cities like NEOM, which has announced air mobility trials. However, regulatory frameworks for personal eVTOLs are still emerging, requiring early engagement [173].
- **Singapore**: Known for its clear and adaptive aviation policies, Singapore is already piloting UAM corridors and has regulatory bodies like CAAS working with industry players [174]. Its dense urban layout and innovation focus make it a highly feasible next market.
- **Qatar**: Qatar's compact geography, high-income population, and strong state-led innovation agenda create favourable conditions for personal air mobility. While current legislation is limited, the centralised governance structure may allow for the efficient development of a tailored regulatory framework for eVTOLs in partnership with national authorities [175].
- **United States:** As a global leader in aviation innovation, the U.S. offers strong long-term potential for Owl-22. Similar to the UAE, the U.S. has a high concentration of wealthy, tech-savvy consumers who are receptive to luxury and personal mobility solutions [176]. Politically, the Federal Aviation Administration (FAA) has made significant strides in preparing for AAM by establishing a powered-lift category and issuing new certification guidelines [177]. However, unlike the UAE's highly centralised and innovation-driven governance, the U.S. regulatory landscape is fragmented across states and municipalities, which could slow implementation. Furthermore, airspace congestion and more restrictive take-off/landing regulations for private property use currently pose

operational constraints [178]. Still, with ongoing national investment in vertiport infrastructure and autonomous flight regulation, the U.S. remains a promising future market, especially for affluent early adopters in innovation hubs like California, Texas, and Florida.

All these countries share common characteristics with the UAE in terms of high income, openness to new technology, innovation investment, and urban congestion, offering natural next steps for Owl-22. However, entry will depend on legal feasibility which in turn, depends on the pace of regulatory evolution.

11.2. Financial Analysis

Owl-22 aims to deliver a luxurious yet accessible experience to urban air mobility. To achieve this balance, a financial analysis was conducted using a set of python scripts *found here*, in which the cost of the product was analysed, and the price was determined based on these costs to examine if it meets all requirements related to REQ-RES. The first step taken to determine the total costs was breaking them down into recurring and non-recurring costs as displayed in Figure 11.2.

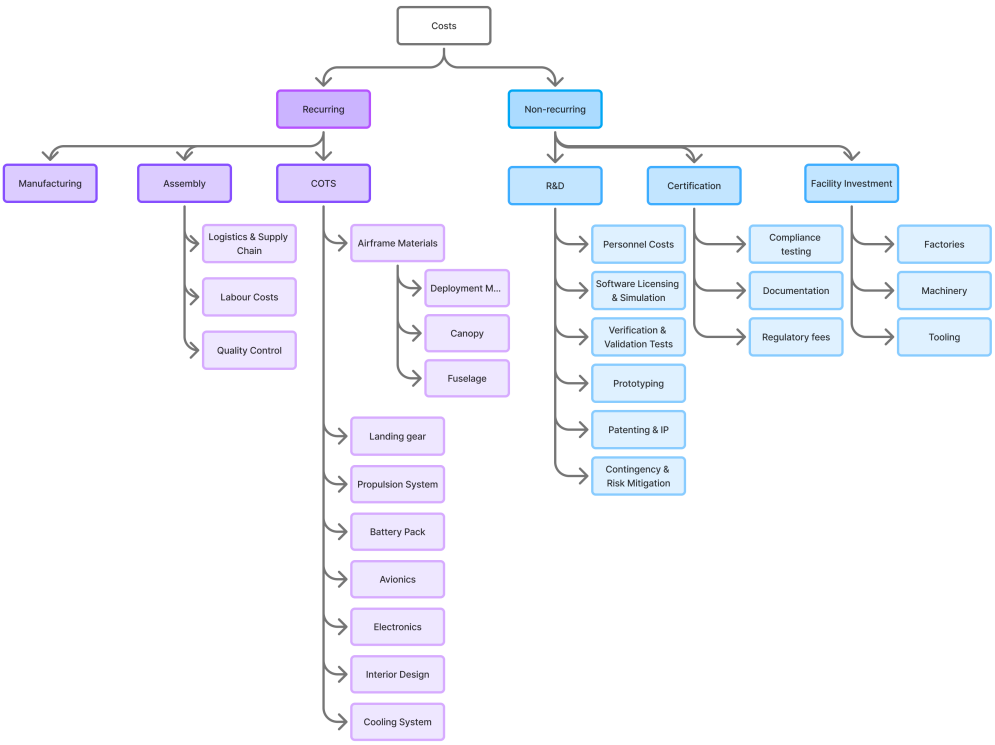

Figure 11.2: Cost breakdown.

The recurring costs represent all costs incurred per unit and are subdivided into:

- **Commercial Off-The-Shelf (COTS)**: These include standard components like batteries, avionics, wiring, and a portion of the propulsion system that is off-the-shelf through the collaboration with Cyclo-Tech. These are mostly mass-produced subsystems purchased from suppliers. To reflect bulk purchasing benefits, the cost of COTS is modelled with a logarithmic price reduction curve fitted to NASA cost estimation data [179]:

$$C_{\text{COTS}}(N) = C_{\text{COTS,base}} \cdot [1 - (0.0721 \cdot \ln(N) - 0.2322)] \tag{11.1}$$

  $C_{\text{COTS,base}}$ is the baseline cost of all COTS subsystems for the production of a single vehicle. This value was determined by estimating the cost of each relevant subsystem individually:

  - *Airframe*: Includes the raw material costs of the fuselage, canopy, and deployable mechanism structure. These material costs, such as the aluminium alloy, are treated as part of the

COTS category due to their fixed per-unit nature. However, the labour-intensive processes such as composite layup, machining, and integration of deployable parts are accounted for separately under manufacturing costs.

- *Battery pack*: Battery costs are estimated using the 2025 $/kWh for a solid-state battery, which is 450$/kWh [180]. This price is discounted by 10 % over a timeline of 5 years, as it is expected that large-scale production of Owl-22 will start after 5 years.
- *Avionics*: Estimated from certified GNSS, onboard computing, and multi-sensor navigation packages typical in high-end drones and light eVTOLs.
- *Propulsion (partial)*: COTS from motor and propellers were priced based on known suppliers. The price for cyclorotors remains enclosed to this day, so this price has been determined by multiplying the costs of the motor and propeller assembly by a contingency of 30%. It has been decided to do it this way due to CycloTech's promise that cyclorotors will cost approximately the same as normal rotors in a couple of years.
- *Landing gear (partial)*: Wheels and aluminium legs were priced separately based on costs from known suppliers, with an integration multiplier to reflect system-level fit.
- *Cooling and wiring systems*: Estimated using comparative data from existing aircraft such as Volocity, adjusted to fit Owl-22 specifications [181].

These costs were derived from public supplier data, industry benchmarks, and parametric relations. A general contingency of 10% was applied over the total COTS to account for uncertainty in supplier pricing, design changes, and excluded systems for which prices could not be determined, such as interior design. These assumptions will be critically examined in the sensitivity study (see Table 11.2). The breakdown of the total budget for the COTS for the production of a single vehicle is displayed in Table 11.3.

Table 11.3: Breakdown of baseline COTS cost per subsystem.

Subsystem	Estimated Cost [$]
Airframe Materials	174.90
Landing Gear (COTS)	1,500.00
Propulsion (COTS)	27,485.00
Battery Pack	7,302.00
Avionics	10,620.00
Electronics (Wiring)	3,000.00
Cooling System (AC)	5,000.00
Subtotal (before contingency)	55,081.90
Contingency (10%)	5,508.19
Total COTS Cost (Base)	60,590.09

- **Manufacturing**: Covers all in-house production activities such as fabrication of the airframe and special treatments like serrated propellers. The learning curve model used assumes the standard aerospace learning rate of 85%, capturing improved efficiency and lower cost with increasing production volume [179]:

$$C_{\text{manuf}}(N) = C_{\text{manuf,base}} \cdot N^{\log_2(0.85)} \tag{11.2}$$

The baseline manufacturing costs per subsystem are shown in Table 11.4. These values serve as the initial inputs to the learning curve model described in Equation 11.2, which accounts for production efficiency gains at larger batch sizes.

The airframe manufacturing cost was estimated using a mass-based approach, applying standard aerospace rates of $350/kg for composite materials and $150/kg for aluminium alloy structures.

These reflect typical fabrication, machining and finishing costs observed in UAV and light aircraft applications.

For the serrated rotors and landing gear, detailed process-level manufacturing data was not available. Therefore, their manufacturing costs were approximated by applying a contingency multiplier to the corresponding COTS cost components. In particular, a 25% uplift was applied to the standard rotor cost to account for additional finishing and serration complexity, and a 10% integration multiplier was used for the landing gear structure. The effects of these contingencies are studied in a sensitivity study in Table 11.2.

Table 11.4: Baseline manufacturing cost per subsystem (before learning-curve scaling).

Subsystem	Manufacturing Cost [$]
Airframe	8,550.00
Landing Gear	152.48
Propulsion	800.00
Total Manufacturing Cost	9,502.48

- **Assembly**: Assembly costs represent final system integration, quality control, logistics and labour costs. Due to their dependence on vehicle complexity rather than learning effects, these are modelled as a fixed share of the COTS and manufacturing cost:

$$C_{\text{assembly}}(N) = 0.4 \cdot (C_{\text{COTS}}(N) + C_{\text{manuf}}(N)) \tag{11.3}$$

This 40% factor reflects the standard percentage used in the aerospace industry for assembly costs [182]. Before this factor is applied, the total assembly costs for the production of a single vehicle would come down to $ 28,156.43.

Having established the baseline recurring costs for the production of a single vehicle, the next step was to apply the cost reduction models defined in Equation 11.1 and Equation 11.2. Since assembly costs are proportional to both COTS and manufacturing costs, they were indirectly affected by both learning effects. By summing the scaled cost components, the total recurring unit cost as a function of production volume was obtained and visualised in Figure 11.3.

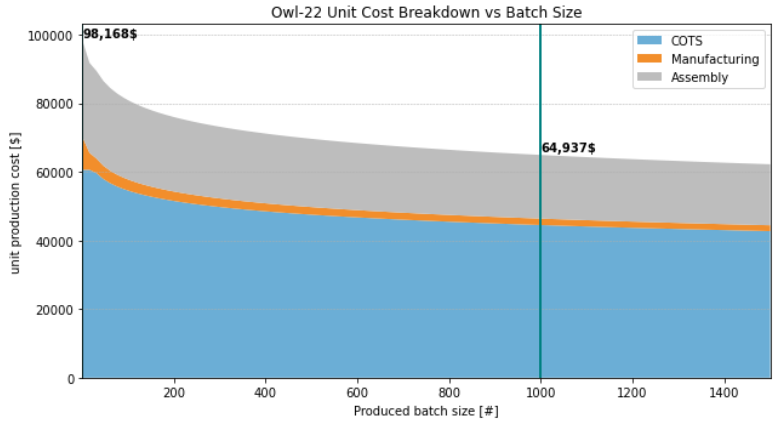

Figure 11.3: Cost scaling with batch size.

From this figure, it can be observed that the recurring cost per unit decreases substantially with increased production. At a target batch size of 1,000 vehicles per year, the total recurring unit cost was estimated at $64,936.89. This is a significant reduction compared to the $98,168 of the production of a single unit.

Although recurring costs represent the per-unit expenditures during serial production, they exclude the significant one-time investments required for product development, regulatory approval, and facility setup. These non-recurring costs are essential for bringing the Owl-22 to market and are amortised across the total expected production run. These amortisations and depreciations need to be (partially) included in the price of Owl-22 in order to ensure breaking even in the lifetime of the investment.

The non-recurring costs (NRCs) of the Owl-22 program were estimated by identifying three major fixed investment categories: research and development (R&D), certification and production facilities. These values were based on public benchmarks, industry analogues, and engineering judgement, with contingency factors applied where appropriate.

- **Research and Development (R&D):** The base R&D cost was budgeted at $450 million, based on Joby Aviation's publicly disclosed expenditures for the development of a comparable eVTOL platform. According to Joby's quarterly financial reports, the company spent approximately $496 million on R&D over the twelve months ending March 31, 2025, with quarterly R&D investments consistently exceeding $130 million [183].

  Given that Owl-22 is expected to remain in production for at least 15 years, with a total project investment lifetime of 20 years, an upfront R&D investment of $450 million is reasonable as well as necessary. This expenditure establishes the technological foundation required to ensure long-term technical maturity and scalability. The inclusion of novel and complex technologies, such as cyclorotors, the semi-autonomous flight control system, and the folding mechanism, demands extensive investment in prototyping, control systems, and software. These elements significantly elevate technical risk and therefore justify higher R&D costs, which also include the risk mitigation budget as displayed in Figure 11.2. Moreover, having said this, it is also common in the aerospace sector that R&D investments increase over time, as programs evolve and additional testing or software upgrades become necessary.

  To account for project-specific needs, an additional $2 million was allocated for the development of semi-autonomous software features [181]. A further $150,000 was included to cover patent applications, legal fees, and intellectual property management. This brings the total required R&D investment to $452.15 million.

- **Certification:** Following FAA guidelines, a base certification cost of $1 million was assumed for aircraft with fewer than three seats [184]. Given the inclusion of semi-autonomous features, this cost was increased by a contingency of 50%, resulting in a total certification budget of $1.5 million.

- **Production Facilities:** A facility size of 2,000 [m^2] was assumed, located in the UAE. Budget items included building construction, tooling, machinery, IT infrastructure, support systems, and installation. A 15% contingency was added to the subtotal, in line with NASA's aerospace cost modelling practices, to account for unforeseen expenditures for the facilities [185]. The total facility investment was budgeted at $11.6 million.

Summing all categories results in a total non-recurring investment of $466,277,000. These costs are considered fixed and are amortised over the full projected production lifetime of 15 years, corresponding to a total output of 15,000 units (1,000 units per year). To comply with the stakeholder-imposed price requirement of $100,000 per unit, only 50% of the R&D cost is carried forward into the per-unit amortisation. This adjustment reflects the assumption that a significant portion of the development cost may be externally funded or covered through the profit margin over the project's lifetime. The remaining non-recurring costs are fully allocated to the per-unit price to ensure financial sustainability across the production timeline.

The final step in determining the unit selling price was selecting an appropriate profit margin. This margin was optimised within the constraints defined by **REQ-RES-COST** to stay below a price of $ 100,000 while minimising the time to break-even. Several profit margins were evaluated iteratively, and a margin of 22.5% was found to be optimal. At this level, the price per unit remained within the acceptable range, and the quickest break-even time would be achieved after approximately 13.5 years, as shown in Figure 11.4.

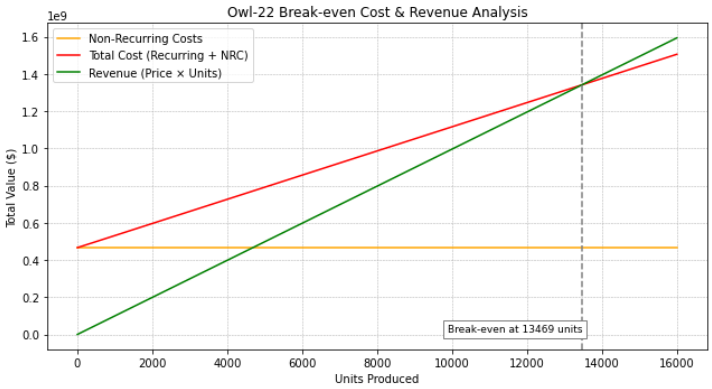

Figure 11.4: Break even analysis Owl-22.

A profit margin of 22.5% results in a final selling price of $99,575 per unit. This value satisfies the constraint imposed by **REQ-RES-COST** while ensuring financial viability. A detailed breakdown of the cost structure and pricing components is provided in Table 11.5.

Table 11.5: Total per-unit price breakdown at a production volume of 1,000 units per year.

Cost Component	**Per-Unit Value [$]**
Recurring Costs	64,936.89
Non-Recurring Costs (Amortised)	16,360.74
Total Cost (before profit)	81,297.63
Per-unit Profit (22.5%)	18,277.46
Final Selling Price	**99,575.09**

Sensitivity Analysis Recurring Costs

To evaluate the robustness of the recurring cost estimations for the Owl-22 system, a sensitivity analysis was conducted by varying the effective cost multipliers for key subsystems and contingency parameters. As clarified in the previous section, contingencies were used to determine the recurring costs of the airframe, propulsion system and landing gear. Moreover, the entire COTS was multiplied by a contingency to account for uncertainties, as well as excluded systems from the current cost estimation, such as interior design.

The initial cost estimations were based on the following contingency assumptions, as summarised in Table 11.6. However, the sensitivity analysis employed a one-at-a-time (OAT) method: each contingency parameter was varied independently across a realistic range (typically 1.0 to 1.4), while all other parameters were held constant. For each variation, the total recurring unit cost was recalculated, allowing direct observation of the effect of each assumption.

Table 11.6: Initial contingency assumptions for recurring cost estimation.

Component	**Contingency Type**	**Value**
Avionics integration	Multiplicative uplift	1.20
COTS cost allowance	Additive contingency	10% (i.e. 1.10 multiplier)
cyclorotor COTS uplift	Multiplicative uplift	1.30
Serrated propeller uplift	Additive manufacturing uplift	25% (i.e. 1.25 multiplier)
Deploy mechanism impact	Multiplicative uplift on manufacturing	1.20

The results, shown in Figure 11.5, reveal which contingencies have the greatest influence on the recurring cost estimate. Notably, the cyclorotor and COTS contingencies produced the largest deviations

in unit cost, indicating that propulsion-related and component uncertainty are key cost drivers. In contrast, the deployment mechanism and the serration uplifts had more moderate effects within the tested range.

This analysis underscores the importance of accurate cost data for novel propulsion components and reinforces the need for conservative assumptions in early-stage design. The plotted trends also demonstrate that the model responds linearly to most contingencies, validating the use of multiplicative uncertainty modelling for this application.

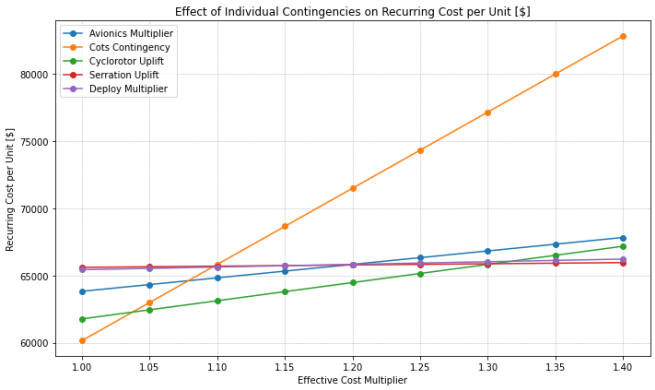

Figure 11.5: Sensitivity analysis recurring costs.

11.3. Investment Analysis

To evaluate the financial viability of Owl-22, an investment analysis was conducted using both a Return on Investment (ROI) and Net Present Value (NPV) analysis. These analyses help assess whether the project yields sufficient financial return to justify the capital invested.

11.3.1. Return on Investment (ROI)

The ROI is used to assess the profitability of the investment as it indicates how much profit or loss an investment generates relative to its cost. For Owl-22, a total of 15,000 units is projected to be sold over the 15-year production life. Each unit yields an estimated gross profit of $34,638.20, based on a selling price of $99,575.09 and recurring production cost of $64,936.89. The resulting ROI is:

$$\text{ROI} = \frac{\text{Total Profit}}{\text{Total NRC}} = \frac{N \cdot (P_{\text{unit}} - C_{\text{rec}})}{C_{\text{NRC}}} = 1.11 \tag{11.4}$$

The ROI is positive, indicating that the project is expected to return $1.11 for every dollar invested in non-recurring development. This suggests that the Owl-22 program can recover its full capital investment and yield an additional 11% profit over its lifetime production of 15,000 units. While the return is modest by aerospace standards, it reflects a financially viable path under the given production assumptions and price constraints.

11.3.2. Net Present Value (NPV)

The NPV evaluates the present-day value of all future cash flows, accounting for the time value of money by discounting cash flows to the start of the investment project as depicted in Equation 11.5. In this analysis, it is again assumed that certification and development will take 5 years, meaning that there will be no cash flows in the first 5 years of the investment lifetime. Positive net cash inflows from sales are assumed to begin in year 6 and continue annually through year 20.

$$\text{NPV} = \sum_{t=1}^{T} \frac{CF_t}{(1+r)^t} - C_{\text{NRC}} \tag{11.5}$$

Due to the early-stage nature of the project, the cash outflows associated with development, certification, and infrastructure during the first five years have not been explicitly modelled on a year-by-year basis. Instead, the total non-recurring cost of $466.28 million is treated as a lump-sum investment at year 0. While this simplification excludes the temporal distribution of development costs, it is considered reasonable at this phase of the analysis, given the limited detail available on the year-specific budget breakdown.

Instead of calculating the NPV for a single discount rate, it has been decided to calculate it for several rates ranging from 4% to 12% to account for the worst case possible. The annual net profit of $34.64 million was discounted back to year 0 for each rate. Figure 11.6 presents the resulting NPV sensitivity curve.

Rather than evaluating the NPV for a single discount rate, a sensitivity analysis was performed across a range of rates from 4% to 12%. This approach provides insight into the financial robustness of the project under both optimistic and conservative assumptions. For each rate, the annual net profit of $34.64 million was discounted back to year 0 for each rate. Figure 11.6 presents the resulting NPV sensitivity curve.

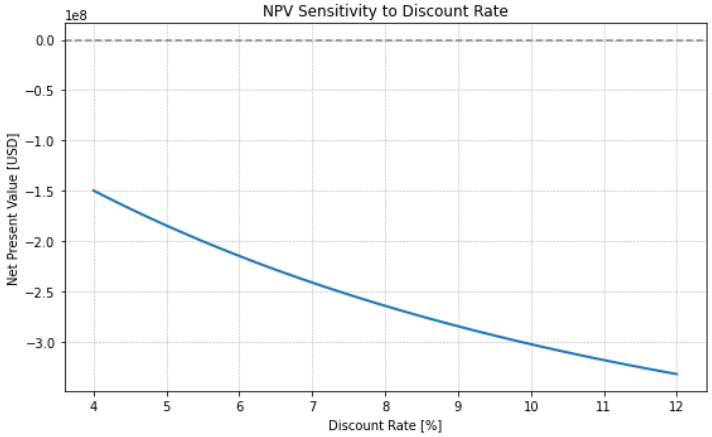

Figure 11.6: Sensitivity of NPV to discount rate (production years 6–20).

Figure 11.6 shows that across the tested range, the NPV remains negative, with an average value of $-256.5 million. This result indicates that, while the project is profitable in absolute terms as shown by ROI, it does not meet the financial return expectations when accounting for the cost of capital.

11.3.3. Interpretation and Conclusion

Together, the ROI and NPV offer a balanced view of the financial viability of Owl-22's investments. The ROI demonstrates that the project could be financially attractive if the cash flows remain constant throughout the project's lifetime. However, due to uncertainties of the actual cash flows throughout the project's lifetime caused by inflation and changing markets, the ROI alone cannot be considered reliable. As the NPV takes into account these economic uncertainties, such as inflation through the discount rate is deemed more reliable to analyse the investment. However, NPV suggest that under traditional financial valuation, the return is insufficient to compensate for investment risk at standard discount rates. To improve investment attractiveness, a positive or less negative NPV is recommended. Ways to improve the NPV are:

- Reducing non-recurring costs through strategic partnerships or grants.
- Increasing production scale beyond 1,000 units annually to benefit from economies of scale.
- Renegotiating the selling price to allow a full reflection of the R&D amortisation within the cost structure.

12 Systems Engineering

The systems engineering process serves as the backbone of the development of Owl-22, ensuring that all technical, operational and safety objectives are met, verified and validated. This chapter breaks down the interdisciplinary activities required to guarantee that the final design meets the needs of the stakeholders. Firstly, a verification and validation plan is presented in Section 12.1 to ensure that the software, as well as components, function as intended to guarantee the safety of Owl-22. Moreover, this section also presents a requirement V&V plan to ensure that the right product is built. Then Subsection 12.2.1 checks whether the requirements set at the beginning of the design project are met by the current design. Lastly, Section 12.3 identifies and evaluates the risks associated with the design, development and manufacturing of Owl-22.

12.1. Verification and Validation

The verification and validation (V&V) of aircraft systems are notoriously difficult. Moreover, significant added complexity is introduced when considering the V&V of the path optimisation and automated VTOL models. As such, this chapter outlines a comprehensive V&V campaign for all components and software. However, note that this chapter only covers the integration and system testing of the software, not the entire vehicle. This is because such tests are typically planned once the detailed vehicle design has been finalised, and the system properties are set in stone.

12.1.1. Software V&V

Aircraft software is incredibly difficult to verify due to its complex embedded architectures and wide set of functions. For instance, the control code, subsystem architectures and data propagation must all be comprehensively verified to ensure certification [186]. As such, it is best to use a toolchain tailored to the verification of such systems. Namely, the Ansys SCADE software environment, shown in Figure 12.1, will be adopted. *SCADE Architect* will be used to design the system and software architecture. Following that, the critical aircraft control software shall be designed and verified in *SCADE Suite*. Simultaneously, the Human-machine Interface (HMI) is designed on *SCADE Display*, a powerful feature of which is its direct compatibility with iOS. By using the Ansys SCADE ecosystem, these diverse systems are seamlessly integrated. This allows for unified verification and certification of the system.

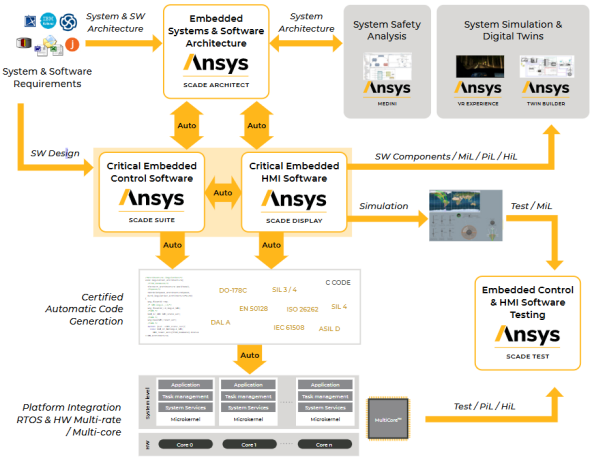

Figure 12.1: Ansys SCADE architecture [186].

Of course, unit, integration and system testing must all be carried out as part of the certification process.

To achieve this, Ansys SCADE employs a mixture of preventative measures and V&V tools, some of which include: the SCADE modelling language is fully deterministic, all possible variables values fire a deterministic transition in a state machine, SCADE Suite Simulator for model debugging, SCADE Suite Design Verifier (DV) for formal verification of functional model properties, and automated validation in accordance with section 11.4.9 of the ISO-26262 safety standard, which demonstrates that the tool complies with its requirements [186].

Lastly, Ansys offers large parts of the SCADE toolbox for free to academic institutes, making it a financially attractive option as well.

AI Testing

Given the extensive use of AI in both path optimisation and vehicle control, it's important to develop a more comprehensive V&V program for these models specifically. This is notoriously difficult for DNNs, since it is difficult to quantify common problems such as overfitting, layer and neuron stability [187]. For the DNNs of both deep RL models, satisfiability modulo theory (SMT) methods are used. SMT essentially determines whether a mathematical formula is satisfiable or not. In this case, SMT-based methods are used as a proof by counter-example; the SMT solver checks for constraint(s) that should be *unsatisfied* if the DNN remains within the expected limits. If not, the solver is satisfied, concluding that the model violates its constraints. Marabou, an open-source, custom SMT-solver, will be used to solve the verification problem [188]. For the path optimisation case, the solver considers constraints on maximum noise pollution, energy consumption, and journey time, while the VTOL DRL model focuses on limiting the maximum absolute vertical velocity, vertical acceleration, and altitude.

Outside of the DNN, the rest of the RL structure needs to be verified. For the flight control case, the established Aerospace SafeRL framework is used [189]. This is a testing environment which features run-time assurance (RTA) and is directly compatible with the VTOL deep RL model architecture. Further verification for the path optimisation algorithm will include a combination of temporal logics (e.g., no collisions will occur, the agent will eventually reach the final location, etc.) and checking for optimality using heuristics that are yet to be determined.

12.1.2. Component Verification

Table 12.1 displays the component-level verification that is necessary to ensure the safety and reliability of Owl-22, as it ensures that each individual subsystem or part performs according to its design specifications before being integrated into a larger system.

Table 12.1: Verification requirements.

Test ID	Test	Purpose	Goals
VER-GNSS-01	Time to First Fix	Verifies the time taken for a GNSS receiver to get satellite signals and calculate its first accurate position to evaluate the startup performance of GNSS receivers [190].	When the receiver has no prior information, the longest TTFF should be 30-60[s]. When the receiver has the almanac and the last known position, the longest TTFF should be 15-30[s]. When the receiver has almanac, ephemeris and position data , the longest TTFF should be 1-5[s] [190].
VER-GNSS-02	Zero Baseline Test [191]	Verify functioning of the GNSS receivers, by connecting a single GNSS antenna to two GNSS receivers [191].	The computed baseline between the two receivers should be less than 2[mm] with a 95% confidence [191].
VER-GNSS-03	Classic Real-time Kinematic Verification Test [191]	Ensures that the GNSS satellites are well-positioned for precise navigation, providing a good position dilution of precision [191].	If PDOP ≤ 2.0 & ≥ 7 satellites, error should be < 0.02[m] horizontally & < 0.04[m] vertically. If PDOP ≤ 3.0 & ≥ 6 satellites, error should be < 0.04[m] horizontally & < 0.05[m] vertically [191].
VER-ACC-01	Static Calibration Test	Verifies and adjusts the accuracy of the accelerometer's output under known, steady-state conditions, e.g. acceleration due to gravity [192].	Assess the zero bias, determine the coefficient matrix and assess linearity of the sensor to match that of the product's manual [193].

Continued from previous page

Test ID	Test	Purpose	Goals
VER-ACC-02	Dynamic Calibration Test	Verifies an accelerometer's performance under time-varying conditions, such as shock, vibrations and oscillations [192].	Identify deviations of the sensor's output from expected results [192]. Identify resonance frequencies that must be filtered using design adjustments [194].
VER-ACC-03	Frequency and Cross-Axis Sensitivity Test	Ensures that the sensor provides accurate data even when subjected to multi-directional forces and assesses the sensor's performance across a range of frequencies [192].	The sensor must meet the IEC60068 and IEC60721 standards [195].
VER-GYR-01	Parameter Curve Determination	Studies the gyroscope's output under controlled angular rates and temperature conditions [196].	Understand the gyroscope's sensitivity and zero point offset (ZPO) between -40[$^\circ C$]-80[$^\circ C$], ensuring its linearity meets EN9100 standards [197].
VER-GYR-02	Voltage Variations Test	Evaluates how fluctuations in the gyroscope's supply voltage affect its ZPO and overall accuracy [196].	Establish acceptable voltage tolerances for the gyroscope and ensure accuracy of the gyroscope is maintained even with moderate power supply instability to meet EN9100 standards [197].
VER-GYR-03	Vibrations Test	Evaluates the sensor's ability to maintain accurate readings under conditions of mechanical vibration present during automotive operations [196].	Establish resonance peaks to apply necessary damping mechanisms when necessary to ensure that sensor outputs remain consistent and free from noise [196].
VER-LID-01	Diffuse Reflectance Test	Calibrate and validate the accuracy and reliability of the LiDAR system's distance measurements and reflectance readings [198].	Use calibrated reflectors at known distances to compare the LiDAR measured distances with the expected values to measure accuracy. The measurement variation should be within a reasonable value, with a confidence of 95%.
VER-LID-02	Field of View (FOV) Test	Evaluates the angular coverage of a LiDAR sensor to determine the area it can effectively scan and detect objects [199].	Ensure the LiDAR's stated horizontal and vertical detection angles are accurate and consistent across its specified range. Any possible blind spots must be identified and eliminated via sensor configuration [199].
VER-OPT-01	Range at First Detection Determination Through Flight Testing	Evaluate the maximum distance at which a camera or sensor can reliably detect a target.	Ensure that the optical camera complies with the Rose Criterion for the minimum signal-to-noise ratio for optimal image processing [200].
VER-OPT-02	Resolution Test	To ensure the optical camera has the necessary resolution for its use in Owl-22.	Use the USAF 1951 test chart to verify if the resolution of the optical camera matches that specified by the manufacturer [201].
VER-USB-01	Software Compliance Test	Ensure that the cable is compliant with the other software in the aircraft.	The cable must meet USB Compliance Test Specifications (CTS) [202].
VER-USB-02	E-marker Verification	Critical in ensuring the safety, performance, and compliance of USB Type-C cables, especially those designed for high power delivery and data transfer rates [203].	Ensures that the e-marker of the cable accurately reports its specifications, preventing situations where a device might draw more power than the cable can handle, thus preventing overheating or failure.
VER-USB-03	Environment Compliance Test	Series of tests performed to ensure airborne equipment can withstand varying conditions that are present in an aircraft [204].	Cable must be compliant with DO-160 standards [204].
VER-BAT-01	Charge-Discharge Destructive Test	Subject the battery to repeated charge and discharge cycles until noticeable degradation occurs [138].	Battery performs according to the manufacturer specifications [138].
VER-BAT-02	Electrochemical Impedance Spectroscopy (EIS) Test	EIS aids in assessing ionic conductivity, evaluating interfacial resistance and detecting potential degradation mechanisms [205].	Based on outcomes, the internal processes must be analysed and the battery performance must be optimised to extend lifespan [205].

Continued from previous page

Test ID	Test	Purpose	Goals
VER-LIFT-01	Wind Tunnel Tests	The main purpose of the test is to assess the aerodynamic performance of the lift devices along with flow visualisation and stability analysis [206].	Quantify aerodynamic coefficients and performance limits to be certified for typ certifications and airworthiness certifications.
VER-LIFT-02	Ground Loading Tests	Simulate the structural integrity of the lift devices in a simulated environment [207].	Verify rotor performance and reliability through structural response measurement, analysis, and fatigue assessment [207].

Sensing and Navigation System Testing

As described in Section 5.2, the accuracy of the attitude, position and velocity determination would be improved with the interaction of the sensors. For this reason, more extensive tests should be performed on the finally integrated system. Firstly, the IMU/GNSS integration would have to be tested. For this, a primary position test will be performed. For example, the integrated system could be driven in a car. Then, after connecting the LiDAR, a similar test could be performed for position, velocity and attitude. A separate test on attitude could be performed with a test rig that rotates the sensors around. Such a rig would have to have the geometry of the aircraft and would be the last major verification before low-altitude test flights. Finally, at this stage, it is not clear whether using the iPad's built-in sensors would be a reliable choice of redundancy for the onboard sensors. Such considerations should be tested under conditions of failure of critical sensors during all the aforementioned system tests. Similarly, the Fault Detection should be verified, ensuring that the system identifies that the sensors give erroneous outputs. The various potential sources of sensor damage should be identified, and the resulting outage modes should be systematically tested.

12.1.3. Requirement V&V

Requirement verification and validation are essential in ensuring that the final product that is built is both the right product and that the final product is being built right. Furthermore, it also ensures that the stakeholder needs are met, thus making the project a greater success. Table 12.2 displays the methods by which requirement verification and validation can be conducted.

Table 12.2: Verification and Validation matrix for one-person eVTOL (detailed, expanded budget).

Requirement ID	Method	Test Details and Facilities	Estimated Cost (USD)
REQ-STR-STAB	Test	Wind-tunnel stability tests up to 15 m/s, expanded to include turbulence simulation and multi-angle testing	100,000
REQ-STR-LOAD	Analysis	Enhanced FEA with environmental variability, fatigue analysis, and third-party validation	10,000
REQ-STR-PIL	Simulation	Mass budgeting + mission performance simulation with pilot load included	20,000
RET-STR-PIL-01	Analysis	CAD sizing analysis with pilot dimensions	10,000
REQ-STR-TPT	Demonstration	Folding mechanism demonstration.	4,500
REQ-STR-TPT-01	Analysis	CAD mass tracking with integrated performance simulation loop	3,500
REQ-STR-PROP	Test	Full-scale structural integration test of propulsion mounting; vibration and stress propagation monitoring to confirm structural isolation from user and avionics	90,000

Continued from previous page

Requirement ID	Method	Test Details and Facilities	Estimated Cost (USD)
REQ-STR-PROP-01	Analysis	High-fidelity FEA to model displacement of structural members under propulsion loads, validating against 1/100th length deflection criterion	8,000
REQ-FP-RAN	Test	Range tests extended to varied terrain and weather conditions + data telemetry logging	100,000
REQ-FP-VEL	Test	Cruise speed verification trials	40,000
REQ-FP-ALT	Test	Altitude determination system informs pilot through interface of the altitude limit.	30,000
REQ-FP-VTOL	Test	VTOL testing with ground footprint measurement.	30,000
REQ-FP-PAY	Simulation	Multivariable payload simulation with cost/safety sensitivity modelling	20,000
REQ-FP-STP	Test	In-flight testing of stopping distance under different conditions	100,000
REQ-OP-POW	Test	Extended duration stress test with redundant propulsion testing rigs	100,000
REQ-OP-COM	Test	Communication system simulation + field test under representative conditions.	80,000
REQ-OP-DEP	Demonstration	Prototype deployment in cold and hot weather conditions, plus time tracking	20,000
REQ-OP-MAIN	Simulation	Fatigue analysis + maintenance simulation with field serviceability feedback integration	10,000
REQ-OP-USE	Analysis	Fatigue analysis + lifecycle simulation on representative load spectra	8,000
REQ-OP-USE-01	Test	Charging station performance testing.	20,000
REQ-CON-SYS	Analysis	GUI testing across devices and simulated mission interruptions	4,000
REQ-CON-DET	Simulation	Simulated fault injection and alert timing tests	30,000
REQ-CON-ENV	Test	In flight testing of protection system	40,000
REQ-CON-DEV	Test	Test and analyse consistency of vehicle responses to standardised pilot inputs across multiple operational trials and control devices	80,000
REC-CON-POS-01	Test	In flight testing	50,000
REC-CON-POS-02	Test	Altitude in flight testing	25,000
REC-CON-POS-03	Test	Attitude in flight testing	25,000
REQ-PHY-VOL	Inspection	Dimensional inspection of folded configuration	5,000
REQ-RES-COST	Analysis	Cost modelling and BOM analysis	5,000
REQ-RES-COST-01	Analysis	Manufacturing process analysis and throughput modelling	4,500
REQ-RES-TIME	Analysis	Resource tracking logs and schedule adherence analysis	1,000
REQ-SAF-PIL	Simulation	Crash energy simulation using composite crash models	15,000
REQ-SAF-PIL-01	Simulation	Loading simulation on cockpit and passenger position	20,000
REQ-SAF-REL	Analysis and Test	Combined FTA and HIL failure injection tests on full control system to validate single-point fault tolerance	50,000
REQ-SAF-CYB	Other	Full penetration testing and zero-day vulnerability scan with red team audit	100,000
REQ-SAF-DES	Test	Hover and descent margin testing using load dump and wind effects	40,000
REQ-SAF-ASC	Test	Hover and descent margin testing using load dump and wind effects	40,000

Continued from previous page

Requirement ID	Method	Test Details and Facilities	Estimated Cost (USD)
REQ-SAF-OBJ	Simulation	3D LiDAR/vision object recognition test simulation in complex environments	40,000
REQ-SUS-MAT	Analysis	Lifecycle assessment (LCA) of all materials used, incorporating embedded carbon metrics and environmental impact factors	5,000
REQ-SUS-MAN	Analysis	Scrap minimization simulation with variable batch sizes	10,000
REQ-SUS-NRG	Inspection	Determination of the carbon footprint of the UAE electricity source.	20,000
REQ-SUS-EOL	Analysis	Full disassembly modeling with recycler consultation	10,000
REQ-SUS-NOI	Test	Urban sound profile testing	80,000
REQ-SUS-BAT-01	Test	Long-term battery cycling with climate simulation	50,000
REQ-SUS-BAT-02	Inspection	Full recharge cycle and degradation tracking	1,000
REQ-SUS-BAT-03	Test	Long-term battery cycling with climate simulation	50,000
REQ-SUS-CO2	Analysis	Full cradle-to-grave LCA	10,000
REQ-REG-GCA	Inspection	GCAA compliance mock certification with external auditor	XXXX
REQ-REG-MUN	Inspection	Review of municipal codes and operational area inspection	XXXX

12.2. Requirement Compliance Analysis

Having determined the initial design, it is important to determine whether this design meets the requirements set at the beginning of the project. This compliance check is done in Subsection 12.2.1, after which a feasibility analysis was done to determine why some requirements are changed, not met or not touched upon in this phase of the design.

12.2.1. Requirement Compliance

Table 12.2.1 checks the compliance of all subsystem requirements set in the beginning stage of the design. System-level requirements have not been included as these can hardly be checked for compliance. The requirement's compliance is categorised in four groups: *Compliant*, *Non-Compliant*, *Partially Compliant*, and *Pending*. A requirement is marked as *Compliant* when it has been fully satisfied and supported by evidence, and an exact value could be found for it. *Non-Compliant* requirements are those that have not been met, either due to technical limitations or conflicting design decisions. *Partially Compliant* indicates that the requirement has been fulfilled to some extent, but not in its entirety, typically due to needing to test the entire system. Finally, *Pending* refers to requirements for which compliance cannot yet be assessed, often due to reliance on external factors that are still evolving, such as regulatory frameworks or detailed development of software. This transparent categorisation ensures that the status of each requirement is traceable, justifiable, and open to future reassessment. For an overview of the requirement abbreviations used, refer to Table 12.3.

Table 12.3: List of requirement abbreviations and their full forms.

REQ	Requirement	VTOL	Vertical Take-Off And Landing	COST	Price
STR	Structure	PAY	Payload	TIME	Design Time
FP	Flight Performance	STP	Stopping Distance	PIL	Pilot
OP	Operations	POW	Power	REL	Reliability
CON	Control	COM	Communication	CYB	Cyber Security
PHY	Physical	DEP	Deployability	DESC	Descent Rate
RES	Resource	MAIN	Maintenance	OBJ	Object Detection
SAF	Safety	USE	Usage	MAT	Material
SUS	Sustainability	SUR	Landing Surface	MAN	Manufacturing
REG	Regulations	SYS	GUI System	NRG	Energy
STAB	Stability	DET	Fault Detection	EOL	End-Of-Life
LOAD	Loading	ENV	Envelope	NOI	Noise
PIL	Pilot	DEV	Control Device	BAT	Battery
TPT	Transport	POS	Position And Attitude	CO2	Carbon Footprint
RAN	Range	VOL	Volume	GCA	Government Regulation
VEL	Speed	BAT	Battery	MUN	Municipal Rules
ALT	Altitude				

Table 12.4: Requirement compliance matrix – one-person eVTOL.

Requirement ID	Description	Compliance	Evidence Reference	R.M.
REQ-STR-LOAD	The structural components of the vehicle shall withstand all flight loads with a minimum safety factor of 1.5, without permanent deformation or structural failure.	Compliant	See Chapter 8	S.L.
REQ-STR-PIL	The vehicle shall be capable of transporting one pilot weighing up to 100 [kg] + 5 [kg] of utilities over a full mission cycle.	Compliant	See Section 8.3	S.L.
RET-STR-PIL-01	The deployed structure shall provide a seating area that accommodates a pilot with a body height between 1.50 [m] and 1.94 [m] and a shoulder breadth up to 0.55 [m], without restricting control input or field of view during any phase of operation.	Compliant	See Section 8.3	S.L.
REQ-STR-TPT	The folded version of the vehicle shall be transportable by 1 person.	Pending	Explicit tests for this requirement to be compliant still have to be conducted, see Subsection 12.1.3.	S.L
REQ-STR-TPT-01	The total mass of the fully assembled vehicle in its operational configuration shall not exceed 200 kg, excluding the pilot and any external control device	Compliant	See Section 8.3	S.L.
REQ-STR-VOL	When fully folded for storage or transport, the vehicle shall fit entirely within a bounding volume of 4 [m^3].	Compliant	See Subsection 8.4.1	S.L.
REQ-STR-PROP	The structures shall house the propulsion elements, transferring the loads without discomfort to the user or other systems.	Compliant	See Subsection 8.3.2	S.L.
REQ-STR-PROP-01	The displacement of structural members supporting the propulsion units shall not exceed 1/100th of the length of the supporting structural member.	Compliant	See Subsection 8.3.2	S.L.
REQ-FP-RAN	The vehicle shall have a minimum operational range of 30 [km] under standard urban flight conditions, based on a full fuel cycle, including take-off, cruise, and landing phases.	Compliant	See Chapter 4	K.S.

Continued from previous page

Requirement ID	Description	Compliance	Evidence Reference	R.M.
REQ-FP-VEL	The vehicle shall be capable of sustaining a cruise speed of at least 60 [km/h] in level flight under standard atmospheric conditions at cruise altitude	Compliant	See Chapter 4	K.S.
REQ-FP-ALT	The vehicle shall maintain a cruise altitude of a minimum of 20 [m] above ground level during standard operational conditions.	Compliant	See Chapter 3	K.S.
REQ-FP-VTOL	The vehicle shall be capable of vertical take-off and landing (VTOL) from a stationary position on flat terrain.	Compliant	See Chapter 3	A.R.
REQ-FP-PAY	The vehicle shall be able to generate sufficient power to lift off a total payload of at least 105 [kg], consisting of one 100 [kg] passenger and 5 [kg] of utilities, over the full mission profile.	Compliant	See Section 3.2, a maximum force of 6336 [N] is generated by the propulsion system.	K.S.
REQ-FP-STP	The vehicle shall have a maximum stopping distance of 8.0 [m].	Pending	Explicit tests for this requirement to be compliant still have to be conducted, see Subsection 12.1.3.	A.M.
REQ-OP-POW	The propulsion system shall be capable of continuously delivering a maximum power output of at least 170 [kW], to enable all phases of flight.	Compliant	See Chapter 4, the maximum power achieved is 172.1 [kW]	A.R.
REQ-OP-DEP	The vehicle shall be deployable from its fully retracted transport configuration to a flight-ready state by a single person in no more than 2 [minutes].	Pending	Explicit tests for this requirement to be compliant still have to be conducted, see Subsection 12.1.3.	J.R.
REQ-OP-MAIN	The vehicle shall require no scheduled or unscheduled maintenance for a period of at least 2 years or 1,000 flight cycles - whichever comes first - under normal usage and environmental conditions.	Compliant	See Chapter 9	J.R.
REQ-OP-USE	The vehicle shall be designed for a minimum operational lifetime of 500 flight cycles per year, assuming regular use of 5 days per week, without requiring performance-degrading maintenance or component replacement.	Compliant	Maintainability, safety and reliability plans as well as the diagnostics have been designed to ensure this requirement is compliant.	J.R.
REQ-OP-USE-01	The vehicle shall have a maximum refuel time of 30 [min].	Pending	See Subsection 12.1.3	J.R.
REQ-OP-SUR	The vehicle shall be capable of performing vertical take-off and landing (VTOL) from and to a flat, unobstructed area no larger than 6 [m^2] under standard atmospheric conditions.	Compliant	See Chapter 9	J.R.
REQ-CON-SYS	The vehicle shall provide a graphical user interface on a personal electronic device that enables the pilot to monitor system status and receive alerts.	Compliant	See Chapter 5, an iPad will be used as the personal electronic device.	A.M.
REQ-CON-DET	The vehicle shall continuously monitor the status of all critical subsystems and provide the pilot with real-time alerts for any detected faults or performance degradation within 1 [s] of detection during all operational phases.	Pending	See Chapter 6 and Subsection 12.1.3	A.M.
REQ-CON-ENV	The vehicle shall incorporate an automated protection system that prevents the pilot from exceeding predefined limits on attitude with a response time of less than 0.2 [s] from threshold exceed detection.	Pending	Flight path assistance system still has to be developed and tested for Owl-22, see Subsection 12.1.3.	A.M.

Continued from previous page

Requirement ID	Description	Compliance	Evidence Reference	R.M.
REQ-CON-DEV	The pilot shall be able to control the vehicle during all operational phases using a personal electronic device, such as a smartphone, tablet, or smartwatch.	Compliant	See Chapter 5, an iPad will be used as the personal electronic device.	A.M.
REQ-CON-POS	The vehicle shall continuously determine and report its full 6-degree-of-freedom (6-DoF) state — including geographic position, altitude, and attitude — with sufficient accuracy and confidence to support safe control and navigation during all phases of flight.	Compliant	See Section 5.2	A.M.
REQ-CON-POS-01	The vehicle shall determine and report its geographic location with 4.0 [m] radius (95% confidence level) during all flight phases.	Compliant	See Chapter 5, Multi-GNSS has an accuracy of $1-4$ [m] (source).	A.M.
REQ-CON-POS-02	The vehicle shall determine and report its altitude with an accuracy better than 2.0 [m] (95% confidence level) during all flight phases.	Partially Compliant	See Chapter 5, single lidar sensor has an accuracy of $\pm 1-5$ [cm], however, the entire system still needs to be tested to ensure complete requirement compliance.	A.M.
REQ-CON-POS-03	The vehicle shall determine and report its attitude with an accuracy better than 2 [m] at a 95% confidence level during all flight phases.	Partially Compliant	See Chapter 5, gyroscopes have an accuracy of $0.5-2$ [m], however, the entire system still needs to be tested to ensure complete requirement compliance.	A.M.
REQ-PHY-VOL	When fully folded for storage or transport, the vehicle shall fit entirely within a bounding volume of 4.0 [m^3].	Compliant	See Subsection 8.4.1	G.F.
REQ-PHY-BAT	The battery's total mass shall not exceed 30% of the vehicle's total mass in operational configuration.	Non-Compliant	See Chapter 4	G.F.
REQ-RES-COST	The target selling price of the vehicle shall not exceed $100,000 per unit.	Compliant	See Section 11.2, Owl-22 has a total selling price of $ 99,575	K.S.
REQ-RES-COST-01	The vehicle shall be designed for a production volume of 1,000 units per year.	Pending	Still needs to be evaluated in the manufacturing plan	K.S.
REQ-RES-TIME	The design of the vehicle shall be completed within a total effort of 4,000 person-hours, based on a team of 10 people working full-time over 50 working days (8 hours per day).	Pending	See Subsection 12.1.3	K.S.
REQ-SAF-PIL	The vehicle shall protect the pilot from life-threatening injury during all phases of nominal operation.	Pending	Explicit tests for this requirement to be compliant still have to be conducted, see Subsection 12.1.3.	F.S.
REQ-SAF-PIL-01	The vehicle shall provide a secured seating position with restraint and energy absorbing features.	Pending	Explicit tests for this requirement to be compliant still have to be conducted, see Subsection 12.1.3.	F.S.
REQ-SAF-REL	The vehicle shall be designed to achieve a minimum reliability of 99.9% per flight, and shall tolerate any single-point subsystem failure without loss of control or violation of safety-critical flight parameters.	Pending	Explicit tests for this requirement to be compliant still have to be conducted, see Subsection 12.1.3.	F.S.

Continued from previous page

Requirement ID	Description	Compliance	Evidence Reference	R.M.
REQ-SAF-CYB	The vehicle's communication and control systems shall be protected against unauthorised access, data corruption, and remote command injection.	Pending	Explicit tests for this requirement to be compliant still have to be conducted, see Subsection 12.1.3.	F.S.
REQ-SAF-DES	The vehicle shall have a maximum steady-state descent rate no greater than 1.5 [m/s] during operation, as measured during vertical landing from a hover at full payload capacity, under standard atmospheric conditions at sea level.	Pending	Not part of the simulation presented in Chapter 7, planning on including this in the future.	F.S.
REQ-SAF-ASC	The vehicle shall have a maximum steady-state ascent rate no greater than 3.0 [m/s] during operation, as measured during vertical landing from a hover at full payload capacity, under standard atmospheric conditions at sea level.	Pending	Not part of the simulation presented in Chapter 7, planning on including.	F.S.
REQ-SAF-OBJ	The vehicle's object detection system shall alert the pilot of potential collisions at a distance exceeding the maximum stopping distance plus a reaction buffer of seconds.	Pending	Explicit tests for this requirement to be compliant still have to be conducted, see Subsection 12.1.3.	F.S.
REQ-SUS-MAT	The vehicle shall be developed with sustainability as an integral design objective, by minimising negative environmental impacts across its production, operation, and disposal phases.	Compliant	See Chapter 10	F.S.
REQ-SUS-MAN	The manufacturing process of the vehicle shall be designed to minimise environmental impact by using energy-efficient production methods and ensuring that at least 70% of production waste (by mass) is either recyclable or reusable.	Pending	Limited information available in Owl-22's manufacturing plan.	F.S.
REQ-SUS-NRG	The vehicle shall operate using an energy source that emits no more than 75 $g\ CO_2/km$.	Compliant	Explicit tests for this requirement to be compliant still have to be conducted, see Subsection 12.1.3.	F.S.
REQ-SUS-EOL	The vehicle shall be designed with an end-of-life strategy that enables at least 80% of its total mass to be reused, recycled, or safely disposed of using environmentally responsible processes.	Pending	Explicit tests for this requirement to be compliant still have to be conducted, see Subsection 12.1.3.	F.S.
REQ-SUS-NOI	The system shall produce noise levels no greater than 75 [dB].	Pending	See Chapter 3, Owl-22 produces a noise of 71 [dB] at an altitude of 20 [m]	F.S.
REQ-SUS-BAT	The vehicle shall include an onboard battery system as part of its energy storage architecture by default.	Compliant	See Chapter 4	F.S.
REQ-SUS-BAT-01	The battery shall retain at least 80% of its original capacity after 1000 full charge-discharge cycles under standard operating conditions (ambient temperature 297.15–318.15 [K]).	Compliant	See Chapter 4	F.S.
REQ-SUS-BAT-02	The battery shall be rechargeable.	Compliant	See Chapter 4	F.S.
REQ-SUS-BAT-03	The battery shall support repeated charge-discharge cycles without replacement during the first 2 years of operation.	Compliant	See Chapter 4	F.S.
REQ-SUS-CO2	The vehicle's complete life-cycle shall have a carbon footprint lower than 20,000 [kg].	Pending	Detailed LCA still needs to be conducted	F.S.

Continued from previous page

Requirement ID	Description	Compliance	Evidence Reference	R.M.
REQ-REG-GCA	The vehicle shall be designed in compliance with all applicable regulations issued by the UAE General Civil Aviation Authority (GCAA).	Pending	Awaiting GCAA personal eVTOL certification framework release	A.A.
REQ-REG-MUN	The vehicle shall comply with applicable municipal regulations in the UAE regarding public safety, noise, privacy, and permitted landing and take-off zones.	Pending	Pending municipal eVTOL guidance in UAE cities	A.A.

12.2.2. Feasibility Analysis

From the compliance matrix displayed in the previous section, it is evident that some requirements have been categorised as either *Non-Compliant* or *Pending*. **REQ-PHY-BAT** is a requirement that was deliberately not met since otherwise, the range requirement **REQ-FP-RAN** could not be met with the design decision of a solid lithium battery. The violation of **REQ-PHY-BAT** would not result in the non-compliance of **REQ-STR-TPT-01**, as the total vehicle mass remained below the 200 kg threshold. Furthermore, the battery choice was critical to achieving sufficient energy density, which directly enables compliance with core functional requirements such as **REQ-OP-POW** and **REQ-OP-USE**. In this case, trade-offs were consciously made in favour of mission-critical performance, while accepting localised non-compliance where it did not compromise safety, transportability, or overall system viability.

Moreover, many of the requirements related to safety (**REQ-SAF**) are categorised as *Pending*, as their verification depends on full-system integration testing, environmental exposure trials, and in-flight validation, none of which could be conducted within the scope of the current design phase. Similarly, requirements concerning path assistance and assisted landing and take-off functionalities are also marked as *Pending*. Although these systems were considered conceptually during the design process, their detailed development, integration, and testing fall outside the scope of this phase and are intended for future implementation, aiming to comply with these requirements in the future.

In addition, several sustainability-related requirements remain *Pending* due to the long-term and system-wide nature of their verification. These include metrics such as recyclability rates, end-of-life material tracking, and lifecycle carbon accounting, which require access to detailed supplier data and manufacturing processes that are not yet finalised at this stage.

Lastly, the regulatory compliance requirements (**REQ-REG**) have also been classified as *Pending*. This is primarily because both national and municipal authorities are still in the process of developing dedicated regulatory frameworks for the integration of personal eVTOLs. While the design has been tailored to align with UAE-specific constraints, such as hot climate conditions and known restricted airspace zones, the absence of formal certification pathways and operational guidelines prevents conclusive verification. Due to this, these requirements remain pending until authoritative regulatory documentation becomes available.

12.3. Risk Analysis

This section identifies and evaluates the risks associated with the design, development and manufacturing of Owl-22. Each subsystem introduces distinct challenges that may impact the overall safety, performance, and feasibility of the eVTOL. The technical risks are summarised in Table 12.5, which also lists the responsible team member assigned to monitor each risk.

The table assesses the likelihood ('L') and consequence ('C') of each risk. Both of these are rated from 1 to 5. In the case of likelihood, 1 means that the event will seldom happen, 2 indicates that it will happen rarely, in a limited number of cases, 3 represents that the event could happen at some point of many aircraft's lifetimes, 4 means that the risk will happen for many aircraft in use, and 5 suggests that the event will occur for most aircraft, potentially repeatedly. For consequence, a score of 1 indicates negligible impact on the aircraft operation, 2 suggests an inconvenience with little operational threat, 3

implies the need for repairs, 4 means the aircraft must be grounded promptly but remains safe for a limited time, and 5 represents an imminent danger to the user. These scores are visualised in the risk map in Table 12.6, which helps to assess the severity of each risk.

Each risk in Table 12.5 is assigned an ID in the format XXX–YY, where XXX denotes the subsystem/category and YY the risk number. For clarity, the risks are grouped into six sub-categories. The energy system (EN) includes the battery system (BAT) and the power system (POW). The structural subsystem (STR) covers all load-bearing and protective elements. The avionic suite comprises several components: the state and obstacle sensing system (SAS), navigation system (NAV), pilot interface display (TAB), on-board computer (OBC), and flight path assistant (FPA). The propulsion system (PROP) encompasses all components responsible for generating and controlling thrust. The production and logistics (PROD) includes the risk related to depending on suppliers (SUP), doing in-house manufacturing (MAN) and the logistics risk (LOG). Lastly, risks related to the V&V (TEST) have also been accounted for. Note that the *responsible member* (RM) column in the table contains the initials of the relevant member. These initials can be cross-referenced with the title page.

Table 12.5: Technical risks with ID, responsible member (RM), and pre-risk T (Total), L (Likelihood), and C (Consequence).

ID	Description	RM	T	L	C
	Energy System				
RS-EN-BAT-01	Even though the solid state reduces the risk of thermal runaway, factors such as manufacturing defects, overcharging or physical damage can still lead to overheating and potential fires.	K.S.	10	2	5
RS-EN-BAT-02	Solid-state batteries can be brittle and susceptible to cracking under mechanical stress. Vibrations and impact during Owl-22 operations could compromise battery integrity, leading to failures.	K.S.	12	3	4
RS-EN-BAT-03	If the battery is allowed to discharge below a critical threshold, it can lead to sudden power loss during flight, posing significant safety risks.	K.S.	15	3	5
RS-EN-POW-01	Power converters and inverters are susceptible to failures due to over-temperature, over-current and over-voltage conditions. These stresses can lead to component degradation or sudden failures.	K.S.	12	3	4
RS-EN-POW-02	Exposure to high or low temperature can degrade power electronics, leading to reduced efficiency, shortened lifespan, or complete system failure.	K.S.	12	4	3
RS-EN-POW-03	Electrical system components can fail due to defects, overheating, or overloading. Such failures can result in loss of critical functions of Owl-22.	K.S.	10	2	5
RS-EN-POW-04	Electromagnetic interference from power electronics can disrupt avionics and communication systems, affecting the reliability of control signals and situational awareness.	K.S.	12	3	4
RS-EN-POW-05	Faulty or damaged wiring can lead to short circuits, loss of electrical power, and potential fires. These issues may result from manufacturing defects, improper installation, or wear and tear over time.	K.S.	15	3	5
	Structure System				
RS-STR-01	The vehicle is intended to be used on a regular basis for repetitive tasks, causing cyclical loads. This can cause fatigue in parts of the battery structure and failures due to weakening in the structure.	S.L.	16	4	4
RS-STR-02	Due to UAE environmental conditions involving sand, prolonged exposure can compromise protective coatings and cause pitting corrosion.	S.L.	12	4	3
RS-STR-03	Manufacturing defects such as voids, improper heat treatment of materials or cracks, could lead to early structural failures.	G.F.	15	3	5
RS-STR-04	Due to high ambient temperatures in UAE, there could be softening of structural adhesives or thermal degradation of sealants, causing delamination.	S.L.	16	4	4
RS-STR-05	The structure is foldable in order to reduce storage space. Friction could damage the surface of the folding parts over the course of the Owl-22 lifetime, making it more difficult or impossible to fold/unfold the structure.	F.S.	12	4	3
RS-STR-06	The structure will be unfolded before flight. If this is not done properly, the structure could be unsafe to fly.	F.S.	20	4	5

ID	Description	RM	T	L	C
	Avionic Suite				
RS-AV-SAS-01	Prolonged exposure to high ambient and surface temperatures can degrade internal electronics of the camera or cause the camera module to shut down to prevent damage, resulting in loss of visual input.	A.M.	8	4	2
RS-AV-SAS-02	Dust accumulation on LiDAR lenses or mirrors can impair detection accuracy.	A.M.	15	5	3
RS-AV-SAS-03	Prolonged exposure of the LiDAR sensors to high ambient temperature may affect sensor calibration or cause thermal drift.	A.M.	12	4	3
RS-AV-SAS-04	Sand can accumulate on the camera lens, blurring the image or damaging the optical coatings. This can compromise object recognition or landing assistance.	A.M.	15	5	3
RS-AV-SAS-05	The UAE's intense sunlight causes overexposure or lens flare, leading to inaccurate obstacle detection or landing assistance.	A.M.	15	5	3
RS-AV-NAV-01	GNSS positioning may be degraded due to signal blockage, for example, by high-rise buildings in big cities like Dubai and Abu Dhabi, which can lead to reduced navigation accuracy or intermittent signal dropouts.	A.M.	12	4	3
RS-AV-NAV-02	Errors in combining GNSS data with other onboard sensors, such as IMU and LiDAR, may lead to discrepancies in vehicle position or heading.	A.M.	12	3	4
RS-AV-NAV-03	Sustained high ambient temperatures may cause drift or performance degradation in GNSS receivers.	A.M.	12	4	3
RS-AV-NAV-04	High processing demands on the OBC could cause delayed or inaccurate navigation updates, especially during dynamic manoeuvres or in high-traffic airspace.	A.M.	9	3	3
RS-AV-NAV-05	Unintentional interference or malicious attack, such as GNSS spoofing or jamming, could disrupt position calculations, causing the vehicle to deviate from its intended flight path or lose situational awareness.	A.M.	10	2	5
RS-AV-TAB-01	The reliance on a single USB-C connection for the data handling and the pilot interface introduces a single point of failure. Accidental disconnection, cable damage or port failure can lead to loss of display functionality and data handling.	A.M.	16	4	4
RS-AV-TAB-02	High ambient temperatures in the UAE can cause the tablet to overheat, leading to automatic shutdown or degraded performance. This can result in the loss of critical flight information during operation.	A.M.	16	4	4
RS-AV-TAB-03	Intense sunlight can cause significant glare on the tablet screen, impairing readability and potentially leading to misinterpretation of flight data.	A.M.	10	5	2
RS-AV-TAB-04	Turbulence or pilot movement can result in unintended touchscreen inputs, potentially altering settings or displaying incorrect information.	A.M.	9	3	3
RS-AV-OBC-01	The OBC may overheat under UAE conditions if not adequately cooled, potentially leading to reduced processing performance, throttling or unexpected shutdowns.	A.M.	16	4	4
RS-AV-OBC-02	Failure or overload of the OBC can affect real-time processing and support functions of the tablet, causing delays, freezing or system resets.	A.M.	15	3	5
RS-AV-FPA-01	The flight path assistance (FPA) system may fail to detect existing obstacles or designated no-fly zones (NFZs), potentially leading to unauthorised airspace incursions or collision hazards.	D.A.	15	3	5
RS-AV-FPA-02	Sudden establishments of new NFZs during flight, without timely updates to the FPA system, can result in inadvertent entry into restricted airspace.	D.A.	12	4	3
	Propulsion System				
RS-PROP-01	The combination of cyclorotors and coaxial rotors can introduce complex gyroscopic effects and dynamic loads, which may lead to structural fatigue failure.	A.R.	12	3	4
RS-PROP-02	High ambient temperatures in the UAE may cause the cyclorotor and biaxial rotor components to overheat, reducing performance or causing system failure.	A.R.	16	4	4

ID	Description	RM	T	L	C
RS-PROP-03	Exposure to sand and dust can cause erosion of rotor blades, accumulation of abrasive particles in moving components, and potential imbalance in the propulsion system. Leading to reduced thrust efficiency, increased vibration an and accelerated wear.	A.R.	15	5	3
RS-PROP-04	The integration of cyclorotors and coaxial rotors increases control system complexity. Inadequate synchronisation between these propulsion systems can lead to flight instability or loss of control.	A.R.	12	3	4
RS-PROP-05	The exposed rotor system is vulnerable to foreign object damage, including birds, plastic, or other airborne debris, which can impair rotor integrity and flight safety	A.R.	15	3	5
RS-PROP-06	The aircraft will be designed with certain flight conditions in mind. Extreme weather conditions like strong winds could cause higher loads on the aircraft than what the control systems are ready to counter, which would increase the risk of an accident.	M.P.	8	2	4
RS-PROP-07	Through impact or electrical connection faults, one of the propulsive devices could fail, thus endangering the pilot and their surroundings.	A.M.	10	2	5
RS-PROP-08	Serrated end pieces will be added to the existing propeller geometry. There is a possibility of detachment and potential danger either to the other propellers or the surroundings.	D.A.	6	3	2
	Production & Logistics				
RS-PROD-SUP-01	Owl-22 require parts and materials from external suppliers. If one of these suppliers starts delaying deliveries for any reason, production would come to a halt.	K.S.	12	4	3
RS-PROD-SUP-02	The Owl-22 structure will need to withstand significant stresses. In case the quality of the supplied aluminium decreases, the structure might fail.	K.S.	10	2	5
RS-PROD-SUP-03	Owl-22 will use several off-the-shelf components. In case a part supplier goes bankrupt, a threat of a long-term production halt would emerge.	K.S.	8	2	4
RS-PROD-MAN-01	The production includes a number of processes, which can result in individual parts or the overall assembly having deficiencies.	J.R.	12	3	4
RS-PROD-MAN-02	Misassembly of the folding mechanism during production may result in mechanical binding, reduced folding functionality, or unsafe structural configurations during deployment.	J.R.	12	3	4
RS-PROD-LOG-01	Transportation of the products will be required from the production facility to the customer. The aircraft could be damaged during this process.	J.R.	9	3	3
	V&V				
RS-TEST-01	Test facility might not be available on the desired date, causing delays to the product timeline.	A.A.	8	4	2

Table 12.6: Pre-mitigation risk map.

5(Very likely)		RS-AV-TAB-03	RS-AV-SAS-02 RS-AV-SAS-04 RS-AV-SAS-05 RS-PROP-03		
4(Likely)		RS-AV-SAS-01 RS-TEST-01	RS-EN-POW-02 RS-STR-02 RS-STR-05 RS-AV-SAS-03 RS-AV-NAV-01 RS-AV-NAV-03 RS-AV-FPA-02 RS-PROD-SUP-01	RS-STR-01 RS-STR-04 RS-AV-TAB-01 RS-AV-TAB-02 RS-AV-OBC-01 RS-PROP-02	RS-STR-06
3(Possible)			RS-AV-NAV-04 RS-AV-TAB-04 RS-PROD-LOG-01	RS-EN-BAT-02 RS-EN-POW-01 RS-EN-POW-04 RS-AV-NAV-02 RS-PROP-01 RS-PROP-04 RS-PROD-MAN-01 RS-PROD-MAN-02	RS-EN-BAT-03 RS-EN-POW-05 RS-STR-03 RS-AV-OBC-02 RS-AV-FPA-01 RS-PROP-05
2(Unlikely)			RS-PROP-08	RS-PROP-06 RS-PROD-SUP-03	RS-EN-BAT-01 RS-EN-POW-03 RS-AV-NAV-05 RS-PROP-07 RS-PROD-SUP-02
1(Negligible)					
Likelihood↑	1(Negligible)	2(Low)	3(Significant)	4(Critical)	5(Catastrophic)
	Consequence				

ACTION: No action | Monitor | Minor management | Major management | Stop, Reevaluate

Based on the identified risks in the pre-mitigation phase, preventative measures and contingency plans have been proposed to reduce both the likelihood and/or consequence of all risks. These measures include design adaptations, system redundancies, and clear operational protocols. In Table 12.7, the updated risk rankings are presented to reflect the impact of these mitigation strategies. By implementing these actions, several risks have been significantly reduced, demonstrating the effectiveness of early-stage risk management within the Owl-22 design process. The risks in Table 12.7 are ranked from highest to lowest total risk score to highlight which issues require the most urgent attention and mitigation efforts during the design and development of Owl-22. These scores also correspond to the positions shown in the risk map in Table 12.8, which visually categorises the risks based on their likelihood and consequence to support intuitive assessment and decision-making.

Table 12.7: Preventive measures and contingency plans of identified technical risks.

			Post-Risk		
ID	**Preventive Measures**	**Contingency Plan**	**T**	**L**	**C**
RS-AV-OBC-01	Ensure robust cooling solutions and continuous temperature monitoring.	Activate cooling protocols and stop tracking non-essential information.	8	2	4
RS-AV-OBC-02	Design the OBC with overload protection and fail-safe mechanisms.	In the case of such surcharges, non-essential information will not be tracked.	8	2	4
RS-AV-FPA-01	The implementation of redundant sensors for obstacle detection and regular NFZ database updates.	Program the aircraft to initiate automated loiter or landing manoeuvres if obstacle or NFZ data becomes unreliable.	8	2	4
RS-PROP-05	The utilisation of an advanced sensing and early detection system to identify and avoid foreign objects.	If damage is detected, limit high-manoeuvrability commands. In severe cases, initiate an emergency landing.	8	2	4

ID	Preventive Measures	Contingency Plan	*Post-Risk* T	L	C
RS-STR-03	Use only aerospace-grade materials with full traceability and supplier quality certifications, along with routine inspections.	Assess extent of damage. If it is minor, reduce speed and manoeuvring intensity. If it is major, initiate an emergency landing.	8	2	4
RS-EN-BAT-02	Ensure the battery housing can endure the vibrations and stress of operation.	Have the BMS disconnect the affected module from the main power system.	6	2	3
RS-STR-01	The system will include a Structural Health Monitoring (SHM) system with sensors to assess structural damage.	The SHM system will assess the extent of damage and modify flight parameters.	6	2	3
RS-STR-04	Apply UV-resistant and heat-reflective coatings to bonded joints to reduce surface temperature exposure.	Restrict payload, manoeuvring, and flight time in extreme heat to reduce thermal stress. If damage occurs, initiate emergency landing.	6	2	3
RS-EN-POW-01	The implementation of a robust BMS that can monitor and control charging, temperature and detect anomalies.	In the case of such surcharges, non-essential systems will be powered down to prevent any irreversible damage.	6	2	3
RS-EN-POW-02	The implementation of an integrated thermal management system with real-time temperature monitoring and active cooling.	Initiate automatic switch to backup systems to introduce redundancy and prevent a complete system shutdown.	6	2	3
RS-STR-05	Allow easy access to the guard rails of the folding mechanism, to ease its maintenance and lubrication.	Offer services to replace worn-out parts or sell replacement parts to the customers.	6	2	3
RS-AV-SAS-02	Incorporate protective housings and self-cleaning mechanisms for LiDAR sensors to prevent dust accumulation and maintain detection accuracy.	Activate self-cleaning mechanisms to clear dust accumulation. If obstructions persist, transition to redundant sensors and engage emergency navigation algorithms.	6	2	3
RS-AV-NAV-01	Augment GNSS with inertial navigation systems and signal quality monitoring to ensure reliable positioning in urban environments with potential signal blockage.	At the occurrence of critical signal loss, the speed will be limited and the pilot will be prompted to land as soon as possible.	6	3	2
RS-AV-NAV-04	Optimise onboard computer processing and implement priority-based task scheduling to ensure accurate navigation updates under high-demand conditions.	If processing overload is detected and cannot be resolved, safe navigation must be engaged to lower max speed and prioritise hover until computation stability is restored.	6	3	2
RS-AV-TAB-01	Design redundant data pathways and secure cable management to eliminate single points of failure in the USB-C connection.	Activate alternate data pathways during the occurrence of cable damage or port failure to prevent loss of display function or data handling.	6	3	2
RS-AV-TAB-02	Use external cooling solutions and operational guidelines limiting tablet exposure to extreme heat to prevent overheating and maintain performance.	Fall back on the OBC to provide critical performance information and landing instructions through audio to ensure pilot safety.	6	3	2
RS-AV-TAB-03	Apply anti-glare screen protectors and use adjustable sunshades to improve tablet screen readability under intense sunlight.	For a given flight condition, if the pilot is executing an unexpected manoeuvre, the OBC could send a confirmation message before performing said manoeuvre.	6	3	2
RS-PROP-02	Implement thermal monitoring and active cooling systems for cyclorotor and biaxial rotor components.	Activate cooling systems, non-essential systems will be powered down to prevent any irreversible damage. If damage cannot be controlled, an emergency landing will be initiated.	6	2	3

ID	Preventive Measures	Contingency Plan	*Post-Risk* T	L	C
RS-PROP-03	Use protective coatings and seals on rotor blades as well as moving parts. Combined with regular cleaning and inspection to prevent sand and dust damage.	In the case of occurrence, adjust rpm or reduce aggressive manoeuvres to minimise stress on potentially compromised blades.	6	3	2
RS-PROD-SUP-01	Request predictions from suppliers regarding part/material availability.	Keep a reserve inventory of parts/materials to allow short-term operation during a shortage.	6	3	2
RS-PROP-04	Develop advanced control algorithms with real-time synchronisation and fail-safe mechanisms to ensure stable coordination.	In extreme cases, execute an autonomous emergency landing in a predefined safe zone.	6	2	3
RS-PROP-06	Weather reports will be examined before flight, and the aircraft will be locked out in case of dangerous conditions.	In case of a sudden weather change for the worse, the cruise altitude will be decreased.	6	2	3
RS-EN-BAT-01	The implementation of an advanced Battery Management System (BMS) to monitor and control charging, temperature and detect anomalies.	Employ cooling or fire suppression protocols in the case of overheating or fires.	5	1	5
RS-STR-01	Employ multi-layer protective coatings to prolong the integrity of the structure of Owl-22.	Assess extent of damage. If it is minor, reduce speed and manoeuvring intensity to reduce load. If it is major, initiate an emergency landing.	4	2	2
RS-EN-POW-05	Ensure proper installation using high-quality wiring with protective insulation, and conduct routine inspection.	Employ cooling or fire suppression protocols in the case of overheating or fires.	4	1	4
RS-AV-SAS-03	Employ cooling or fire suppression protocols in the case of overheating or fires.	Transition to redundant sensors and engage emergency navigation algorithms.	4	2	2
RS-AV-NAV-02	Apply sensor fusion algorithms with real-time validation and calibration to minimise discrepancies between GNSS, IMU, and LiDAR data.	Cross-reference real-time LiDAR point clouds with pre-mapped terrain to adjust vehicle position.	4	2	2
RS-AV-NAV-03	Incorporate thermal management and heat-resistant components.	Transition to Inertial Navigation Systems (INS) using IMU data for dead reckoning when GNSS signals become unreliable.	4	2	2
RS-AV-NAV-05	Implement anti-spoofing and jamming detection techniques along with secure navigation algorithms.	Use the communication links to contact authorities and initiate emergency landing procedures.	4	1	4
RS-PROP-07	Run the diagnostic system before each flight to assess the propulsion system condition.	The propulsion system has sufficient thrust to fly with one propulsion device inoperative.	4	1	4
RS-AV-FPA-02	Incorporate real-time NFZ update capabilities and an automated alert system to adjust flight paths during sudden airspace changes.	Program the aircraft to initiate automated loiter if NFZ data becomes unreliable to allow the navigation system to recalibrate.	4	2	2
RS-PROD-MAN-01	Establish rigid work frameworks and properly train the manufacturing staff.	Introduce quality control personnel, analyse defective products.	4	2	2
RS-PROD-LOG-01	Include padding for sensitive components of the Owl-22 during transport to the customer.	Perform quality control again after transporting the aircraft.	4	2	2

ID	Preventive Measures	Contingency Plan	*Post-Risk* T	L	C
RS-EN-BAT-01	A minimum state of charge (SoC) threshold of 20% is enforced through the BMS to prevent deep discharge and ensure sufficient reserve power for safe operations or make an emergency landing.	In the case of occurrence, the system will initiate controlled emergency landing procedures.	3	1	3
RS-EN-POW-03	Use high-reliability electrical components with built-in protection features, implement system-level redundancy and diagnostics to prevent as well as detect failures.	Employ the redundancy systems to use isolated power buses to power the critical systems of Owl-22	3	1	3
RS-STR-06	Owl-22 will identify the status of the structure and provide visual and audible feedback to the user when the structure is unfolded correctly.	The aircraft will not allow take-off when the structure is not correctly unfolded.	3	1	3
RS-AV-SAS-01	Implement thermal insulation and active cooling of camera electronics.	Employ cooling protocols in the case of overheating.	3	3	1
RS-AV-SAS-04	Equip cameras with protective covers and automatic cleaning systems to prevent sand build-up and protect optical surfaces.	In case of severe sand obstruction, switch to redundant camera systems to maintain situational awareness and landing assistance.	3	3	1
RS-AV-SAS-05	Use sunshades, optical filters, and HDR imaging to reduce overexposure and lens flare under intense sunlight.	Use LiDAR as a complementary system to validate optical obstacle detection systems while in extreme sunlight.	3	3	1
RS-PROP-O1	Perform detailed dynamic analysis and reinforce structural components to withstand gyroscopic effects and cyclic loads from cyclorotors and biaxial rotors.	If detected, the pilot should reduce manoeuvring to stabilise the aircraft. If control is lost, the system initiates landing, followed by the suspension of flights pending inspection.	3	1	3
RS-PROD-SUP-02	Sign the supply contract with an established, reputable company. Perform regular quality checks.	Arrange emergency supply with an alternative company.	3	1	3
RS-PROD-SUP-03	Regularly analyse the financial condition of the suppliers.	Keep a reserve inventory of parts. Draw up a list of alternative suppliers. Establish contact with these suppliers early to enable a fast switch from one supplier to the other.	3	1	3
RS-PROD-MAN-02	Use alignment jigs and visual QA steps for telescoping components. Modularised folding structure for easier assembly.	Isolate faulty units. Inspect the affected batch and rework the folding system using a trained technician team.	3	1	3
RS-EN-POW-04	Apply electromagnetic shielding, proper grounding, and filtering techniques to power electronics to minimise EMI and protect the integrity of avionics as well as communication systems.	Activate shielding and reconfiguration protocols to isolate affected components.	2	1	2
RS-AV-TAB-04	Implement touchscreen input lock features and physical stabilisers to prevent unintended commands during turbulence or pilot movement.	During turbulence or big pilot movements, the OBC will send a confirmation message before executing any touchscreen inputs.	2	1	2
RS-TEST-01	Plan the testing procedure far ahead. Determine potential alternative dates for the testing procedure.	Make a flexible plan such that delay in testing does not require the project actions to stop and wait.	2	2	1

ID	Preventive Measures	Contingency Plan	*Post-Risk* T	L	C
RS-PROP-08	Perform solid joining method and material selection, such that it complements the challenging environmental conditions of the target market location.	Analyse the potential paths that an ejected serrated piece could take. Provide extra protection to the components on these paths. Offer replacement services.	2	2	1

Table 12.8: Post-mitigation risk map.

5(Very likely)					
4(Likely)					
3(Possible)	RS-AV-SAS-01 RS-AV-SAS-04 RS-AV-SAS-05	RS-AV-NAV-01 RS-AV-NAV-04 RS-AV-TAB-01 RS-AV-TAB-02 RS-AV-TAB-03 RS-PROP-03 RS-PROD-SUP-01			
2(Unlikely)	RS-TEST-01 RS-PROP-08	RS-STR-01 RS-AV-SAS-03 RS-AV-NAV-02 RS-AV-NAV-03 RS-AV-FPA-02 RS-PROD-MAN-01 RS-PROD-LOG-01	RS-EN-BAT-02 RS-STR-01 RS-STR-04 RS-EN-POW-01 RS-EN-POW-02 RS-AV-SAS-02 RS-PROP-02 RS-PROP-04 RS-PROP-06 RS-STR-05	RS-AV-OBC-01 RS-AV-OBC-02 RS-AV-FPA-01 RS-PROP-05 RS-STR-03	
1(Negligible)		RS-EN-POW-04 RS-AV-TAB-04	RS-EN-BAT-01 RS-EN-POW-03 RS-PROP-01 RS-STR-06 RS-PROD-SUP-02 RS-PROD-SUP-03 RS-PROD-MAN-02	RS-EN-POW-05 RS-AV-NAV-05 RS-PROP-07	RS-EN-BAT-01
Likelihood↑	1(Negligible)	2(Low)	3(Significant)	4(Critical)	5(Catastrophic)
	Consequence				

13 Project Design and Development Logic

The post-DSE development of the Owl-22 is structured into six phases from design finalisation to market deployment. Each phase incrementally increases the integration of the system, allowing for structured validation. This section outlines the design and development logic employed for the vehicle. A visual overview of the development phases can be seen in Figure 13.1.

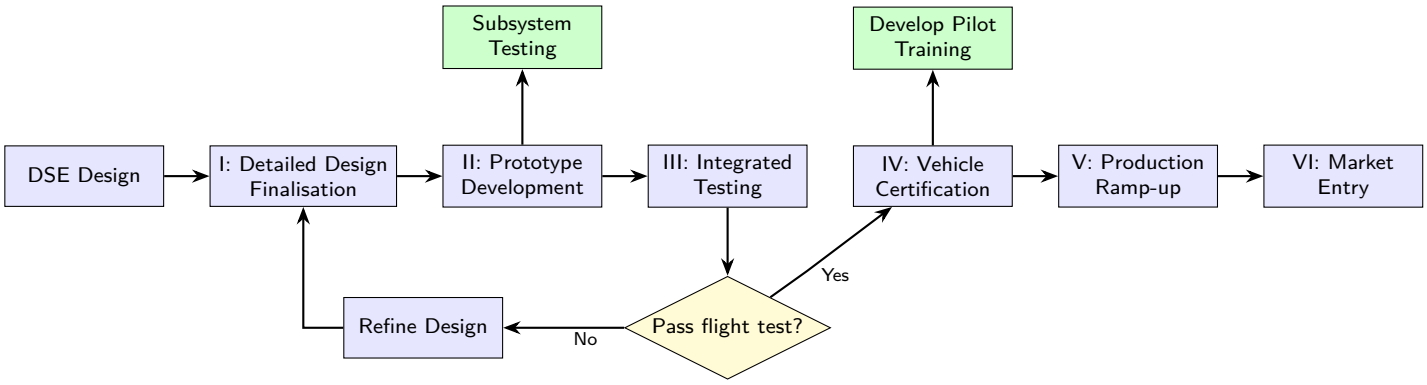

Figure 13.1: Development and certification path of the Owl-22.

13.1. Phase I – Detailed Design Finalisation

The development and certification of the Owl-22 follows a structured, phased approach aimed at achieving design maturity and airworthiness. Starting from the conceptual design, the vehicle evolves through detailed design and simulation, gradually incorporating higher levels of fidelity until a fully integrated, certifiable system is reached.

During early development, hardware-in-the-loop (HIL) and software-in-the-loop (SIL) testing are employed to validate control logic, sensor integration, and safety-critical subsystems. These simulation environments enable rapid iteration and risk reduction prior to physical prototyping. Following this, a functional prototype is constructed and subjected to bench testing and full-vehicle integration trials to evaluate mechanical, electrical, and aerodynamic performance.

13.2. Phase II – Prototype Development

In this stage, the first prototype is constructed and assembled with the goal of verifying how well the different subsystems interact and perform under realistic ground-based conditions. As the assembly progresses, particular care is taken to confirm that the design can be built as intended, not just in theory but in practice.

To support this effort, dedicated test setups are developed in parallel for components such as the battery management system and controls. These setups enable subsystem bench testing, in which each component is tested under controlled conditions to validate its stand-alone functionality. This approach allows potential faults to be isolated early. By identifying and resolving issues at the subsystem level, the bench testing phase significantly reduces the risk of unexpected failures during integrated vehicle testing.

13.3. Phase III – Integrated Vehicle Testing

In this phase, the validated subsystems are integrated into a full-scale prototype for system-level testing. The primary objective is to assess the performance of the complete vehicle under realistic operational conditions. Ground tests are first conducted to verify the integrity of software integration, sensor fusion, and real-time responsiveness of the control system.

Once ground verification is complete, the prototype proceeds to initial flight testing, where the vehicle's stability, control authority, and overall performance are evaluated in line with expected mission profiles. These tests are critical for identifying any discrepancies between simulated and actual behaviour, particularly under dynamic or edge-case conditions. Should the vehicle fail to meet key performance or safety criteria during flight testing, the team re-enters a design refinement loop. In this case, the results are used to isolate the root causes. If the vehicle successfully passes all aspects of the flight test, it progresses to the certification phase. This gate ensures that only viable designs continue through the development pipeline, reducing risk and ensuring that resources are focused on certifiable configurations.

13.4. Phase IV – Certification Readiness

This phase is centred on getting the vehicle ready for certification by relevant aviation authorities, such as the GCAA. To support this process, early-stage safety analyses (including a preliminary system safety assessment and a failure modes and effects analysis) are carried out. These analyses help identify potential failure points and critical interdependencies between subsystems, forming a foundation for discussions with regulators.

At the same time, the design of the human-machine interface is evaluated through human-piloted simulations. These tests provide insights into pilot workload, usability, and response times. To facilitate a smooth transition toward real-world use, standard operating procedures are developed, along with supporting training materials. These resources are aimed at ensuring early users can become familiar with the system efficiently and operate it safely from the outset.

13.5. Phase V – Production Ramp-Up

Once the design has been validated, attention turns toward preparing for full-scale production. To support this, an initial production batch is assembled. This step serves to evaluate whether the planned manufacturing approach is workable in practice, with a focus on verifying assembly timelines, tooling performance, and the reliability of part deliveries.

During this phase, quality assurance processes are fine-tuned. Tolerances, inspection routines, and acceptable variation limits are reviewed and adjusted based on real-world feedback from the initial builds. In parallel, traceability systems are implemented to link each vehicle to its specific components, including serial numbers and testing records. This is essential to meet airworthiness regulations and to support maintenance tracking. Finally, the broader supply chain is stress-tested under production-like conditions to ensure that sourcing, shipping, and lead times are sufficiently stable to support production ramp-up without disruption.

13.6. Phase VI – Market Entry

As the vehicle enters the market, a limited number is delivered to initial customers. During this phase, a system is put in place to monitor fleet performance in real time, tracking key indicators such as battery condition, control system behaviour, and user-reported feedback. Insights gathered from this data feed directly into iterative updates to both the technical documentation and the post-deployment support strategy. In parallel, the necessary customer support systems are launched. These include practical user training, logistics for spare parts, and clearly defined legal procedures for warranty claims and repairs. To position the vehicle within its intended market segment, a focused marketing campaign is initiated. This campaign targets urban users, helping to strengthen the product's identity as a modern mobility solution. Furthermore, this stage provides the opportunity to reassess the final selling price of the vehicle, as unforeseen factors and actualised costs, emerging from production, deployment, and support operations, can now be comprehensively evaluated.

A Gantt chart providing an overview of these phases is presented in the next page.

Project Gantt

Read-only view, generated on 20 Jun 2025

Instagantt

	ACTIVITIES	START	DUE	STATUS	IDENTIFIER
	Post-DSE Plan:	19/Jun	20/Dec		-
	Detailed Design Finalisation	19/Jun	27/Feb	Not start	1
2	Final Components and Vendor Selection	19/Jun	29/Sep	Not start	1.1
3	Confirm Integration Layout of Avionics and Battery	18/Jul	17/Oct	Not start	1.2
4	Conduct Final Simulations	05/Sep	04/Dec	Not start	1.3
5	Conduct Internal Preliminary Design Review	19/Sep	25/Dec	Not start	1.4
6	Freeze Detailed CAD	30/Oct	13/Feb	Not start	1.5
7	Secure IP for Key Innovations	30/Jul	27/Feb	Not start	1.6
	Subsystem Development and Testing	24/Nov	15/Dec	Not start	2
9	Fabricate Propulsion Prototypes	24/Nov	06/Mar	Not start	2.1
10	Conduct Noise Tests	06/Mar	04/Jun	Not start	2.2
11	Integrate Battery and BMS with OBC	16/Feb	20/Apr	Not start	2.3
12	Conduct Battery Pack Thermal and Mechanical tests	22/Apr	14/Jul	Not start	2.4
13	Evaluate PHM Modules in Simulation	27/Mar	16/Sep	Not start	2.5
14	Vibration and Shock Testing on Structure and Batteries	01/May	22/Jul	Not start	2.6
15	Conduct Ground Integration of Subsystems	01/May	30/Sep	Not start	2.7
16	Make Model Refinements Based on Preliminary Tests	17/Jul	15/Dec	Not start	2.8
	Prototype Development	27/Feb	20/Oct	Not start	3
18	Order Materials	27/Feb	03/Jul	Not start	3.1
19	Build Full-Scale Fuselage	19/Jun	15/Jan	Not start	3.2
20	Assemble Propulsion, Avionics and Batteries Into Full Prototype	18/Dec	15/Jun	Not start	3.3
21	Execute Full Software and Hardware Integration	20/Jan	20/Jun	Not start	3.4
22	Integrate Folding Mechanism	20/Mar	20/Jul	Not start	3.5
23	Conduct Ground-based Redundancy Tests	20/Jul	20/Oct	Not start	3.6
	Integrated Vehicle Testing	20/Oct	20/Sep	Not start	4
25	Perform First Tethered Hover Tests	20/Oct	20/Feb	Not start	4.1
26	Conduct Transition Flight Envelop Testing	20/Feb	20/Aug	Not start	4.2
27	Evaluate Performance In Varied Weather Conditions	20/Feb	20/Nov	Not start	4.3
28	Run Fail-Safe Behaviour Simulations	20/Jun	20/Dec	Not start	4.4
29	Refine Flight Control Tuning	20/Apr	20/Nov	Not start	4.5
30	Validate Noise Produced Estimations	20/Sep	20/Dec	Not start	4.6
31	Operational Testing of PHM and Diagnostics	20/Dec	20/Apr	Not start	4.7
32	Make System Improvements Based on Tests	20/Feb	20/Sep	Not start	4.8
	Certification and Production Ramp-Up	20/Aug	18/Sep	Not start	5
34	Begin Regulatory Engagement	20/Aug	20/Jul	Not start	5.2
35	Compile Technical Documentation for Certification	20/Sep	20/Jul	Not start	5.1
36	Conduct Certification Tests	20/Jul	20/Dec	Not start	5.4
37	Execute Manufacturing and Quality Assurance	21/Aug	18/Sep	Not start	-
38	Make a Final Version of the V&V and Requirement Traceability	20/May	20/Oct	Not start	5.3
39	Draft User Training Manual and Maintenance Plan	20/May	20/Apr	Not start	5.5
	Market Readiness and Launch	20/Mar	20/Dec	Not start	6
41	Launch Marketing and Branding Strategy	20/Mar	20/Nov	Not start	6.1
42	Develop Web Portal and Customer Interface	20/Oct	20/Jun	Not start	6.2
43	Evaluate After-Sales, Maintenance, and Update Pathways	20/Jun	20/Oct	Not start	6.3
44	Prepare Market Expansion Roadmap Beyond UAE	20/Jun	20/Dec	Not start	6.4

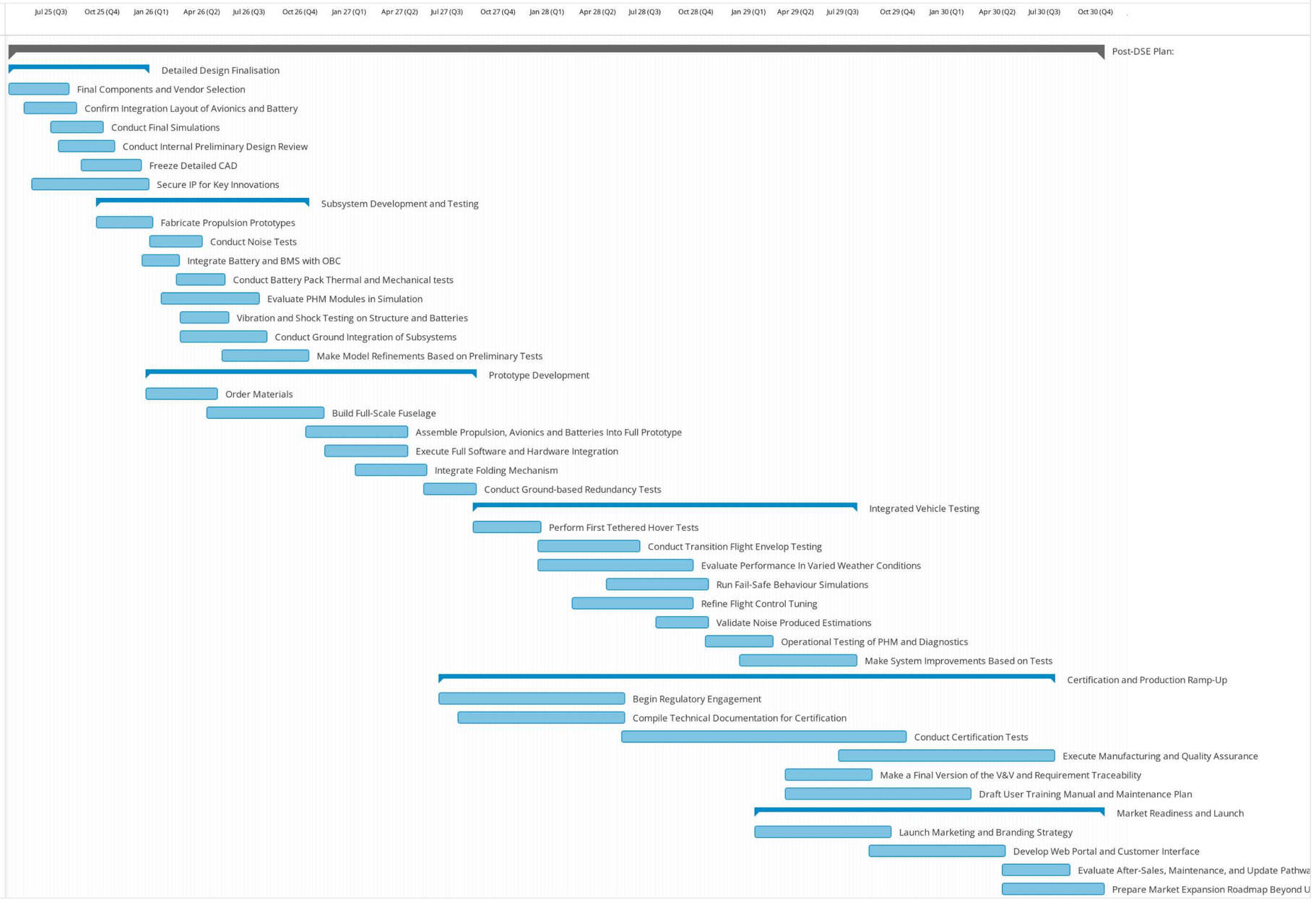

14 Innovations

Owl-22's vision is twofold. First, to provide a completely new solution to traffic congestion. In Western cities, traffic congestion is typically solved in one of three ways: road expansion, improved walkability/active transport, or public transportation. The latter two solutions are especially effective in such cities due to their conventional urban planning, public transportation heritage and hospitable climates. In postmodern cities, however, characterised by their recent construction and unorthodox city planning, these solutions are far less applicable. In the case of Dubai, for example, it unconventionally contains several centres spread along the coast, leading to a fragmented distribution of the population. The large distances between these hubs make it functionally impossible to walk between them, emphasising the need for robust transportation. Moreover, the relative novelty of the city means that it has little public transport infrastructure beyond its limited metro. Thus, unlike most Western cities, which can build on their long-existing systems through prolonged, sustained investments, Dubai would require providing a huge influx of capital to lay the foundations for an accessible public transport system. To avoid this, the local government addresses existing congestion issues by simply building more roads. Such a method is ecologically unsustainable, requires continuous maintenance and is a short-term solution to a constant problem.

By providing a low-altitude, privately owned eVTOL, Owl-22 offers a solution that is not constrained by land connections. Furthermore, it allows for the continuous expansion of travel corridors through the introduction of vertical layers. Such an expansion is not only a long-term solution to congestion, but it also requires little to no physical infrastructure to achieve and requires no maintenance. Thus, such an innovation is not only attractive to consumers, but also to governments that must continuously address the ever-increasing issue of congested roads. Additionally, unlike existing air-taxi solutions, a privately owned vehicle provides the user with flexibility akin to owning a car, taking off from home and travelling at one's convenience instead of commuting to a vertiport, paying for the service and taking off at predetermined times. The minimal infrastructure required to facilitate this vertical expansion is also important when addressing the sustainability of Owl-22. Assuming that vertiport construction would be the main source of infrastructure building, this vehicle doesn't carry the ecological implications that are associated with cars (which require roads), making it far better for the local environment.

The second vision of Owl-22 is to redefine the daily commute experience. In highly congested cities like Dubai, travelling to work typically requires leaving at unconventional times to avoid rush hour and a general feeling of dread is associated with the entire experience. Through this vehicle, which introduces intuitive, aerial travel, users can not only reduce their travel times, but also come to enjoy the experience of going back and forth from work. Another benefit is related to the living locations of users. In Dubai, for example, the majority of congestion is centred around Sheikh Zayed Road [148]. As such, expats in particular have to make well-informed decisions about where they live in order to minimise the chance of traffic when travelling to work. This, in turn, narrows the number of locations considered by expats and consequently drives the prices of certain neighbourhoods up. Owl-22's 30 [km] range circumvents this problem to a large extent, opening up previously sidelined neighbourhoods as feasible housing locations. Thus, purchasing this vehicle can also be viewed as an investment, enabling users to live in cheaper areas without suffering from constant traffic.

Regarding the specific design, Owl-22 innovates in two main ways. For one, its longitudinal foldability is a unique solution to enable easy storage at users' homes. By leveraging telescoping beams, as well as an accordion-like side-skin composite of Dyneema and PPSU, the vehicle's bounding box reduces by over 6 [m^3] to a total of 4 [m^3]. This reduction aligns Owl-22's volume with that of cars, allowing for convenient storage. Secondly, the unique combination of coaxial and cyclorotors allows for a more comfortable ride for users compared to conventional multicopter configurations. Namely, the thrust vectoring provided by the cyclorotors eliminates any tilting in forward flight and minimises it for turning. This allows for a more relaxing, comfortable flight compared to existing VTOLs such as helicopters.

15 Conclusion

As urban environments have exhausted traditional ground transportation systems, the Owl-22 project emerges as a bold response to the growing demand for efficient, personal mobility solutions in environments such as the UAE. This report details the concept design, establishing a framework for the design process of Owl-22. The content details finalising the design in the context of the design enabler, stakeholder requirements, system architecture and interface definition.

Based on the framework outlined, the subsystem design was performed, starting with the propulsion subsystem. The propulsion subsystem, consisting of 2 front cyclorotors and 2 rear coaxial rotors, is designed to carry 305 [kg] in optimal performance conditions, perform vertical take-off and landing, and achieve a total of 71 [dB]. The lower noise levels were achieved through the use of corotating coaxial rotors, with the upper blade larger than the lower blade, as well as serrated propeller blades. Following that, the source of power for Owl-22, being a solid-state lithium battery, was designed to be 33.2% of total vehicle mass, such that a range of 30 [km] and a cruise velocity of 60 [km/h] is achieved. The health of the battery was ensured with the use of a robust battery management system that takes care of managing the health, safety and thermal characteristics of the battery.

A critical component of flight safety in Owl-22 is the integration of a robust avionics suite. The avionics suite includes a communications suite, with displayed instruments equipped for Visual Flight Rules (VFR) operations, easing the transitions for users from cars. For situational awareness and safety, the suite features a 360-degree LiDAR sensing, providing a 20-meter omnidirectional detection range. This feature is supported by real-time mapping RTAB-Map, with future upgrades potentially leveraging AI for dynamic avoidance protocols and path planning. Furthermore, Owl-22 employs automated take-off and landing with semi-autonomous cruise flight enabled by an actor-critic control architecture. Following through with the concept of safety and reliability, prognostics and health management enhance the vehicle's resilience by enabling real-time awareness of system health and predictive maintenance strategies. A general architecture for the prognostics and health monitoring system has been established, leveraging an onboard, communications and ground-layer.

A preliminary control system was developed for nominal operations under small-angle assumptions with full actuator saturation. However, the verification and validation revealed system instability and the absence of rate saturation for control action. Future work should address these limitations to ensure stable and reliable performance across all flight phases.

Figure 15.1: Owl-22 external view.

With all the subsystems defined, the structural design of Owl-22 was finalised. The main airframe is constructed from aerospace-grade Aluminium 7068-T6511, selected for its high strength-to-weight ratio. The structure was sized for vibrational and static loads experienced during take-off, cruise, landing, and ground transportation. The final structure was verified using a Finite Element Analysis to ensure its safety under loads. Furthermore, the shape of the structure was optimised based on an aerodynamic analysis to minimise flow separation and drag, enhancing performance during flight, resulting in the final design presented in Figure 15.1. Preliminary assessments indicated that the structure remains over-designed. The total integrated vehicle mass currently stands at 197 [kg]. However, a sensitivity analysis proved that this value can be reduced to 175 [kg] with further structural optimisation tailored to the mission profile. This sets a lower bound mass estimate and a goal for future development stages.

The operational and logistical needs prove that Owl-22 is a user-friendly, low-maintenance personal

aerial vehicle due to its six-phase mission profile, intuitive iPad-based control, and minimal infrastructure demands. Designed for manufacturability in the UAE, it leverages modular construction and predictive diagnostics to reduce service needs. At the end-of-life, a circular approach enables easy disassembly and recycling through a digital material passport. Together, these features ensure Owl-22 is practical and scalable.

The sustainability strategy addresses environmental, social and economic dimensions. Environmentally, the vehicle incorporates recyclable materials and energy-efficient propulsion while adhering to noise emission standards. The environmental impact, conducted via a life cycle assessment, indicates that Owl-22 has a comparable carbon footprint to conventional vehicles. However, as it transports only one person at a time, its per-passenger emissions are higher than those of a multi-passenger vehicle. The social sustainability assessment focuses on enhancing community well-being by increasing local jobs, as well as reducing travel times and reimagining daily travel as an enjoyable experience. Economically, Owl-22 contributes by reinforcing the UAE's image as a futuristic city and creating employment opportunities through local manufacturing and service infrastructure.

Owl-22 targets UAE's high-income market, leveraging the country's supportive regulations and luxury-oriented consumer base. Owl-22's design is differentiated by its private ownership, foldable design and relative affordability. The financial analysis estimates the cost breakdown presented in Table 15.1.

Table 15.1: Total per-unit price breakdown at a production volume of 1,000 units per year.

Cost Component	**Per-Unit Value [$]**
Recurring Costs	64,936.89
Non-Recurring Costs (Amortised)	16,360.74
Total Cost (before profit)	81,297.63
Per-unit Profit (22.5%)	18,277.46
Final Selling Price	**99,575.09**

The Return On Investment (ROI) of 1.11 suggested that this project would get modest returns. On the contrary, the negative Net Present Value (NPV) indicates financial risks due to high initial investments. This can be curbed using strategic scaling of production, securing partnerships and optimising costs.

The systems engineering procedure conducted included a verification and validation plan, a requirement compliance assessment, and a risk management framework to ensure reliability. Following this, a structured six-phase development roadmap was established to guide Owl-22 from design finalisation through prototyping, testing, certification, and market entry.

Advancing Owl-22 toward market readiness, the next steps start with developing the embedded systems, such as flight control, battery management and communication protocol. These are essential for safe, semi-autonomous operation. Once implemented, these systems must be verified and validated through rigorous hardware and software simulation to ensure reliability. Simultaneously, a production plan must be established to define manufacturing processes, to optimise costs, followed by forming strategic partnerships for certification support and scaling operations.

The Owl-22 introduces two key innovations that position it uniquely in the urban air mobility landscape. It provides a practical personal aerial mobility solution for cities like Dubai and a convenient commuting experience. Its low-altitude, privately owned electric vertical take-off and landing design reduces reliance on road infrastructure while offering sustainable and flexible travel. With a 30 [km] range, it enables residential freedom and helps ease urban housing demand. Key design features, such as compact longitudinal folding and a coaxial-cyclorotor propulsion system, enhance storage convenience and deliver a smooth flight, making everyday aerial travel more accessible and comfortable.

References

[1] *Cyclo Tech*. 2025. URL: https://www.cyclotech.at.

[2] I. Surname, I. Surname, and I. Surname. *Aeeroacoustcs of Flight Vehicles: Theory and Practice*. 1st ed. Virginia, United States: NASA, 1991.

[3] P.N.Sorensen and D.R.Cuppoletti. "Rotor-Rotor Interaction Noise of CounterRotating vs CoRotating Rotors for Air Mobility Applications". In: *noise* 10.25 (2021), pp. 6–14.

[4] P.V.Makeev et al. "Comparative Study of a Conventional, Coaxial Counter-Rotating, and Co-Rotating Rotor Aerodynamics in Hover". In: *Russian Aeronautics* 64.2 (2021), 233–239.

[5] Z. Wei et al. "The Title of the Article". In: *The Title of the Journal* 15.4337 (2024), pp. 1–10.

[6] Airplane Academy. *What's the Difference Between 2, 3, and 4-Bladed Propellers?* 2024. URL: https://airplaneacademy.com/whats-the-difference-between-2-3-and-4-bladed-propellers/ (visited on 06/13/2025).

[7] Website Name <OR> I. Surname, I. Surname, and I. Surname. *Title of the Website*. 2000. URL: https://example.com (visited on 12/24/2020).

[8] Hobbywing. *Hobbywing*. 2025. URL: https://www.hobbywing.com/en/.

[9] Ohad Gur. *Propeller Design*. 1st ed. Virginia, United States: Aerospace Industries, 2024.

[10] APC. *Engineering Design Process Used to Develop APC Propellers*. 2025. URL: https://www.apcprop.com/technical-information/engineering/?v=796834e7a283 (visited on 06/13/2025).

[11] J. Baltazar, J. de Campos, and D. Rijpkema. "Prediction of the Propeller Performance at Different Reynolds Number Regimes with RANS". In: *The Title of the Journal* 9.10 (2021), p. 1115.

[12] Aero Toolbox. *Reynolds Number Calculator*. 2022. URL: https://aerotoolbox.com/reynolds-number-calculator/ (visited on 06/16/2025).

[13] Airfoil Tools. *TAirfoltools*. 2025. URL: http://airfoiltools.com/.

[14] M.S.Howe. "Aerodynamic noise of a serrated trailing edge". In: *Fluids and Structures* 5.1 (1991), pp. 33–45.

[15] P.Kholodov and S.Moreau. "Optimization of trailing-edge serrations with and without slits for broadband noise reduction". In: *Journal of Sound and Vibration* 490.2 (2021), p. 115736.

[16] S. Dougherty, N. Lin Oo, and D.Ahao. "Effects of propeller separation and onset flow condition on the performance of quadcopter propellers". In: *Aerospace Science and Technology* 145.108837 (2023), p. 8041.

[17] My Aircraft Cost. *What Are Airplane Propellers Made Of? A Material Guide*. 2025. URL: https://myaircraftcost.com/what-are-airplane-propellers-made-of-a-material-guide/ (visited on 06/13/2025).

[18] OMNI. *Distance Attenuation Calculator*. 2024. URL: https://www.omnicalculator.com/physics/distance-attenuation (visited on 06/18/2025).

[19] D.B.Hanson. "Helicoidal Surface Theory for Harmonic Noise of Propellers in the Far Field". In: *Aeronautics* 18.10 (2012), p. 1213.

[20] J. Goyal. *TU Delft Explore*. 2024. URL: https://gitlab.tudelft.nl/jatindergoyal/hanson-model-helicoidal-theory/-/releases/v3.0 (visited on 06/18/2025).

[21] Hyo Wan Kim, Duraisamy Karthikeyan, and Brown Richard. "Aeroacoustics of a coaxial rotor in level flight". In: *Rotorcraft Aeromechanics Laboratory* (2008), p. 14.

[22] J.H.Dittmar. *SOmee Design Philosophy for Reducing the Community Noise of Advancd CounerRotational Propellers*. 1st ed. Virginia, United States: Nasa, 1985.

[23] Noise Tools. *Source Model*. 2006. URL: https://noisetools.net/noisecalculator (visited on 06/18/2025).

[24] *Ansys Workbench | Simulation Integration Platform*. Ansys, Inc. URL: https://www.ansys.com/products/ansys-workbench (visited on 06/24/2025).

[25] AdFem. *Steady-state Navier-Stokes equations in 3D space*. 2021. URL: https://kailaix.github.io/AdFem.jl/dev/SteadyStateNavierStokes3D/ (visited on 06/17/2025).

[26] M. Lohry. *Turbulent flow simulations for wall-bounded flows - Reynolds-averaged Navier Stokes and Large Eddy Simulations*. Jan. 2012. URL: https://www.princeton.edu/~hammett/turbulence/2011/13%2016-2%20Lohry%20Large%20Eddy%20Simualtions.pdf?.

[27] Ansys Inc. *Closure of RANS Equations*. 2020. URL: https://innovationspace.ansys.com/courses/wp-content/uploads/sites/5/2020/09/Basics-of-Turbulent-Flows-Lesson-5-Handout.pdf.

[28] SimScale. *K-Epsilon Turbulence Models*. 2023. URL: https://www.simscale.com/docs/simulation-setup/global-settings/k-epsilon/ (visited on 06/17/2025).

[29] N. V. Budko. "Finite Volume Method in 2D, Straight and skewed boundaries, Properties of 2D FVM Laplacian matrix". Lecture given by Dr. Neil Budko at TU Delft as a part of the Numerical Methods for Differential Equations course.

[30] Benedict Moble. "Fundamental understanding of the cycloidal-rotor concept for micro air vehicle applications". English. Copyright - Database copyright ProQuest LLC; ProQuest does not claim copyright in the individual underlying works; Last updated - 2023-03-03. PhD thesis. University of Maryland, 2010, p. 312. ISBN: 978-1-124-48531-7. URL: https://www.proquest.com/dissertations-theses/fundamental-understanding-cycloidal-rotor-concept/docview/855603491/se-2.

[31] M. Kanoglu, Y. A. Cengel, and J. M. Cimbala. *EXTERNAL FLOW: DRAG AND LIFT*. http://contents.kocw.net/KOCW/document/2015/hanbat/chadongjin/3.pdf. 2010.

[32] Tianwei Jin et al. "Structural batteries: Advances, challenges and perspectives". In: *ScienceDirect* 62 (2023), pp. 151–167. DOI: 10.1016/j.mattod.2022.12.001. URL: https://www.sciencedirect.com/science/article/pii/S1369702122003364.

[33] Constantin Rotaru and Michael Todorov. "Helicopter Flight Physics". In: *Flight Physics*. Ed. by Konstantin Volkov. Rijeka: IntechOpen, 2017. Chap. 2. DOI: 10.5772/intechopen.71516. URL: https://doi.org/10.5772/intechopen.71516.

[34] GridX. *What is Battery Degradation and How to Prevent It*. URL: https://www.gridx.ai/knowledge/what-is-battery-degradation-and-how-to-prevent-it (visited on 06/18/2025).

[35] Smart Propel. *Solid-State Batteries: The Rising Star of Future Energy Storage*. https://www.smartpropel.com/solid-state-batteries-the-rising-star-of-future-energy-storage. Accessed: 2025-05-16. 2024.

[36] EVBox Team. *How Much Do Electric Car Batteries Weigh?* 2024. URL: https://blog.evbox.com/ev-battery-weight.

[37] Battery Ecosystem Partnership (BEP) Association. *The Case for Solid-State Batteries*. 2024. URL: https://bepassociation.eu/the-case-for-solid-state-batteries/.

[38] Marc A. Rosen and Aida Farsi. "Chapter 6 - Battery system design". In: *Battery Technology*. Ed. by Marc A. Rosen and Aida Farsi. Academic Press, 2023, pp. 161–198. ISBN: 978-0-443-18862-6. DOI: https://doi.org/10.1016/B978-0-443-18862-6.00006-9. URL: https://www.sciencedirect.com/science/article/pii/B9780443188626000069.

[39] Andrea Reindl, Meier Hans, and Michael Niemetz. "Scalable, Decentralized Battery Management System Based on Self-organizing Nodes". In: July 2020, pp. 171–184. ISBN: 978-3-030-52793-8. DOI: 10.1007/978-3-030-52794-5_13.

[40] G. Vykunta Rao et al. "Modular battery management system architecture for commercial vehicle applications". In: *Materials Today: Proceedings* 92 (2023). 2nd International Conference on Multifunctional Materials, pp. 1538–1543. ISSN: 2214-7853. DOI: https://doi.org/10.1016/j.matpr.2023.06.017. URL: https://www.sciencedirect.com/science/article/pii/S2214785323033953.

[41] Leo Allen S. Tayo et al. "Comparative Analysis of Centralized and Distributed BMS Topologies for LEV Applications". In: *2024 IEEE Transportation Electrification Conference and Expo, Asia-Pacific (ITEC Asia-Pacific)*. 2024, pp. 524–530. DOI: 10.1109/ITECAsia-Pacific63159.2024.10738574.

[42] Emre Biçer et al. "Solid-State Batteries: Chemistry, Battery, and Thermal Management System, Battery Assembly, and Applications—A Critical Review". In: *Batteries* 11.6 (2025). ISSN: 2313-0105. DOI: 10.3390/batteries11060212. URL: https://www.mdpi.com/2313-0105/11/6/212.

[43] Zhen Yin et al. "Battery Management System Towards Solid-State Batteries". In: *CHAIN* 1.4 (2024), pp. 319–353. DOI: 10.23919/CHAIN.2024.000011.

[44] A.A. Hakeem Akinlabi and Davut Solyali. "Configuration, design, and optimization of air-cooled battery thermal management system for electric vehicles: A review". In: *Renewable and Sustainable Energy Reviews* 125 (2020), p. 109815. ISSN: 1364-0321. DOI: https://doi.org/10.1016/j.rser.2020.109815. URL: https://www.sciencedirect.com/science/article/pii/S1364032120301106.

[45] Chakib Alaoui. "Solid-State Thermal Management for Lithium-Ion EV Batteries". In: *IEEE Transactions on Vehicular Technology* 62.1 (2013), pp. 98–107. DOI: 10.1109/TVT.2012.2214246.

[46] Foo Shen Hwang et al. "Review of battery thermal management systems in electric vehicles". In: *Renewable and Sustainable Energy Reviews* 192 (2024), p. 114171. ISSN: 1364-0321. DOI: https://doi.org/10.1016/j.rser.2023.114171. URL: https://www.sciencedirect.com/science/article/pii/S1364032123010298.

[47] F. Asgari Sima, A. Ghafari, and S. Akbari. "Enhancing Solid-State Battery Performance through Advanced Thermal Management Techniques". In: *NanoScience Technology* 14 (2024). Accepted: 6 August 2024, Published by: 21 August 2024, pp. 1–19. URL: https://jnanoscitec.com.

[48] Angelo Maiorino et al. "A review on thermal management of battery packs for electric vehicles". In: *Applied Thermal Engineering* 238 (2024), p. 122035. ISSN: 1359-4311. DOI: https://doi.org/10.1016/j.applthermaleng.2023.122035. URL: https://www.sciencedirect.com/science/article/pii/S1359431123020641.

[49] Neha Khan et al. "A critical review of battery cell balancing techniques, optimal design, converter topologies, and performance evaluation for optimizing storage system in electric vehicles". In: *Energy Reports* 11 (2024), pp. 4999–5032. ISSN: 2352-4847. DOI: https://doi.org/10.1016/j.egyr.2024.04.041. URL: https://www.sciencedirect.com/science/article/pii/S2352484724002506.

[50] R Kurmaev, V Struchkov, and V Novak. "Experience in the development of an effective thermal management system for the high-voltage battery of the vehicle". In: *IOP Conference Series: Materials Science and Engineering* 819 (May 2020), p. 012020. DOI: 10.1088/1757-899X/819/1/012020.

[51] Chang-Ching Tu et al. "Industry perspective on power electronics for electric vehicles". In: *Nature* (June 2024). DOI: 10.1038/s44287-024-00055-4.

[52] Xiqian Yu et al. "Battery Safety: From Lithium-Ion to Solid-State Batteries". In: *Engineering* 21 (2023), pp. 9–14. ISSN: 2095-8099. DOI: https://doi.org/10.1016/j.eng.2022.06.022. URL: https://www.sciencedirect.com/science/article/pii/S2095809922006282.

[53] Federal Aviation Authority. *Integration of Powered-Lift: Pilot Certification and Operations; Miscellaneous Amendments Related to Rotorcraft and Airplanes_2024*. 2024.

[54] Shizhuang Wang et al. "Enhancing navigation integrity for urban air mobility with redundant inertial sensors". In: *Aerospace Science and Technology* 126 (July 2022), p. 107631. DOI: 10.1016/j.ast.2022.107631.

[55] Nurlan Boguspayev et al. "A Comprehensive Review of GNSS/INS Integration Techniques for Land and Air Vehicle Applications". In: *Applied Sciences* 13.8 (2023), p. 4819. ISSN: 2076-3417. DOI: 10.3390/app13084819. URL: https://www.mdpi.com/2076-3417/13/8/4819.

[56] Haiyang Qiu et al. "A Study on Graph Optimization Method for GNSS/IMU Integrated Navigation System Based on Virtual Constraints". In: *Sensors* 24.13 (2024), p. 4419. ISSN: 1424-8220. DOI: 10.3390/s24134419. URL: https://www.mdpi.com/1424-8220/24/13/4419.

[57] Y.-T Chiu et al. “IMPROVEMENT OF LiDAR-SLAM-BASED 3D NDT LOCALIZATION USING FAULT DETECTION AND EXCLUSION ALGORITHM”. In: *The International Archives of the Photogrammetry, Remote Sensing and Spatial Information Sciences* XLIII-B1-2022 (May 2022), pp. 189–195. DOI: 10.5194/isprs-archives-XLIII-B1-2022-189-2022.

[58] Antonio Angrisano. “GNSS/INS Integration Methods”. Dottorato di ricerca in Scienze Geodetiche e Topografiche, XXIII Ciclo. Ph.D. thesis. Napoli, Italia: Dipartimento di Scienze Applicate, Università degli Studi di Napoli Parthenope, 2009.

[59] Ahmad Merei et al. “A Survey on Obstacle Detection and Avoidance Methods for UAVs”. In: *Drones* 9.3 (2025). ISSN: 2504-446X. DOI: 10.3390/drones9030203. URL: https://www.mdpi.com/2504-446X/9/3/203.

[60] Wolfram Burgard, Oliver Brock, and Cyrill Stachniss. “Map-Based Precision Vehicle Localization in Urban Environments”. In: *Robotics: Science and Systems III*. MIT Press, 2008, pp. 121–128.

[61] Mathieu Labbé and François Michaud. “RTAB□map as an open□source lidar and visual simultaneous localization and mapping library for large□scale and long□term online operation”. In: *Journal of Field Robotics* 36.2 (Oct. 2018), pp. 416–446. DOI: 10.1002/rob.21831.

[62] Matheus Ladeira and Emmanuel Grolleau. “Towards a Modular and Customisable Model-Based Architecture for Autonomous Drones”. In: *2020 IEEE 44th Annual Computers, Software, and Applications Conference (COMPSAC)*. July 2020, pp. 1127–1128. DOI: 10.1109/COMPSAC48688.2020.0-107.

[63] European Union Aviation Safety Agency. *Urban Air Mobility (UAM)*. Accessed: 2025-05-17. 2025. URL: https://www.easa.europa.eu/en/domains/drones-air-mobility/drones-air-mobility-landscape/urban-air-mobility-uam.

[64] Sabitri Poudel, Muhammad Yeasir Arafat, and Sangman Moh. “Bio-Inspired Optimization-Based Path Planning Algorithms in Unmanned Aerial Vehicles: A Survey”. In: *Sensors* 23.6 (2023). ISSN: 1424-8220. DOI: 10.3390/s23063051. URL: https://www.mdpi.com/1424-8220/23/6/3051.

[65] Wenjie Liu et al. “A Deep Reinforcement Learning-Based Path Planning Algorithm for Urban eVTOL Aircraft”. In: *2024 8th CAA International Conference on Vehicular Control and Intelligence (CVCI)*. 2024, pp. 1–6. DOI: 10.1109/CVCI63518.2024.10830128.

[66] S. B. Liu et al. “Reinforcement learning based multi-perspective motion planning of manned electric vertical take-off and landing vehicle in urban environment with wind fields”. In: *Engineering Applications of Artificial Intelligence* 149 (2025), p. 110392. DOI: 10.1016/j.engappai.2025.110392.

[67] V. Klein and E. A. Morelli. *Aircraft system identification: theory and practice*. 2006. DOI: 10.2514/4.861505.

[68] Julian Ibarz et al. “How to train your robot with deep reinforcement learning: lessons we have learned”. In: *The International Journal of Robotics Research* 40.4-5 (Jan. 2021), pp. 698–721. DOI: 10.1177/0278364920987859.

[69] E. Kaufmann et al. “Champion-level drone racing using deep reinforcement learning”. In: *Nature* 620 (7976 2023), pp. 982–987. DOI: 10.1038/s41586-023-06419-4.

[70] Pierre Beckmann, Guillaume Köstner, and Inês Hipólito. *Rejecting Cognitivism: Computational Phenomenology for Deep Learning*. Feb. 2023. DOI: 10.48550/arXiv.2302.09071.

[71] M. Homola, Y. Li, and E. V. Kampen. “Uncertainty-driven distributional reinforcement learning for flight control”. In: *AIAA SCITECH 2025 Forum* (2025). DOI: 10.2514/6.2025-2793.

[72] Eivind Bøhn et al. “Deep Reinforcement Learning Attitude Control of Fixed-Wing UAVs Using Proximal Policy optimization”. In: *2019 International Conference on Unmanned Aircraft Systems (ICUAS)*. 2019, pp. 523–533. DOI: 10.1109/ICUAS.2019.8798254.

[73] Tuomas Haarnoja et al. “Soft Actor-Critic: Off-Policy Maximum Entropy Deep Reinforcement Learning with a Stochastic Actor”. In: *CoRR* abs/1801.01290 (2018). arXiv: 1801.01290. URL: http://arxiv.org/abs/1801.01290.

[74] R. S. Sutton. *Reinforcement learning*. Bradford Books, 1992. DOI: 10.1007/978-1-4615-3618-5.

[75] *SparkFun GNSS Receiver Breakout - MAX-M10S (Qwiic)*. URL: https://www.sparkfun.com/sparkfun-gnss-receiver-breakout-max-m10s-qwiic.html (visited on 06/18/2025).

[76] Daniel Kraus, Hristo Ivanov, and Erich Leitgeb. “Approach for an Optical Network Design for Autonomous Vehicles”. In: *2019 21st International Conference on Transparent Optical Networks (ICTON)*. 2019 21st International Conference on Transparent Optical Networks (ICTON). July 2019, pp. 1–6. DOI: 10.1109/ICTON.2019.8840176. URL: https://ieeexplore.ieee.org/document/8840176 (visited on 06/18/2025).

[77] Rui Li, Wim J.C. Verhagen, and Richard Curran. “A systematic methodology for Prognostic and Health Management system architecture definition”. In: *Reliability Engineering and System Safety* 193 (2020), p. 106598. DOI: 10.1016/j.ress.2019.106598. URL: https://doi.org/10.1016/j.ress.2019.106598.

[78] Chetan Kulkarni et al. *A Prognostics Framework for Battery Health Monitoring Integrated with Thermal Modeling*. Tech. rep. KBR Inc, Intelligent Systems Division. Moffett Field, CA: NASA Ames Research Center, n.d.

[79] John T. Warner. *Lithium-Ion Battery Chemistries: A Primer*. Elsevier, 2019.

[80] Bin Xu et al. “Decoupling the thermal and non-thermal effects of discharge C-rate on the capacity fade of lithium-ion batteries”. In: *Journal of Power Sources* 510 (2021), p. 230390. DOI: 10.1016/j.jpowsour.2021.230390.

[81] Jimin Oh et al. “Comprehensive understanding of the effects of imbalanced cell via battery module tests for further usage of cycled batteries”. In: *Journal of Power Sources* 631 (2025), p. 236282. DOI: 10.1016/j.jpowsour.2025.236282. URL: https://doi.org/10.1016/j.jpowsour.2025.236282.

[82] Manuel Ank, Tobias Brehler, and Markus Lienkamp. “Wire bond contact defect identification in battery modules of electric vehicles using pulses and differential voltage analysis”. In: *eTransportation* 18 (2023), p. 100284. DOI: 10.1016/j.etran.2023.100284.

[83] Tianfeng Gao et al. “Hazardous characteristics of charge and discharge of lithium-ion batteries under adiabatic environment and hot environment”. In: *International Journal of Heat and Mass Transfer* 141 (2019), pp. 419–431. DOI: 10.1016/j.ijheatmasstransfer.2019.06.075.

[84] Ozge Yetik and Tahir Hikmet Karakoc. “Thermal and electrical analysis of batteries in electric aircraft using nanofluids”. In: *Journal of Energy Storage* 52 (2022), p. 104853. DOI: 10.1016/j.est.2022.104853.

[85] Edoardo Locorotondo et al. “Development of a battery real-time state of health diagnosis based on fast impedance measurements”. In: *Journal of Energy Storage* 38 (2021), p. 102566. DOI: 10.1016/j.est.2021.102566.

[86] Wenxue Liu et al. “Enabling high-fidelity electrothermal modeling of electric flying car batteries: A physics-data hybrid approach”. In: *Journal of Power Sources* 560 (2023), p. 232690. DOI: 10.1016/j.jpowsour.2022.232690.

[87] Quan Quan. *Introduction to Multicopter Design and Control*. 1st. Singapore: Springer Singapore, 2017, pp. xxvi + 384. ISBN: 978-981-10-3381-0. DOI: 10.1007/978-981-10-3382-7.

[88] VIJAY DESAI. “Modeling, Simulation and Complete Control of a Quadcopter”. MA thesis. National Institute of Technology Karnataka, 2017. URL: https://harikrishnansuresh.github.io/assets/quadcopter_control_project_report.pdf.

[89] Zaid Tahir, Waleed Tahir, and Saad Ali Liaqat. “State Space System Modelling of a Quad Copter UAV”. Version v2. In: *arXiv* (Sept. 13, 2019). Revised version (v2), submitted 13 September 2019. arXiv: 1908.07401 [cs.RO].

[90] Coen de Visser. “Aerospace Systems and Control Theory - A closer look at dynamics”. 2024.

[91] Federal Aviation Administration(FAA). *14 CFR Part 23 – Airworthiness Standards: Normal, Utility, Acrobatic, and Commuter Category Airplanes*. Available at GovInfo: CFR□2011□title14□vol1□part23.pdf. Jan. 2011. URL: https://www.govinfo.gov/content/pkg/CFR-2011-title14-vol1/pdf/CFR-2011-title14-vol1-part23.pdf.

[92] European Union Aviation Safety Agency (EASA). *SC□VTOL□01 – Special Condition for Small□Category VTOL Aircraft*. July 2019. URL: https://www.easa.europa.eu/sites/default/files/dfu/SC-VTOL-01.pdf.

[93] Scott Openshaw et al. *Ergonomics and Design: A Reference Guide*. Tech. rep. White paper published by Oregon State University EHS. Muscatine, Iowa: Allsteel Inc., 2006. URL: https://ehs.oregonstate.edu/sites/ehs.oregonstate.edu/files/pdf/ergo/ergonomicsanddesignreferenceguidewhitepaper.pdf.

[94] Max Roser, Cameron Appel, and Hannah Ritchie. *Human Height*. https://ourworldindata.org/human-height. Our World in Data, Global Change Data Lab. Accessed June 12, 2025. 2021.

[95] Healthline Editorial Team. *Average Shoulder Width: For Men and Women*. Accessed: 2025-06-12. 2023. URL: https://www.healthline.com/health/average-shoulder-width.

[96] Department of Mechanical Engineering, City University of Hong Kong. *Chapter 2.17. Shoulder Breadth (Bideltoid)*. Accessed: 2025-06-12. n.d. URL: https://personal.cityu.edu.hk/meachan/online%20anthropometry/chapter2/Ch2-17.htm.

[97] Dhaval Patel et al. *DroneX UAV Design for IMechE UAS Competition*. https://www.researchgate.net/publication/343933362_DroneX_UAV_Design_for_IMechE_UAS_Competition. ResearchGate publication. May 2020. DOI: 10.13140/RG.2.2.18452.12166.

[98] URL: https://help.solidworks.com/2025/english/SolidWorks/cworks/c_simp_method_topology.htm?verRedirect=1.

[99] Flight Medicine Systems Pty Ltd. *Understanding Blade Pass Frequency*. Technical Report / Presentation. Examines the concept of blade pass frequency and its effect on vibration in helicopters. Flight Medicine Systems Pty Ltd, 2021. URL: https://flightmed.com.au/wp-content/uploads/2021/05/Understanding-Blade-Pass-Frequency.pdf.

[100] Electic Motors. *The Engineering Toolbox*. 2024. URL: https://www.engineeringtoolbox.com/electrical-motors-hp-torque-rpm-d_1503.html (visited on 06/23/2025).

[101] Australian Aluminium Council. *Aluminium Extrusion Manual*. February 2023. Accessed June 2025. Feb. 2023. URL: https://aluminium.org.au/wp-content/uploads/2023/01/Aluminium-Extrusion-Manual-Feb23.pdf.

[102] D.L. Monette. “Coating removal techniques in the aerospace industry”. In: *Corrosion Control in the Aerospace Industry* (2009), pp. 225–247. DOI: 10.1533/9781845695538.3.225.

[103] Howard D. Curtis. *Fundamentals of Aircraft Structural Analysis*. New York: McGraw-Hill, 2001. ISBN: 9780071163166.

[104] *Jetson 1 Technical Specifications*. 2025. URL: https://jetson.com/jetson-one.

[105] V. T. T. Nguyen. *Basic Mechanical Vibrations*. Technical Report. Uploaded by the author on March 10, 2015. Industrial University of Ho Chi Minh City, 2011. URL: https://www.researchgate.net/profile/V-T-T-Nguyen/publication/273330566_Basic_Mechanical_Vibrations/links/54fecf170cf2741b69f164f2/Basic-Mechanical-Vibrations.pdf.

[106] Daniel J. Inman. *Engineering Vibration*. 4th ed. Boston: Pearson, 2014. ISBN: 978-0-13-287169-3.

[107] Priem Motorsport. *Sparco EVO QRT FIA*. Online product listing. 2025. URL: https://www.priemmotorsport.nl/kuipstoelen/sparco-evo-qrt-fia.

[108] DSM Dyneema. *Dyneema® high-strength, high-modulus polyethylene fiber: Comprehensive Factsheet (UHMWPE)*. Fact sheet CIS YA100. Issued 01-01-2008, 4 pages. Geleen, The Netherlands: DSM Dyneema / Pelican Rope, Jan. 2008. URL: https://pelicanrope.com/content/PDFs/Dyneema-Comprehensive-factsheet-UHMWPE.pdf.

[109] DataIntelo. *PPSU for Aerospace Market Research Report 2032*. https://dataintelo.com/report/ppsu-for-aerospace-market. Accessed: 2025-06-16. 2025.

[110] Electron Retracts. *Set Wheels + Brakes 200 mm (Pair)*. Accessed: 2025-06-12. 2025. URL: https://www.electron-retracts.com/product/set-wheels-brakes-200-mm-pair/.

[111] Digital Canal. *Aluminum Design Report*. https://www.digitalcanalstructural.com/site3/wp-content/uploads/2020/08/AluminumSampleReport.pdf. Sept. 2018.

[112] European Aviation Safety Agency (EASA). *Easy Access Rules for Normal, Utility, Aerobatic and Commuter Category Aeroplanes (CS-23)*. Initial Issue. 2018. URL: https://www.easa.europa.eu/sites/default/files/dfu/CS-23%20Initial%20issue.pdf.

[113] Ansys Inc. *Granta Selector 2025 R1*. Metals plus database. May 18, 2025. URL: https://www.ansys.com/products/materials/granta-selector.

[114] R. Biswas and R. C. Strawn. *Tetrahedral and Hexahedral adaptation for CFD problems*. Technical Report. NASA, 1997. URL: https://www.nas.nasa.gov/assets/nas/pdf/techreports/1997/nas-97-007.pdf.

[115] J. McIver. *Cessna Skyhawk II / 100*. Performance Assessment. Temporal Images, 2003. URL: http://www.temporal.com.au/c172.pdf.

[116] PAUL K. CHANG. "CHAPTER XII - Control of Separation of Flow". In: *Separation of Flow*. Ed. by PAUL K. CHANG. Pergamon, 1970, pp. 716–752. ISBN: 978-0-08-013441-3. DOI: https://doi.org/10.1016/B978-0-08-013441-3.50016-2. URL: https://www.sciencedirect.com/science/article/pii/B9780080134413500162.

[117] H. Bijl and N. Timmer. "Laminar and turbulent flows". Lecture given by Dr. N. Timmer at TU Delft as a part of the Introduction to Aerospace Engineering course.

[118] Aircraft Spruce Europe. *Plexiglas*. Accessed: 2025-06-11. 2025. URL: https://www.aircraftspruce.eu/metals---plastics/plexiglas/plexiglas.html.

[119] Evonik Industries AG. *PLEXIGLAS® for Aviation*. Brochure in PDF. Accessed: 2025-06-11. Evonik. 2023. URL: https://www.plexiglas.de/files/plexiglas-content/pdf/broschuere/122-3-PLEXIGLAS-for-aviation-web.pdf.

[120] Federal Aviation Administration. *Advisory Circular 25.775□1: Windows and Windshields*. 25.775-1. Advisory Circular. Active as of 2003-01-17, guidance for compliance with 14 CFR part 25 § 25.775 :contentReference[oaicite:1]index=1. U.S. Department of Transportation. Jan. 2003. URL: https://www.faa.gov/documentLibrary/media/Advisory_Circular/AC_25_775-1.pdf (visited on 06/12/2025).

[121] *Walksnail Avatar HD Camera Pro*. NordFPV. URL: https://nordfpv.com/products/walksnail-avatar-hd-camera-pro (visited on 06/18/2025).

[122] Benewake (Beijing) Co., Ltd. *TF02-Pro LiDAR – Specification Datasheet*. Datasheet. Version A02 (PDF). Benewake (Beijing) Co., Ltd, Apr. 2024. URL: https://en.benewake.com/uploadfiles/2024/04/20240426135509321.pdf.

[123] Ltd.) Slamtec (Shanghai Slamtec Co. *RPLIDAR S3 360° Laser Scanner (40 m) – Product Page & Datasheet*. 2025. URL: https://eu.robotshop.com/nl/products/slamtec-rplidar-s3-360-laser-scanner-40-m.

[124] Dynalabs (DynaLabs) Inertial Systems. *8000 Series Inertial Measurement Unit (IMU) – Datasheet*. Datasheet. DynaLabs, Ankara, Turkey, July 2022. URL: https://www.dynalabs.com.tr/wp-content/uploads/2022/08/IMU_8000_Datasheet.pdf.

[125] Apple Inc. *iPad (11□inch, 11th generation) – Technical Specifications*. Technical Specifications. Apple Inc., 2025. URL: https://www.apple.com/nl/ipad-11/specs/.

[126] Samsung Electronics GmbH. *990 EVO Plus 2 TB SSD (MZ□V9S2T0BW) – Product Page*. Accessed June 20, 2025; M.2 2280, PCIe 4.0 ×4 PCIe 5.0 ×2, sequential read/write up to 7250/6300 MB/s, 1 000 000/1 350 000 IOPS, 9 g, 5□year warranty. 2025. URL: https://www.alternate.nl/Samsung/990-EVO-Plus-2-TB-SSD/html/product/100080170.

[127] Holybro (Holybro, Inc.) *Pixhawk 6C Flight Controller – Technical Specification*. Technical Specification. STM32H743 STM32F103 processors, ICM□42688□P/BMI055 accelerometer/gyro, IST8310 mag, MS5611 barometer; Power: USB 5 V, servo rail 0–36 V; 84.8 × 44 × 12.4 mm; 59.3 g (aluminum case). Holybro, 2024. URL: https://docs.holybro.com/autopilot/pixhawk-6c/technical-specification.

[128] Garmin Ltd. *GTR 205 COMM Radio – Technical Specifications*. Technical Specification. Slim bezel (1.3″), full□color LCD, frequency lookup, 10 W Tx, 16 W upgrade option; TSO C146e/C157b/C165a/C195b certified. Garmin Ltd., June 2025. URL: https://www.garmin.com/en-US/p/721555/#specs.

[129] Welotec GmbH. *TK100 Series Industrial 4G LTE Router – Technical Specifications*. Technical Specification. LTE Cat 4 (Quectel EC25□EC chipset), dual SIM, 2×10/100 Ethernet (1 configurable WAN), 9–36 V DC power, IP30 enclosure, –20 °C to +70 °C, metal housing, firewall/OpenVPN/IPsec, wall/DIN□rail mounting. Welotec GmbH, Oct. 2023. URL: https://welotec.com/products/4g-lte-industrial-router-tk100?variant=41722772226129.

[130] SRE-PA & D-TEC Department Staff. *Margin philosophy for science assessment studies*. European Space Agency, 2012.

[131] StatCounter GlobalStats. *Tablet Vendor Market Share United Arab Emirates*. Accessed: 2025-05-19. 2025. URL: https://gs.statcounter.com/vendor-market-share/tablet/united-arab-emirates.

[132] *Vacuum Infusion Process (VIP) Results in High Strength Composites*. AEROVAC. URL: https://www.compositesone.com/vacuum-infusion-process-vip-results-in-high-strength-composites/ (visited on 06/23/2025).

[133] *Vacuum Infusion Technique*. KBS. URL: https://kbs-delivery.gr/en/content/7-vacuum-infusion-technique? (visited on 06/23/2025).

[134] Maria Roszkowska-Menkes, Maria Aluchna, and Bogumił Kamiński. "True Transparency or Mere Decoupling? The Study of Selective Disclosure in Sustainability Reporting". In: *Critical Perspectives on Accounting* 98 (Jan. 1, 2024), p. 102700. ISSN: 1045-2354. DOI: 10.1016/j.cpa.2023.102700. URL: https://www.sciencedirect.com/science/article/pii/S1045235423001612 (visited on 06/16/2025).

[135] Olga Hawn and Ioannis Ioannou. "Mind the Gap: The Interplay between External and Internal Actions in the Case of Corporate Social Responsibility". In: *Strategic Management Journal* 37.13 (2016), pp. 2569–2588. ISSN: 1097-0266. DOI: 10.1002/smj.2464. URL: https://onlinelibrary.wiley.com/doi/abs/10.1002/smj.2464 (visited on 06/16/2025).

[136] Ben Purvis, Yong Mao, and Darren Robinson. "Three pillars of sustainability: in search of conceptual origins". In: *Sustainability Science* 14.3 (2019), pp. 681–695. DOI: 10.1007/s11625-018-0627-5. URL: https://doi.org/10.1007/s11625-018-0627-5.

[137] S. Delbecq et al. "Aviation and Climate: a literature review." In: *ISAE-SUPAERO* (2022). DOI: https://doi.org/10.34849/a66a-vv58.

[138] ESPEC Corporation. *Battery Charge-Discharge Test*. https://www.espec.co.jp/english/products/trustee/test/charge.html. Accessed: 2025-05-20.

[139] *The Battery Mineral Loop*. RMI. URL: https://rmi.org/insight/the-battery-mineral-loop/ (visited on 06/17/2025).

[140] João Lopes et al. "A Life Cycle Assessment of Commercial Aircraft Considering Technological and Operational Improvements". In: *Sustainability* 14.17 (2022). Accessed: 2025-05-16, p. 10598. DOI: 10.3390/su141710598. URL: https://www.mdpi.com/2071-1050/14/17/10598.

[141] Jens F. Peters et al. “On the environmental competitiveness of sodium-ion batteries under a full life cycle perspective – a cell-chemistry specific modelling approach”. In: *Sustainable Energy Fuels* 5 (24 2021), pp. 6414–6429. DOI: 10.1039/D1SE01292D. URL: http://dx.doi.org/10.1039/D1SE01292D.

[142] Patent PC. *Solid State Batteries in 2020-2030: Adoption, Performance Gains, and Market Projections*. https://patentpc.com/blog/solid-state-batteries-in-2020-2030-adoption-performance-gains-and-market-projections. Accessed: 2025-05-16. 2023.

[143] Jens F. Peters et al. “On the environmental competitiveness of sodium-ion batteries under a full life cycle perspective – a cell-chemistry specific modelling approach”. In: *Sustainable Energy Fuels* 5 (24 2021), pp. 6414–6429. DOI: 10.1039/D1SE01292D. URL: http://dx.doi.org/10.1039/D1SE01292D.

[144] Khaula Alkaabi. “Analyzing the travel behaviour and travel preferences of employees and students commuting via the dubai metro”. In: *Arab World Geographer* 17 (Jan. 2014), pp. 42–65.

[145] G. Sajwani and H. Al–Othman. “Sustainable Development: An Analytical Vision for Smart Dubai City Social Policies”. In: *Information Sciences Letters* 12.7 (2023), pp. 87–2889. DOI: 10.18576/isl/120716.

[146] *A new era of smart mobility: SAVI cluster in Masdar City*. SAVI website. Located in Abu Dhabi’s Masdar City with plans for 15,000 new jobs and AED22billion GDP impact. 2023. URL: https://www.savi.ae/what-is-savi.

[147] Emirates247 Staff. ““Make it in the Emirates” concludes with new industrial projects valued over AED 11 billion”. In: *Emirates247* (May 22, 2025). Coverage of Make it in the Emirates 2025 event, including industrial deals totaling AED11billion. URL: https://www.emirates247.com/business/economy-finance/make-it-in-the-emirates-concludes-with-new-industrial-projects-valued-over-aed11-billion-2025-05-22-1.739498.

[148] The Phoenix Review. *Guide to Dubai commute and transport statistics for residents and visitors*. Online article. 2025. URL: https://www.thephoenixreview.com/guide-to-dubai-commute-and-transport-statistics-for-residents-and-visitors/.

[149] Yuta J. Masuda, Jason R. Williams, and Heather Tallis. “Does Life Satisfaction Vary with Time and Income? Investigating the Relationship Among Free Time, Income, and Life Satisfaction”. In: *Journal of Happiness Studies* 22 (2021), pp. 2051–2073. DOI: 10.1007/s10902-020-00307-8. URL: https://www.ncbi.nlm.nih.gov/pmc/articles/PMC8336732/.

[150] Morgan Stanley Research. *Flying Cars: Investment Implications of Urban Air Mobility*. Projects a total addressable market of $1.5 trillion for autonomous aircraft by 2040, with a more bullish forecast placing the market at $2.9 trillion. 2021. URL: https://www.morganstanley.com/ideas/autonomous-aircraft.

[151] Emirates NBD. *Green Auto Loan*. Offers financing up to 80% of the vehicle cost, including accessories, with interest rate discounts of 0.25% to 0.5%. 2025. URL: https://www.emiratesnbd.com/en/loans/auto-loans/green-auto-loan.

[152] Abu Dhabi Commercial Bank (ADCB). *Green Car Loans*. Provides financing up to 80% of the car value, with interest rates starting from 1.94% flat per annum. 2025. URL: https://www.adcb.com/en/personal/loans/car-loans/green-car-loans.

[153] Dubai Islamic Bank (DIB). *EVolve Green Financing*. Offers green financing solutions with low profit rates starting from 1.89% per annum. 2025. URL: https://www.uab.ae/personal/loans/green-auto-loans.

[154] HSBC. *Green Car Loans*. Offers green car loans with interest rate discounts of up to 0.25% on the applicable flat interest rate. 2025. URL: https://evlife.world/mena/financing-your-electric-dreams/.

[155] RAKBANK. *Green Auto Loan*. Provides green auto loans with interest rates starting from 2.27% per annum. 2025. URL: https://www.thephoenixreview.com/guide-to-dubai-commute-and-transport-statistics-for-residents-and-visitors/.

[156] MarketsandMarkets. *Urban Air Mobility Market Size, Share, Trends, Companies & Industry*. Accessed: 2025-05-07. 2025. URL: https://www.marketsandmarkets.com/Market-Reports/urban-air-mobility-market-251142860.html.

[157] Grand View Research. *Middle East & Africa Urban Air Mobility (UAM) Market Size & Outlook, 2030*. Accessed: 2025-05-07. 2024. URL: https://www.grandviewresearch.com/horizon/outlook/urban-air-mobility-uam-market/mea.

[158] UAE General Civil Aviation Authority. *UAS Registration | General Civil Aviation Authority (GCAA) of UAE*. 2023. URL: https://www.gcaa.gov.ae/en/pages/uasregistration.aspx.

[159] WAM. *General Civil Aviation published world first national regulation related to vertiports*. 2022. URL: https://www.wam.ae/en/details/1395303114515.

[160] Reuters. *UAE begins mapping corridors for air taxis and cargo drones*. 2025. URL: https://www.reuters.com/world/middle-east/uae-begins-mapping-corridors-air-taxis-cargo-drones-2025-02-13/.

[161] World Bank Open Data. *World Bank Open Data*. 2025. URL: https://data.worldbank.org/indicator/NY.GDP.PCAP.CD?locations=AE.

[162] The Official Portal of the UAE Government. *The UAE’s Future Roadmap*. 2025. URL: https://u.ae/en/about-the-uae/uae-in-the-future/uae-future.

[163] UAE Ministry of Investment: Invest in UAE. *A Global Investment Hub*. 2025. URL: https://www.investuae.gov.ae.

[164] B.D. Augustine. *UAE ranks high in technology adoption in financial services.* 2018. URL: https://gulfnews.com/business/banking/uae-ranks-high-in-technology-adoption-in-financial-services-1.2136502?.

[165] J Gambrell. *Dubai choked by traffic as it becomes victim of its own popularity*. 2025. URL: https://www.independent.co.uk/travel/news-and-advice/dubai-uae-tourists-flight-traffic-jams-housing-b2693890.html.

[166] Gulftoday. *UAE reveals forward-looking vision in aviation sector*. 2024. URL: https://gulfnews.com/business/banking/uae-ranks-high-in-technology-adoption-in-financial-services-1.2136502?.

[167] The Official Portal of the UAE Government. *UAE Net Zero 2050*. 2025. URL: https://u.ae/en/more/uae-net-zero-2050.

[168] Joby Aviation. *Joby to Launch Air Taxi Service in UAE*. Accessed: 2025-05-07. 2024. URL: https://www.jobyaviation.com/news/joby-to-launch-air-taxi-service-uae/.

[169] Archer Aviation. *Abu Dhabi and Archer Announce Agreement With Cross-Industry Stakeholders To Launch First Commercial Electric Air Taxi Flights*. Accessed: 2025-05-07. 2024. URL: https://investors.archer.com/news/news-details/2024/Abu-Dhabi-and-Archer-Announce-Agreement-With-Cross-Industry-Stakeholders-To-Launch-First-Commercial-Electric-Air-Taxi-Flights/default.aspx.

[170] Eve Air Mobility and Kookiejar. *Eve and Kookiejar to Develop Urban Air Traffic Management System for Operations in Dubai*. Accessed: 2025-05-07. 2023. URL: https://www.eveairmobility.com/eve-and-kookiejar-to-develop-urban-air-traffic-management-system-for-operations-in-dubai/.

[171] AutoFlight. *AutoFlight*. Accessed 2025-06-18. AutoFlight. 2025. URL: https://www.autoflight.com/en/.

[172] XPENG AeroHT. *XPENG AEROHT: eVTOL Flying Car*. Accessed 2025-06-18. Guangdong Huitian Aerospace Technology Co., Ltd. 2025. URL: https://www.aeroht.com/.

[173] NEOM & Volocopter. *NEOM and Volocopter: First Electric Air Taxi Flight in Saudi Arabia*. Accessed 2025-06-12. NEOM. June 21, 2023. URL: https://www.neom.com/en-us/newsroom/neom-volocopter-evtol.

[174] Civil Aviation Authority of Singapore (CAAS) & European Union Aviation Safety Agency (EASA). *CAAS and EASA Agreement to Support Development, Deployment and Safe Operation of eVTOL Aircraft*. Accessed 2025-06-12. AAM International. Oct. 21, 2022. URL: https://www.aaminternational.com/2022/10/caas-and-easa-agreement-to-support-development-deployment-and-safe-operation-of-evtol-aircraft.

[175] Chris Stonor. *Middle East: "Air Taxis a Major Agenda at Qatar NDS3 Event"*. Accessed 2025-06-12. eVTOL Insights. Aug. 21, 2024. URL: https://evtolinsights.com/2024/08/middle-east-air-taxis-a-major-agenda-during-qatar-nds3-event.

[176] InsightTrendsWorld. *Insight of the Day: Luxury Consumers Are Still Willing to Spend, with Younger Ones Leading the Way*. Accessed 2025-06-12. InsightTrendsWorld. URL: https://www.insighttrendsworld.com/post/insight-of-the-day-luxury-consumers-are-still-willing-to-spend-with-younger-ones-leading-the-way.

[177] Federal Aviation Administration (FAA). *Powered Lift Part 194 SFAR Frequently Asked Questions (FAQ)*. Last updated October 22, 2024; Accessed 2025□06□12. Federal Aviation Administration. Oct. 22, 2024. URL: https://www.faa.gov/air-taxis/FAQ.

[178] Federal Aviation Administration (FAA). *Advanced Air Mobility (Air Taxis)*. Last updated July 18, 2023; Accessed 2025□06□12. Federal Aviation Administration. July 18, 2023. URL: https://www.faa.gov/air-taxis/.

[179] NASA Johnson Space Center Cost Analysis Division. *Cost Estimation Handbook: Learning Resources*. Archived August 30, 2012; Accessed 2025-06-17. NASA Johnson Space Center. 2012. URL: https://web.archive.org/web/20120830021941/http://cost.jsc.nasa.gov/learn.html.

[180] Zed Rockford. *NASA's Sulfur Selenium Solid□State Battery Technology Impact on eVTOL Aircraft Development*. Accessed 2025-06-18. Business Aviation. Feb. 16, 2025. URL: https://businessaviation.aero/evtol-news-and-electric-aircraft-news/electric-aircraft/nasas-sulfur-selenium-solid-state-battery-technology-impact-on-evtol-aircraft-development?utm_source=chatgpt.com.

[181] Davide Ferretto and Daniele Carugo. "Development and Production Costs Estimation Methodology for eVTOL". Accessed 2025-06-17. MSc thesis. Politecnico di Torino, Apr. 2024. URL: https://webthesis.biblio.polito.it/31312/1/tesi.pdf.

[182] FARO Technologies. *Trends in Aerospace Assembly: An Introduction*. Accessed 2025-06-17. FARO Technologies. URL: https://www.faro.com/en/Resource-Library/Article/trends-in-aerospace-assembly-introduction.

[183] Joby Aviation, Inc. *2025 Proxy Statement and 2024 Annual Report (Form 10-K/A and Proxy Statement)*. SEC filing (PDF). Accessed 2025-06-18. May 2025. URL: https://ir.jobyaviation.com/sec-filings/all-sec-filings/content/0001819848-25-000330/joby-2025xars.pdf.

[184] Ben Sampson and Aerospace Testing International. *In this Issue – SHOWCASE 2019*. Accessed 2025-06-18. Aerospace Testing International. Oct. 23, 2018. URL: https://www.aerospacetestinginternational.com/online-magazines/in-this-issue-showcase-2019.html.

[185] National Aeronautics and Space Administration (NASA). *Exploration Systems Architecture Study: Final Report, NASA□TM□2005□214062*. Technical Memorandum NASA□TM□2005□214062. Archived PDF hosted by NSS; Accessed 2025□06□18. NASA, Nov. 2005.

[186] Ansys. 2022. URL: https://www.ansys.com/content/dam/amp/2022/april/webpage-requests/2022-ansys-scade-handbook.pdf.

[187] Caterina Urban and Antoine Miné. *A Review of Formal Methods applied to Machine Learning*. 2021. arXiv: 2104.02466 [cs.PL]. URL: https://arxiv.org/abs/2104.02466.

[188] Guy Katz et al. "The Marabou framework for verification and analysis of deep neural networks". In: 2019. DOI: 10.1007/978-3-030-25540-4_26.

[189] U. Ravaioli et al. "Safe reinforcement learning benchmark environments for aerospace control systems". In: *2022 IEEE Aerospace Conference (AERO)* (2022), pp. 1–20. DOI: 10.1109/aero53065.2022.9843750.

[190] Keysight Technologies. *GPS Receiver Testing*. Application Note 5990-4943EN. Keysight Technologies, July 2014. URL: https://www.keysight.com/us/en/assets/7018-05194/application-notes/5990-4943.pdf.

[191] Office of the Surveyor-General and Land Information, ACT Government. *GNSS Equipment Verification, Guideline No. 9*. Version 2.0, General revision resulting from GDA2020 introduction. Dickson, ACT, Australia, Nov. 2023. URL: https://www.planning.act.gov.au/survey-spatial-data-and-maps/survey-control-and-geodesy/geodetic-calculator-spreadsheets/calculations-on-adg66act-standard-grid.

[192] Ascend Technologies. *How to Effectively Test a Vibration Accelerometer Sensor*. https://www.ascend-tech.com/blog/how-to-effectively-test-a-vibration-accelerometer-sensor. Accessed: 2025-05-15. July 2017.

[193] Kian Sek Tee et al. "Triaxial Accelerometer Static Calibration". In: *Proceedings of the World Congress on Engineering 2011*. Vol. III. London, U.K.: IAENG, July 2011, pp. 2164–2167. ISBN: 978-988-19251-5-2.

[194] C.z. Li, Y. Chen, and T. Zhou. "Dynamic Calibration Methods of Accelerometer in Vibration-Temperature Combined Environment". In: *Mechanical and Materials Engineering of Modern Structure and Component Design*. Ed. by A. Öchsner and H. Altenbach. Vol. 70. Advanced Structured Materials. Springer, Cham, 2015. DOI: 10.1007/978-3-319-19443-1_36. URL: https://doi.org/10.1007/978-3-319-19443-1_36.

[195] International Electrotechnical Commission (IEC). *New Key Standards for Testing*. https://www.iec.ch/blog/new-key-standards-testing. Accessed: 2025-05-15. Sept. 2020.

[196] H. Sternberg and C. Schwalm. *Qualification Process for MEMS Gyroscopes for the Use in Navigation Systems*. Technical Report. HafenCity University Hamburg, Department of Geomatics and University of the Bundeswehr Munich, Institute of Geodesy, 2007.

[197] Kistler Group. *EN 9100 (AS9100) Certification*. https://www.kistler.com/NL/en/en-9100-as9100-certification/C00000672. Accessed: 2025-05-16.

[198] Imatest LLC. *LiDAR Testing*. https://www.imatest.com/solutions/lidar-testing/. Accessed: 16-May-2025. 2025.

[199] Keysight Technologies. *How to Verify Lidar Sensors*. https://www.keysight.com/us/en/solutions/verify-lidar-sensors.html. Accessed: 16-May-2025. 2025.

[200] Cyrus Minwalla et al. “Flight Test Evaluation of a Prototype Optical Instrument for Airborne Sense-and-Avoid Applications”. In: *AIAA Journal of Aerospace Information Systems* 8387 (2012). DOI: 10.2514/1.XXXXX.

[201] Pyser-SGI Limited. *Resolution Charts and Gratings*. Product catalog for optical resolution test charts, including USAF 1951, Ronchi rulings, and grids. Pyser-SGI Limited. Fircroft Way, Edenbridge, Kent, TN8 6HA, United Kingdom, Apr. 2010. URL: https://www.pyser-sgi.com/.

[202] Keysight Technologies. *S94USBCB USB Type-C Interconnects Compliance Test Software*. https://www.keysight.com/us/en/product/S94USBCB/usb-type-c-interconnects-compliance-test-software.html. Accessed: 16-May-2025. 2025.

[203] Brendan Murphy. *What is an E-Marker in a USB Type-C Cable and How Does It Work?* https://www.totalphase.com/blog/2020/10/what-is-e-marker-how-does-it-work/. Accessed: 16-May-2025. Oct. 2020.

[204] Federal Aviation Administration. *Advisory Circular 21-16G: RTCA Document DO-160 versions D, E, F, and G, “Environmental Conditions and Test Procedures for Airborne Equipment”*. Advisory Circular AC 21-16G. Identifies RTCA/DO-160G as an acceptable standard for environmental qualification of airborne equipment. U.S. Department of Transportation, Federal Aviation Administration, June 2011. URL: https://www.faa.gov/regulations_policies/advisory_circulars/.

[205] Pooja Vadhva et al. “Electrochemical Impedance Spectroscopy for All-Solid-State Batteries: Theory, Methods and Future Outlook”. In: *ChemElectroChem* 8.11 (2021), pp. 1930–1947. DOI: 10.1002/celc.202100108.

[206] John C. Lin et al. “High Lift Common Research Model for Wind Tunnel Testing: An Active Flow Control Perspective”. In: *55th AIAA Aerospace Sciences Meeting*. AIAA SciTech Forum. Grapevine, Texas: AIAA, Jan. 2017. DOI: 10.2514/6.2017-0319.

[207] Jiahong Zheng. “A Flight Load Test Method for Helicopter Rotor Blade”. In: *International Journal of Mechanical Engineering and Applications* 9.5 (2021), pp. 75–78. DOI: 10.11648/j.ijmea.20210905.11. URL: http://www.sciencepublishinggroup.com/j/ijmea.